



---

**POZNAŃ UNIVERSITY OF TECHNOLOGY**

---

---

**DOCTORAL DISSERTATION**

---

Modelling and experimental research  
of polypropylene fibre reinforced high performance concrete  
regarding ductility

---

mgr inż. Michał Demby

Supervisor:  
prof. dr hab. inż. Mieczysław Kuczma

Poznań 2022



# Spis treści

<b>Preface</b>	<b>v</b>
<b>Abstract</b>	<b>vii</b>
<b>Streszczenie</b>	<b>ix</b>
<b>Notations</b>	<b>xi</b>
<b>1 Motivation</b>	<b>1</b>
<b>2 Aim and scope of the research</b>	<b>3</b>
<b>3 PFRHPC - the state-of-the-art</b>	<b>5</b>
<b>4 Experimental research</b>	<b>15</b>
4.1 Test specimens . . . . .	15
4.2 Used materials . . . . .	19
4.3 Apparatus . . . . .	33
4.4 Preliminary tests and mix proportions . . . . .	35
4.5 Determination of compressive strength . . . . .	37
4.5.1 Description of testing . . . . .	37
4.5.2 Results of tests . . . . .	38
4.6 Determination of material parameters . . . . .	41
4.6.1 Description of testing . . . . .	41
4.6.2 Results of tests . . . . .	44
4.7 Testing of laboratory beams (10x10x50cm) . . . . .	50
4.7.1 Description of testing . . . . .	50
4.7.2 Results of tests . . . . .	51
4.8 Testing of full-scale beams (12x24x260cm) . . . . .	54
4.8.1 Description of testing . . . . .	54
4.8.2 Results of tests . . . . .	56
<b>5 Modelling</b>	<b>71</b>
5.1 Formulation of the problem . . . . .	71
5.2 Model of the concrete . . . . .	73

5.3	Computational model . . . . .	79
5.4	Convergence test . . . . .	82
<b>6</b>	<b>Ductility of PFRHPC beams</b>	<b>85</b>
6.1	Measurements of ductility . . . . .	85
6.2	Ductility of laboratory beams (10x10x50cm) . . . . .	88
6.3	Ductility of full-scale beams (12x24x260cm) . . . . .	89
<b>7</b>	<b>Conclusions and future research</b>	<b>95</b>
7.1	Conclusions . . . . .	95
7.2	Future research directions . . . . .	98
<b>Appendix A</b>		
	Force-displacement graphs in full-scale beams	99
<b>Appendix B</b>		
	Maps of horizontal strains in full-scale beams	107
<b>Bibliography</b>		<b>107</b>
<b>List of figures</b>		<b>143</b>
<b>List of tables</b>		<b>148</b>

# Preface

*The pessimist sees difficulty in every opportunity.  
The optimist sees opportunity in every difficulty.  
/Winston Churchill/*

*To everyone on my way who have contributed to make me the optimist*

First of all, I would like to thank my family and my closest friends - you are the best support team I could ever dream of. You believed in me even when I didn't believe in myself.

I have no words to express my gratitude to Professor Mieczyslaw Kuczma who is the supervisor of this thesis and my mentor. His help and efforts to make me a good researcher are invaluable.

I am grateful to the laboratory staff headed by Doctor Justyna Grzymisławska. The exploration of the specific nature of laboratory work was pure pleasure - even though I used to leave laboratory not so clean. I cannot fail to mention that the support of my colleagues from Division of Structural Engineering has been priceless. In particular I would like to thank Professor Janina Bogucka, Doctor Teresa Grabiec-Mizera and Doctor Jacek Scigallo. Our discussions were very encouraging.

This thesis was supported by grants: 01/11/DSMK/0902 (2017), 01/11/DSMK/0011 (2018) and 01/11/SBAD/0032 (2019) from the Ministry of Science and Higher Education. Laboratory tests were carried out using modern measuring devices purchased within the grant from Professor Kuczma (6571/IA/SP/2016). The experimental research would not be possible without the support of industry environment. My acknowledgements go to following companies: COLAS, GORAZDZE, PEKABEX and SIKA.



# Abstract

Concrete, which is the second after the water most consumed material in the world, is also one of the oldest and the fastest developing structural material. This rapid advancement results in not just increase of its compressive strength but also in improvement of other material properties, what is consistent with the idea of *high performance concrete* (HPC). It is a known fact that higher compressive strength is related to higher brittleness of concrete. To overcome this downside of concrete and enhance the ductility of concrete structure fibre reinforcement can be applied. Among many different fibres used nowadays as the concrete reinforcement, next to steel ones, polypropylene fibres are very popular. Their advantages over steel fibres include smaller weight, higher resistance against corrosion and what is important - the smaller cost. The following thesis concerns polypropylene fibre reinforced high performance concrete (PFRHPC).

In this dissertation, the fundamental properties of the abovementioned material are discussed. Basic information about high performance concrete (HPC) as well as polypropylene fibre reinforced concrete (PFRC) is presented. The world research interest in this field with examples of application of PFRHPC are also provided.

The experimental research was conducted in the laboratory of Poznan University of Technology. In the research many specimens (132) were subjected to different tests. Thanks to the cooperation with industry partners the used constituents of concrete mix were of the highest quality. The considerable industry interest in this research may indicate on desirability of undertaken project. Among conducted testing of materials used in the research the determination of flexural and compressive strength (both standard and early strengths) of cement and cement-silica fume mix as well as determination of bulk density of aggregates can be mentioned. The advanced contact-free measuring system ARAMIS 6M based on the principle of digital image correlation (DIC) was applied in the research. The series of preliminary tests had to be done to determine the final concrete mix proportions.

The compressive strength was determined on the cube as well as cylinder specimens. For one of the variants the compression test was carried out also after one year after concreting. High dosage of polypropylene fibres will result in a decrease in compressive strength of concrete; on the other hand the mechanism of failure under compression changes and in case of the polypropylene fibres presence is not so destructible

Cylinder specimens were also used in determination of material parameters like modulus of elasticity and Poisson's ratio. The method A according to Standard EN12390-13 [208] assumed in the research enabled the establishment of initial as well as stabilized

Young's modulus. Some 5 to 10 percentage increase of initial value after stabilization was recorded.

The testing of laboratory beams (10x10x50 cm) was conducted in order to determine the difference in failure mechanism of bended specimen with and without polypropylene fibres.

Among all specimens full-scale beams (12x24x260 cm) shall be highlighted. Beams reinforced by polypropylene fibres, steel longitudinal bars and mix of mentioned types of reinforcement were subjected to three-point bending. There is also other diversity with regard to used materials (silica fume and aggregates) from the other manufacturer, place of preparation of samples (laboratory vs industrial conditions) and the length of polypropylene fibre. In the test the cyclic loading-unloading procedure with gradually increased mid-span deflection was provided. The force-displacement graphs as hysteresis and the envelopes for the maximum values of forces were plotted. Displacements of the beams were recorded simultaneously by using three different measurement systems: testing machine INSTRON 8505, linear variable differential transformer and non-contact measuring system ARAMIS 6M. The obtained results are in very good agreement.

Experimental research was complemented by modelling and numerical analysis of PFRHPC beams. After the formulation of the problem and description of Concrete Damage Plasticity model of concrete the computational model of beam under monotonous mid-span deflection is presented. The model was prepared by using selected results of own experiments and literature proposals. The fibre reinforcement was included in the model by the modification of tensile stress-strain of concrete. The mesh-sensitivity verification was carried out also.

A special attention is paid to the ductility issue. A review of different measurements of ductility has been done. The ductility parameters like fracture energy, characteristic length, ductility length and toughness indices were calculated based on my own experimental results. The increase of all considered ductility parameters in comparison with specimens without polypropylene fibres - was observed.

The summary and all conclusions are presented in chapter 7 of the thesis. The possible directions of further work are also included there. After the main part of the work two appendixes are situated. In appendix A force-displacement graphs from three-point bending tests of full-scale beams are included, whereas in the appendix B maps of horizontal strains in selected loading-unloading cycles in abovemention tests are located. The notation of symbols and abbreviations used in the thesis reader may find at the beginning of the work, whereas the bibliography, list of figures and list of tables are provided at the end of this dissertaton.

# Streszczenie

Beton, będący drugim (po wodzie) najbardziej używanym materiałem na świecie, jest jednym z najstarszych i najszybciej rozwijających się materiałów konstrukcyjnych. Ten gwałtowny rozwój skutkuje nie tylko wzrostem wytrzymałości na ściskanie, ale również poprawą innych właściwości materiałowych, co jest zgodne z ideą *betonu wysokowartościowego* — *high performance concrete* (HPC). Dobrze znanym jest fakt, iż większa wytrzymałość na ściskanie jest związana z większą kruchością betonu. Aby przezwyciężyć tę podstawową wadę tego materiału konstrukcyjnego i polepszyć ciągliwość konstrukcji betonowych stosuje się zbrojenie betonu w postaci włókien. Wśród wielu różnych włókien stosowanych dziś do betonu, włókna polipropylenowe, obok stalowych, cieszą się dużą popularnością. Mają one przewagę nad włóknami metalowymi głównie jeśli chodzi o mniejszy ciężar, lepszą odporność korozyjną i - co istotne - mniejszy koszt. Niniejsza rozprawa dotyczy betonu wysokowartościowego zbrojonego włóknami polipropylenowymi – PFRHPC (z języka angielskiego: *polypropylene fibre reinforced high performance concrete*).

W pracy opisano podstawowe właściwości materiału PFRHPC. Zaprezentowane zostały istotne informacje zarówno na temat betonu wysokowartościowego jak i betonu zbrojonego włóknami polipropylenowymi. Tematyka PFRHPC budzi duże zainteresowanie świata naukowego, jak i wynika z potrzeb jego zastosowania w praktyce budowlanej.

Badania doświadczalne zostały przeprowadzone w laboratorium Politechniki Poznańskiej. Różnego typu testom poddano wiele próbek (łącznie 132 sztuki). Dzięki współpracy z renomowanymi partnerami przemysłowymi (COLAS, GÓRAŹDŹE, PEKABEX and SIKKA) zastosowane materiały były najwyższej jakości. Duże zainteresowanie przemysłu prowadzonymi badaniami świadczy o zasadności podjęcia tego tematu badawczego. Wśród przeprowadzonych badań materiałów, które użyto do przygotowania betonu PFRHPC, wymienić można między innymi badanie wytrzymałości (zarówno standardowej jak i wcześniejszej) na zginanie i ściskanie cementu oraz mieszanki cementu z pyłem krzemionkowym i określenie gęstości nasypowej użytych kruszyw. W badaniach wykorzystano zaawansowany bezdotykowy system pomiarowy ARAMIS 6M bazujący na zasadzie cyfrowej korelacji obrazu (DIC). W celu określenia proporcji składników mieszanki betonowej przeprowadzono także szereg testów wstępnych.

Wytrzymałość betonu na ściskanie została określona zarówno na próbkach sześciennych jak i walcowych. Dla jednego z wariantów badawczych badanie wykonano również po dłuższym okresie czasu - jednego roku od czasu zabetonowania. Przyjęte wysokie dozowanie włókien skutkowało obniżeniem wytrzymałości na ściskanie; z drugiej jednak strony mechanizm zniszczenia przy ściskaniu uległ wyraźnej zmianie i w przypadku zastosowania włókien polipropylenowych nie był tak destrukcyjny (beton był mniej kruchy).

Próbki walcowe zostały także wykorzystane do określenia parametrów materiałowych, jakimi są moduł sprężystości podłużnej Younga oraz współczynnik Poissona. Przyjęcie metody A zgodnie z normą EN12390-13 [208] pozwoliło określić zarówno wstępną jak i ustabilizowaną wartość modułu Younga. Zaobserwowano kilkuprocentowy (5-10%) wzrost wartości modułu po stabilizacji w porównaniu z wartością wstępną.

Badania belek laboratoryjnych (10x10x50 cm) zostały przeprowadzone, by wyznaczyć różnicę w mechanizmie zniszczenia próbek z i bez włókien polipropylenowych.

Wśród wszystkich zbadanych próbek należałoby podkreślić szczególne znaczenie pełnowymiarowych belek (12x24x260 cm). Elementy te zbrojone włóknami polipropylenowymi, podłużnymi prętami stalowymi lub dwoma wspomnianymi rodzajami zbrojenia poddano trójpunktowemu zginaniu. Dokonano również dywersyfikacji pod względem: (1) zastosowanych materiałów (różne pyły krzemionkowe i kruszywa), (2) miejsca przygotowania próbek (warunki betonowania laboratoryjne i przemysłowe) oraz (3) różne długości włókien (48 mm i 60 mm). W badaniach cyklicznego obciążenia-odciążenia przyjęto stopniowe (co 1 mm) zwiększanie przemieszczenia w środku rozpiętości belki. Zaprezentowano wykresy siła-przemieszczenie zarówno w formie histerezy jak i obwiedni maksymalnych wartości sił. Przemieszczenia były rejestrowane jednocześnie za pomocą trzech różnych systemów pomiarowych: maszyną wytrzymałościową INSTRON 8505, liniowym czujnikiem przemieszczeń oraz bezdotykowym systemem pomiarowym ARAMIS. Otrzymane wartości liczbowe wykazują pełną wzajemną zgodność.

Badania doświadczalne zostały uzupełnione modelowaniem i numeryczną analizą belek wykonanych z PFRHPC. Po sformułowaniu problemu i opisanu założeń modelu plastyczno-degradacyjnego (*Concrete Damage Plasticity - CDP*) zaprezentowano model obliczeniowy belek poddanych trójpunktowemu zginaniu. Model ten został przygotowany w oparciu o wybrane wyniki własnych eksperymentów laboratoryjnych oraz propozycje literaturowe. Zbrojenie rozproszone uwzględniono w modelu obliczeniowym poprzez modyfikację związków konstytutywnych betonu, co ma duże znaczenie w strefie rozciąganego betonu. Przeprowadzono również weryfikację wrażliwości gęstości siatki elementów skończonych na przebieg ścieżki siła-przemieszczenie.

Specjalną uwagę poświęcono w pracy zagadnieniu ciągliwości. Dokonany został przegląd różnych miar ciągliwości proponowanych w literaturze. Parametry ciągliwości, takie jak energia pęknięcia, długość charakterystyczna, długość ciągliwości czy wskaźniki ciągliwości zostały obliczone w oparciu o wyniki własnych badań laboratoryjnych. W próbkach z PFRHPC zanotowano znaczący wzrost każdego z tych parametrów w porównaniu do próbek nie zawierających włókien polipropylenowych.

Podsumowanie i wnioski końcowe zostały zaprezentowane w rozdziale 7 pracy, gdzie zawarto też spis planowanych kierunków przyszłych prac badawczych. Dodatkowo w pracy zamieszczono dwa załączniki. W załączniku A przedstawiono uzupełniające wykresy siła-przemieszczenie z trójpunktowego zginania pełnowymiarowych belek, podczas gdy w załączniku B zawiera mapy rozkładu i koncentracji odkształceń w wybranych cyklach obciążania-odciążania badanych belek. Objasnienia symboli i skrótów użytych w pracy podano na początku rozprawy, podczas gdy Bibliografię, Spis rysunków i Spis tabel umieszczono na końcu tej dysertacji.

# Notations

## Operators:

$a$	scalar
$\vec{a}$	vector
$\mathbf{A}$	tensor
$\Delta$	finite difference
$\dot{a}$	first derivative of $a$ with respect to time
$\ddot{a}$	second derivative of $a$ with respect to time
$\nabla$	gradient operator
div	divergence
$\mathbf{A}^T$	transposition of $\mathbf{A}$

## Latin capitals:

$A_d$	area of the damaged cross-section
$A$	area of the cross-section
$D_l$	ductility length
$\mathbf{E}$	fourth-order stiffness tensor
$E_c$	modulus of elasticity of concrete
$E_{c,0}$	initial secant modulus of elasticity of concrete
$E_{c,s}$	stabilized secant modulus of elasticity of concrete
$F$	yield function
$G$	plastic potential function
$G_f$	fracture energy
$\mathbf{I}$	identity tensor (matrix)
$I$	toughness index
$\mathbf{K}$	stiffness matrix
$K_c$	the ratio of the second stress invariant on the tensile meridian
$\bar{\mathbf{S}}$	effective stress deviator

**Latin small letters:**

$d$	scalar damage variable
$d_c$	compressive damage variable
$d_t$	tensile damage variable
$\mathbf{f}$	vector (column matrix) of nodal forces
$f_{ct}$	tensile strength of concrete
$l_{ch}$	characteristic length
$\bar{p}$	hydrostatic pressure
$\bar{q}$	von Mises equivalent effective stress
$\mathbf{q}$	vector (column matrix) of nodal displacements
$\bar{\mathbf{u}}$	displacement vector

**Greek letters:**

$\boldsymbol{\varepsilon}$	infinitesimal strain tensor
$\boldsymbol{\varepsilon}^{el}$	elastic strain
$\boldsymbol{\varepsilon}^{pl}$	plastic strain
$\tilde{\boldsymbol{\varepsilon}}_c^{pl}$	compressive equivalent plastic strain
$\tilde{\boldsymbol{\varepsilon}}_t^{pl}$	tensile equivalent plastic strain
$\epsilon$	eccentricity
$\lambda$	nonnegative plastic multiplier
$\rho$	mass density
$\boldsymbol{\sigma}$	Cauchy stress tensor
$\bar{\sigma}$	effective stress
$\sigma_{t0}$	uniaxial tensile stress at failure
$\hat{\sigma}_{max}$	maximum principal effective stress
$\sigma_{b0}$	initial equibiaxial compressive yield stress
$\sigma_{c0}$	initial uniaxial compressive yield stress
$\Psi$	dilation angle measured in the $p-q$ plane at high confining pressure

**Abbreviations:**

CDP	concrete damage plasticity
HPC	high performance concrete
HSC	high strength concrete
PFRC	polypropylene fibre reinforced concrete
PFRHPC	polypropylene fibre reinforced high performance concrete
SFRC	steel fibre reinforced concrete
UHPC	ultra high performance concrete

# Chapter 1

## Motivation

Concrete with its nine thousand year old tradition has played an important role in shaping our civilization. Although the binding has changed since ancient times from crushed plaster used by the Egyptians and lime used by the Romans into Portland cement (1824) the development of concrete did not end in the 19th or 20th century. On the contrary, it has been estimated that nowadays 25 billion tons of concrete are produced annually [3], which makes it the second (after water) most consumed material in the world [40]. To imagine the pace of this rapid advancement it should be enough if we realize that according to *Global Cement Report* [212] China consumed more cement during the last two years than the United States during the whole 20th century.

The wide application of concrete as the structural material is completely justified by its advantages: possibility to create individual shapes and dimensions of members, opportunity to use local constituents and connected with this fact a relatively low price of the structure. Concrete is also characterised by long service life, which is relevant in terms of sustainable development. Observing the recent trends in architecture, it is impossible not to notice that there is more to concrete than just carrying loads and it often has architectural function (so called *decorative concrete*).

The main criterion in the classification of concrete is its excellent compressive strength. In the early 1990s in *American Concrete Institute Materials Journal* we can find references to concrete with the compressive strength higher than 42 MPa as a "high strength concrete", which today is perceived as the ordinary one. Nowadays, information about concrete with 200 MPa compressive strength is not surprising or unbelievable. However, the development of concrete is not a one-parameter task - the idea of *high performance concrete* also assumes the improvement of other features than compressive strength such its durability.

It must be emphasized, however, that concrete has two serious drawbacks. They are its relatively low tensile strength (approximately equaled 10% of compressive strength) and its brittleness, which in other words can be expressed as the lack of ductility. The brittle nature of concrete poses a problem for structures designers as the ability of a structure to undergo large plastic deformations prior to failure can be crucial. In addition, there is a reverse relation between strength of concrete and its ductility: the higher the concrete strength, the lower is its ductility [20, 180]. This is the reason why the ductility issue is

so important in high performance concrete considerations.

The way to improve the situation is the modification of concrete mix proportions by adding fibre reinforcement. Actually, the concept of using fibres to enhance structural materials was used even in ancient Egypt, where mud bricks were reinforced with natural fibres like cut pieces of straw or horsehair [87, 98]. Nevertheless, the beginning of using fibres in structural engineering practice is dated to 1960s (Romualdi and Baston [149]). The presence of fibres completely changes the mechanism of failure in bended structural members and allows one to overcome the brittle nature of concrete. Among many different fibres used as concrete reinforcement, next to steel ones, polypropylene fibres are very popular. They have the advantage of smaller weight and resistance against corrosion [122]. New polypropylene fibres are often presented as the cheaper replacement of steel fibres. Even though it is hard to expect the great increase of concrete strength due to inclusion of polypropylene fibres, the improvement of concrete ductility is undeniable [12].

Among many applications of PFRHPC in structural engineering we can distinguish pavements [76], floors, overlays, industrial slabs, road and airport surfaces [125], prefabricated thin-walled elements [138], shotcrete or tunnel linings [27]. The wide range of application can be even further extended if we have more thorough knowledge and sufficient research on polypropylene fibre reinforced high performance concrete.



**Fig. 1.1:** Author of the dissertation with his supervisor at PEKABEX's facilities

In the dissertation the effort of experimental research and modelling of high performance polypropylene fiber reinforced concrete was made. The particular emphasis was put on the ductility phenomenon.

## Chapter 2

# Aim and scope of the research

The interest of the academia as well as industrial communities in the issue of polypropylene fibre reinforced high performance concrete was demonstrated at national and international conferences [43, 44, 92, 93]. In view of the above and considering the motivation presented in chapter 1 the following hypothesis of the dissertation was made:

**The polypropylene fibre reinforcement significantly improves the flexural behaviour and ductility of high performance concrete beams.**

In the scope of this dissertation we decided to undertake the following tasks of:

1. conducting of experimental tests on polypropylene fibre reinforced high performance concrete (PFRHPC),
2. modelling and numerical simulation of PFRHPC,
3. determination of the ductility in PFRHPC beams.

For this purpose a wide literature survey was done. The state-of-the-art is presented in chapter 3 of the thesis. The properties of polypropylene fibre reinforced high performance concrete are also shown there.

The experimental research (Task 1) was conducted in the laboratory of Poznan University of Technology. In the research 132 specimens were subjected to different types of tests. Thanks to the cooperation with renowned industry partners (COLAS, GORAZDZE, PEKABEX and SIKA), the constituents of concrete mix we used were of the highest quality. The considerable industry interest in this research may indicate the need of undertaken project. Among conducted tests of materials used in the research the testing of flexural and compressive strength (both standard and early strengths) of cement and cement-silica fume mix, as well as determination of bulk density of aggregates can be distinguished. The advanced contact-free measuring system ARAMIS 6M, which is based on the principle of digital image correlation (DIC), was used in the laboratory experiments. Firstly, a series of preliminary tests was done to determine the final concrete mix proportions.

The compressive strength was determined by means of tests on cube as well as cylinder specimens. For one of the variants also the compression test was carried out after one

year after concreting. Cylinder specimens were also used in determination of material parameters like Young's modulus of elasticity and Poisson's ratio. Method A employed in the research, in accordance to Standard EN12390-13 [208], enabled the establishment of initial as well as stabilized Young's modulus. The testing of laboratory beams (10x10x50 cm) was conducted in order to investigate the difference in failure mechanism of a bended specimens with and without polypropylene fibres.

Among all specimens full-scale beams (12x24x260 cm) shall be highlighted. The beams reinforced with polypropylene fibres, steel longitudinal bars and mix of the mentioned types of reinforcement were subjected to three-point bending. The specimens were diversified with regard to: (1) used materials (different silica fume and aggregates), (2) site of preparation of samples (under laboratory and industrial conditions) and (3) length of polypropylene fibre (48 mm and 60 mm). In the three-point bending test, the cyclic loading-unloading procedure with gradually increased mid-span deflection was utilized, in which the deformation process was displacement-controlled. The obtained force-displacement graphs show the characteristic hysteresis loops indicating energy dissipation.

The modelling of polypropylene fibre reinforced high performance beams (Task 2) is presented in chapter 5. The problem was formulated and the Concrete Damage Plasticity model was described in detail. In the computational model of three-point bending beam the modification of tensile stress-strain relation allows us to take into account the influence of the polypropylene fibres on the force-displacement relationship.

The determination of ductility in PFRHPC beams (Task 3) required the definition of measurement of ductility. The influence of polypropylene fibres on toughness indices in laboratory beams calculated according to different standards (ASTM and JSCE) was investigated. For full-scale beams the ductility parameters like fracture energy, characteristic length, ductility length and as well as toughness indices (according to JSCE) were calculated based on the own experimental research results.

The summary and final conclusions are presented in chapter 7. The future research directions are also included there.

## Chapter 3

# PFRHPC - the state-of-the-art

The polypropylene fibre reinforced high performance concrete (PFRHPC) is the subject of interest of many scientists from all over the world. In this chapter general knowledge about properties of PFRHP concrete and the recent developments in this field are presented.

The **high performance concrete (HPC)** is the type of concrete in which higher than usual compressive strength is combined with improvement of other properties, like its durability for instance. In the definition of *high performance concrete* according to Federal Highway Administration (the United States) even eight performance characteristics are mentioned. Next to compressive strength we can find freeze-thaw durability, scaling resistance, abrasion resistance, chloride penetration, modulus of elasticity, shrinkage and creep [172]. Nevertheless, the compressive strength still remains one of the main criterion of concrete classification. According to Eurocode 2 [210] concrete grades higher than C50/60 are perceived as high strength concrete grades. Admittedly, the term *high* (as well as *ultra-high*) in referring to the performance (or strength) of concrete taking its rapid advance into account is rather relative. In order to illustrate this relativity the reference to American Concrete Institute Materials Journal from 1992 [180] can be done - by term *high strength concrete* concrete with compressive strength higher than 42 MPa was meant. Nowadays in practice such concrete grades are perceived as ordinary ones. The reasonable classification of concrete is presented in [79], where compressive strength equaled 55 MPa is the border for *high* performance concrete, strengths above 100 MPa are classified as *very high* strengths whereas concrete with the strength exceeding 150 MPa is called as the *ultra-high* strength/performance concrete.

Ample attention of worldwide research is also devoted to testing on **ultra high performance concrete (UHPC)** where it can be assumed that minimum cylinder compressive strength equals 150 MPa [178]. Various mechanical properties of UHPC are investigated. The mean compressive strength converting factors in UHPC differ from those of high strength or ordinary concrete, where cube specimens get higher compressive strength than cylinder ones. In research [95] cube:cylinder ratio was determined as 0.89. The tensile strength behaviour of UHPC was investigated at Kassel University by the same team of scientists (Kusumawardaningsih, Fehling et al. [96]). The equation to predict the modulus of elasticity of ultra-high performance concrete was proposed by [15], the structural behaviour of beams subjected to bending is presented in [188], whereas the dynamic strength

of UHPC was the subject of research in [65]. The promising results of testing of anchorage zones and bond between reinforcing steel and concrete can be found in [178] - as authors indicate, the reduction of dimensions of regions with stress concentrations is possible.

The mechanical properties of high strength concrete (HSC) and high performance concrete (HPC) were collected in the state-of-the-art published by the International Federation for Structural Concrete (fib) as *Bulletin 42: Constitutive modelling of high-strength/high-performance concrete* [52]. According to Schmidt [154] the same four principles are foundation of both high compressive strength and the improved durability of concrete:

- a very low water-cement ratio,
- the use of higher amount of effective superplasticizers,
- a high packing density,
- the use of steel or other fibres.

The **low water-cement ratio** is the landmark of high-performance concrete. This ratio should be taken smaller than 0.35, very often - as in this research - is approximately 0.25 and sometimes it is possible to get values even below 0.20 [79, 128]. The inverse relation between the water-cementitious ratio and the strength of concrete is well-known (smaller w/c ratio, greater strength of concrete), however we have to bear in mind workability problems related to small amount of water in concrete mix. Therefore effective **superplasticizer** is required. Neville [128] points to its high dosage (between 5 and 15 litre per cubic meter of concrete) and underlines the need of compatibility between superplasticizer and Portland cement.

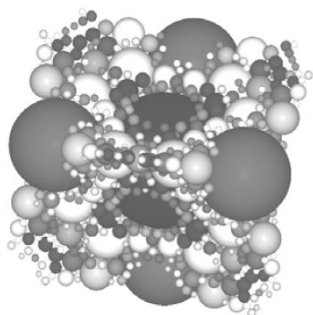


**Fig. 3.1:** Packing effect (source: [154])

Based on the idea of **packing effect** (very dense microstructure - fig. 3.1) the usage of **silica fume** to enhance the strength of concrete become self-explanatory. Particles of silica fume are approximately one hundred times smaller than cement particles [128], and due to very high reactivity of silica fume with calcium hydroxide there is the option to replace some part of cement by silica fume (usually between 5% to 15% of mass of cementitious material). No wonder that so many works on this issue were done [55, 117, 130, 150, 173, 196]. The effect of silica fume on mechanical properties of high strength concrete was investigated i.a. by [117]. Assuming the fixed water/binder ratio (0.35) and constant

total binder content ( $500 \text{ kg/m}^3$ ) the following percentages of cement were substituted by silica fume: 0%, 6%, 10% and 15%. The increase of proportion of silica fume resulted in decrease of workability and improvement of short-term mechanical properties (28-day compressive strength and secant modulus of elasticity). According to [3] replacement of 10% of cement into silica fume also enhanced tested mechanical parameters of concrete. The properties of silica fume are described in more detail in section 4.2 of this dissertation.

The packing effect and related dense microstructure of concrete are the basis of many scientific works nowadays. For instance, Nancy Soliman and Arezki Tagnit-Hamou investigated the possibility of using glass sand instead of quartz sand in UHPC [163], which is not only cost-effective, but also environmentally friendly solution.

The fourth, indicated by Schmidt [154] HPC principle (after the low water-cement ratio, the using of superplasticizer and the high packing density) is **the use of fibres**. The increasing strength is inseparably connected with the increasing brittleness - this is the reason why ductility issue is so important in high performance concrete considerations. In order to eradicate the brittle nature of concrete, the modification of mix proportions by adding the fibre reinforcement is widely used. The change of failure mechanism of concrete member after inclusion fiber reinforcement in concrete mix is presented in figure 3.2, which is adopted from [116]. Effects of fibres on properties of concrete in fresh state and hardened concrete are the subject of many works [128, 183]. In the author's opinion the book [28] written by Bentnur and Mindness deserves special attention. It can be perceived as the compendium of knowledge about fibre reinforced cementitious materials.

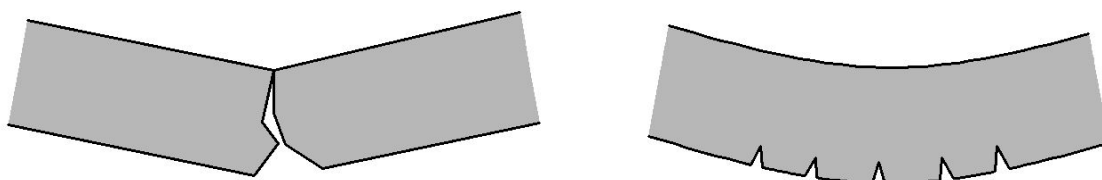


**Fig. 3.2:** Failure mechanism of concrete members without and with fiber (based on [116])

The very thorough and vast overview of different fibres was done by Mohajerani et al. [122]. They have presented properties of fibres and their applications in construction materials and referred to waste and natural fibres, which are important due to the sustainable development point of view. Among other papers on fibres, review work [136] can be pointed. The most common classification of fibres used in concrete structures is based on the material of fibre - we can distinguish among others steel, glass and synthetic fibres:

- The common use of **steel fibres** is due to many improvements in the overall properties: increase of fracture energy, increase of compressive and tensile strengths and decrease of tendency to cracking [79], improvement of resistance to fatigue and impact and blast loading [122]. The plethora of researches on properties of steel fibre

reinforced concrete has been conducted (i.a. [2, 5, 21, 62, 171, 179, 180]). As the cooperation with industry the author has the opportunity to participate in laboratory tests of SFRC (steel fibre reinforced concrete) for one of the leading concrete producer in Poland [45, 46, 94]. However, the investigation of residual flexural tensile strength of SFRC beams is not the subject of this thesis and the obtained results still constitutes a trade secret.

- Adding **glass fibres** to concrete is also possible - among their advantages we can find the reduction of internal stresses in fresh concrete mix [61, 79]. Due to their amazing properties in strenghtening, glass fibres are often used in resins and composites [122].
- Next to steel and glass fibres the whole range of **synthetic (polymer) fibres** is very common nowadays - it is not only because of the attractive price, but also due to their properties. Generally, synthetic fibres can be divided into two groups according to level of their modulus of elasticity [28]. In low modulus fibres we can distinguish polypropylene ones (which are the subject of consideration in this thesis) and the others like acrylic, nylon, polyester, polyethylene [152] or polyolefin [9, 198]. In the group of high modulus fibres we can find carbon fibres, aramid, high-strength acrylic and polyvinyl alcohol (PVA).

The comparisons of using different type of fibers in concrete mix are very common in the literature [5, 13, 38, 66, 67, 74, 98, 104, 121, 144, 161, 164, 179]. Nevertheless, a lot of attention in worldwide research is given to different hybrid fibre combinations. The mix of two different types of fibre reinforcement can lead to improvement of mechanical properties of concrete [159]. Nothing stands in the way of exploiting the advantages of various fibres in order to enhance the concrete performance [160]. There are researches about mechanical properties of fibre combinations: steel-polypropylene [5, 11, 36, 66, 120, 124, 160, 190], steel-polyester [160], steel-glass [160], basalt-polypropylene [50, 156, 183] and many others. The mix of different poylpropylene fibers can be also considered [73]. However, undeniable benefits of using hybrid fibre combinations do not mean that research on concrete with one type of fibre is exploited or pointless. This is confirmed by a plethora of continuously carried out worldwide scientific investigations.

In this dissertation polypropylene fibre reinforcement is considered. According to standard [209] polymer fibres are straigth or deformed pieces of extruded, orientated and cut polymer material, which are suitable to be homogenously mixed into concrete or mortar. The classification of polymer fibres [209] is presented in the table 3.1 and there is worth mentioning only II class fibres can be taken into account as the structural reinforcement.

**Tab. 3.1:** Classification of polymer fibers according to [209]

Class	Diameter	Fibres
Ia	< 0.30 mm	micro
Ib		mono-filamented fibrillated
II	> 0.30 mm	macro

The density of polypropylene fibres is approximately  $0.90 \text{ g/cm}^3$ , their tensile strength varies from 350 MPa to 700 MPa whereas the modulus of elasticity can be equaled between 3.5 and 10 GPa [136]. Among many advantages of applying polypropylene fibres in concrete mix the following can be distinguished: the decrease of microcracks, the improvement of fire-resistance, the constraint of early shrinkage of concrete [79].

Many papers on **mechanical properties** of polypropylene fibre reinforced concrete have been created [6, 12, 20, 24, 31, 73, 102, 116, 124, 125, 153, 158, 160, 180, 183]. Among the most frequently tested properties the compressive strength and the flexural strength can be pointed out. As indicated by Alhozaimy [12], contradictory experiment results could have reason in differences in matrix composition, polypropylene fibre type and volume fraction as well. For example, the addition of polypropylene fibre to concrete mix results in the marginal improvement of compressive strength in works [58, 138, 158], the decrease in [125], whereas no impact on compressive strength can be observed according to [33, 98]. The examination of the effects of various dosages of monofilament polypropylene fibers on compressive strength of concrete was the purpose of work [146]. As Richardson explains, the reason of decrease in compressive strength of concrete due to the addition of polypropylene fibres is in their low bond strength form, which breaks in the CSH bond between the cement and aggregate [146]. The influence of amount of cement grout and different types of fibres on compressive strength was presented in [170]. In case of polypropylene fibre addition the smaller amount of fibre results in more effective impact of cement grout.

Effects of polypropylene fibres on compressive strength and flexural strength of concrete were explored by Mashrei et al [116] (2018). In their experimental research, where the 12mm length long and 34 microns in diameter fibres were used, three different mixes and five percentage of polypropylene fibre (0%, 0.1%, 0.2%, 0.3% and 0.5% of the weight of the cement) were tested. As well compressive as flexural strength increases with increase of the percentage of polypropylene fibres up to 0.3%. The further growth of PF amount (up to 0.5%) caused the decrease of compressive and flexural strength.

When it comes to flexural strength testing in the work [158] the addition of 0.25% of fibers results in 51.05% increase in flexural strength, whereas according to [12] no significant effects on flexural strength of concrete, but increased flexural toughness and impact resistance were recorded. The influence of various proportions of polypropylene fibers (between 0.1% and 0.5% by volume of concrete) on the mechanical properties of PPFRC is considered in [6], where the reduction in modulus of elasticity and the increase in flexural strength and splitting tensile strength was noted.

From the subject of the thesis point of view it is impossible not to mention about the **ductility**. It is not surprising that high strength concrete is characterised by higher brittleness and rapid mechanism of failure. Polypropylene fibres help to overcome this downside. The detailed review of different measurements of ductility and their interpretation is presented in chapter 6 of the thesis. At this point it is worth to notice that many researchers use toughness indices (according to ASTM C1018 [201] and JSCE SF-4 [211]) to measure the ductility of fibre reinforced concrete beams [2, 9, 16, 21, 22, 50, 66, 71, 104, 130, 152, 164, 165, 189, 190].

The comparison of abovementioned standards with the emphasis on the problem of

lack of harmonisation the rules of determination of toughness indices within the academic community was presented in [104].

The toughness indices in concrete reinforced by two different forms of polypropylene fibers (including monofilament and staple fibers) was considered in [73]. In comparison to plain concrete,  $I_5$ ,  $I_{10}$  and  $I_{30}$  determined according to [201] increased slightly when staple fibers was provided. On the other hand, in the case of monofilament great improvement of ductility was recorded. Higher ductility was observed when longer fibers were used also in experiment of full-scale beams (15x22x250 cm) reinforced by steel fibers [192]. The superiority of macro polypropylene fibers over micro fibres in the enhancement of ductility in self-compacting lightweight concrete was proved by [16]: whereas the using of micro PP fibres does not have any impact on the ductility, implication of above 1.5 kg/m<sup>3</sup> (0.165%) macro PP fibres results in the toughness index on level 19.76 kNmm (calculated according to [211]). On the other hand, according to [102] the toughness index results with PP mesh fiber reinforcement were higher than those obtained with PP monofilament fiber reinforcement. As the reason of this, the fiber characteristics, such as geometrical shape, tensile strength and Young's modulus as well as interfacial bonding strength between fiber and cement paste were indicated.

There are many others measures of ductility, as ductility factor  $\mu$ , which can be expressed as the ratio of ultimate curvature to yield curvature. Kwan et al. [97] proposed the simplified design method of RC beams, where as well strength as ductility requirements can be met.

Attempt to increasing ductility in high-performance concrete by the use of alkali-resistance glass fibres or by polymer-dispersions was made by [106] - however any significant enhancement was concluded - only high steel fibre content shows the improvement of ductility. Interestingly, in the work [107] using AR-glass fibers and some particular polymer modification results even in losses in ductility of high performance concrete.

Mechanical properties of PFRHPC are not the only subjects of scientific considerations when it comes to this material. In the era of sustainable development the strong emphasis has been placed on **durability** of structure (and extending of its life) [30, 38, 54, 84, 109, 119, 123, 142, 144, 150, 196].

Rashid [144] investigated into durability characteristics of FRC girders exposed to open atmosphere for 36 months. Different fibre reinforcement variants were considered: steel, polypropylene and hybrid (steel-polypropylene). As the conclusion the beneficial effect of polypropylene fibres on the improvement of durability by the natural weathering exposure is indicated. In case of hybrid fibre reinforcement the negation of effect of steel fibres by polypropylene ones was observed. Greater resistance to sulfate attack and freezing-thawing resistance of high-performance synthetic fibers reinforced concrete in comparison with ordinary concrete was ascertained by [119].

The influence of cracks on the reduction of durability is undeniable and one of the reason of cracking is **drying shrinkage**. The effect of fibres on this undesirable by us phenomenon was investigated in i.a. [193], where it has been showed that the drying shrinkage strength is highly dependent on fibers' modulus of elasticity and polypropylene fibers show better performance in preventing crack developments in comparison with polyolefin and steel fibers. The positive effect of polypropylene fibers in reducing the drying

shrinkage strain was also noticed in research of lightweight cementitious composite with perlite microspheres [101]. The reduction of drying shrinkage in hybrid steel-polypropylene FRC compared with plain concrete was presented in [3], whereas in [114] the effect of shrinkage reducing admixture and polypropylene fibers on drying shrinkage behaviour of concrete was investigated.

Reduction of permeability because of polypropylene fibres presence results in the delay in starting the degradation process of concrete [82]. The reduction of permeability and capillary porosity by pore blocking effect was proved using Scanning Electron Microscope (SEM) by [142]. The cracking strongly influences on permeability of concrete, which leads to deterioration of durability. The addition of polypropylene fibers made the crack surface more tortuous and rough in comparison with plain concrete surface [105]. Cracking patterns analysis of cement paste with the addition of polypropylene fibres was done also by [168].

The very low permeability in high performance concrete (associated with low water-cement ratio and packing effect) could also have negative impact on performance in fire. The steam produced in concrete at high temperatures requires the escape route [147]. Otherwise, some additional internal stresses are generated, which can lead to violent expelling of concrete pieces from the surface of member. To prevent this unfavourable phenomenon, called as explosive **spalling**, fibre reinforcement comes to the rescue again. The polypropylene fibres, whose melting temperature is around 150 degree Celsius [168] (according to [68] depending on type of PP fibres between 120<sup>0</sup>C and 170<sup>0</sup>C) under high temperature are start melting and as a consequence microcracks occur [85]. Taking into account the fact that spalling occurs between 190<sup>0</sup>C and 250<sup>0</sup>C [83] we have got prepared abovementioned pathways for gas in concrete microstructure. High-temperature behaviour of high performance concrete and desired impact of polypropylene fibres addition on increase permeability after fibre melting was investigated in i.a. [17, 131, 132, 173, 177, 195]. For example, Algourdin et al. [11] concluded that addition of 0.75 kg/m<sup>3</sup> of polypropylene fibres into concrete containing steel fibres (60kg/m<sup>3</sup>) is effective in preventing spalling.

The positive influence of polypropylene fibres on properties of concrete can be observed also in its impact resistance [23, 130, 145] and abrasian resistance [64, 72, 125].

The improvement of structure durability is doubtlessly a good direction to fulfilling eco-friendliness requirements. However, bearing in mind that natural resources are not unlimited we can also try to use **recycled materials** in order to protect our environment. The plethora of research works on this issue certified that eco-aspects are treated seriously in concrete development. Intensive research on recycled polypropylene fibres are carried out at Military University of Technology (in cooperation with Building Research Institute) in Poland by Małek et al. [111, 112, 113]. Polypropylene fibre waste was also considered in [55, 123, 140]. The influence of polypropylene fibres on performance of recycled aggregate concrete is investigated by [7, 8, 40] - their essential function in enhancing concrete mechanical properties is highlighted. The concrete with palm oil biomass clinker, which is waste by-product, as partial replacement of fine aggregates was under consideration in [181].

Referring to eco-aspects and being conscious of high cement content required in high performance concrete, there is worth to mention the work of Portuguese researchers [59],

**Tab. 3.2:** Influence of polypropylene fiber inclusion to the concrete on different properties [30]

Property	Influence
crack limitation	very positive
toughness	
impact resistance	
spalling resistance	
freeze-thaw resistance	
durability	
tensile strength	positive
flexural strength	
abrasian resistance	
eco-friendly	
economic	
elasticity modulus	neutral/difficult to assess
compressive strength	
workability	negative
water absorption	difficult to assess
porosity	
permeability	

who developed and presented mixture design method for eco-efficient UHPC based on statistical mixture design (SMD) approach. The substitution of cement in concrete mixture by less-energy-intensive cementitious materials was the subject of interest of Randl et al. [143] - according to their study this replacement is possible up to approximately 45% by weight of cement without significant degradation of mechanical properties and workability. Technological, economical and environmental advantages because of using non-absorptive glass powder particles in UHPC are presented by [163], and positive influence on workability of high-performance concrete due to replacement by fillers like quartz sand the part of the cement can be found in [194].

In an accessible manner the influence of polypropylene fiber on different concrete properties is presented in table 3.2, which was based on [30].

The using of polypropylene fibre reinforcement is under investigation in many different types of concrete as for example: lightweight concrete [16, 17, 21, 101, 104, 173, 191], self-compacting concrete [16, 18, 58, 85, 124, 133, 141, 150, 185], fly ash concrete [84, 105, 150, 196], concrete with silica fume [130, 196].

Also not without significance is the **bond** between polypropylene fiber and cement matrix. Due to chemically inert and hydrophobic characteristics of polypropylene the interaction between fibres and hydration products in alkaline environment can require improvement. For this purpose different modification have been done like by nano calcium carbonate [53]. The substantial enhancement of bond between PP fibres and cementitious material can be obtained by adding nanosilica [70]. Polish scientists (Broda et al. [34]) have been investigated the influence of organic pigments and flame retardants on the

structure of polypropylene fibres. In the work of Bantia and Gupta from University of British Columbia in Canada the influence of polypropylene fiber geometry on plastic shrinkage cracking in concrete has been considered [22]. Their investigation not only proved that polypropylene fibers are effective in controlling plastic shrinkage cracking, but also indicated that a finer fiber is more effective than a coarser one the same way that a longer fiber is better than a shorter one. The interesting problem of optimization of fiber geometry for fiber reinforced composites was the subject of consideration in the work [86].

A lot of information about strains and cracking in PFRC 1:1 scale beams were provided also by [176]. In an accessible manner information about fibre reinforced concrete is collected for Polish engineer in [60]. The review of properties of fibre reinforced concrete can be found in [4, 32, 98, 115, 194, 199].

Due to their properties there are many examples of **application** of polypropylene fibers in civil engineering like pavements [76], floors, overlays, industrial slabs, road and airport surfaces [125], prefabricated thin-walled elements [138], shotcrete or tunnel linings [27]. According to [88] roughly 100 000 m<sup>3</sup> of fiber reinforced concrete have been produced annually of which 60% was applied in slabs on grade, 25% in fiber shotcrete, 5% in precast members and last 10% was used in other applications. The calculation of design thickness of pavement with addition of different types of fibres was carried out by [74]. In comparison to normal strength concrete the design thickness of pavement can be reduced by 35%, 17% and 22% by the inclusion of 1% volume fraction of steel, polypropylene and glass fibres respectively. Nevertheless, the authors take the cost-to-benefit analysis into account, which shows that steel fiber is not economical and using of polypropylene fibers despite worse mechanical strength allows one to get commercially viable solution. Economic benefits of fibre reinforcement cement composite application in jointed plain concrete pavement are also considered in [13]. The simplified method of calculation of the thickness of slabs on grade is showed by [60]. Interesting case study is presented in [30], where the application of polypropylene fiber reinforced concrete in architecture of public spaces is discussed. The authors indicate harsh conditions of use, which architectural forms as footbridges or skateparks are subjected to, and compare them with positive in this respect properties of PFRC.

The complexity of properties of even plain concrete makes **modelling** of this material a great challenge. The linear elasticity material model is not able to reflect the behaviour of concrete amongst other because of different fracture mechanisms under compression and tension, plastic properties of material and degradation of stiffness due to cracking. When it comes to concrete plasticity a good summary of various proposed mathematical models with numerical application examples is presented by Chen [39]. Among many works about fracture and damage mechanics there is the duty to mention those by Bažant [25], Peerlings [135], De Borst [42] and Geers [57]. The combination of theory of plasticity with damage mechanics resulted in damage plasticity mechanics, which nowadays is the most widely applied attitude in modelling of concrete. One of the model based on the coupling between degradation and plasticity is widespread Concrete Damage Plasticity (CDP) proposed by Lubliner [108] and developed further by Lee and Fenves [100]. The interpretation of particular parameters of CDP model has been the subject of many

works [47, 77, 78, 89, 129, 137, 166, 167]. The modification of flow rule, a new plastic potential in concrete damage plasticity model was presented in [169]. The model for concrete subjected to cycling loading was proposed by [18] - four components should be considered then: an envelope curve, an unloading curve, a reloading curve and a transition curve. The computational homogenization in modelling of concrete, where the behaviour at macro-scale was described using micro-scale phenomena is well-described by [48, 49]. The more detailed description of modelling of the concrete is presented in chapter 5 of the dissertation.

The development of a good theoretical model, which will reflect the behaviour of polypropylene fiber reinforced high performance concrete would allow for even wider than described above application of the material. For this purpose the experimental verification is necessary. The testing and modelling can help to get a better understanding of PFRHPC.

# Chapter 4

## Experimental research

### 4.1 Test specimens

In the experimental research generally four types of specimens<sup>1</sup> (fig. 4.1) were considered:

- full-scale beams B (with dimensions of 12x24x260 [cm]),
- laboratory beams b (with dimensions of 10x10x50 [cm]),
- cubes K (with dimensions of 10x10x10 [cm]),
- cylinders W (with dimensions of 10/20 [cm]).

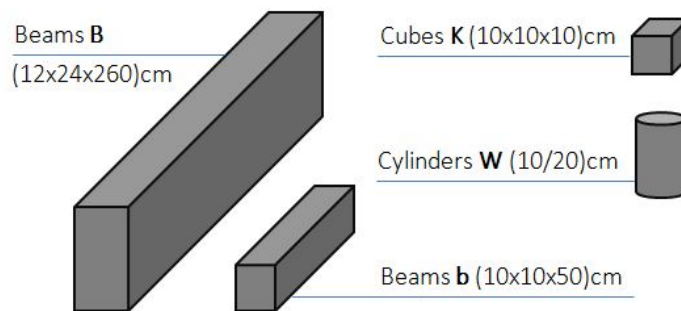


**Fig. 4.1:** Types of specimens used in the research

The decision to the replacement of more popular dimensions of cube (15x15x15 [cm]) and cylinders (15/30 [cm]) by smaller ones (10x10x10 [cm] and 10/20 [cm], respectively) was motivated by the limitation of the testing machine. The maximum possible load by INSTRON 8505 is 2 MN, what taking into account the area 15x15x15 [cm] cube

---

<sup>1</sup>This list does not include additional specimens required to complementary testing of cement (small beams with dimensions of 4x4x16 [cm]). Full particulars about this issue can be found in section 4.2 of the thesis.

face corresponds to stresses of 90 MPa approximately. Considering the higher predictable compressive strength of material I have decided to use the smaller samples.

Concreting of researching members have occurred in the academic batching plant situated in the laboratory of Poznan University of Technology as well as in Prefabricated Elements Plant 'PEKABEX'. The decision about different place of concreting specimens had the aim of comparison influence of laboratory and industrial conditions on received results.

Therefore experimental research programme was divided into three stages:

- 0 - preliminary experiments, (more information in section 4.4 of this work),
- I - testing of specimens concreted in the academic batching plant (PUT),
- II - testing of specimens concreted in prefabricated elements plant ('PEKABEX').

All specimens were transported into the academic laboratory, where the testing took place. Over 130 samples has been tested - details about amount of specimens according to type of sample and the stage of work are summarized in the table 4.1.

**Tab. 4.1:** Amount of specimens according to their type and stage of work

No.	Type of specimen	Dimensions [cm]	Amount of specimens [pcs.]			
			Stage of work			Overall
			0	I	II	
1	beam(B)	12x24x260	1	12	6	19
2	beam(b)	10x10x50	12	12	6	30
3	cube(K)	10x10x10	20	9	6	35
4	cylinder(W)	10/20	18	18	12	48
Overall			51	51	30	132

Beside the variation of place of concreting some other variants based on differences in composition of concrete mix were provided. The source of these differences is in the manufacturer of silica fume and aggregate and in the presence of polypropylene fibers in concrete mix or their length. Due to the multitude of variants an appropriate way of marking of samples was required. To put this in order the applied labelling of members is presented in the figure 4.2. The summary of differences among particular variants are assembled in table 4.2

Each label of specimen starts with Roman numeral, which corresponds to stage of hereinbefore mentioned stage of work. Afterwards, Arabic numeral gives information about number of variant in this particular stage of work. The differences between variants have their source in composition of cement mixture and are tabulated in subsection 5.4 of this work. The last part of specimen's tag is associated with type of specimen and its number.

In the case of full-scale beams with substantial length (260 cm) and, consequently, weight (almost 200 kg) there was a need of application mounting brackets not only to

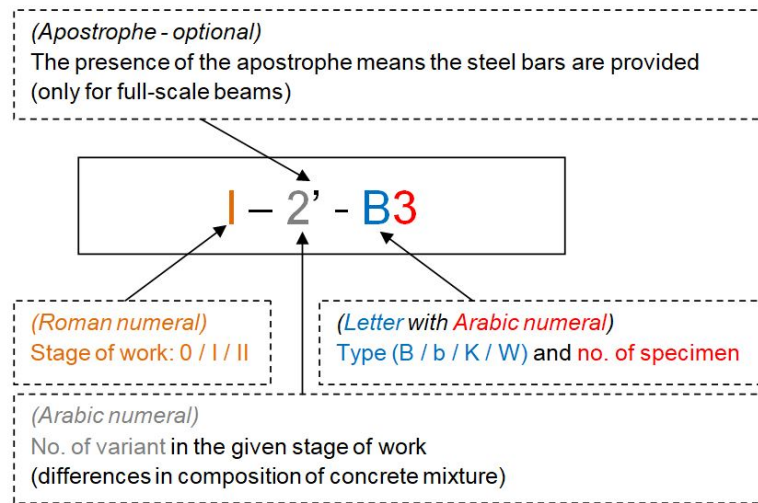


**Fig. 4.2:** The method of interpretation of the specimens notation (explanation of symbols in the text)

**Tab. 4.2:** Research variants

Variant	Place of concreting	Silica fume + aggregate	Polypropylene fibre length
I-1	Academic batching plant	Set A	50mm
I-2		Set B	
I-3		-	
II-1	Prefabricated batching plant	Set A	50 mm
II-2			60 mm

The additional apostrophe in description of variant indicates the steel bars are provided (applies only to full-scale beams).

transport specimens from the prefabricated elements plant to the laboratory but also to arrange them in the testing machine. Due to the wish of reflecting typical conditions encountered in the factory, the lifting anchors ordinarily used in PEKABEX were applied. The lifting capacity of one mounting bracket, which equals 4.25 t, is incomparably larger than required, but it is the smallest one accessible in the plant. Their arrangement in the beam is illustrated in figure 4.3. In the most of full-scale specimens also some minimum structural reinforcement (fig. 4.4) was applied. The exception is represented by beams no I-2-(B4-B6), where there is no reinforcing steel in order to compare its influence on received results.

The author had the fortune to be actively engaged in each stage of preparation of specimens what allowed him to better comprehension of the matter.

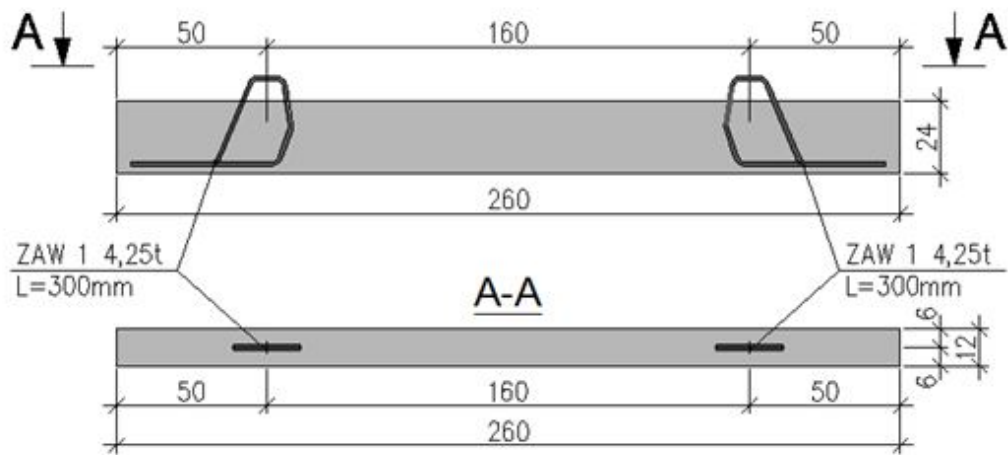


Fig. 4.3: Arrangement of mounting brackets in the full-scale beam

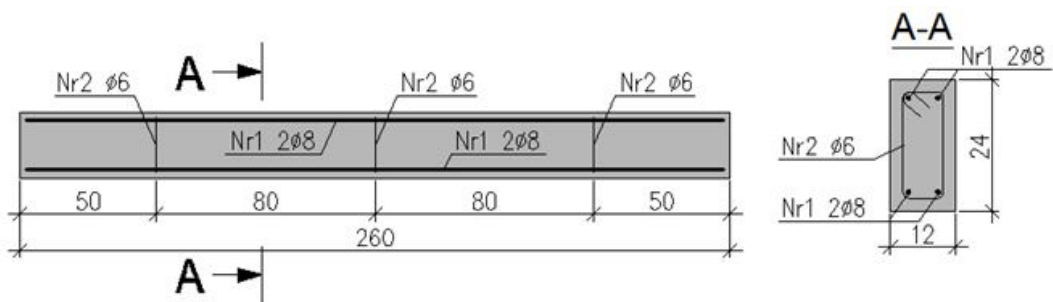


Fig. 4.4: Steel reinforcement in most of full-scale beams



Fig. 4.5: PEKABEX concrete batching plant

## 4.2 Used materials

In this section details and properties of materials used in laboratory tests are presented. Some additional experimental results are shown also.

### Cement

In the production of high performance concrete the appropriate quality of cement, which is the basic ingredient of the concrete mix and its binder, is particularly important. Therefore, Portland cement CEM I 52.5 R produced by GORAŹDŹE was used in the research. It is worth emphasizing that amount of cement used in high performance concrete is much greater than in normal strength concretes. The generally used cement content in normal strength concrete is approximately  $300 \text{ kg/m}^3$ , whereas in high performance concrete reaches value of  $600 \text{ kg/m}^3$  for instance.

Although there was the Producer guarantee of quality of cement, basic testing of material as the determination of strength was carried out. The prismatic specimens with dimensions  $40 \times 40 \times 160 \text{ mm}$  were used in testing of flexural strength, and subsequently, after three point bending and failure the mentioned specimens, halves of prisms were used in testing of compression. The schemes of loading for determination of flexural strength is presented in figure 4.6. With the aim of preparation specimens the typical moulds with three horizontal compartments were used. Each batch for three specimens consisted of:

- 450 g of cement,
- 1350 g of sand (according to EN 196-1 CEN Standard) and
- 225 g of water.

In order to determine the compressive strength class of cement both standard strength (28 days) and early strength (2 days) must be checked. Results of testing are shown in tables 4.3 – 4.6.

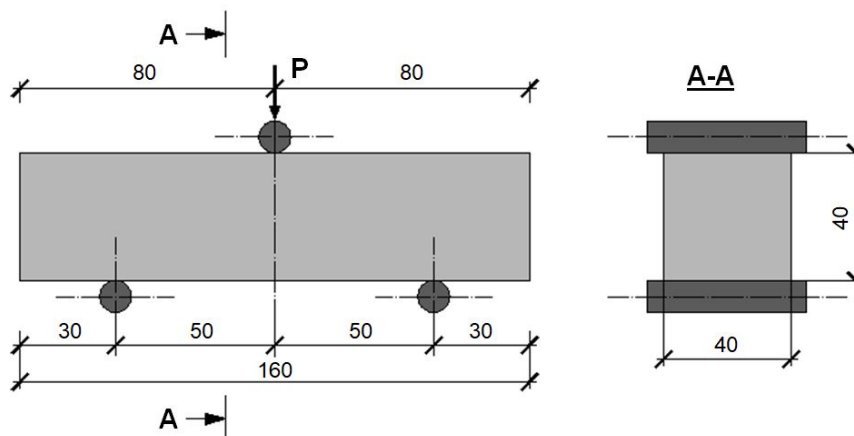


Fig. 4.6: Scheme of loading for determination of flexural strength [mm]

**Tab. 4.3:** Standard (28 days) flexural strength of cement - test results

No.	Label of specimen	Maximum flexural force [kN]	Maximum flexural stress [MPa]	Displacement (for max. flex. stress) [mm]
1	28-C-1	3.84	9.01	1.26
2	28-C-2	3.78	8.86	1.20
3	28-C-3	3.78	8.86	1.23
<b>Mean value</b>		<b>3.80</b>	<b>8.91</b>	<b>1.23</b>
Standard deviation		0.04	0.09	0.03
Coefficient of variation		1.1%	1.0%	2.4%

**Tab. 4.4:** Early (2 days) flexural strength of cement - test results

No.	Label of specimen	Maximum flexural force [kN]	Maximum flexural stress [MPa]	Displacement (for max. flex. stress) [mm]
1	2-C-1	2.39	5.59	0.99
2	2-C-2	2.37	5.56	1.06
3	2-C-3	2.52	5.92	1.16
<b>Mean value</b>		<b>2.43</b>	<b>5.69</b>	<b>1.07</b>
Standard deviation		0.08	0.20	0.09
Coefficient of variation		3.3%	3.5%	8.4%

**Fig. 4.7:** Prism half during compression test

**Tab. 4.5:** Standard (28 days) compressive strength of cement - test results

No.	Label of specimen	Maximum compressive force [kN]	Maximum compressive stress [MPa]	Displacement (for max. compressive stress) [mm]
1	28-C-1a	94.466	59.04	2.81
2	28-C-1b	95.273	59.55	3.09
3	28-C-2a	93.500	58.44	2.84
4	28-C-2b	88.226	55.14	2.86
5	28-C-3a	93.514	58.45	2.85
6	28-C-3b	90.849	56.78	2.65
<b>Mean value</b>		<b>92.638</b>	<b>57.60</b>	<b>2.85</b>
Standard deviation		6.892	2.70	0.02
Coefficient of variation		7.4%	4.7%	0.7%

**Tab. 4.6:** Early (2 days) compressive strength of cement - test results

No.	Label of specimen	Maximum compressive force [kN]	Maximum compressive stress [MPa]	Displacement (for max. compressive stress) [mm]
1	2-C-1a	62.199	38.87	2.39
2	2-C-1b	60.789	37.99	2.46
3	2-C-2a	58.947	36.84	2.08
4	2-C-2b	63.641	39.78	2.19
5	2-C-3a	60.996	38.12	2.10
6	2-C-3b	61.156	38.22	2.22
<b>Mean value</b>		<b>61.288</b>	<b>38.30</b>	<b>2.24</b>
Standard deviation		2.440	0.96	0.02
Coefficient of variation		4.0%	2.5%	0.9%

The mean value of maximum compressive stress measured after 28 days, which is equaled to 57.60 MPa, (table 4.5) exceeds the value of 52.5 MPa, what allows to classify the cement as in the 52.5 class. Due to the early strength measured after 2 days (38.30 MPa - table 4.6) greater than 30 MPa the classification cement used in the research as 52.5 R is approved.

## Silica fume

Application of silica fume has the great significance in production of high performance concrete [128] and even though it is not the one of the cheapest cementitious material the use of silica fume continues to increase. As the one of the most popular and very reactive pozzolana is the by-product of the manufacture of silicon and ferrosilicon alloys from high-purity quartz and coal [128]. In the result of oxidation and condensation of gaseous silicon oxide (SiO) we get amorphous silica (SiO<sub>2</sub>). Their reaction with calcium hydroxides (due to the hydration of ordinary Portland cement) has the influence on decreased porosity, permeability and bleeding of concrete [117]. The very fine diameter of silica fume particles is not meaningless. The mean diameter usually does not exceed 0.1 μm [128], what considering the packing effect idea is crucial. I will never forget the first time I took a piece of microsilica in my hand - very low density (2.20 g/cm<sup>3</sup> [128]) is impressive.

In this research two different silica fumes were used. Specimens in variants I-2 and I-3 were prepared with SILIMIC produced by HUTA ŁAZISKA SA (this type of silica fume was denoted as 'KL' in the thesis), and in the rest of specimens (variants I-1, II-1 and II-2) SIKAFUME produced by SIKAFUME was provided (denoted as 'KS' in the thesis). The second one is actually the filler with silica fume.

I have been decided to test flexural and compressive strength of cement with silica fume. For this purpose the part of cement in the mix was replaced by silica fume. The procedure of testing was the same like in the case of testing of cement compressive and flexural strength. The silica fume constitutes almost 15% of all cementitious material (and approximately 17% of cement by weight). To keep the same proportions between these two cementitious materials in all research (see section 4.4 of the thesis) the following mix proportions were determined:

- 385 g of cement,
- 65 g of silica fume,
- 1350 g of sand (according EN 196-1 CEN Standard sand was used) and
- 225 g of water.

Detailed results of testing are situated in tables 4.7-4.14, whereas the summary of experiment results are presented in the table 4.15. The maximum flexural stress as well as maximum compressive stress are illustrated also in figures 4.9 and 4.10 as the column diagrams. The replacement of the part of cement with the silica fume at an early age (testing after 2 days since concreting) results in a small decrease of maximum flexural and compressive force in comparison with probes with cement only. On the other hand testing after 28 days clearly shows the increase of abovementioned quantities. The differences between various silica fume (KS vs. KL) are fairly small.

**Tab. 4.7:** Standard (28 days) flexural strength of cement mixed with silica fume (KL) - test results

No.	Label of specimen	Maximum flexural force [kN]	Maximum flexural stress [MPa]	Displacement (for max. flex. stress) [mm]
1	28-KL-1	4.28	10.04	1.22
2	28-KL-2	4.08	9.55	1.13
3	28-KL-3	4.03	9.45	1.17
<b>Mean value</b>		<b>4.13</b>	<b>9.68</b>	<b>1.17</b>
Standard deviation		0.13	0.32	0.05
Coefficient of variation		3.2%	3.3%	3.8%

**Tab. 4.8:** Early (2 days) flexural strength of cement mixed with silica fume (KL) - test results

No.	Label of specimen	Maximum flexural force [kN]	Maximum flexural stress [MPa]	Displacement (for max. flex. stress) [mm]
1	2-KL-1	2.36	5.54	1.11
2	2-KL-2	2.12	4.97	1.19
3	2-KL-3	2.23	5.24	1.07
<b>Mean value</b>		<b>2.24</b>	<b>5.25</b>	<b>1.12</b>
Standard deviation		0.12	0.29	0.06
Coefficient of variation		5.4%	5.4%	5.4%

**Tab. 4.9:** Standard (28 days) flexural strength of cement mixed with silica fume (KS) - test results

No.	Label of specimen	Maximum flexural force [kN]	Maximum flexural stress [MPa]	Displacement (for max. flex. stress) [mm]
1	28-KS-1	3.98	9.32	1.20
2	28-KS-2	3.94	9.23	1.20
3	28-KS-3	4.09	9.58	1.13
<b>Mean value</b>		<b>4.00</b>	<b>9.38</b>	<b>1.18</b>
Standard deviation		0.08	0.18	0.04
Coefficient of variation		1.9%	1.9%	3.4%

**Tab. 4.10:** Early (2 days) flexural strength of cement mixed with silica fume (KS) - test results

No.	Label of specimen	Maximum flexural force [kN]	Maximum flexural stress [MPa]	Displacement (for max. flex. stress) [mm]
1	2-KS-1	2.35	5.50	1.13
2	2-KS-2	2.17	5.09	1.18
3	2-KS-3	2.29	5.36	1.31
<b>Mean value</b>		<b>2.27</b>	<b>5.32</b>	<b>1.21</b>
Standard deviation		0.09	0.21	0.09
Coefficient of variation		4.0%	3.9%	7.7%

**Tab. 4.11:** Standard (28 days) compressive strength of cement mixed with silica fume (KL) - test results

No.	Label of specimen	Maximum compressive force [kN]	Maximum compressive stress [MPa]	Displacement (for max. compressive stress) [mm]
1	28-KL-1a	105.924	66.20	3.08
2	28-KL-1b	106.188	66.37	3.01
3	28-KL-2a	106.334	66.46	3.03
4	28-KL-2b	107.030	66.89	2.68
5	28-KL-3a	102.118	63.82	2.88
6	28-KL-3b	105.498	65.94	2.74
<b>Mean value</b>		<b>105.515</b>	<b>65.95</b>	<b>2.90</b>
Standard deviation		3.025	1.18	0.03
Coefficient of variation		2.9%	1.8%	0.9%

**Tab. 4.12:** Early (2 days) compressive strength of cement mixed with silica fume (KL) - test results

No.	Label of specimen	Maximum compressive force [kN]	Maximum compressive stress [MPa]	Displacement (for max. compressive stress) [mm]
1	2-KL-1a	57.777	36.11	2.13
2	2-KL-1b	54.139	33.84	1.90
3	2-KL-2a	57.756	36.10	2.14
4	2-KL-2b	58.653	36.66	2.08
5	2-KL-3a	54.404	34.00	2.06
6	2-KL-3b	54.477	34.05	2.15
<b>Mean value</b>		<b>56.201</b>	<b>35.13</b>	<b>2.07</b>
Standard deviation		4.273	1.67	0.01
Coefficient of variation		7.6%	4.8%	0.4%

**Tab. 4.13:** Standard (28 days) compressive strength of cement mixed with silica fume (KS) - test results

No.	Label of specimen	Maximum compressive force [kN]	Maximum compressive stress [MPa]	Displacement (for max. compressive stress) [mm]
1	28-KS-1a	111.472	69.67	2.34
2	28-KS-1b	106.393	66.50	2.29
3	28-KS-2a	108.474	67.80	2.48
4	28-KS-2b	114.144	71.34	2.63
5	28-KS-3a	105.824	66.14	2.17
6	28-KS-3b	106.338	66.46	2.45
<b>Mean value</b>		<b>108.774</b>	<b>67.99</b>	<b>2.39</b>
Standard deviation		11.302	4.41	0.03
Coefficient of variation		10.4%	6.5%	1.1%

**Tab. 4.14:** Early (2 days) compressive strength of cement mixed with silica fume (KS) - test results

No.	Label of specimen	Maximum compressive force [kN]	Maximum compressive stress [MPa]	Displacement (for max. compressive stress) [mm]
1	2-KS-1a	54.298	33.94	2.27
2	2-KS-1b	53.805	33.63	2.04
3	2-KS-2a	56.124	35.08	2.27
4	2-KS-2b	49.709	31.07	2.00
5	2-KS-3a	55.699	34.81	2.01
6	2-KS-3b	56.908	35.57	2.29
<b>Mean value</b>		<b>54.424</b>	<b>34.02</b>	<b>2.15</b>
Standard deviation		6.663	2.60	0.02
Coef. of variation		12.2%	7.6%	1.0%

**Tab. 4.15:** Comparison of test results for cement and cement mixed with silica fume

Mechanical property	Time of testing	Cement	Cement mixed with silica fume (KL)	Cement mixed with silica fume (KS)
<b>Testing of flexural strength</b>				
Maximum flexural force [kN]	2 days	2.43	2.24	2.27
	28 days	3.80	4.13	4.00
Maximum flexural stress [MPa]	2 days	5.69	5.25	5.32
	28 days	8.91	9.68	9.38
Displacement (for max. flexural stress) [mm]	2 days	1.07	1.12	1.21
	28 days	1.23	1.17	1.18
<b>Testing of compressive strength</b>				
Maximum compressive force [kN]	2 days	61.288	56.201	54.424
	28 days	92.638	105.515	108.774
Maximum compressive stress [MPa]	2 days	38.30	35.13	34.01
	28 days	57.60	65.95	67.98
Displacement (for max. compressive stress) [mm]	2 days	2.24	2.07	2.14
	28 days	2.85	2.90	2.39

**Fig. 4.8:** Silica fume used in the research

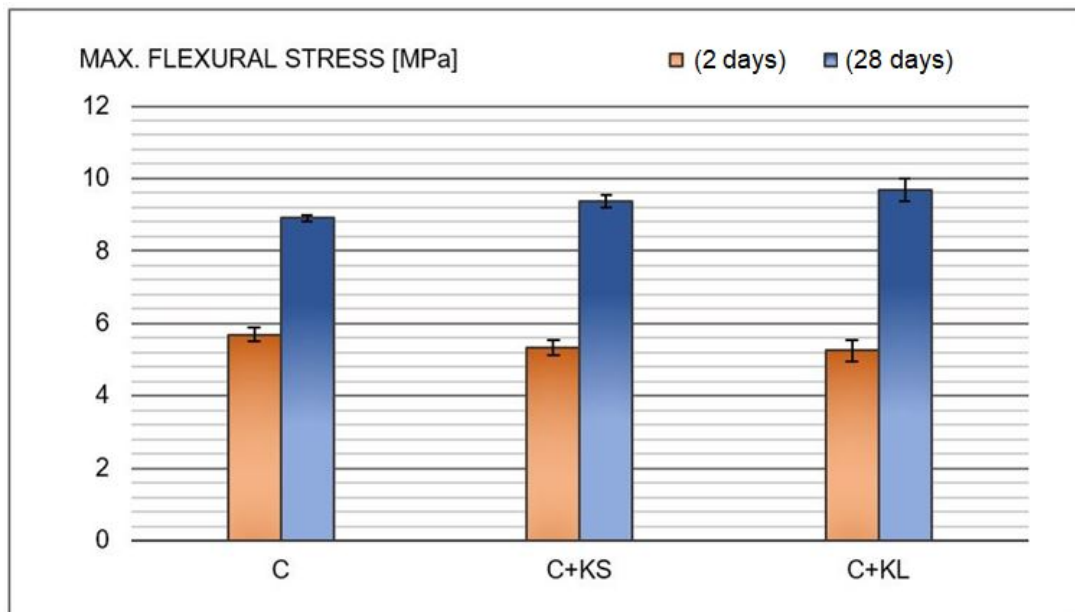


**Fig. 4.9:** Max. flexural stress [MPa] of cement and cement mixed with silica fume - column diagram

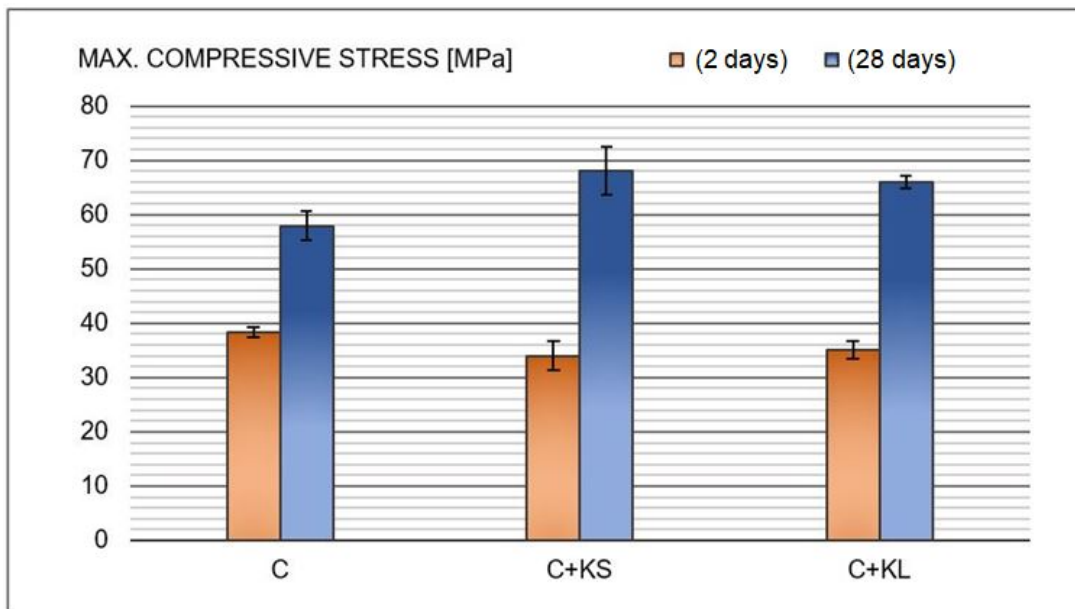


**Fig. 4.10:** Max. compressive stress [MPa] of cement and cement mixed with silica fume - column diagram

**Tab. 4.16:** Different providers of aggregate

Set	No. of measurement	Provider of aggregate	
		fine aggregate	coarse aggregate
A	I-1, II-1, II-2	PEKABEX	PEKABEX
B	I-2, I-3	SIKA	COLAS

## Aggregate

In the experimental research two different sets of aggregates were utilized. The first one, denoted by A assumed using the same aggregates as in the daily manufacturing in the prefabricated element factory (PEKABEX). In this way variants I-1, II-1 and II-2 were prepared. On the other hand in variants I-2 and I-3 aggregates provided by the other manufacturer are applied (set B) (table 4.16). In both sets basalt with maximum particle size of 16 mm as a coarse aggregate and sand as a fine aggregate were taken. The grading curves of used aggregates are presented in figures 4.12-4.15.

**Fig. 4.11:** Coarse aggregate (basalt) used in the research (COLAS)

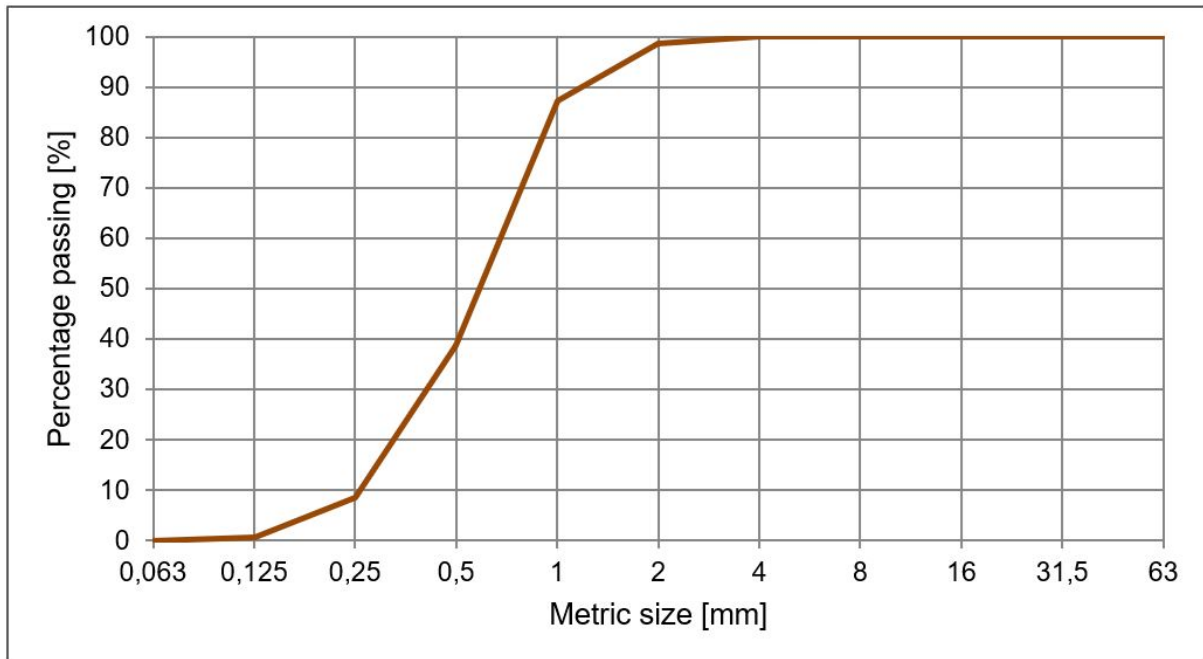


Fig. 4.12: Grading curve for fine aggregate (PEKABEX)

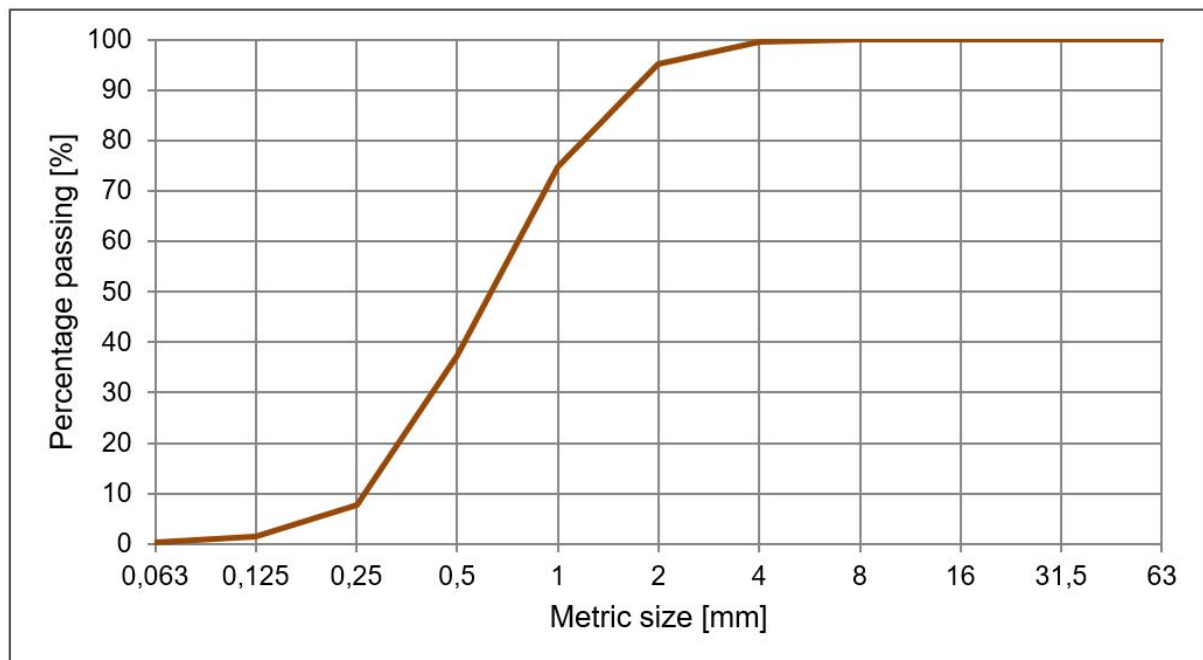


Fig. 4.13: Grading curve for fine aggregate (SIKA)

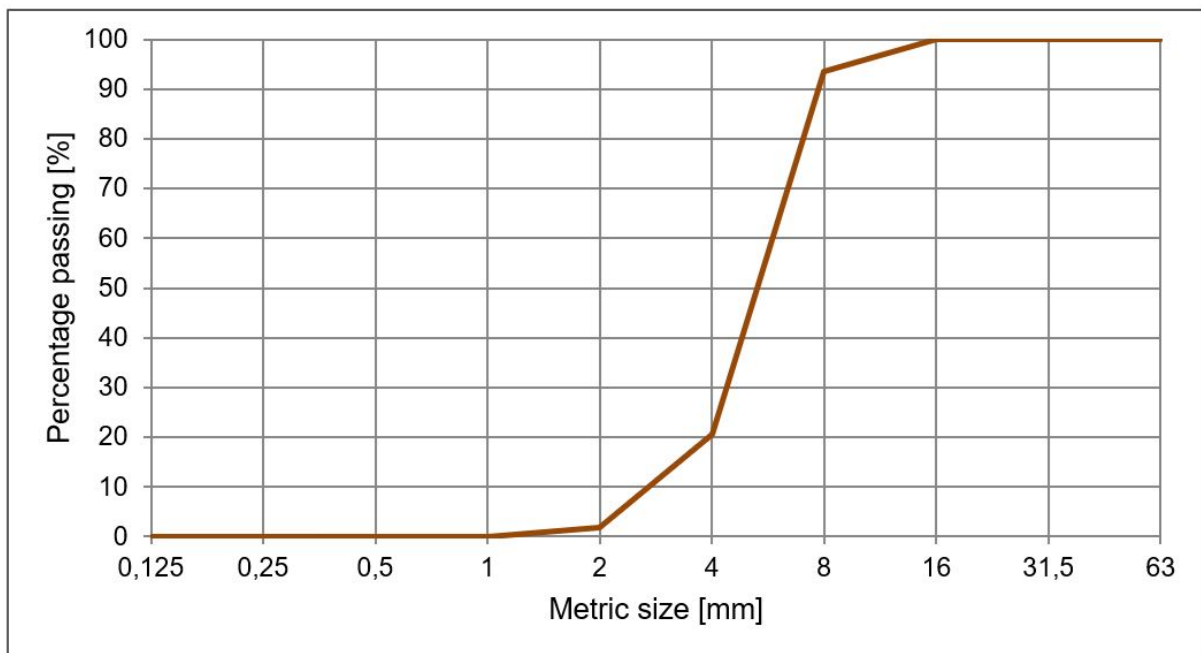


Fig. 4.14: Grading curve for coarse aggregate (PEKABEX)

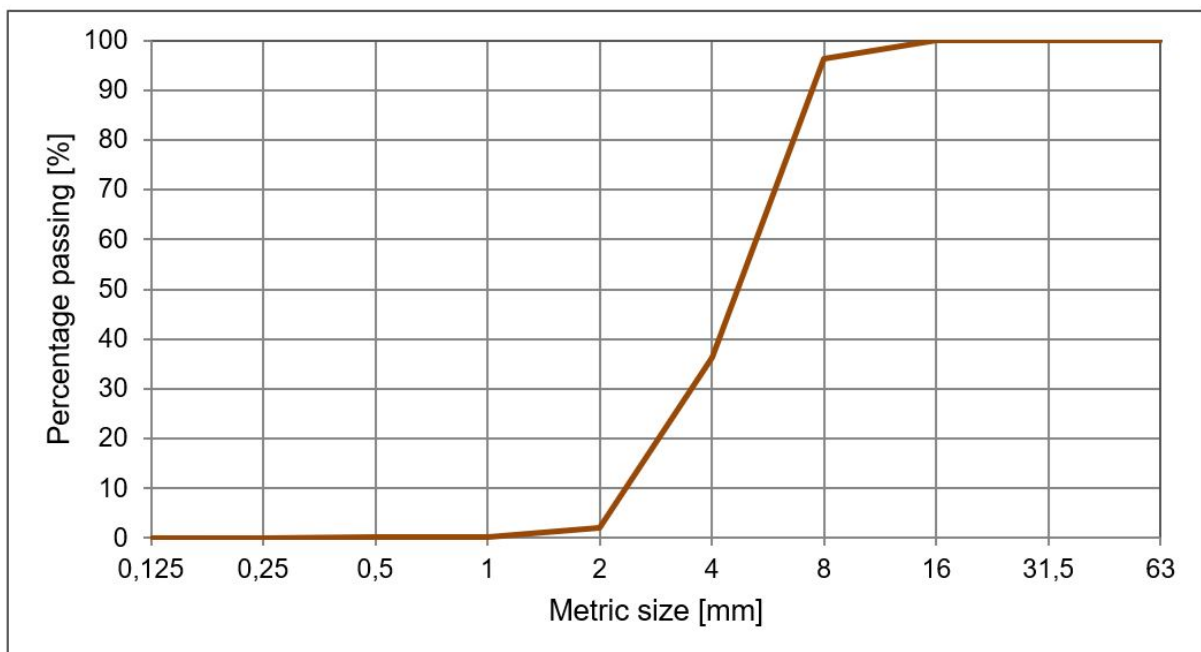


Fig. 4.15: Grading curve for coarse aggregate (COLAS)

**Tab. 4.17:** Results of testing of bulk density

Aggregate	No. of measurement	Bulk density [kg/dm <sup>3</sup> ]	
		loose degree	compacted degree
<b>Fine aggregate - sand</b>			
PEKABEX	1st measurement	1.48	1.70
	2nd measurement	1.48	1.70
	<b>Mean value</b>	<b>1.48</b>	<b>1.70</b>
SIKA	1st measurement	1.40	1.68
	2nd measurement	1.36	1.64
	<b>Mean value</b>	<b>1.38</b>	<b>1.66</b>
<b>Coarse aggregate - basalt</b>			
PEKABEX	1st measurement	1.60	1.92
	2nd measurement	1.57	1.89
	<b>Mean value</b>	<b>1.59</b>	<b>1.91</b>
COLAS	1st measurement	1.56	1.85
	2nd measurement	1.56	1.89
	<b>Mean value</b>	<b>1.56</b>	<b>1.87</b>

In addition, the bulk density test was carried out. The bulk density which is the weight per unit volume was determined according to Standard PN-EN 1097-3:2000 [202]. The results of testing are presented in table 4.17. There is a slight difference between bulk density of aggregates to the advantage of PEKABEX ones, but in general we can consider them as aggregates with similar bulk densities.

**Fig. 4.16:** Bulk density test setup

## Water and superplasticizer

As it was mentioned before, in high performance concrete the low water cement ratio is crucial. In this research the mean water cementitious ratio is around 0.25 (details are presented in table 4.18), what would not be possible without applying appropriate superplasticizer. The SIKA ViscoCrete-98RS produced by SIKA has been chosen. The acting of this yellowish, homogeneous liquid is based on the electrostatic repulsion mechanism, what allows one to considerably diminish the quantity of water in the mix. The recommended dosage of the applied polymeric admixture is defined as between 0.2% and 2.0% of the weight of cement. However, based on the executed preliminary tests in this research a greater amount of superplasticizer was required to get appropriate workability of concrete (over 3% of cement by weight).

## Polypropylene fibre

In the research polypropylene fibers on the basis of Polyolefin produced by SIKA were used: SikaFiber Force-60 and SikaFiber Force-48. White, straight, embossed fibres have following properties: density  $0.91 \text{ kg/dm}^3$ , melting temperature  $\sim 164^{\circ}\text{C}$ , tensile strength  $\sim 465 \text{ MPa}$  and modulus of elasticity  $\sim 7.5 \text{ GPa}$ . The diameter of provided fibres is 0.84 mm, whereas its length depending on research variant equals 48 mm or 60 mm. Applied polypropylene fibres are classified into II class according to Standard EN14889-2 [209], so they can be treated as the structural reinforcement. In the research the maximum possible fibre content dosage (due to workability on the basis of preliminary tests) was provided ( $20 \text{ kg/m}^3$ ). I am conscious that it exceeds daily-used content dosage of polypropylene fibres. Nevertheless, I would like to check the influence of the high fibre content dosage on the ductility and other mechanical properties of PFRHPC.



**Fig. 4.17:** Polypropylene fibre used in the research

## 4.3 Apparatus

During experimental research a lot of different kind of apparatus was used. Most important of them are presented below.

### Cement mixer

For the purpose of this research the new cement mixer was purchased in the laboratory of Poznan University of Technology (figure 4.18). The gravity concrete mixer with the working capacity of 200 l and 1500 W power enabled efficient preparation of specimens in the academic batching plant.



**Fig. 4.18:** Cement mixer in the laboratory of Poznań University of Technology

### Testing machines - INSTRON

The damaging experiments of specimens were conducted by means of two testing machines: INSTRON 8505 and INSTRON SATEC 300DX (figure 4.19). Both of them are hydraulic devices with accuracy class of 0.5. The first one, with the maximum possible load of 2 MN, was used to investigate full-scale beams (12x24x260 cm) under bending and to make compression testing of cubes (10x10x10 cm) and cylinders (10/20 cm). The latter, with the maximum possible load of 300 kN, was used during testing of laboratory beams (10x10x50 cm) and research of properties of cement and silica fume.

### ARAMIS

In the experimental research advanced contact-free measuring system - ARAMIS 6M - was used. The special method based on the principle of digital image correlation (DIC) allowed one to obtain results from one more (than testing machine) source of information. The basis of DIC method is the comparison of digital photographs of a component at



**Fig. 4.19:** Testing machines: INSTRON 8505 (on the left) and INSTRON SATEC 300DX (on the right)

different stages of deformation [118]. The deformation vector fields and strain maps are built up thanks to tracking pixels blocks. The pixel blocks, which should be unique and random, require relevant contrast and intensity. All full-scale beams (12x24x260 cm) were tested with usage of the above described professional non-contact measuring system. This work demands from the researcher an appropriate preparation of specimen's surface. The adequate quantity, magnitude and density of black pixels on prepared in advance white background was the virtual lesson of patience for the author - nevertheless, it was worth it.



**Fig. 4.20:** Contact free measuring system ARAMIS 6M

## 4.4 Preliminary tests and mix proportions

In order to select the mix proportion a series of preliminary tests was carried out. For this purpose eight different batches of concrete were prepared and examined. To sum up, over 50 specimens were subjected to testing during this initial stage of work. Detailed results of these experiments except final concrete mix proportions are not presented in the thesis. In addition one full-scale beam (0-B1) (fig. 4.22) was purposefully prepared with the aim of the verification and trying of the advanced laboratory apparatus as ARAMIS is.

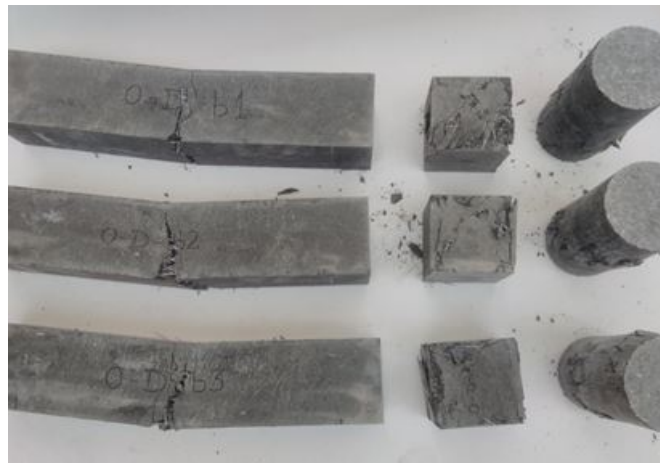


**Fig. 4.21:** A few specimens after testing in the preliminary stage of work



**Fig. 4.22:** Full-scale beam in a test stand subjected 3-point bending in the preliminary stage of work

The mix proportions, which were eventually established, are presented in table 4.18.

There is one singled out mix proportion with some diversifications. The I-2 differ from I-1 by the type of used silica fume and aggregates. The I-3 on the other hand has the same mix proportions like I-2 except the presence of fibre reinforcement. The last two variants were prepared in the industrial conditions: II-1 has the same amount and type of ingredients like I-1, whereas II-2 has different length of polypropylene fibres. In all variants the water/cementitious material ratio is on the level of approximately 0.25. It is worth reminding that in case of full-scale beams the apostrophe in the description of specimen indicates the presence of longitudinal steel bars.

**Tab. 4.18:** Mix proportions

Variant	I-1	I-2	I-3	II-1	II-2
Ingredient	Amount of ingredient [kg/m <sup>3</sup> ]				
1 Portland cement CEM I 52.5R	600	600	600	600	600
2 Silica fume SIKA FUME HR	100	-	-	100	100
Silica fume SILMIC (Łaziska)	-	100	100	-	-
3 Fine aggregate (PEKABEX)	600	-	-	600	600
Fine aggregate (Wiechlice)	-	600	600	-	-
4 Coarse aggregate (PEKABEX)	1000	-	-	1000	1000
Coarse aggregate (COLAS)	-	1000	1000	-	-
5 Water	172	180	180	172	172
6 Superplasticizer SIKA Viscocrete-98RS	21	21	21	21	21
7 Polypropylene fibre SikaFiber Force-60	20	20	-	20	-
Polypropylene fibre SikaFiber Force-48	-	-	-	-	20
Water/cementitious material ratio	0.246	0.257	0.257	0.246	0.246

## 4.5 Determination of compressive strength

### 4.5.1 Description of testing

The experimental procedure complied with PN-EN 12390-3 Standard [205]. The compressive strength of concrete was investigated by means of INSTRON 8505 (fig. 4.23). Testing was carried out on cube as well as on cylinder specimens. The examples of samples after compressive strength test are presented in figure 4.24.



**Fig. 4.23:** Cylinder specimen mounted on compressive strength test setup



**Fig. 4.24:** Examples of specimens after compressive strength test

### 4.5.2 Results of tests

The results of testing for each variant are catalogued in table 4.19, where the mean values of compressive strength with standard deviations and coefficients of variation are shown.

Taking into account the small amount of samples there are no huge differences between particular variants except variant no. I-3, which did not contain polypropylene fibres in concrete mix (plain concrete). In every other variant compressive cylinder strength is between 90 and 100 MPa, whereas the cube strength fluctuates between 110 and 125 MPa. In the case of concretes without the polypropylene fibres, the compressive strength reaches the magnitude of almost 140 MPa. Moreover, there is no the usual difference between cylinder and cube strengths, what confirms the literature study on high strength concrete's property. The studies, where cylinder strength is even greater than cube one in the case of HSC, are known [95]. The clear decline in compressive strength after including polypropylene fibres in the concrete mix is not really surprising [6], especially if we take into account the provided high dosage of fibres. On the other hand, the difference in failure mechanisms under compression of specimens with and without fibre reinforcement also deserves attention and should be considered. Whereas in figure 4.24 the failure of sample with PP fibres is depicted, the figure 4.26 shows the even academic failure of no-fiber-reinforced concrete under compression. The positive influence of fibres can be observed.

The mean compressive strength results from table 4.19 are also illustrated by bar diagrams, where the standard deviations are marked (fig. 4.25). Samples without PP fibres have much smaller standard deviations.

There is a requirement of commenting the amount of cylinder specimens in variants II-1 and II-2. There are members concreted in Prefabricated Elements Plant and unfortunately, after removing of formwork insufficient density of concrete mix in specimens II-1-W3 and II-2-W3 was observed. Due to large amount of pores it was decided to not test and consider these cylinders in the research.

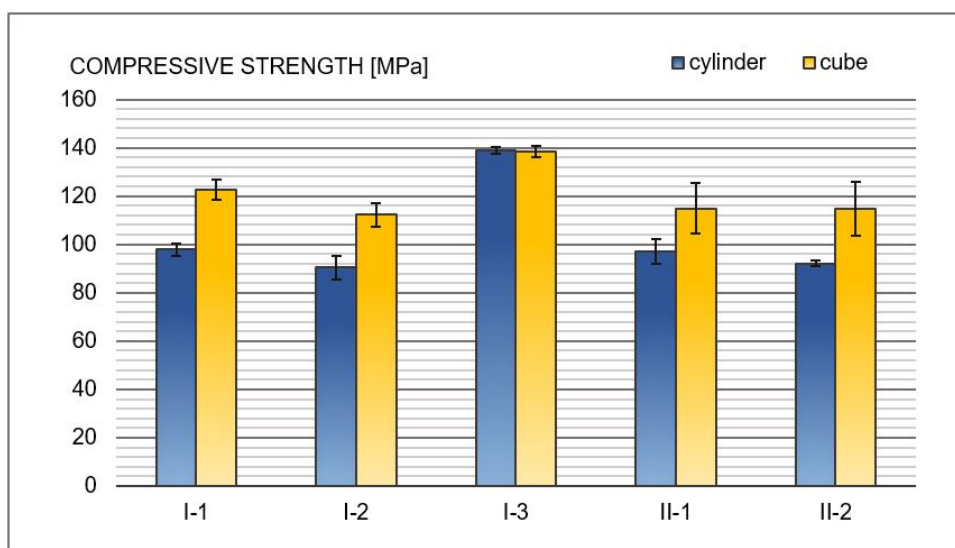


**Fig. 4.25:** Compressive strength [MPa] test results (after 28 days) - column diagram

**Tab. 4.19:** Results of compressive strength test

Variant	No. of specimen	Cylinder strength [MPa]	No. of specimen	Cube strength [MPa]
I-1	I-1-W1	97.40	I-1-K1	125.62
	I-1-W2	95.73	I-1-K2	117.72
	I-1-W3	100.49	I-1-K3	124.05
	<b>Mean value</b>	<b>97.87</b>	<b>Mean value</b>	<b>122.46</b>
	Stand. deviation	2.42	Stand. deviation	4.18
	Coef. of variation	2.5%	Coef. of variation	3.4%
I-2	I-2-W1	93.33	I-2-K1	107.52
	I-2-W2	93.19	I-2-K2	111.78
	I-2-W3	84.74	I-2-K3	117.39
	<b>Mean value</b>	<b>90.42</b>	<b>Mean value</b>	<b>112.23</b>
	Stand. deviation	4.92	Stand. deviation	4.95
	Coef. of variation	5.4%	Coef. of variation	4.0%
I-3	I-3-W1	140.42	I-3-K1	139.34
	I-3-W2	137.84	I-3-K2	139.85
	I-3-W3	138.60	I-3-K3	135.64
	<b>Mean value</b>	<b>138.95</b>	<b>Mean value</b>	<b>138.28</b>
	Stand. deviation	1.33	Stand. deviation	2.30
	Coef. of variation	1.0%	Coef. of variation	1.7%
II-1	II-1-W1	100.53	II-1-K1	102.98
	II-1-W2	93.59	II-1-K2	118.36
	II-1-W3	-	II-1-K3	123.21
	<b>Mean value</b>	<b>97.06</b>	<b>Mean value</b>	<b>114.85</b>
	Stand. deviation	4.91	Stand. deviation	10.56
	Coef. of variation	5.1%	Coef. of variation	9.2%
II-2	II-2-W1	92.90	II-2-K1	120.53
	II-2-W2	91.31	II-2-K2	121.95
	II-2-W3	-	II-2-K3	101.81
	<b>Mean value</b>	<b>92.11</b>	<b>Mean value</b>	<b>114.76</b>
	Stand. deviation	1.12	Stand. deviation	11.24
	Coef. of variation	1.2%	Coef. of variation	9.8%

**Tab. 4.20:** Cube strength [MPa] after 28 days and 1 year (variant I-1)

Variant	No. of specimen	Cube strength (after 28 days) [MPa]	No. of specimen	Cube strength (after 1 year) [MPa]
I-1	I-1-K1	125.62	I-1-K4	130.95
	I-1-K2	117.72	I-1-K5	123.80
	I-1-K3	124.05	I-1-K6	127.03
	<b>Mean value</b>	<b>122.46</b>	<b>Mean value</b>	<b>127.26</b>
	Stand. deviation	4.18	Stand. deviation	3.58
	Coef. of variation	3.4%	Coef. of variation	2.8%

**Fig. 4.26:** The failure of cylinder under compression - specimen without polypropylene fibres (I-3-W1)

In the table 4.20 the comparison of compressive cube strength results for one variant (I-1) depending on the age of concrete is presented. After 1 year after concreting approximately 4% increase of strength was recorded.

## 4.6 Determination of material parameters

### 4.6.1 Description of testing

The testing of essential materials parameters as modulus of elasticity and Poisson's ratio were carried out on cylindrical specimens (100/200 mm) for every research variant. In order to measure strains, extensometers and electric resistance wire strain gauges were applied.



**Fig. 4.27:** Preparation of specimens for testing of material parameters

The implementation of electric resistance wire strain gauges and support stands for extensometers (as well as subsequent assembly of extensometers) require high precision. Before the measuring devices are stuck on concrete area there is the obligation of appropriate preparation of cavities. To refill the pores DURACYL ® Plus, which is usually applied for dental purposes, was used. The specimens in the process of preparation for testing are presented in figure 4.27, whereas figure 4.28 shows prepared specimens.

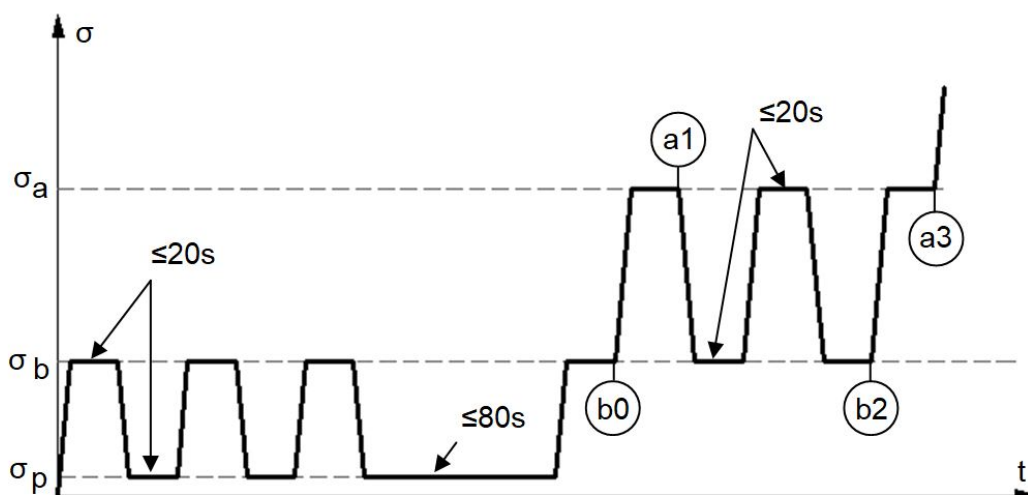


**Fig. 4.28:** Cylinder specimens for testing of material parameters

**Tab. 4.21:** The characteristics of applied electric resistance wire strain gauges

Type	KC-60-120-A1-11
Gage factor (24°C, 50%RH)	$2.07 \pm 1.0\%$
Gage length	60 mm
Gage resistance (24°C, 50%RH)	$120.2 \pm 0.2 \Omega$
Adoptable thermal expansion	10.8 PPM/°C
Temperature coefficient of gage factor	+0.015 %/°C

The testing of Young's modulus was carried out according to requirements of Standard [208]. From two available methods of determination of secant modulus of elasticity the method A (which is more complex and allows one to find out the stabilized as well as the initial value of modulus) was chosen. The course of testing is presented in the stress-time graph (figure 4.29).

**Fig. 4.29:** Cycles for determination of initial and stabilized secant modulus of elasticity

Before the relevant testing starts, there are requirements of checking the wiring stability and specimen positioning. To this end three preloading cycles are carried out. Each preloading cycle consists of applying stress up to the lower stress  $\sigma_b$ , holding this level of stress for a period not exceeding 20 seconds and reducing the stress down to preload  $\sigma_p$ . The rate of applying stresses as well as their reducing equals  $0.6 \pm 0.2$  MPa/s. The lower stress  $\sigma_b$  was assumed as  $0.15f_{cm}$  (where permissible range of this value according to Standard [208] equals  $0.10 - 0.15f_{cm}$ ). The preload stress value was taken as 2.0 MPa (where the minimum recommended value is 0.5 MPa and as the maximum  $\sigma_b$  shall be taken).

In order to check the wiring stability (what is called in Standard [208] as the first check), the variation of strains between the second cycle and the third cycle should not exceed 10% on each measuring line. The meeting the condition of the second check (chec-

king of specimen positioning) is more difficult - here the strains at the third cycle on both measuring lines shall not differ from their average by more than 20%. Otherwise, the specimen must be re-centred and the test must be restarted. The results of the second (more demanding) check are presented in table 4.22. The high and suspicious accuracy in specimen I-2-W4 arises from the following mistake - the unintended additional initial load was applied on this specimen, what has got a bearing on results of tested material parameters. The similar story took place in testing of II-2-5. Therefore the values are presented in brackets.

After positive results of both checks two loading cycles are carried out with the range between from  $\sigma_b$  into  $\sigma_a = f_{cm}/3$ . The last, third cycle is executing until the damage of specimen. It is worth mentioning here that described levels of stresses were determined on the basis of compressive strength measured in companion specimens (W1-W3) for each research variants independently. This is the reason why the numbers of specimens here starts with W4 - not with W1)

**Tab. 4.22:** Strains along measuring line at lower stress after third preloading cycle

Variant	No of specimen	Compressive strain [%]			Difference [%]
		measuring line 1	measuring line 2	mean value	
I-1	I-1-W4	0.0456	0.0340	0.0398	14.6
	I-1-W5	0.0386	0.0308	0.0347	11.2
	I-1-W6	0.0411	0.0302	0.0357	15.3
I-2	I-2-W4	(0.0306)	(0.0299)	(0.0303)	(1.2)
	I-2-W5	0.0374	0.0310	0.0342	9.4
	I-2-W6	0.0292	0.0413	0.0353	17.2
I-3	I-3-W4	0.0480	0.0404	0.0442	17.2
	I-3-W5	0.0469	0.0396	0.0433	16.9
	I-3-W6	0.0468	0.0429	0.0449	8.7
II-1	II-1-W4	0.0307	0.0339	0.0323	5.0
	II-1-W5	0.0295	0.0372	0.0334	11.5
	II-1-W6	0.0303	0.0359	0.0331	8.5
II-2	II-2-W4	0.0338	0.0309	0.0324	4.5
	II-2-W5	(0.0283)	(0.0264)	(0.0274)	(3.5)
	II-2-W6	0.0332	0.0297	0.0315	5.6

On the grounds of recorded strains at the particular stress levels (see figure 4.29) there is the opportunity to compute values of initial and stabilized modulus of elasticity according to following formulas:

$$E_{c,0} = \frac{\sigma_{a,1} - \sigma_{b,0}}{\varepsilon_{a,1} - \varepsilon_{b,0}} \quad (4.1)$$

$$E_{c,s} = \frac{\sigma_{a,3} - \sigma_{b,2}}{\varepsilon_{a,3} - \varepsilon_{b,2}} \quad (4.2)$$

### 4.6.2 Results of tests

As the example, in figure 4.30 the stress-strain relationship for one specimen (I-1-W4) is shown. In order to emphasize the difference between initial and stabilized values of Young's modulus in this graph the part of last damaging loading cycle is omitted. We can observe a clear change in the inclination of stress-strain line.

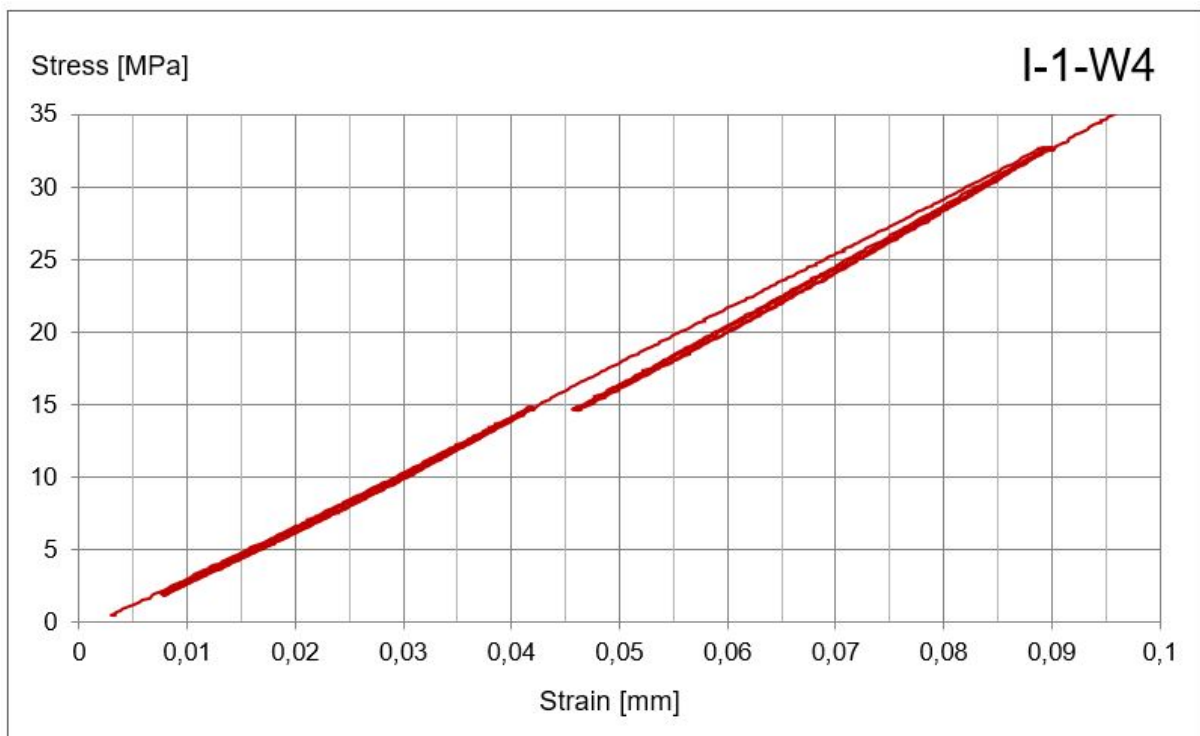


Fig. 4.30: Stress - strain graph for cylinder I-1-W4

The results of calculations of the initial as well as the stabilized **modulus of elasticity** for all of specimens are catalogued in table 4.23. The last column of the table shows the percentage increase of Young's modulus after the stabilization. We should not forget about the consequences of problems with samples I-2-W4 and II-2-W5 described in subsection 4.6.1. Testing results of these specimens are presented in brackets and they are not taken into consideration. The mean values for each variant with error bars are presented in the column diagram (fig. 4.31). In all tested specimens the increase of Young's modulus after stabilization has been confirmed. It is interesting that the industrial conditions of preparation of samples result in higher secant modulus of elasticity (initial as well as stabilized) - please compare variants I-1 and II-1. The highest magnitudes are obtained in variant I-3 (without polypropylene fibre), what was for compression test results rather predictable. The decrease of Young's modulus was recorded also in other works [6].

The ratio of transverse strain to axial strain, which is called in material science as **Poisson's ratio**  $\nu$  was also determined in the research. The magnitudes of Poisson's ratio were calculated on three different steps of the testing: a1, b2 and a3 (see fig.4.29). In table 4.24 results of calculations with mean values and standard deviations for each

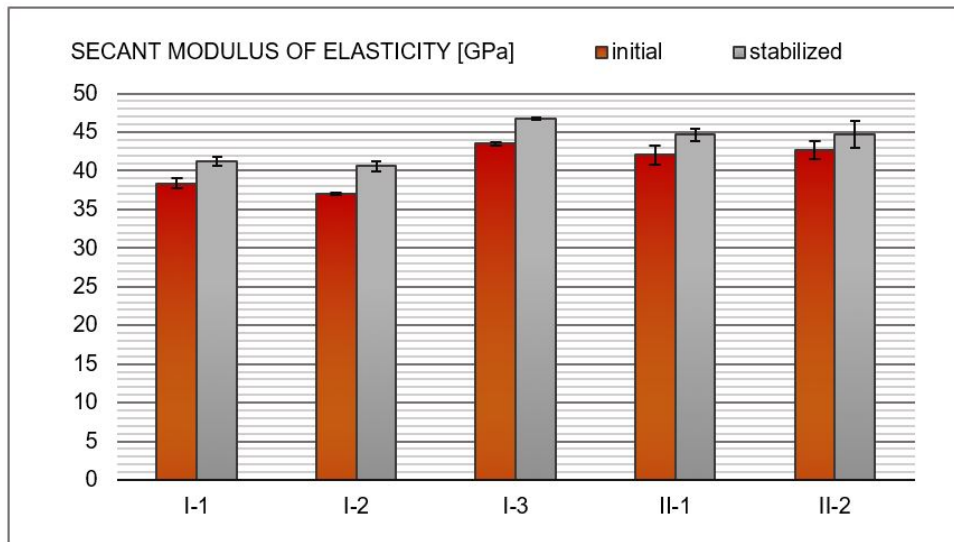


Fig. 4.31: Secant modulus of elasticity - column diagram

variant of concrete mix are presented. Due to the same reasons as in determination of modulus of elasticity, values in brackets (specimens I-2-W4 and II-2-W5) are not taken into consideration. The conducted research leaves no doubt - in investigated concrete Poisson's ratio can be approximately taken as 0.20, which is commonly-known as value of Poisson's ratio of concrete.

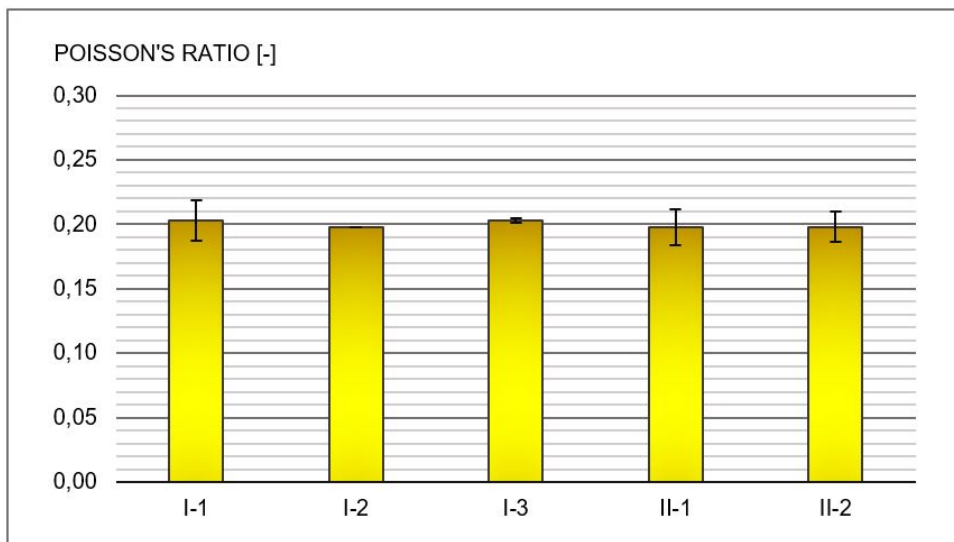


Fig. 4.32: Poisson's ratio - column diagram

**Tab. 4.23:** Initial and stabilized secant modulus of elasticity - results of calculation

Variant	No of specimen	Secant modulus of elasticity [GPa]		$\frac{E_{c,s}-E_{c,0}}{E_{c,0}}100\%$
		$E_{c,0}$ (initial)	$E_{c,s}$ (stabilized)	
I-1	I-1-W4	37.561	40.818	8.67
	I-1-W5	38.827	41.825	7.72
	I-1-W6	38.714	41.005	5.92
	<b>Mean value</b>	<b>38.367</b>	<b>41.216</b>	<b>7.44</b>
	Stand. deviation	0.701	0.536	1.40
	Coef. of variation	1.8%	1.3%	18.8%
I-2	I-2-W4	(40.462)	(44.063)	(8.90)
	I-2-W5	37.136	41.072	10.60
	I-2-W6	36.933	40.068	8.49
	<b>Mean value</b>	<b>37.035</b>	<b>40.570</b>	<b>9.53</b>
	Stand. deviation	0.144	0.710	1.51
	Coef. of variation	0.4%	1.7%	15.8%
I-3	I-3-W4	43.316	46.657	7.71
	I-3-W5	43.493	46.840	7.70
	I-3-W6	43.605	46.601	6.87
	<b>Mean value</b>	<b>43.471</b>	<b>46.699</b>	<b>7.43</b>
	Stand. deviation	0.146	0.125	0.48
	Coef. of variation	0.3%	0.3%	6.5%
II-1	II-1-W4	43.455	45.414	4.51
	II-1-W5	41.155	43.870	6.60
	II-1-W6	41.596	44.717	7.50
	<b>Mean value</b>	<b>42.069</b>	<b>44.667</b>	<b>6.20</b>
	Stand. deviation	1.221	0.773	1.53
	Coef. of variation	2.9%	1.7%	24.7%
II-2	II-2-W4	43.521	45.876	5.41
	II-2-W5	(44.776)	(47.071)	(5.13)
	II-2-W6	41.901	43.459	3.72
	<b>Mean value</b>	<b>42.711</b>	<b>44.668</b>	<b>4.57</b>
	Stand. deviation	1.146	1.709	1.20
	Coef. of variation	2.7%	3.8%	26.3%

**Tab. 4.24:** Poisson's ratio

Variant	No of specimen	Poisson's ratio [-]			
		(a1)	(b2)	(a3)	mean value
I-1	I-1-W4	0.192	0.193	0.194	0.193
	I-1-W5	0.193	0.197	0.195	0.195
	I-1-W6	0.218	0.223	0.221	0.221
	<b>Mean value</b>	<b>0.201</b>	<b>0.204</b>	<b>0.203</b>	<b>0.203</b>
	Stand. deviation	0.015	0.016	0.015	0.016
	Coef. of variation	7.3%	8.0%	7.5%	7.7%
I-2	I-2-W4	(0.255)	(0.254)	(0.255)	(0.255)
	I-2-W5	0.199	0.197	0.199	0.198
	I-2-W6	0.199	0.197	0.199	0.198
	<b>Mean value</b>	<b>0.199</b>	<b>0.197</b>	<b>0.199</b>	<b>0.198</b>
	Stand. deviation	0.000	0.000	0.000	0.000
	Coef. of variation	0.0%	0.0%	0.0%	0.0%
I-3	I-3-W4	0.208	0.193	0.206	0.202
	I-3-W5	0.207	0.194	0.207	0.203
	I-3-W6	0.210	0.197	0.209	0.205
	<b>Mean value</b>	<b>0.208</b>	<b>0.195</b>	<b>0.207</b>	<b>0.203</b>
	Stand. deviation	0.002	0.002	0.002	0.002
	Coef. of variation	0.7%	1.1%	0.7%	0.8%
II-1	II-1-W4	0.210	0.209	0.210	0.210
	II-1-W5	0.187	0.176	0.186	0.183
	II-1-W6	0.201	0.203	0.202	0.202
	<b>Mean value</b>	<b>0.199</b>	<b>0.196</b>	<b>0.199</b>	<b>0.198</b>
	Stand. deviation	0.012	0.018	0.012	0.014
	Coef. of variation	5.8%	9.0%	6.1%	7.0%
II-2	II-2-W4	0.191	0.181	0.194	0.189
	II-2-W5	(0.252)	(0.276)	(0.254)	(0.261)
	II-2-W6	0.203	0.210	0.206	0.206
	<b>Mean value</b>	<b>0.197</b>	<b>0.196</b>	<b>0.200</b>	<b>0.198</b>
	Stand. deviation	0.008	0.021	0.008	0.012
	Coef. of variation	0.0%	0.1%	0.0%	0.1%

For the one of the research variant (II-2) the attempt of using non-contact measuring system ARAMIS in determination of modulus of elasticity was taken. Strains measured by means of extensometers and ARAMIS were recorded simultaneously. The results of Young's modulus calculations are in table 4.25. Despite the fact that the one of the sample (before-mentioned II-2-W5) cannot be taken into consideration and the drawing conclusions on the grounds of two results is rather not effective, still the huge coefficient of variation in the case of ARAMIS measurement can be disturbing. Nevertheless, it is not the fault of ARAMIS measuring system. It is well-known fact that the testing of modulus of elasticity is very vulnerable when it comes to situation of specimen - this is the explanation why two controls mentioned in section 4.6.1 are required. Due to alignment of ARAMIS device the above-mentioned controls were conducted in perpendicular plane to plane observed by ARAMIS cameras (extensometers are situated in both opposite sides of sample). Thus, the proper situation of specimen was done only in one plane - the ARAMIS, which has to be located only from one side of specimen does not have this opportunity. Unfortunately, I made this conclusion during interpretation of results after the testing.



**Fig. 4.33:** ARAMIS system during the testing of modulus of elasticity



**Fig. 4.34:** The cylinder II-2-W4 subjected to testing

**Tab. 4.25:** Modulus of elasticity by the means of extensometers and Aramis [GPa]

Variant	No of specimen	Extensometers		ARAMIS	
		$E_{c,0}$	$E_{c,s}$	$E_{c,0}$	$E_{c,s}$
II-2	II-2-W4	43.521	45.876	39.493	41.682
	II-2-W5	(44.776)	(47.071)	(41.898)	(44.445)
	II-2-W6	41.901	43.459	48.168	49.805
	<b>Mean value</b>	<b>42.711</b>	<b>44.668</b>	<b>43.831</b>	<b>45.744</b>
	Stand. deviation	1.146	1.709	6.134	5.744
	Coef. of variation	2.68%	3.83%	14.00%	12.56%

## 4.7 Testing of laboratory beams (10x10x50cm)

### 4.7.1 Description of testing

The investigated beams (10x10x50cm) referred to as *laboratory beams* and labeled by small "b" letter were subjected to three-point bending test. This investigation was conducted in order to present the difference in failure mechanism of bended specimens with and without polypropylene fibres. As the testing machine the INSTRON 300DX was used (fig. 4.35). Initial load was assumed as 500 N and the pace of testing was fixed as 1 mm per minute. The effective length of span was takes as 40 cm (fig. 4.36).



Fig. 4.35: Laboratory beam (10x10x50cm) mounted on test setup

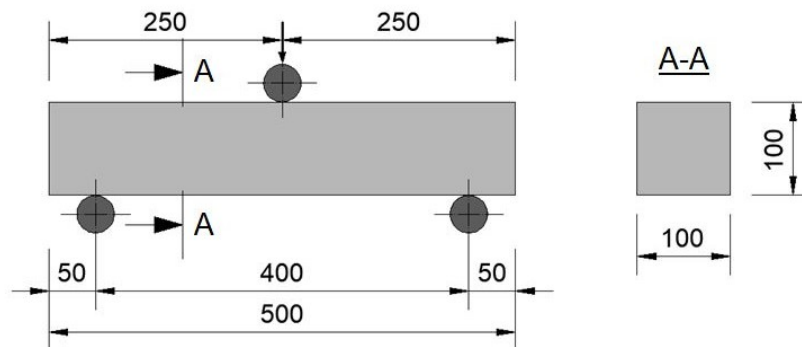


Fig. 4.36: Static scheme of laboratory beam

### 4.7.2 Results of tests

The conducted experimental tests have confirmed the substantial impact of polypropylene fibre reinforcement on failure mechanism of bended concrete members. In the case of polypropylene fibre reinforced beams (variants I-1, I-2, II-1, II-2) testing was carrying on until mid-span deflection reaches value of 15 mm, whereas for specimens without fibres (variant I-3) it was impossible to get this displacement because the failure was really rapid and brittle. The difference between failure mechanisms is presented in the photos (fig. 4.37) and in the force-displacement charts (fig. 4.38). The force-displacement relationship in beams without polypropylene fibre was marked by dashed line, whereas the continuous one represents specimens of the variant with the fibre reinforcement. The more complex interpretation of chart (fig. 4.38) regarding ductility is presented in chapter 6 of this dissertation. It is worth to mention that the dispersion of test results is greater in case of beams concreted in the prefabricated element plant (variants II-1, II-2) rather than in specimens prepared in the academic batching plant (except I-1 what is explained below).



**Fig. 4.37:** The failure mechanism of beam without (on the left) and with (on the right) polypropylene fibre reinforcement

In table 4.26 maximum forces and corresponding bending stresses are shown. Actually in each variant results are approximately (12-13) kN and (7-8) MPa, respectively. In addition, mean values of maximum elastic forces with standard deviations are presented in figure 4.39. The huge coefficient of variation in variant I-1 results from greater magnitude of force in specimen I-1-b2. Not taking into account this sample would result in coefficient of variation equaled 5.77%, but the mean value and standard deviation would be calculated based on two results only. It should be acknowledged that the amount of specimen is rather small and in further research I would like to repeat some tests considering greater number of samples.

**Tab. 4.26:** Max. force [kN] and corresponding flexural stress [MPa] in laboratory beams

Variant	No. of specimen	Maximum elastic force [kN]	Flexural stress (for max. elastic force) [MPa]
I-1	I-1-b1	10.989	6.59
	I-1-b2	15.052	9.03
	I-1-b3	11.923	7.15
	<b>Mean value</b>	<b>12.655</b>	<b>7.59</b>
	Stand. deviation	2.13	1.28
	Coef. of variation	16.8%	16.8%
I-2	I-2-b1	12.001	7.20
	I-2-b2	12.063	7.23
	I-2-b3	12.507	7.50
	<b>Mean value</b>	<b>12.190</b>	<b>7.31</b>
	Stand. deviation	0.28	0.17
	Coef. of variation	2.3%	2.3%
I-3	I-3-b1	11.880	7.13
	I-3-b2	11.954	7.17
	I-3-b3	12.473	7.48
	<b>Mean value</b>	<b>12.102</b>	<b>7.26</b>
	Stand. deviation	0.32	0.19
	Coef. of variation	2.7%	2.7%
II-1	II-1-b1	13.502	8.10
	II-1-b2	11.117	6.67
	II-1-b3	12.169	7.30
	<b>Mean value</b>	<b>12.263</b>	<b>7.36</b>
	Stand. deviation	1.20	0.72
	Coef. of variation	9.7%	9.7%
II-2	II-2-b1	10.888	6.53
	II-2-b2	13.521	8.11
	II-2-b3	12.198	7.32
	<b>Mean value</b>	<b>12.202</b>	<b>7.32</b>
	Stand. deviation	1.32	0.79
	Coef. of variation	10.8%	10.8%

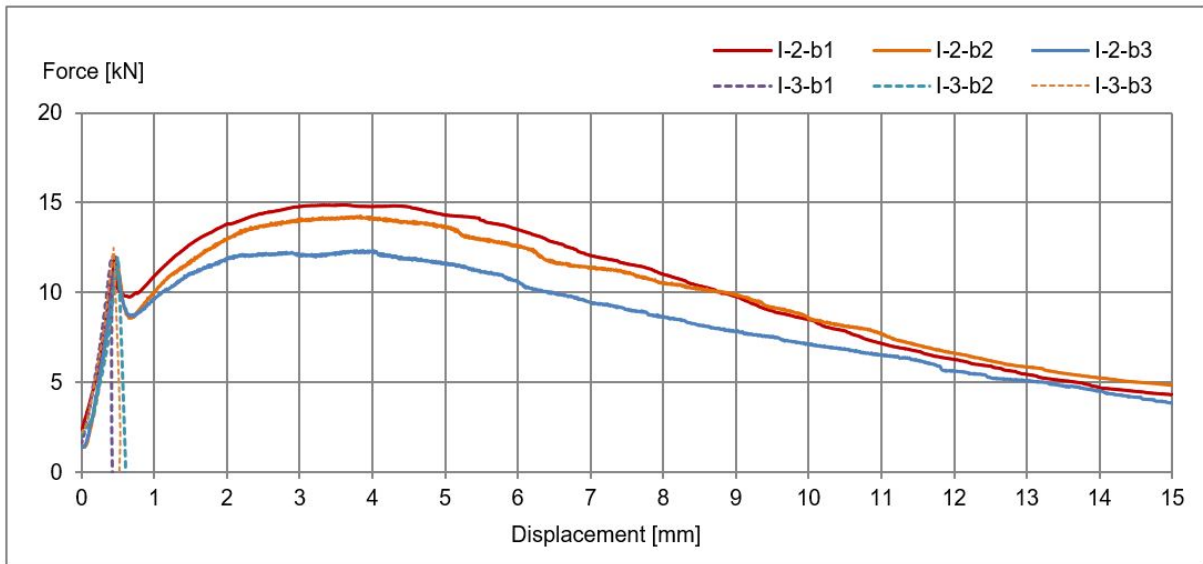


Fig. 4.38: Force-displacement graphs for beams without (I-3) and with (I-2) polypropylene fibre

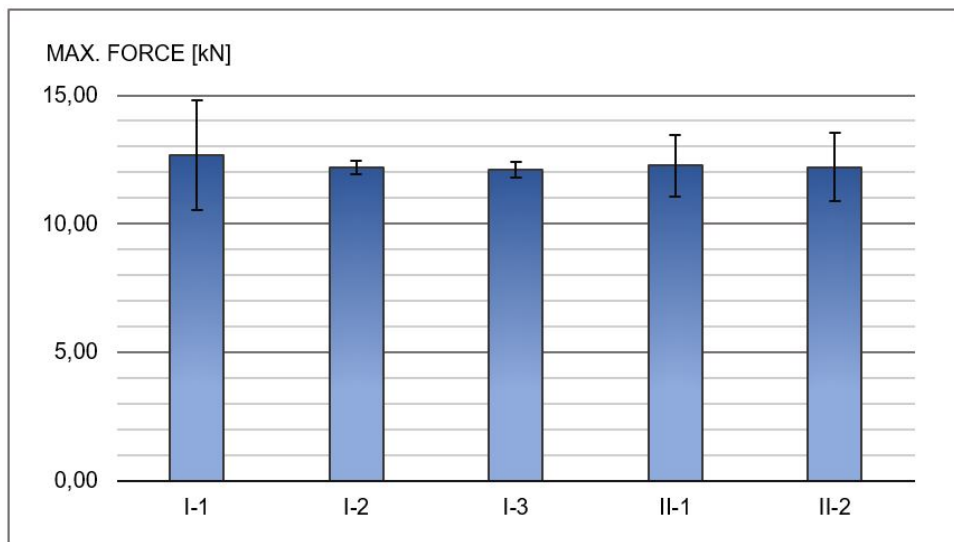


Fig. 4.39: Forces [kN] - column diagram

## 4.8 Testing of full-scale beams (12x24x260cm)

### 4.8.1 Description of testing

The testing of full-scale beams was the main area of the experimental research in this thesis. The 18 beams with dimensions of 12x24x260 cm, where the effective length of span is 240 cm, were subjected to three-point bending test. The beams with only fibre reinforcement, only longitudinal steel bars as well as with both of abovementioned types of reinforcement were examined. There were no beams without any reinforcement due to predictable rapid failure and associated with it hardships with removing the sample from the test setup. The influence of polypropylene fibres on concrete without steel bars and comparison with plain concrete was done by the means of laboratory beams (section 4.7). Details about the applied reinforcement can be found in section 4.1.

It is worth underlining that during experiments three different measuring systems (fig. 4.40) were used simultaneously:

- the testing machine INSTRON 8505,
- linear variable differential transformer (LVDT) situated under the specimen in the middle of the span,
- contact free measuring system ARAMIS which is based on the principle of digital image correlation (DIC).

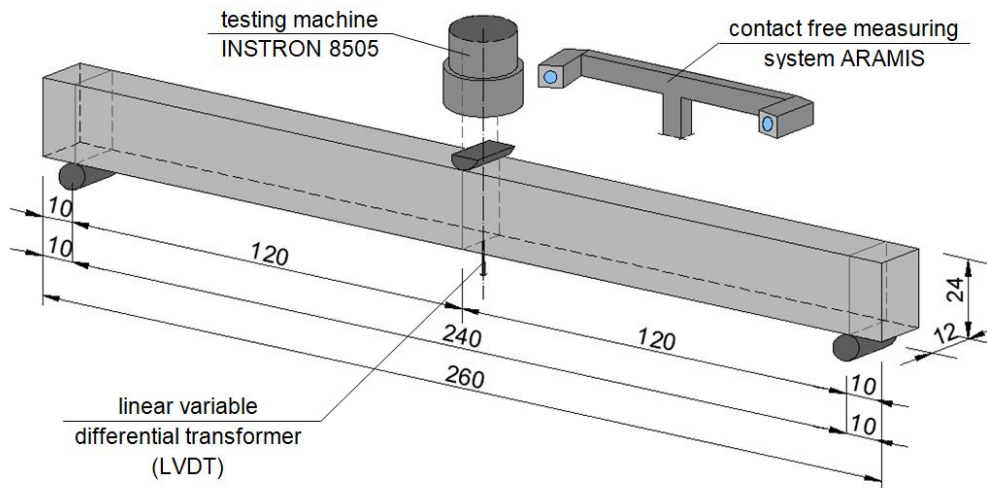


**Fig. 4.40:** Three measuring systems used simultaneously in testing of full-scale beams

The procedure of testing was as follows: firstly the load causing the mid-span deflection equaled 1 mm was applied. After the unloading and coming back to the initial position the next cycle, leading to achievement of 2 mm deflection in the middle of the span, took place. In this way, with increasing deflection by 1 mm in each cycle, testing was carrying



Fig. 4.41: The full-scale beam during testing

on until the damage of specimen. The pace of loading and unloading was assumed as 15 mm per 1 minute, what in consequence results in roughly 4-hours-long testing. Taking into account mounting the specimen on the test setup, preparatory works and laboratory constraints, the research of one beam per day was workable.

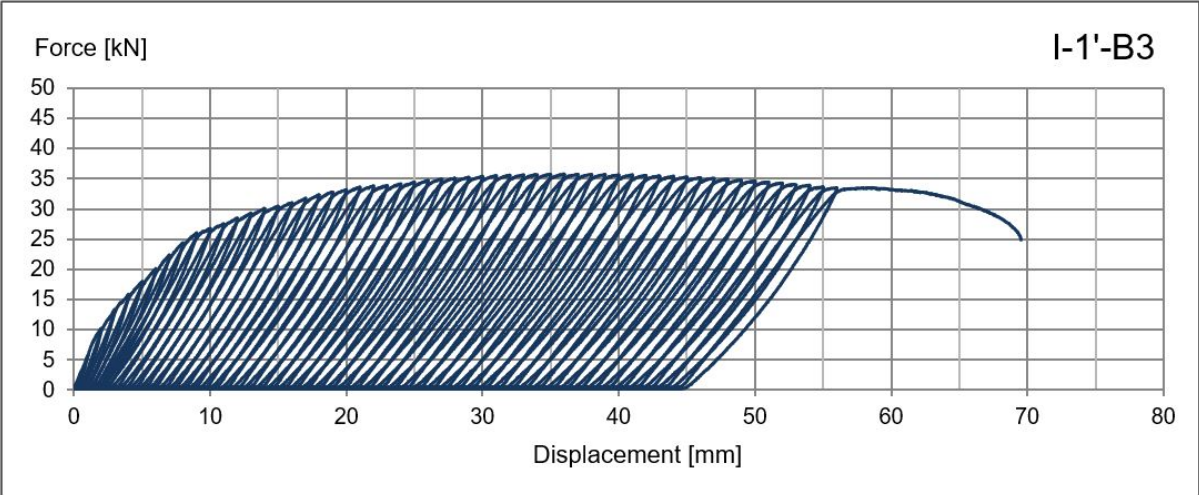


Fig. 4.42: Force-displacement graph for one of the full-scale beam

## 4.8.2 Results of tests

Throughout the three-point bending test the force as well as the mid-span deflection of the beam were recorded. It allowed one to present the force-displacement relationship. In the table 4.27 magnitudes of forces in a few selected (5th, 10th, 20th and 30th) loading cycles for individual specimens are gathered. These cycles correspond to mid-span deflections 5 mm, 10 mm, 20 mm and 30 mm, respectively. Mean values of forces for each variant with standard deviations and coefficients of variation are also presented in the table 4.27. In addition, the mean values are also graphically represented by column diagram (fig. 4.43), where bar errors are marked. All force-displacement graphs are included in Appendix A.

The forces in tested beams prepared in industrial conditions are quite smaller and with greater coefficients of variation in comparison with the same beams prepared in laboratory. The clear difference between variants I-2', I-2 and I-3' can be noticed. The combined effect of polypropylene fibres and steel bars results in higher forces than in cases where only one type of reinforcement was provided.

Coefficient of variation in variant I-2 for 30th loading cycle could be disturbing on the first sight. Its magnitude reaches approximately 30%. However, we need to be aware that the described case concerns beams without steel reinforcing bars and 30th loading cycle what corresponds to 30 mm deflection (which is 1/80 of effective length span).

The shape of force-displacement curve in selected cycles is presented in figures 4.44. It is worth noting at this point the clear difference between the behaviour of beams with and without steel longitudinal bars. The variant I-2 (the one with polypropylene fibre, but without steel reinforcement) is characterised by not only greater scatter of results, but also shows the different shape of force-displacement curve.

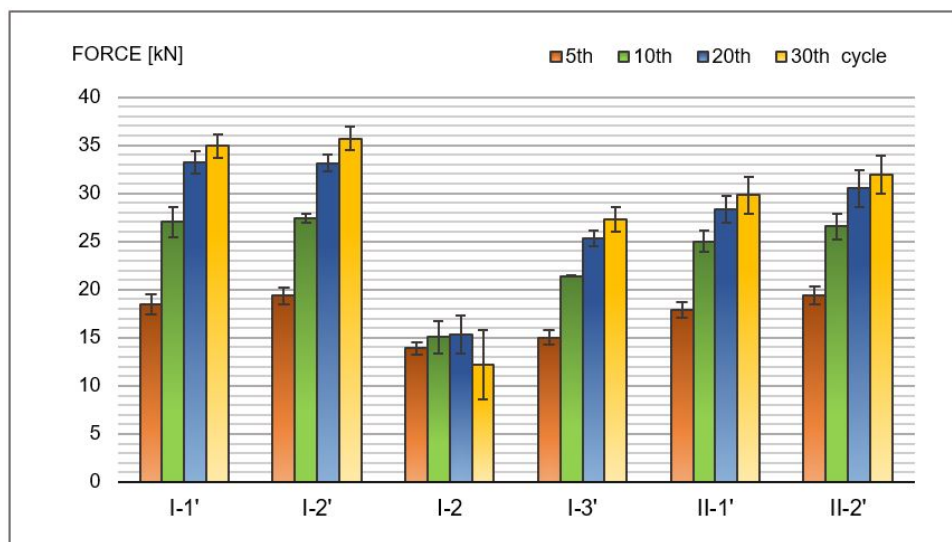


**Fig. 4.43:** Forces [kN] in 5th, 10th, 20th and 30th cycle of loading - column diagram

To make the comparison of results between individual specimens within a variant as well as between different variants the envelopes of maximum forces were used. The way to get the envelope was depicted graphically in figure 4.45 (for beam I-1'-B3, for example).

**Tab. 4.27:** Forces [kN] in 5th, 10th, 20th and 30th loading cycle in testing of full-scale beams

Variant	No. of specimen	Force [kN]			
		No of cycle:			
		5th	10th	20th	30th
I-1'	I-1'-B1	19.625	28.703	34.413	35.842
	I-1'-B2	17.780	25.614	32.093	33.516
	I-1'-B3	18.002	26.771	33.198	35.383
	<b>Mean value</b>	<b>18.469</b>	<b>27.029</b>	<b>33.235</b>	<b>34.914</b>
	Stand. deviation	1.007	1.561	1.160	1.232
	Coef. of variation	5.5%	5.8%	3.5%	3.5%
I-2'	I-2'-B1	19.810	27.793	33.270	35.156
	I-2'-B2	18.390	26.848	33.884	37.061
	I-2'-B3	19.935	27.516	32.194	34.804
	<b>Mean value</b>	<b>19.378</b>	<b>27.382</b>	<b>33.116</b>	<b>35.674</b>
	Stand. deviation	0.858	0.486	0.855	1.214
	Coef. of variation	4.4%	1.8%	2.6%	3.4%
I-2	I-2-B4	14.050	14.376	13.168	8.510
	I-2-B5	13.207	13.880	16.976	15.738
	I-2-B6	14.403	16.990	15.972	12.405
	<b>Mean value</b>	<b>13.887</b>	<b>15.082</b>	<b>15.372</b>	<b>12.218</b>
	Stand. deviation	0.615	1.671	1.974	3.618
	Coef. of variation	4.4%	11.1%	12.8%	29.6%
I-3'	I-3'-B1	15.560	21.388	24.663	26.344
	I-3'-B2	14.130	21.491	26.205	28.768
	I-3'-B3	15.291	21.329	25.090	26.869
	<b>Mean value</b>	<b>14.994</b>	<b>21.403</b>	<b>25.318</b>	<b>27.327</b>
	Stand. deviation	0.760	0.082	0.796	1.275
	Coef. of variation	5.1%	0.4%	3.1%	4.7%
II-1'	II-1'-B1	17.671	25.610	29.548	31.249
	II-1'-B2	17.236	23.779	26.754	27.652
	II-1'-B3	18.766	25.683	28.735	30.570
	<b>Mean value</b>	<b>17.891</b>	<b>25.024</b>	<b>28.346</b>	<b>29.824</b>
	Stand. deviation	0.788	1.079	1.437	1.911
	Coef. of variation	4.4%	4.3%	5.1%	6.4%
II-2'	II-2'-B1	18.956	25.036	29.075	29.932
	II-2'-B2	18.850	26.893	29.779	31.972
	II-2'-B3	20.382	27.683	32.668	33.928
	<b>Mean value</b>	<b>19.396</b>	<b>26.539</b>	<b>30.507</b>	<b>31.944</b>
	Stand. deviation	0.982	1.359	1.904	1.998
	Coef. of variation	5.1%	5.1%	6.2%	6.3%

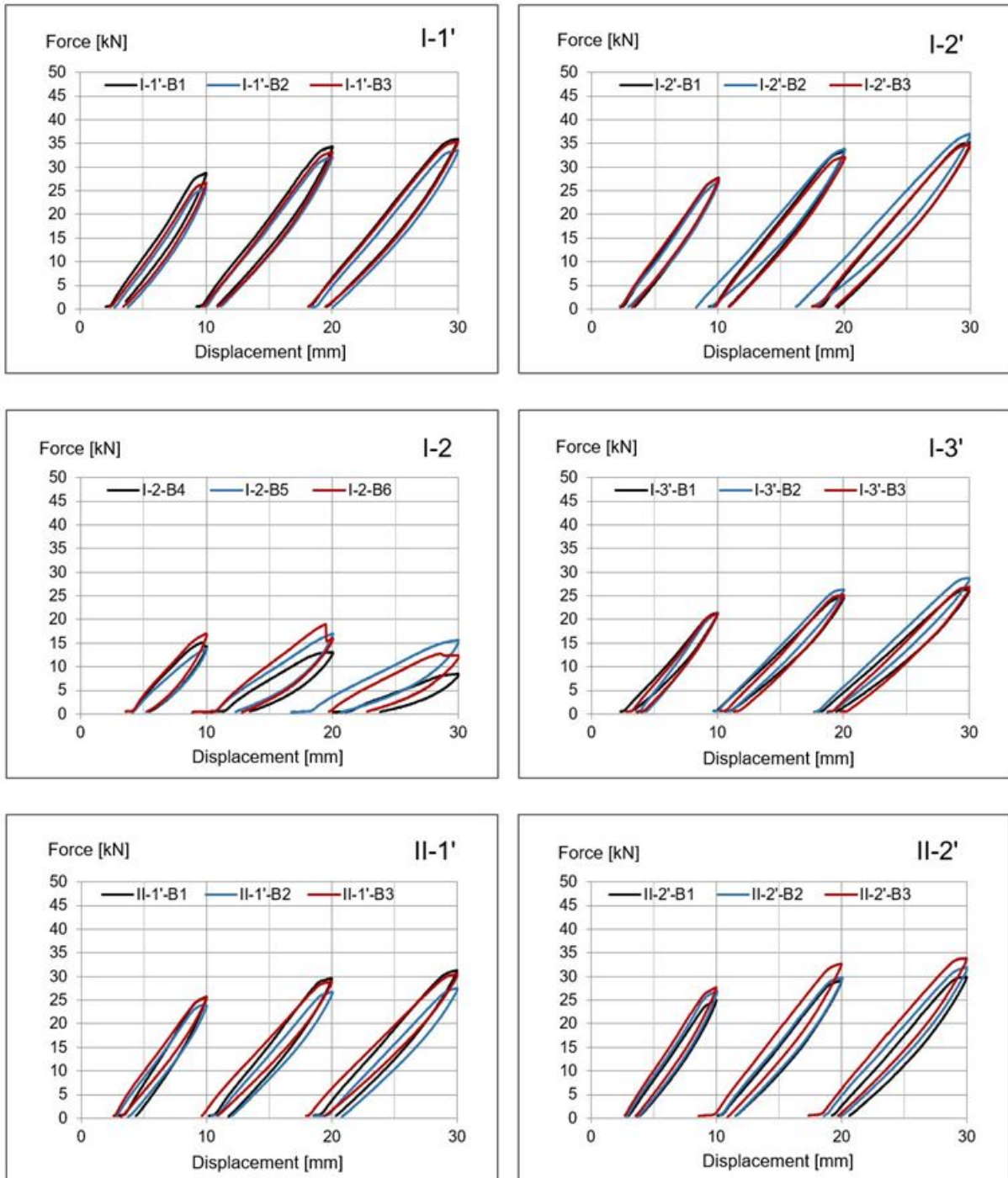
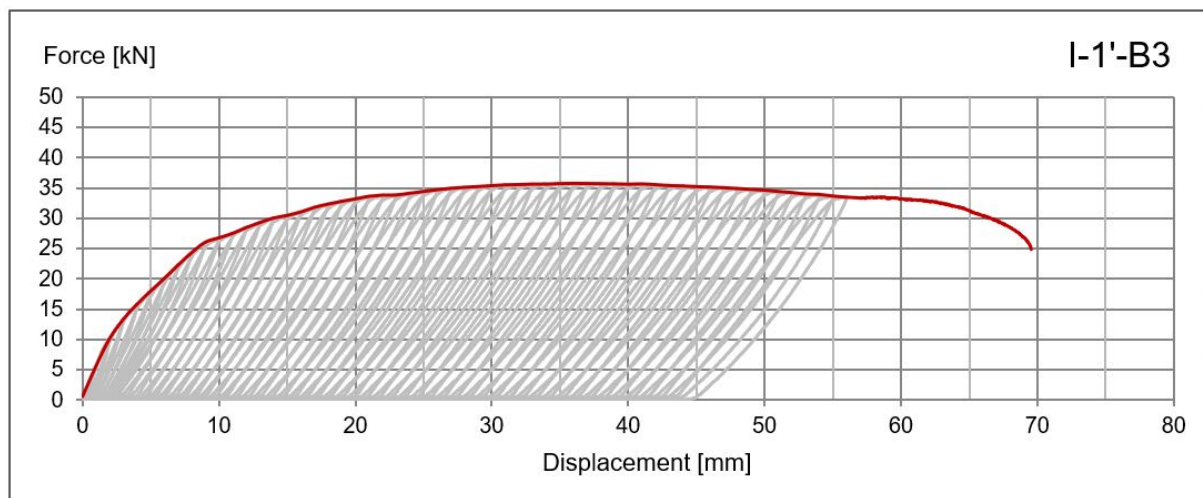


Fig. 4.44: Force-displacement graphs (selected cycles) in full-scale beams (I-1' and I-2')



**Fig. 4.45:** Force-displacement graph (envelope) for the full scale beam I-1'-B3

The specimen II-2'-B1 requires a comment (fig. 4.47). The clear drop of force around 38th cycle of loading is the result of damage of one of the steel bars and associated with this a reduction of stiffness.

After every cycle of unloading the permanent part of mid span deflection was recorded. In the same manner like forces (table 4.27 and fig. 4.43) the results for selected cycles in the table 4.28 as well as in the column diagram (fig. 4.48) are presented. The highest permanent part of deflection was noted for the variant with polypropylene fibres but without steel bars (I-2). The result is in the line with expectations - the lack of longitudinal traditional reinforcement results in smaller stiffness of member, what in consequence leads to higher value of deflections.

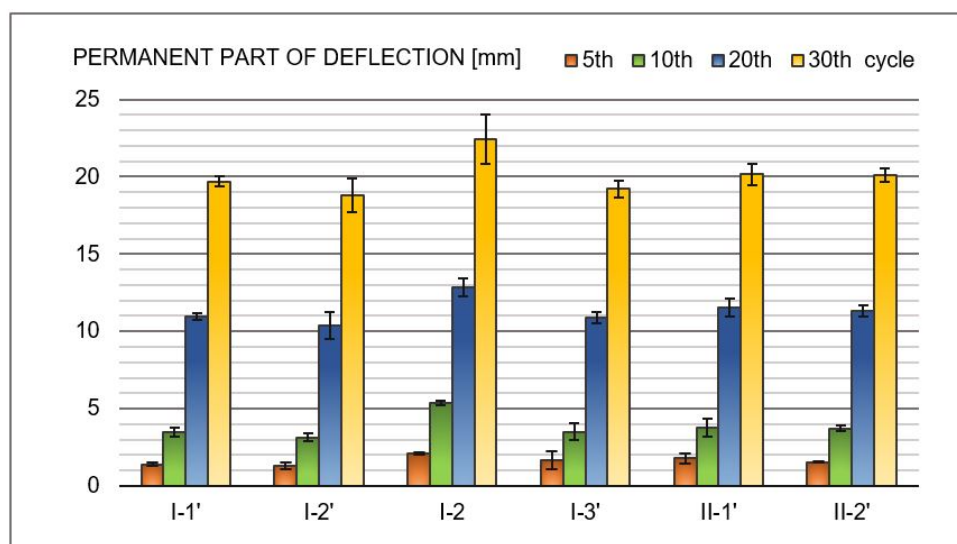


**Fig. 4.46:** Permanent part of deflection [mm] in 5th, 10th, 20th and 30th cycle of loading - column diagram

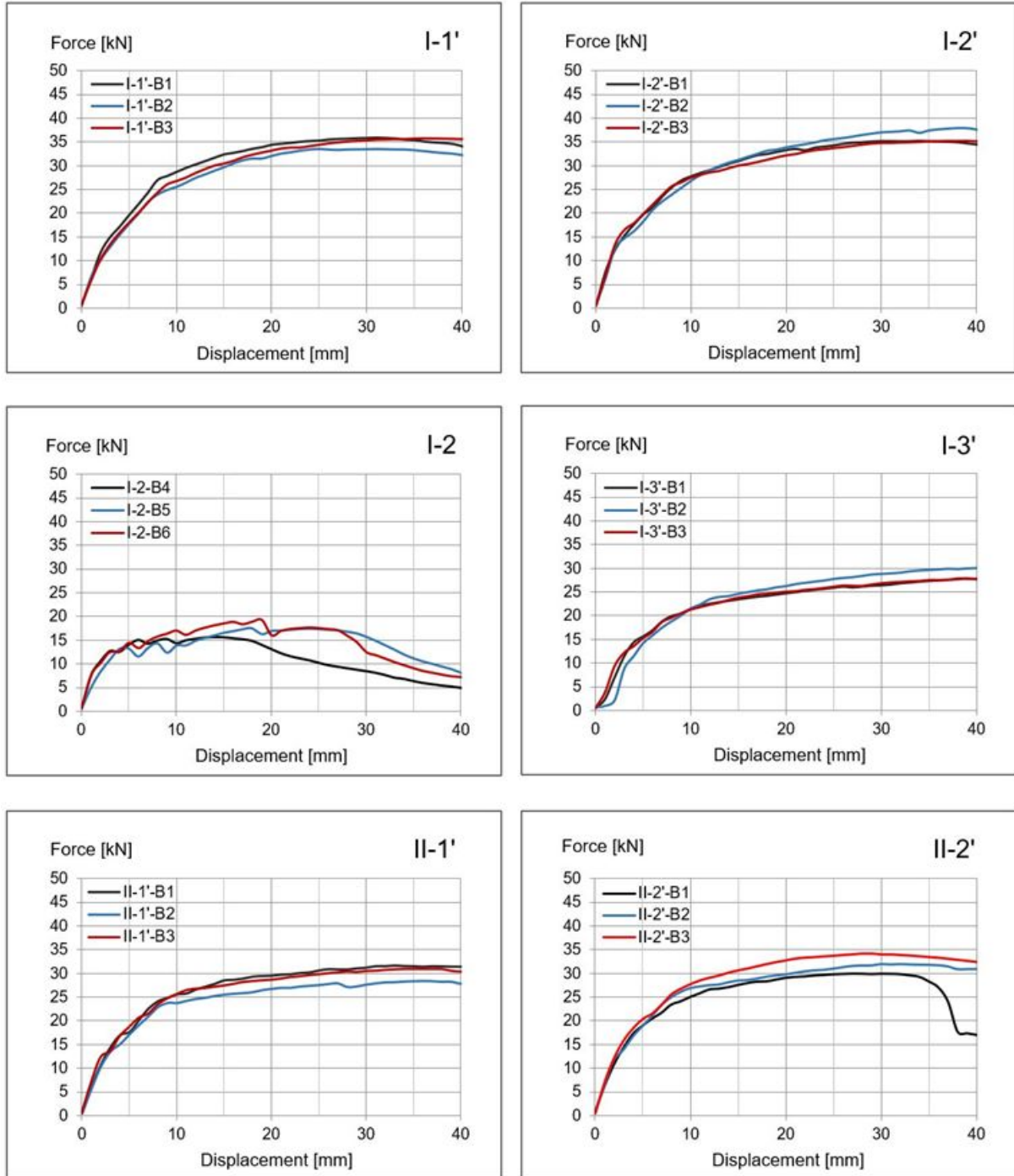


Fig. 4.47: Force-displacement graphs (envelopes) in full-scale beams

**Tab. 4.28:** Permanent part of deflection after 5th, 10th, 20th and 30th loading cycle in testing of full-scale beams

Variant	No. of specimen	Permanent part of deflection [mm]			
		No of cycle:			
		5th	10th	20th	30th
I-1'	I-1'-B1	1.279	3.244	10.817	19.583
	I-1'-B2	1.434	3.799	11.208	20.038
	I-1'-B3	1.476	3.459	10.906	19.434
	<b>Mean value</b>	<b>1.396</b>	<b>3.501</b>	<b>10.977</b>	<b>19.685</b>
	Stand. deviation	0.104	0.280	0.205	0.315
	Coef. of variation	7.4%	8.0%	1.9%	1.6%
I-2'	I-2'-B1	1.499	3.363	10.881	19.488
	I-2'-B2	1.386	2.894	9.402	17.536
	I-2'-B3	1.085	3.202	10.900	19.337
	<b>Mean value</b>	<b>1.323</b>	<b>3.153</b>	<b>10.394</b>	<b>18.787</b>
	Stand. deviation	0.214	0.238	0.859	1.086
	Coef. of variation	16.2%	7.6%	8.3%	5.8%
I-2	I-2-B4	2.119	5.529	13.477	23.798
	I-2-B5	2.155	5.219	12.314	20.695
	I-2-B6	2.033	5.357	12.830	22.739
	<b>Mean value</b>	<b>2.102</b>	<b>5.368</b>	<b>12.874</b>	<b>22.411</b>
	Stand. deviation	0.063	0.155	0.583	1.577
	Coef. of variation	3.0%	2.9%	4.5%	7.0%
I-3'	I-3'-B1	1.224	2.904	10.623	19.145
	I-3'-B2	2.343	3.977	10.701	18.682
	I-3'-B3	1.511	3.668	11.307	19.787
	<b>Mean value</b>	<b>1.693</b>	<b>3.516</b>	<b>10.877</b>	<b>19.205</b>
	Stand. deviation	0.581	0.552	0.374	0.555
	Coef. of variation	34.3%	15.7%	3.4%	2.9%
II-1'	II-1'-B1	2.117	4.371	11.775	20.284
	II-1'-B2	1.709	3.823	11.974	20.786
	II-1'-B3	1.537	3.206	10.889	19.433
	<b>Mean value</b>	<b>1.788</b>	<b>3.800</b>	<b>11.546</b>	<b>20.168</b>
	Stand. deviation	0.298	0.583	0.578	0.684
	Coef. of variation	16.7%	15.3%	5.0%	3.4%
II-2'	II-2'-B1	1.573	3.912	11.527	20.599
	II-2'-B2	1.564	3.699	11.537	19.986
	II-2'-B3	1.526	3.549	10.883	19.697
	<b>Mean value</b>	<b>1.554</b>	<b>3.720</b>	<b>11.316</b>	<b>20.094</b>
	Stand. deviation	0.025	0.182	0.375	0.461
	Coef. of variation	1.6%	4.9%	3.3%	2.3%

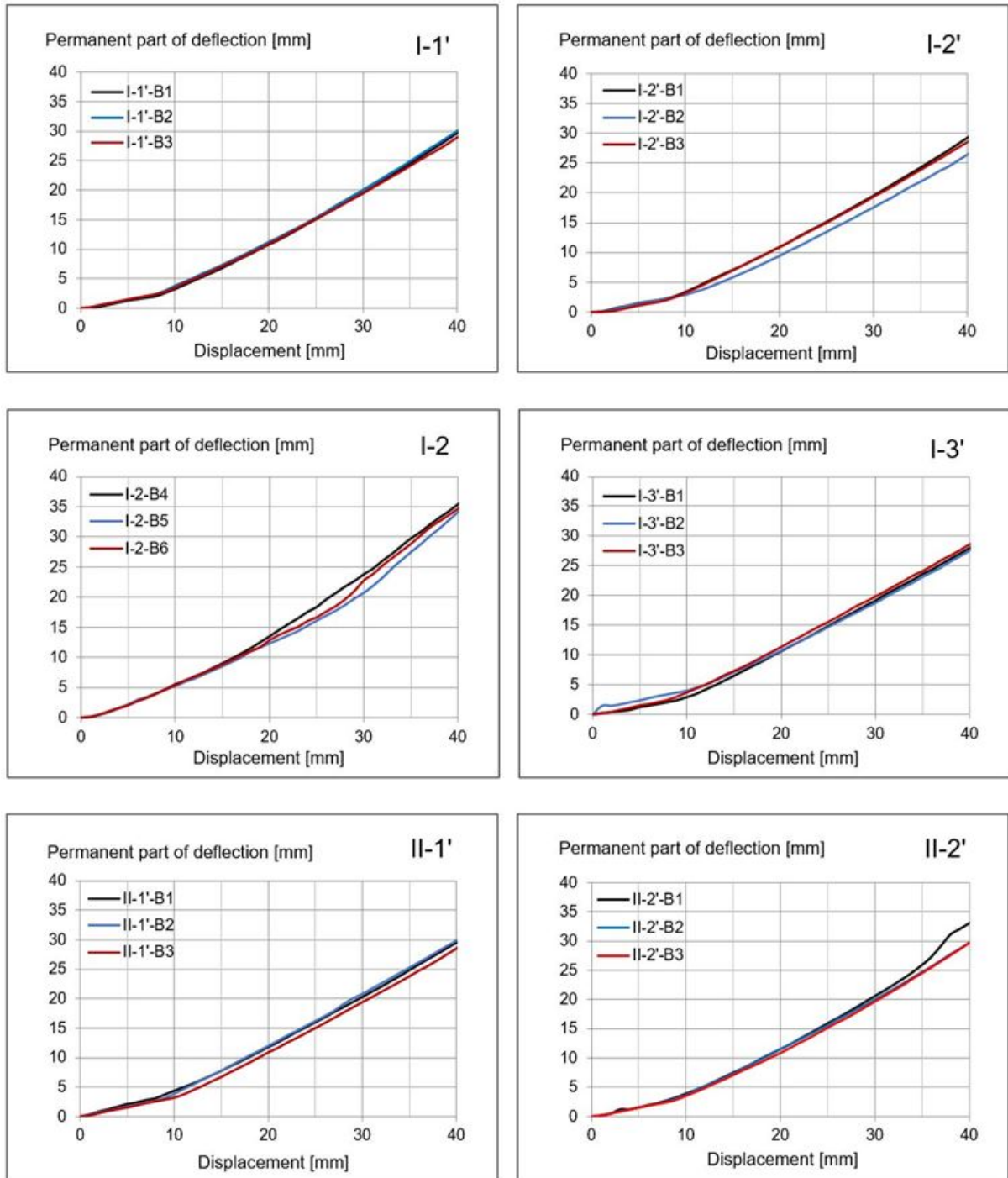
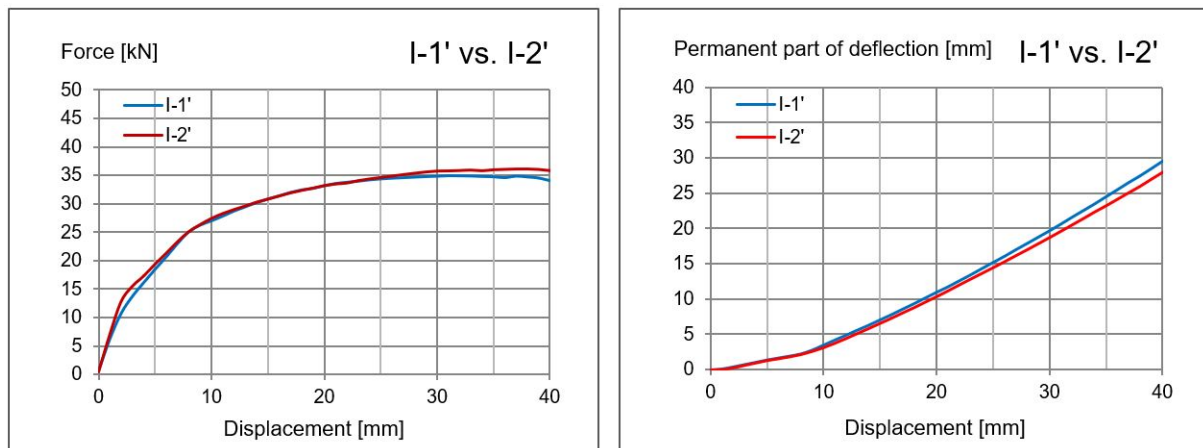


Fig. 4.48: Permanent part of mid-span deflection in full-scale beams

In the figures 4.49-4.53 the mean force-displacement envelopes are presented for comparisons between particular variants. The difference between I-1' and I-2' has the source in ingredients of concrete mix: the silica fume and aggregates were provided by two different manufacturers. As we can see in the figure 4.49 it is hard to say about any influence of this change of the ingredients on the force-displacement relationship as well as on permanent part of deflection.



**Fig. 4.49:** Comparison of results depending on used silica fume and aggregate (I-1' vs. I-2')

Comparison of results in beams with polypropylene fibres and beams with both of considered reinforcement types indicates on huge differences (fig. 4.50). The disparity in permanent part of deflection was discussed earlier, and the force-displacement graphs have visibly different shapes.

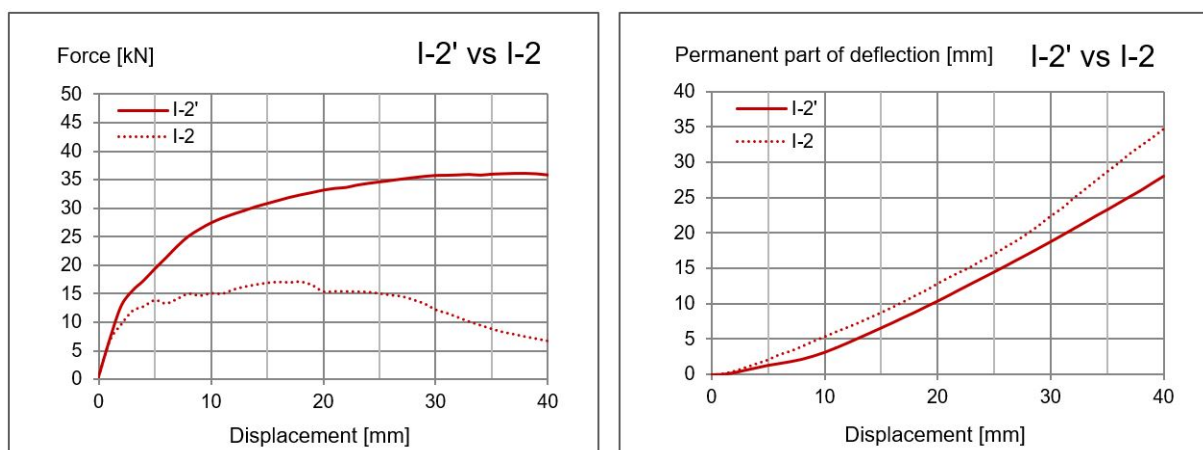


**Fig. 4.50:** Comparison of results depending on the presence of steel bars (I-2' vs. I-2)

On the other hand, comparison of variants I-2' and I-3' allows one to capture the positive effect of polypropylene fibre as the addition to the traditional reinforcement (fig. 4.51). The forces are approximately 25% greater than in case of beams reinforced only by steel bars. The addition of fibres does not change the permanent part of deflection.

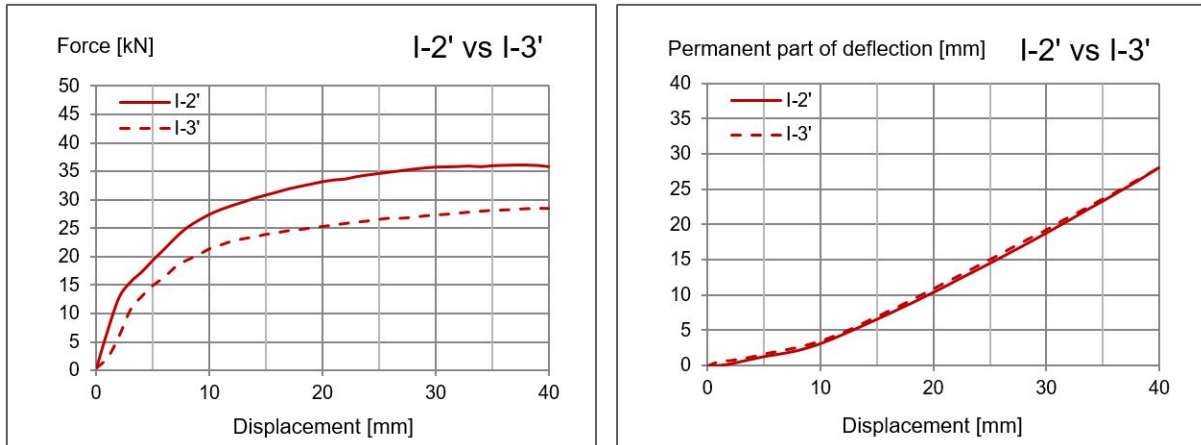


**Fig. 4.51:** Comparison of results depending on the presence of polypropylene fibres (I-2' vs. I-3')

Samples prepared in laboratory conditions show some better results of obtained forces than specimens concreted in industrial conditions (fig. 4.52), although a first linear part of the load-displacement path is the same. Here, like in previous comparison it is hard to say about any difference in permanent part of deflection due to the same stiffness of member.

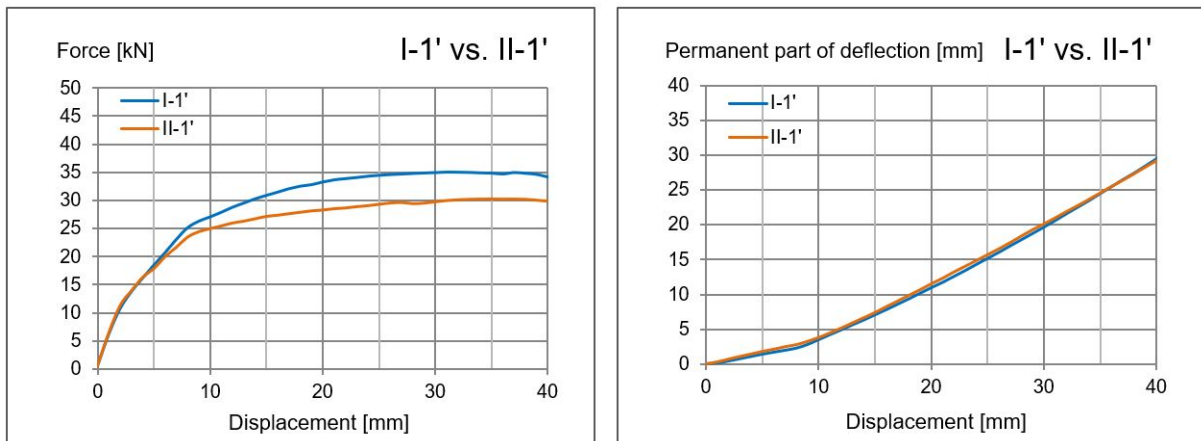


**Fig. 4.52:** Comparison of results depending on place of concreting (I-1' vs. II-1')

The last comparison was done between variants II-1' and II-2', where the only difference was in the length of polypropylene fibres. In this research the influence of small difference in the length of fibres (60 mm vs 48 mm) cannot be captured (fig. 4.53).

As it was mentioned before, three different measuring systems were provided during the testing of full-scale beams. The comparison of measurements of mid-span deflection for

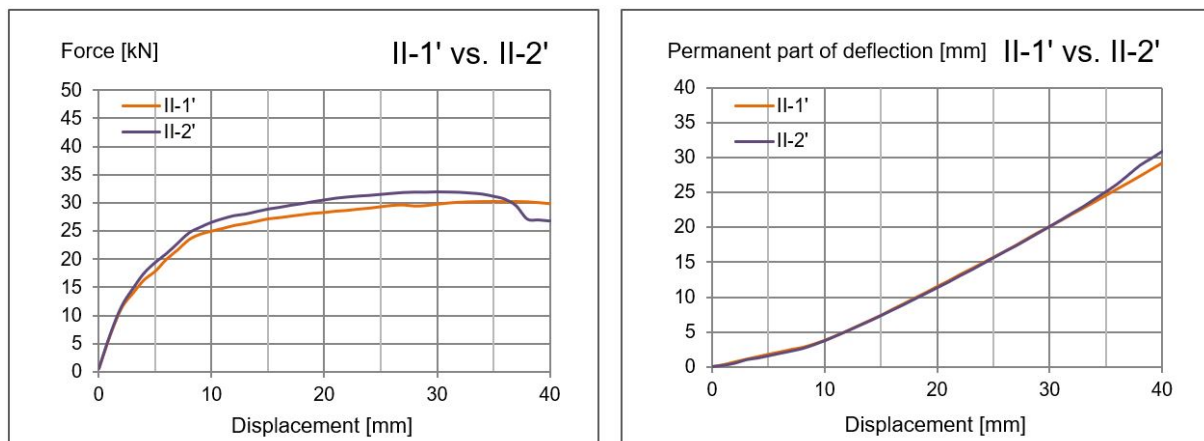


**Fig. 4.53:** Comparison of results depending on polypropylene fibre length (II-1' vs. II-2')

the example of full-scale beam (I-1'-B1) by particular systems is presented in figure 4.54. To make it more readable only a part of the test is shown (the first 850 seconds). By red line the displacement recorded by testing machine (INSTRON) is marked. The procedure of testing was configured to come back to starting position after every cycle of loading, what is visible in the chart - red line every time returns to the intersection with horizontal axis. In fact, it is the movement of testing machine plate, whereas the blue line (LVDT) and green line (ARAMIS) refers directly to the displacement of beam: the lower edge (in case of LVDT) and the middle of the height of beam (in case of ARAMIS). In the beautiful way the increasing permanent part of deflection is visible. Some small differences between peaks of graphs are understandable and predictable: after all we consider displacement of three different points among the height of the section: the upper one (INSTRON), the middle one (ARAMIS) and the lower one (LVDT) - they cannot be exactly the same. The compatibility of presented results gives the full right to treat conducted measurement as valid one.

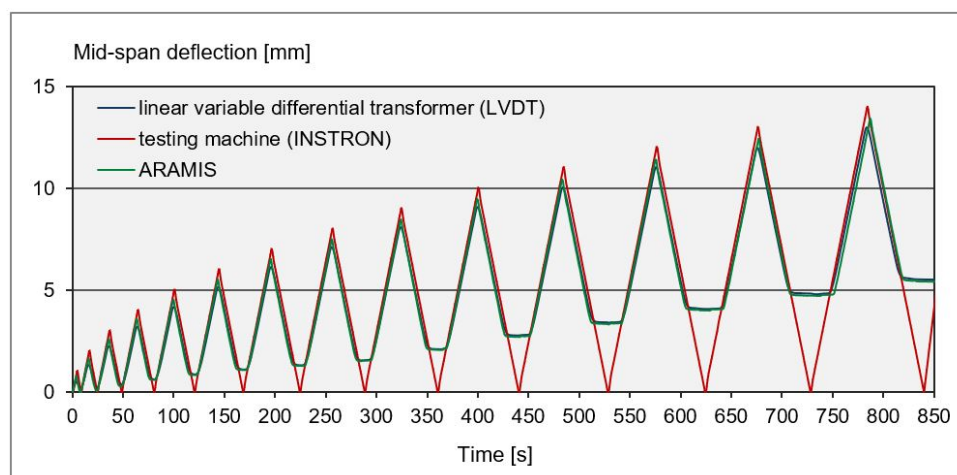


**Fig. 4.54:** Mid-span deflection according to time (first 850 sec) in full-scale beam (I-1'-B1) measured by different measuring systems



Fig. 4.55: The ARAMIS system during testing of full-scale beam

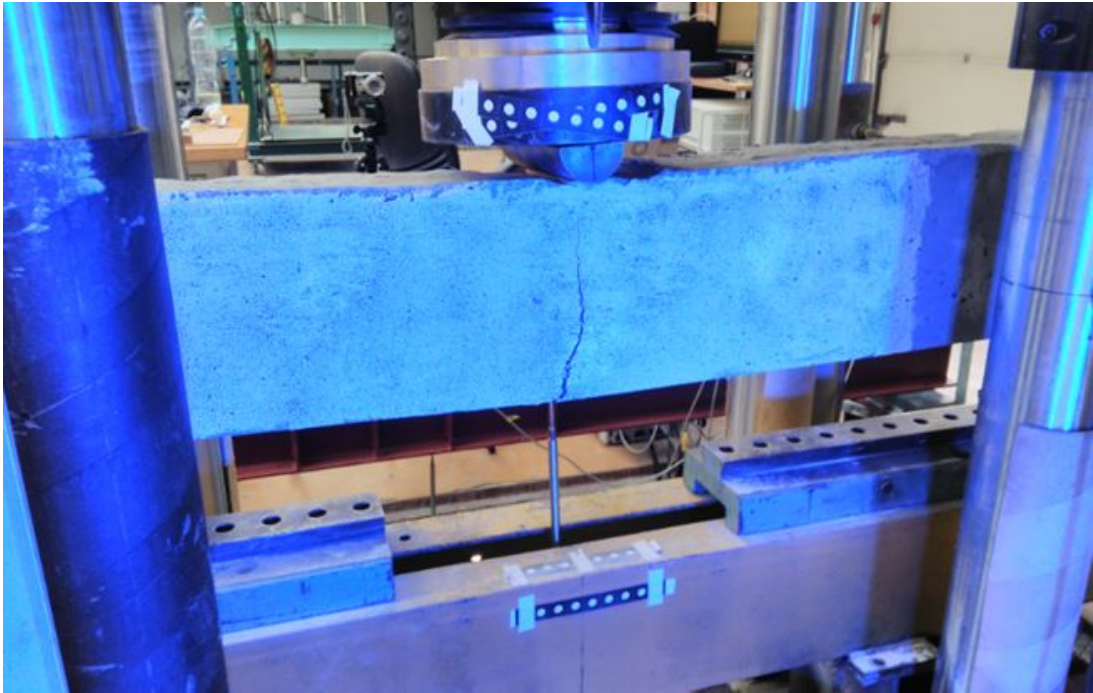


Fig. 4.56: The full-scale beam during testing – view from the side of ARAMIS

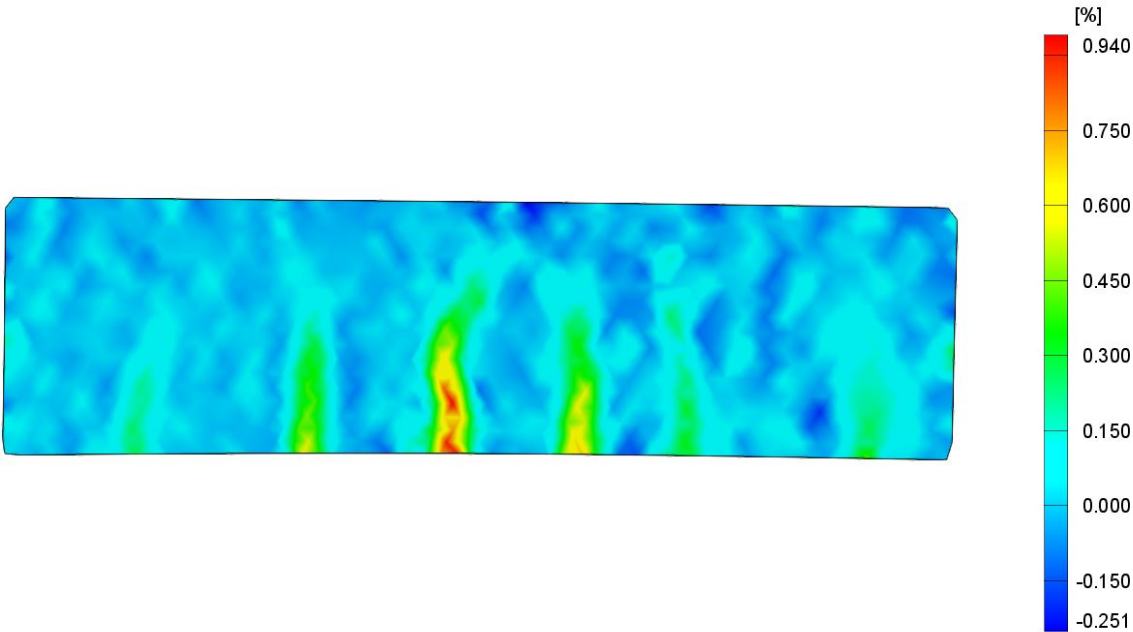


Fig. 4.57: Map of horizontal strain in beam I-2'-B1 after 5th cycle of loading

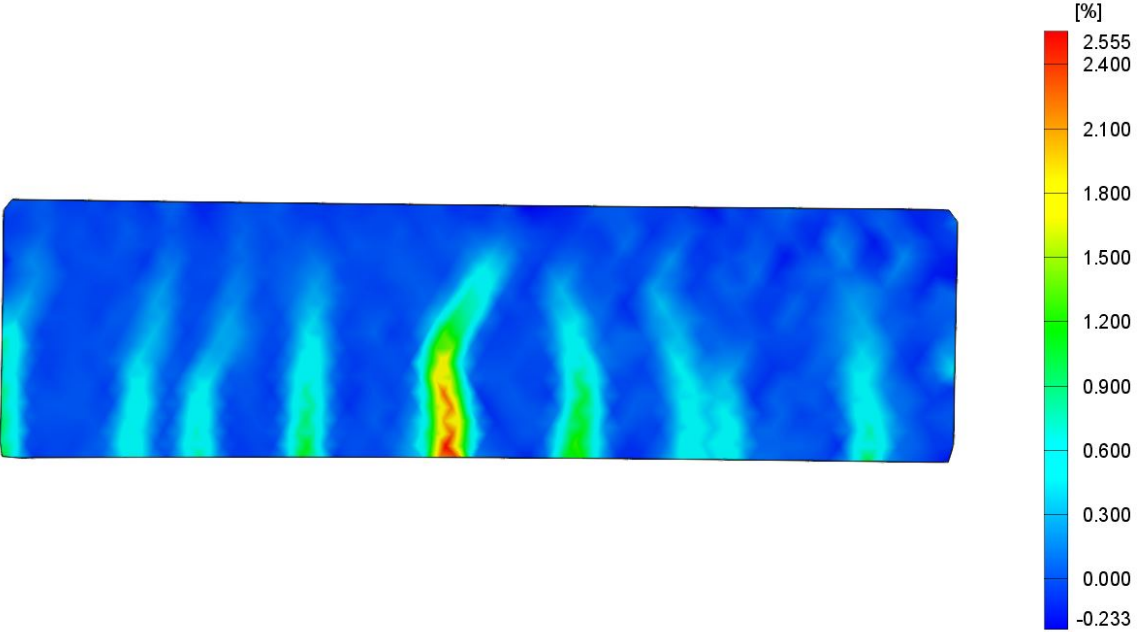
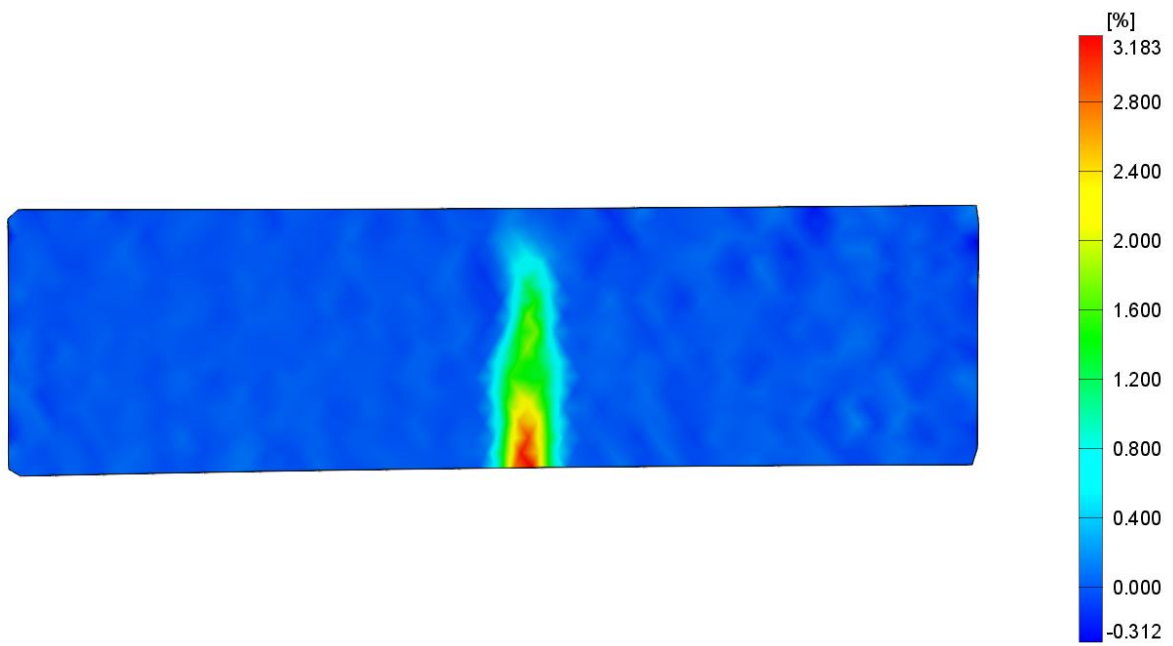
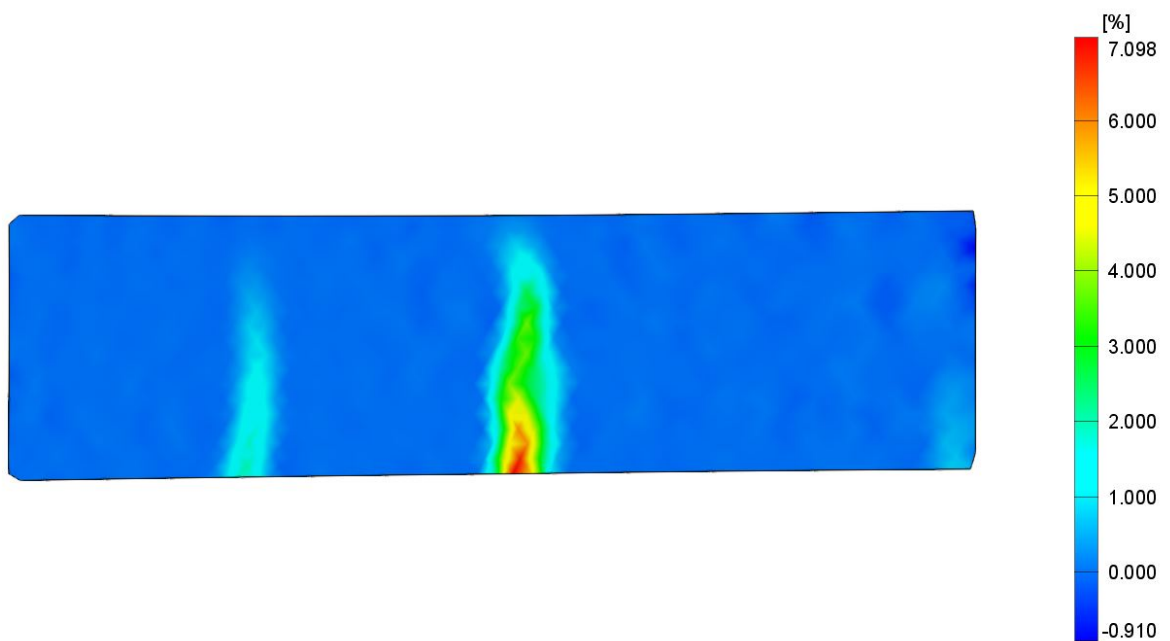


Fig. 4.58: Map of horizontal strain in beam I-2'-B1 after 10th cycle of loading



**Fig. 4.59:** Map of horizontal strain in beam I-2-B4 after 5th cycle of loading



**Fig. 4.60:** Map of horizontal strain in beam I-2-B4 after 10th cycle of loading

It is worth noting that there is a clear difference in horizontal strain distribution according to provided reinforcement. The presence of longitudinal steel bars results in cracks distributed along the beam (fig. 4.57, 4.58), whereas in beams where polypropylene fibres are the only one type of reinforcement we observe only one (optionally a few) greater, concentrated horizontal strains (fig. 4.59, 4.60). Maps for other beams are included in Appendix D of the thesis.



# Chapter 5

## Modelling

### 5.1 Formulation of the problem

The purpose of the analysis is to elaborate a computational model that will reflect properly the behaviour of polypropylene fibre reinforced high performance concrete beams.

The quasi-static deformation process considered is governed by the following system of equations:

- equilibrium equations (three partial differential equations):

$$\operatorname{div}\boldsymbol{\sigma} + \rho\ddot{\vec{u}} = \vec{0} \quad (5.1)$$

- linear strain-displacement equations (six partial differential equations):

$$\boldsymbol{\varepsilon} = \frac{1}{2}[\nabla\vec{u} + (\nabla\vec{u})^T] \quad (5.2)$$

- constitutive laws expressed here for linear elastic behaviour (six algebraic equations):

$$\boldsymbol{\sigma} = \mathbf{E} : \boldsymbol{\varepsilon} \quad (5.3)$$

which will be later on extended to the case of the elastic-plastic behaviour with damage.

In the above formulas the following notations are used:  $\boldsymbol{\sigma}$  is Cauchy stress tensor,  $\boldsymbol{\varepsilon}$  is the infinitesimal strain tensor,  $\vec{u}$  is the displacement vector,  $\rho$  is the mass density and  $\mathbf{E}$  denotes the fourth-order stiffness tensor.

The equations (5.1)-(5.3) should be complemented with proper boundary conditions to be imposed on the field of independent quantity which for the considered problem is the displacement field.

It should be noted that in case of concrete we are dealing with strong material non-linearity. Therefore, obviously constitutive laws (5.3) have to be modified. It is relevant to consider different fracture mechanisms under compression and tension, plastic properties

of material and those related to cracking degradation of stiffness. The complexity of the issue has caused the modelling of concrete to be the subject of interests for many scientists.

Before the compressive crushing occurs, the concrete is subjected to the plastic flow [137]. The theory of plasticity has undeniable advantage of taking into account permanent, irreversible strains. Therefore, the total strains may be expressed as the sum of elastic part (reversible one)  $\boldsymbol{\varepsilon}^{\text{el}}$  and plastic part (irreversible)  $\boldsymbol{\varepsilon}^{\text{pl}}$ :

$$\boldsymbol{\varepsilon} = \boldsymbol{\varepsilon}^{\text{el}} + \boldsymbol{\varepsilon}^{\text{pl}} \quad (5.4)$$

The limitation to plasticity in concrete modelling without considering microcracks and related to them material degradation would be inappropriate. Among many works about fracture mechanics and damage mechanics it is worth to mention about works of Bažant [25, 26], Peerlings [135], De Borst [42] and Geers [57]. As a pioneer in the Continuum Damage Mechanics (CDM) Kachanov [81] is considered. He assumed that damage can be represented by decreasing effective area. Introduced by Rabotnow damage indicator  $d$  (scalar damage variable) takes values from 0 (for non-damaged material) to 1 (for full-damaged material) and can be expressed by formula:

$$d = \frac{A_d}{A} \quad (5.5)$$

where  $A_d$  means area of damage whereas  $A$  is the area of whole section. In continuum damage mechanics calculation of stresses should be done with the effective area of section ( $\bar{A} = A - A_d$ ) taken into account. Thereby in equations (5.1) and (5.3) Cauchy tensor stress  $\boldsymbol{\sigma}$  should be substituted by effective tensor stress  $\bar{\boldsymbol{\sigma}}$ . The relation between them is easy to derive and looks as follows:

$$\bar{\boldsymbol{\sigma}} = \frac{\boldsymbol{\sigma}}{1 - d} \quad (5.6)$$

Currently in modelling of concrete the damaged plasticity mechanics is the most widely applied. This is a combination of plasticity theory (fig. 5.1a) and damage mechanics (fig. 5.1b). Schematically the idea of this coupling is shown in the figure 5.1c.

The finding a solution of described above task explicitly by integration of partial differential equations system is very difficult, if not impossible. Therefore it is appropriate to use an approximate numerical method, i.e. the finite element method (FEM) [197]. In this method the continuum is discretized into a finite number of smaller parts. Then the solution for each element is described with simple linear or quadratic equations, which are stitching back together to get the global solution. The main equilibrium equation (in the static case) can be written as:

$$\mathbf{K}\mathbf{q} = \mathbf{f} \quad (5.7)$$

where:  $\mathbf{K}$  is the stiffness matrix,  $\mathbf{q}$  is the vector (column matrix) of nodal displacements and  $\mathbf{f}$  contains nodal forces.

However, taking into account described above material non-linearity, the solution of the system of equations (5.7) can be ambiguous (stiffness matrix  $\mathbf{K}$  depends on nodal displacements  $\mathbf{q}$ ). Among methods to solve nonlinear equations the most popular are incremental iterative methods, e.g. Newton-Raphson method.

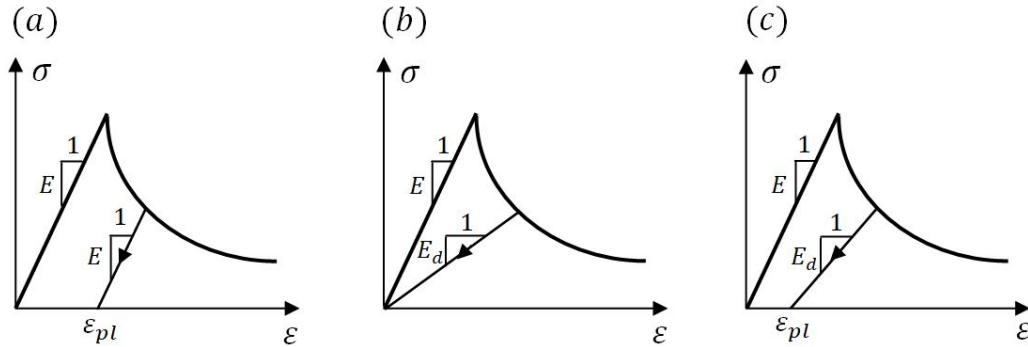


**Fig. 5.1:** The idea of coupling between plasticity and degradation: (a) plastic model, (b) degradation model, (c) plasticity-based damaged model

To sum up, the task is to determine appropriate constitutive law (5.3) including plasticity-based damage model of concrete in the way reflecting the behaviour of PFRHPC beams. We have decided to make use of the Concrete Damage Plasticity (CDP) model.

## 5.2 Model of the concrete

Concrete Damage Plasticity is one of the most widespread model based on the coupling between degradation and plasticity. The model, which was described by Lubliner [108], then developed by Lee and Fenves [100], is known in the literature also as *Barcelona model* - named after the town, where it was presented for the first time. Concrete Damage Plasticity is also one of the available concrete model in ABAQUS software [1]. The thorough interpretation of CDP parameters has been the subject of many researches [47, 77, 129, 137, 167, 169].

Among the main assumptions of Concrete Damage Plasticity model related to the theory of plasticity following should be listed:

- the incremental theory of plasticity is used, therefore the strain rate can be decomposed into elastic strain rate and plastic strain rate:

$$\dot{\varepsilon} = \dot{\varepsilon}^{\text{el}} + \dot{\varepsilon}^{\text{pl}} \quad (5.8)$$

- the plastic flow and the yield function are described by invariants of effective stress tensor  $\bar{p}$  (the hydrostatic pressure stress) and  $\bar{q}$  (von Mises equivalent effective stress):

$$\bar{p} = \frac{1}{3} \bar{\sigma} : \mathbf{I} \quad \bar{q} = \sqrt{\frac{3}{2} \bar{\mathbf{S}} : \bar{\mathbf{S}}} \quad (5.9)$$

where  $\mathbf{I}$  means identity matrix and  $\bar{\mathbf{S}}$  is the effective stress deviator:

$$\bar{\mathbf{S}} = \bar{\boldsymbol{\sigma}} + \bar{p} \mathbf{I} \quad (5.10)$$

- the plastic flow is non-associated (fig. 5.2) and the relationship between the plastic strain rate and the plastic potential function  $G$  is described by:

$$\dot{\varepsilon}^{\text{pl}} = \dot{\lambda} \frac{\partial G(\bar{\sigma})}{\partial \bar{\sigma}} \quad (5.11)$$

where:  $\dot{\lambda}$  is nonnegative plastic multiplier. The assumption of non-associated plastic flow leads to nonsymmetrical material stiffness matrix [1].

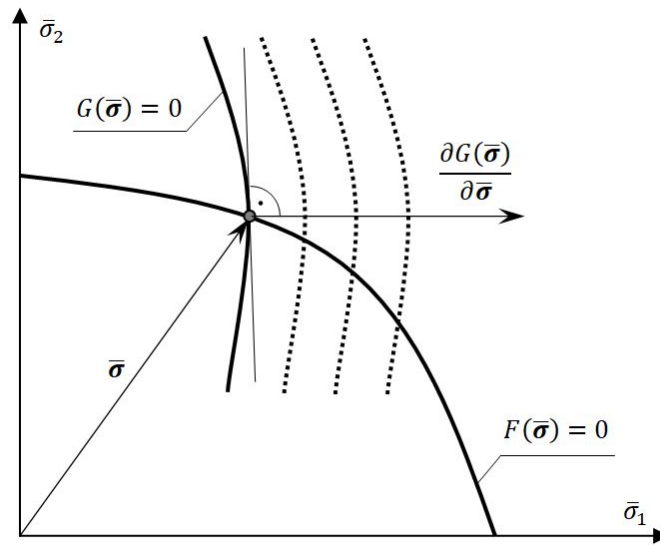


Fig. 5.2: Non-associated plastic flow [137]

- the plastic potential function  $G$  is the Drucker-Prager hyperbolic function:

$$G = \sqrt{(\epsilon \sigma_{t0} \tan \Psi)^2 + \bar{q}^2} - \bar{p} \tan \Psi \quad (5.12)$$

where:  $\epsilon$  is a parameter, referred to as the eccentricity, that defines the rate at which the function approaches the asymptote,  $\sigma_{t0}$  is the uniaxial tensile stress at failure and  $\Psi$  is the dilation angle measured in the  $p - q$  plane at high confining pressure. The hyperbolic surface of plastic potential in meridional plane and the physical interpretation of the eccentricity  $\epsilon$  and the dilation angle  $\Psi$  is depicted in the figure 5.3. It is apparent that smaller magnitudes of eccentricity result in plastic potential function is approaching to linear.

- the yield function is expressed by formula:

$$F(\bar{\sigma}, \tilde{\varepsilon}^{\text{pl}}) = \frac{1}{1 - \alpha} (\bar{q} - 3\alpha\bar{p} + \beta(\tilde{\varepsilon}^{\text{pl}}) \langle \hat{\sigma}_{max} \rangle - \gamma(-\hat{\sigma}_{max})) - \bar{\sigma}_c(\tilde{\varepsilon}_c^{\text{pl}}) \quad (5.13)$$

where:

$$\alpha = \frac{(\sigma_{b0}/\sigma_{c0}) - 1}{2(\sigma_{b0}/\sigma_{c0}) - 1} \quad 0 \leq \alpha \leq 0.5 \quad (5.14)$$

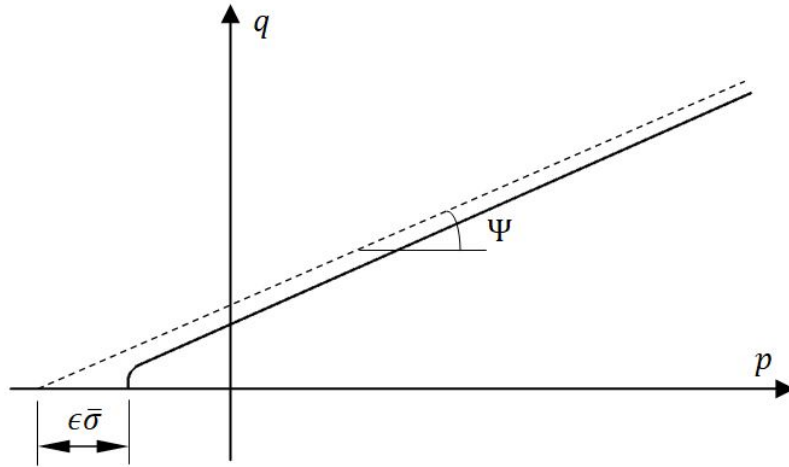


**Fig. 5.3:** The physical interpretation of the eccentricity  $\epsilon$  and the dilation angle  $\Psi$

$$\beta(\hat{\epsilon}^{\text{pl}}) = \frac{\bar{\sigma}_c(\hat{\epsilon}_c^{\text{pl}})}{\bar{\sigma}_t(\hat{\epsilon}_t^{\text{pl}})}(1 - \alpha) - (1 + \alpha) \quad (5.15)$$

$$\gamma = \frac{3(1 - K_c)}{2K_c - 1} \quad (5.16)$$

In the above formulas  $\hat{\sigma}_{max}$  denotes the maximum principal effective stress,  $\sigma_{b0}/\sigma_{c0}$  is the ratio of initial equibiaxial compressive yield stress to initial uniaxial compressive yield stress and  $K_c$  means the ratio of the second stress invariant on the tensile meridian to that on the compressive meridian at initial yield for any given value of the pressure invariant  $p$  such that the maximum principal stress is negative [1]. The magnitude of  $K_c$  should be between 0.5 and 1.0. The influence of this coefficient on the shape of deviatoric cross section of failure surface is presented in the figure 5.4, where two cross sections for  $K_c = 1.00$  and  $K_c = 0.667$  (the later is default according to [1]) are shown. By  $\bar{\sigma}_c(\hat{\epsilon}_c^{\text{pl}})$  and  $\bar{\sigma}_t(\hat{\epsilon}_t^{\text{pl}})$  effective compressive and tensile cohesion stresses were denoted, respectively. In the case of biaxial compression (when the maximum principal effective stress  $\hat{\sigma}_{max} = 0$ ) the yield condition (5.13) is reduced into Drucker-Prager condition.

The yield function  $F$  (eq. 5.13) as well as the plastic multiplier  $\dot{\lambda}$  (in eq. 5.11) are to satisfy Kuhn-Trucker conditions (loading/unloading conditions) [91]:

$$\dot{\lambda}F = 0 \quad \dot{\lambda} \geq 0 \quad F \leq 0 \quad (5.17)$$

It is worth to mention that the state of knowledge about plasticity parameters in CDP model is still developing. For example, the modification of flow rule and proposition of a new plastic potential as the extension of Concrete Damage Plasticity was the subject of consideration in [169].

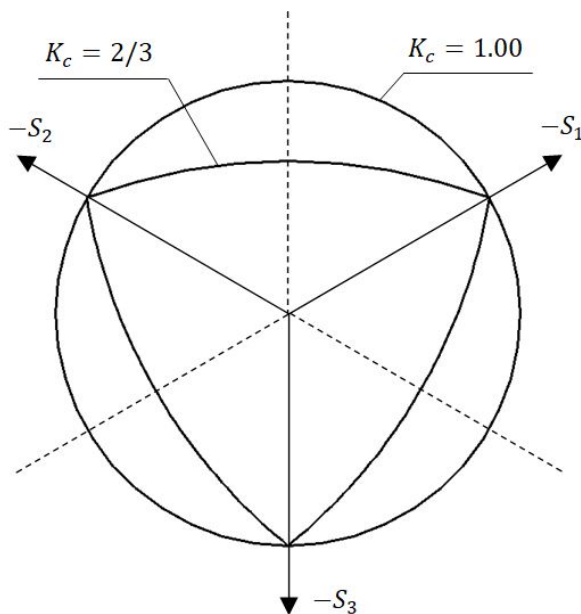


**Fig. 5.4:** Yield surfaces in the deviatoric plane [1]

**Tab. 5.1:** Applied Concrete Damage Plasticity parameters

Dilatation angle	Eccentricity	$f_{b0}/f_{c0}$	$K$	Viscosity parameter
30	0.08	1.16	0.667	0.0001

The last but not least plasticity parameter required to define Concrete Damage Plasticity model in Abaqus software is the viscosity parameter (relaxation time). By default it could be taken as zero, but according to [167] the value of 0.0001 is recommended.

The values of plasticity parameters used in this work are presented in table 5.1. It is worth to mention that obtained results very often crucially depends on their magnitudes [78]. The strong influence of dilation angle and viscosity parameter is presented in [167].

In Concrete Damage Plasticity model two different damage mechanisms are considered: tensile cracking and compressive crushing of concrete. Each of them is described by independent damage parameter: scalar compression damage variable  $d_c$  and scalar tension damage variable  $d_t$ . The proper determination of the scalar damage variables is important in order to extract the plastic part from inelastic strains. The graphic definition of inelastic and plastic strains is presented in figures 5.6 and 5.7 for compression and tension, respectively.

Compressive inelastic strain can be calculated as:

$$\tilde{\varepsilon}_c^{\text{in}} = \varepsilon_c - \varepsilon_{0c}^{\text{el}} \quad (5.18)$$

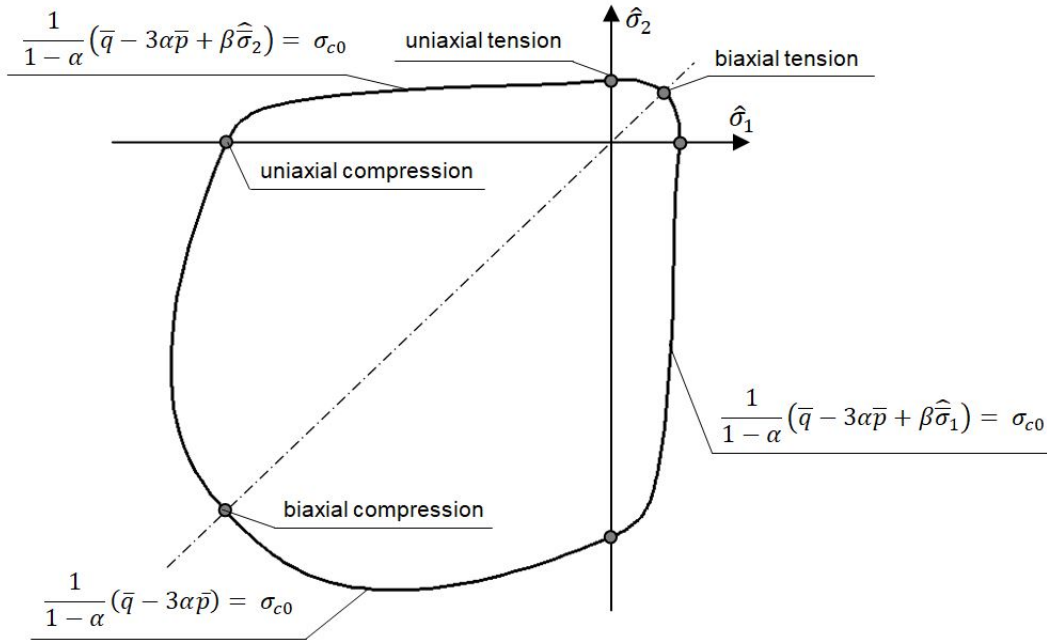


**Fig. 5.5:** Yield surface in plane stress [1]

where  $\varepsilon_c$  denotes total compressive strain and  $\varepsilon_{0c}^{\text{el}}$  means elastic one calculated as:

$$\varepsilon_{0c}^{\text{el}} = \frac{\sigma_c}{E_0} \quad (5.19)$$

in which  $\sigma_c$  is compressive stress and  $E_0$  is initial elastic modulus of undamaged concrete.

In order to get the plastic strain  $\tilde{\varepsilon}_c^{\text{pl}}$  we have to subtract from inelastic strain  $\tilde{\varepsilon}_c^{\text{in}}$  the difference between  $\varepsilon_c^{\text{el}}$  and  $\varepsilon_{0c}^{\text{el}}$ :

$$\tilde{\varepsilon}_c^{\text{pl}} = \tilde{\varepsilon}_c^{\text{in}} - (\varepsilon_c^{\text{el}} - \varepsilon_{0c}^{\text{el}}) \quad (5.20)$$

On the ground of figure 5.6 the following can be written:

$$\frac{\sigma_c}{\varepsilon_c^{\text{el}}} = (1 - d_c)E_0 \quad \Rightarrow \quad \varepsilon_c^{\text{el}} = \frac{\sigma_c}{E_0(1 - d_c)} \quad (5.21)$$

$$\frac{\sigma_c}{\varepsilon_{0c}^{\text{el}}} = E_0 \quad \Rightarrow \quad \varepsilon_{0c}^{\text{el}} = \frac{\sigma_c}{E_0} \quad (5.22)$$

By putting (5.21) and (5.22) into (5.20) we get the compressive plastic strain as a function of the scalar compression damage variable:

$$\tilde{\varepsilon}_c^{\text{pl}} = \tilde{\varepsilon}_c^{\text{in}} - \frac{d_c}{1 - d_c} \frac{\sigma_c}{E_0} \quad (5.23)$$

In the similar way the formula for tensile plastic strain can be derived:

$$\tilde{\varepsilon}_t^{\text{pl}} = \tilde{\varepsilon}_t^{\text{ck}} - \frac{d_t}{1 - d_t} \frac{\sigma_t}{E_0} \quad (5.24)$$

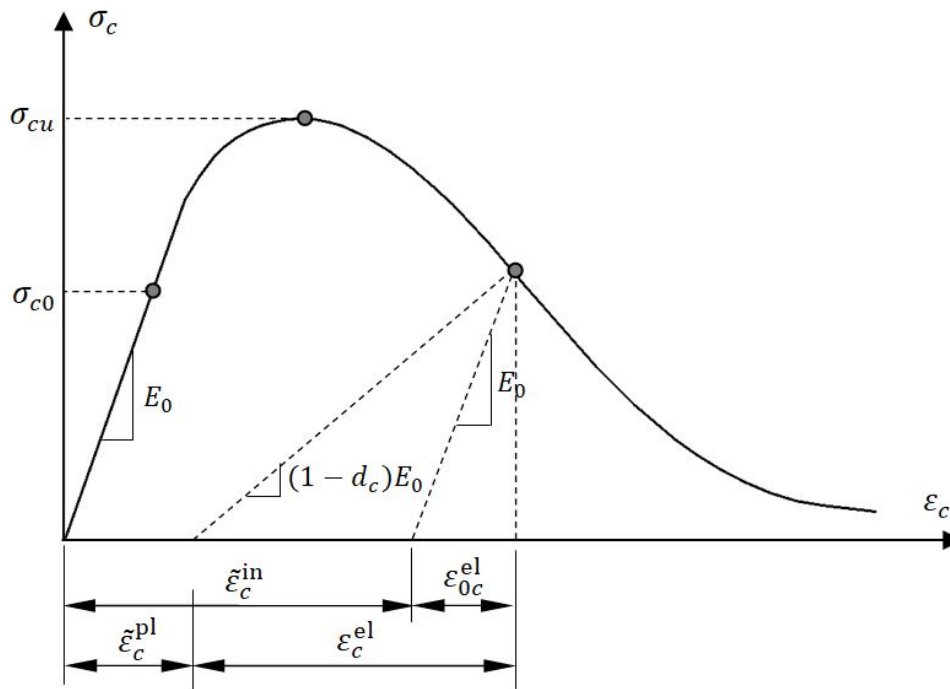


Fig. 5.6: General stress-strain relation for concrete in compression [1]

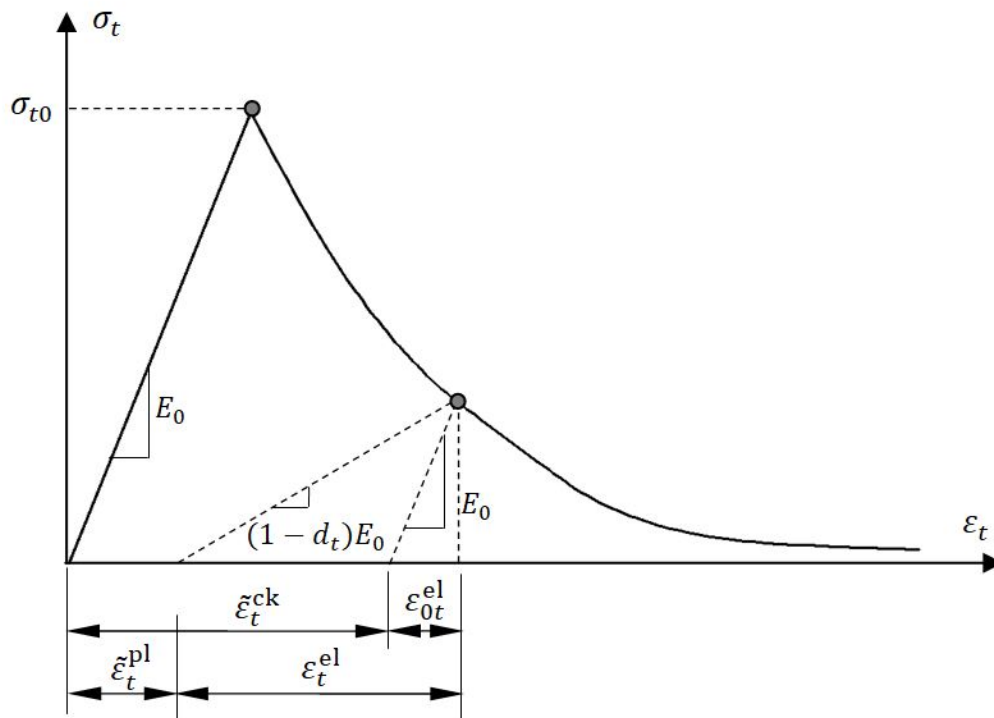
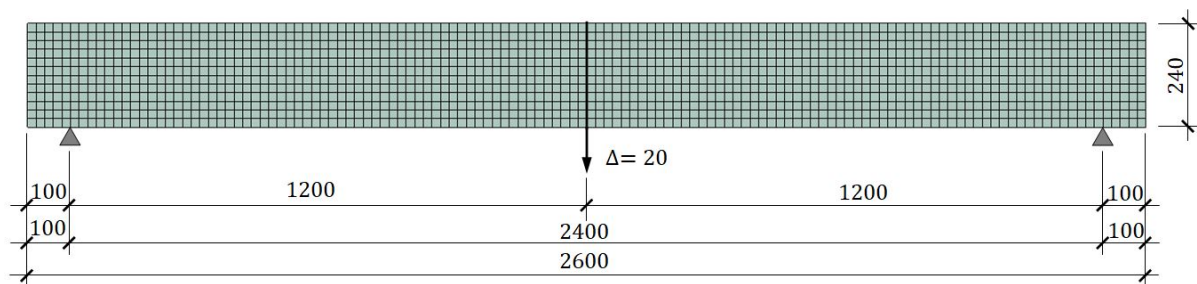


Fig. 5.7: General stress-strain relation for concrete in tension [1]

### 5.3 Computational model

In order to deal with problem described in section 5.1, ABAQUS software suite by Dassault Systems SIMULIA (version 6.19) was employed.

The simply supported PFRHPC beam model is defined. The concrete beam is modelled as deformable shell part with total length of 2600 mm (effective length of the span equals 2400 mm) and the height of the section of 240 mm, whereas the shell tickness equals 120 mm. Two layers (top and bottom) of longitudinal reinforcement as truss wire embedded in concrete region was included in the model. The provided area of each wire was taken as the area of two bars with the diameter of 8 mm. Boundary conditions are imposed on vertical displacements at the ends as shown in figure 5.8. As loading, the mid-span deflection of 20 mm is taken. Based on the convergence test, the size of finite elements was assumed as 20 mm. The concrete is modelled by using four noded plain strain element with reduced integration formulation (CPE4R), whereas steel bars embedded in concrete by two-noded truss (T2D2) elements. The discretization of the structure with the boundary conditions and geometric parameters are depicted in figure 5.8.



**Fig. 5.8:** Geometric parameters of the computational model (dimensions in mm)

In the future work the author would like to prepare model which reflects the loading and unloading process in PFRHPC beams. Then there is a need to model the rigid pin and the contact parameters between the pin and the upper surface of beam. Taking into account material non-linearity the issue appears to be much more complex than it might seem. In the computational part of the dissertation the attention was mainly paid to modelling of beams under monotonous loading.

When it comes to the model of the concrete the determination of plasticity parameters (which were described in section 5.2) is not the only one task in the process of material model preparation. In order to get the full definition of Concrete Damage Plasticity model the stress-strain relation as a set of points for compression as well as for tension should be input.

There are, of course, many different propositions of description of the nonlinear behaviour of concrete like according to Madrid parabola, Desay & Krishnan formula, Majewski formula [110] or Wang & Hsu formula [182]. One of the very detailed proposition of stress-strain relation with a 3rd order polynomial in the denominator is proposed by Saenz [89].

After studying few of them the relationship between compressive stress and strain in

the analysis was taken according to EN 1992-1-1 [210] and can be presented by formula:

$$\sigma_c = f_{cm} \frac{k\eta - \eta^2}{1 + (k-2)\eta} \quad (5.25)$$

where:

$$k = 1.05 E_{cm} \frac{\varepsilon_{c1}}{f_{cm}} \quad \eta = \frac{\varepsilon_c}{\varepsilon_{c1}} \quad (5.26)$$

When it comes to definition of stress-strain relation for tension, according to ABAQUS user's manual the reduction of stresses after reaching the tensile strength can be assumed as a linear for the total strain ten times higher than strain corresponded to the moment of reaching the tensile strength [1, 89]. On the other hand, in the literature some better more accurate propositions can be found like for instance one described by formulas:

$$\sigma_t = E_c \varepsilon_t \quad \text{if } \varepsilon_t \leq \varepsilon_{cr} \quad (5.27)$$

$$\sigma_t = f_{cm} \left( \frac{\varepsilon_{cr}}{\varepsilon_t} \right)^{0.4} \quad \text{if } \varepsilon_t > \varepsilon_{cr} \quad (5.28)$$

The exponent in the formula (5.28) can be replaced by any other fraction  $n$ . Then the expression (5.28) takes the form:

$$\sigma_t = f_{cm} \left( \frac{\varepsilon_{cr}}{\varepsilon_t} \right)^n \quad \text{if } \varepsilon_t > \varepsilon_{cr} \quad (5.29)$$

what was used in the calibration of the model in this work. The provided relations between tensile stresses and strains for concrete with and without polypropylene fibres are presented in figure 5.9. The tensile strengths of concrete were calculated on the ground of results of own laboratory beams testing and equal 7.26 MPa and 8.44 MPa for the case without and with polypropylene fibres, respectively. The magnitudes of exponent in equation 5.29 were taken finally as  $n = 1.00$  for the case without polypropylene fibres and  $n = 0.5$  when they are present.

Naturally force-displacement results from this analysis should not be compared directly with results of experimental research, when the procedure of testing assumed loading-unloading cycles. Nevertheless, there is a quite good correlation between force corresponded to 20 mm mid-span deflection: according to numerical analysis the value for the case with PP fibres equals 34.195 kN (whereas in experiments was on the level of 33.116 kN). In case of lack of PP fibres magnitudes of forces according to ABAQUS and experimental research equal 25.833 kN and 25.318 kN, respectively. Results obtained from numerical analysis are slightly greater than from experiments, what is in line with expectations.

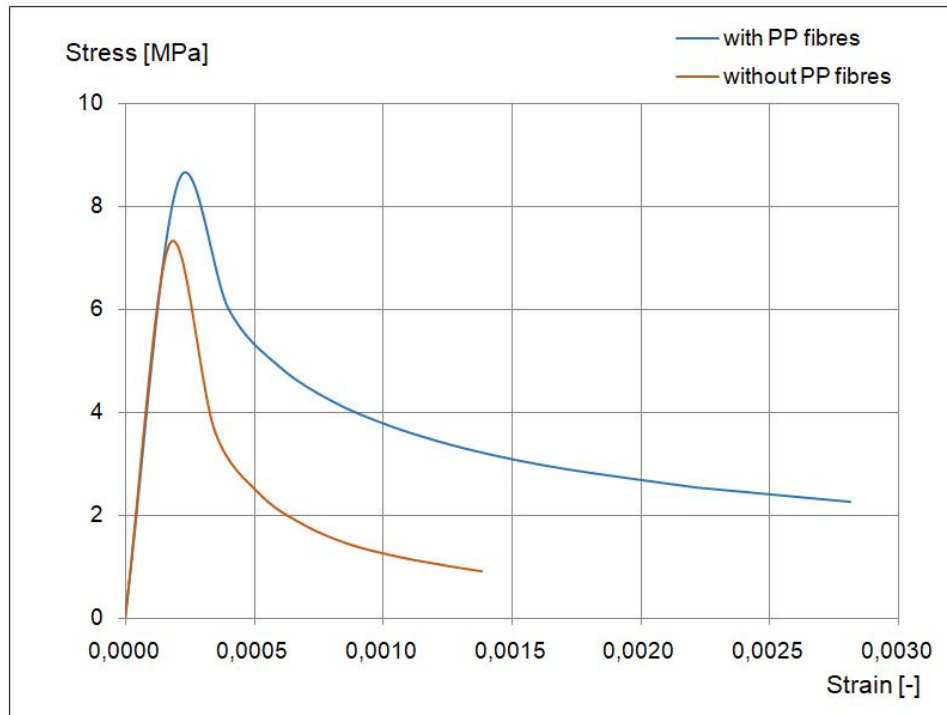


Fig. 5.9: Tensile stress-strain relations provided in the analysis

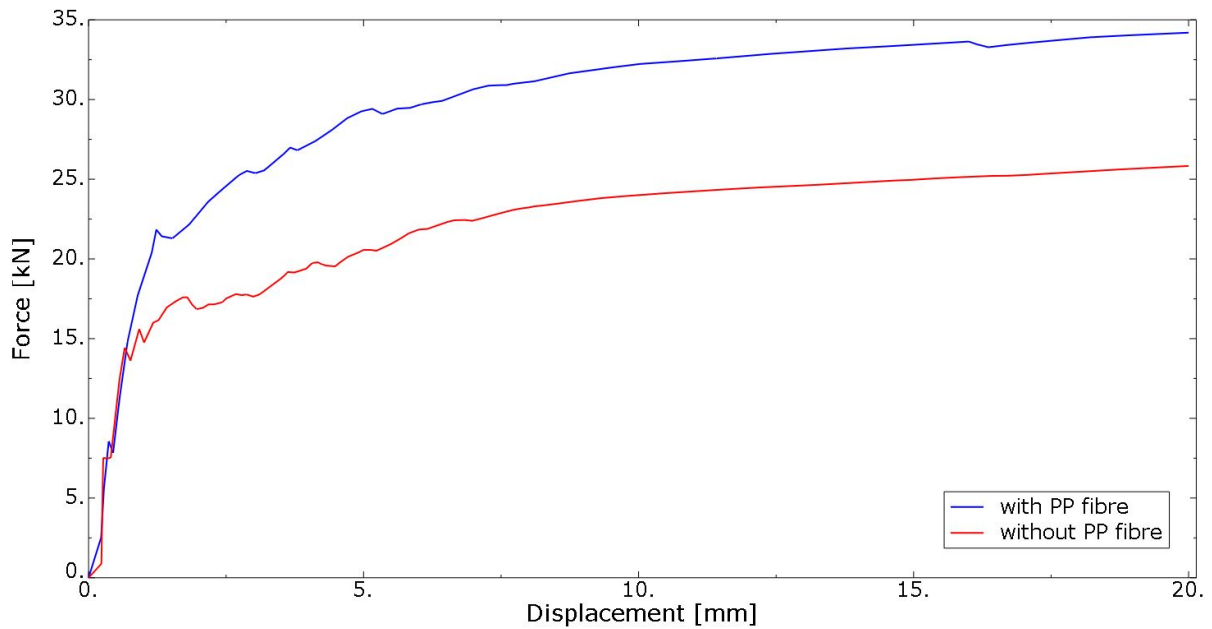


Fig. 5.10: Force-displacement graphs obtained in the analysis

## 5.4 Convergence test

It is well-known that the size of the finite element can have a considerable effect on the results of FEM analysis. Therefore, in the work mesh-sensitivity verification was carried out. Four different sizes of a finite element mesh were taken into consideration: 80 mm, 40 mm, 20 mm and 10 mm (fig. 5.11). Figure 5.12 presents the force-displacement graphs obtained with different meshing size for polypropylene fibre reinforced beam subjected to monotonous loading with the mid-span deflection of 20 mm.

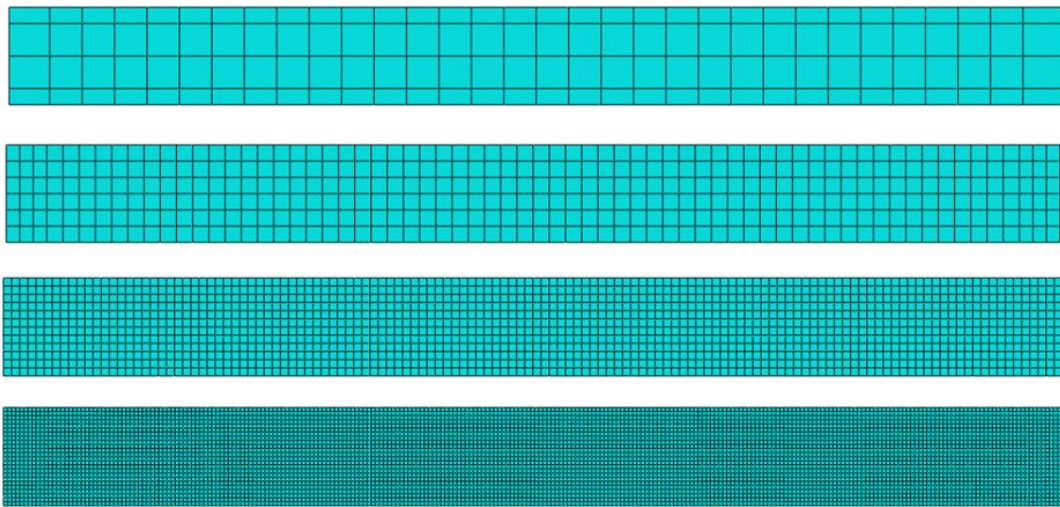


Fig. 5.11: Different density of meshes with FE size: 80 mm, 40 mm, 20 mm, 10 mm

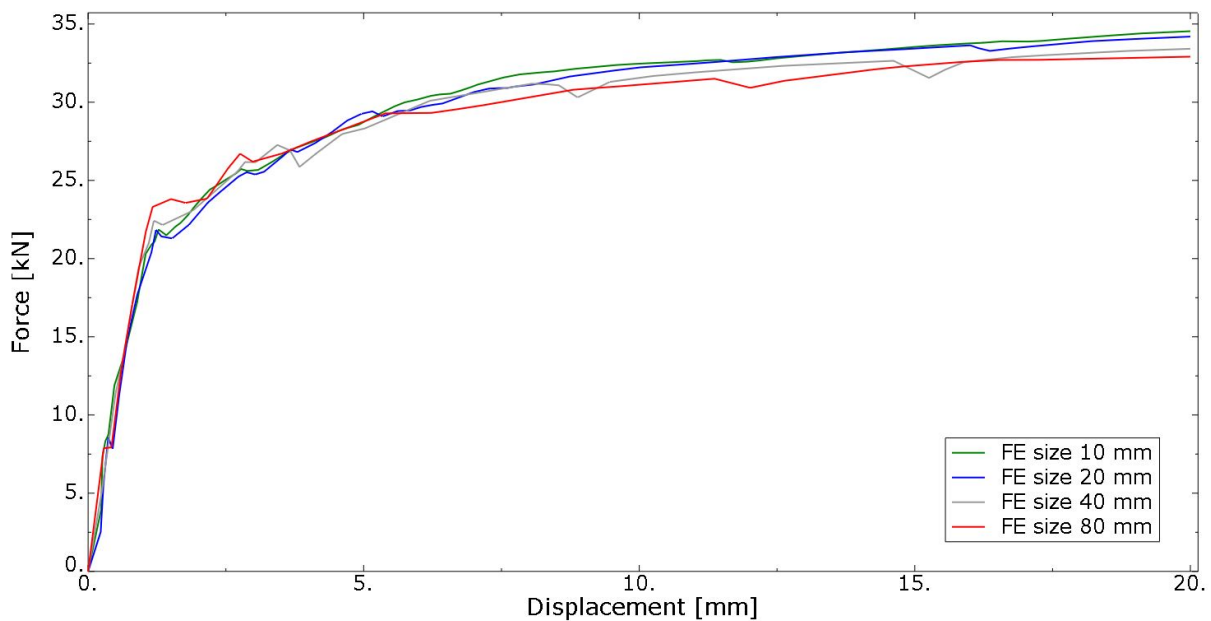


Fig. 5.12: Force-displacement graphs for different FE size: 80 mm, 40 mm, 20 mm, 10 mm

As can be seen in figure 5.12 the coarse mesh (FE size of 80 mm) generates the less regular force-displacement graph. The finer mesh will result in the smoothing of the graph and increase of the force in the final stage of loading. Although, in the first part of the force displacement graph the overrating of the force can be noticed in the case of coarse mesh. There is no great difference in results when 10 mm and 20 mm mesh is compared - on the other hand the time of calculation is significantly longer in the case of finer mesh. Therefore in the analysis 20 mm was taken as the size of finite element.



## Chapter 6

# Ductility of PFRHPC beams

### 6.1 Measurements of ductility

The ductility (the opposite of brittleness) is the mechanical property, which describes the ability of structure to undergo large plastic deformations prior to failure. This feature has obviously many references in metal science. In the case of concrete the brittle nature is one of the biggest material weakness and there is hard to say about any ductility. The problem is much more demanding in the consideration of high performance/strength concrete: the higher compressive strength, the material is more brittle. The application of fibre reinforcement in concrete mix allows one to overcome or at least diminish this downside. In such circumstances the question arises how to measure the ductility of fiber reinforced high performance concrete beams.

One of the basic measurement of ductility is the **ductility factor**  $\mu$ , which can be expressed in terms of deflection, curvature or rotational ductility [192]. Considering deflection ductility the factor can be presented as ratio of mid-span deflection at the peak load  $\delta_p$  to mid-span deflection at the steel rebar yielding  $\delta_y$ :

$$\mu = \frac{\delta_p}{\delta_y} \quad (6.1)$$

In the literature some other propositions of expression of ductility factor can be found. For example, according to [157] the mid-span deflection at the peak load  $\delta_p$  from the equation (6.1) is replaced by the mid-span deflection at the ultimate limit state  $\delta_u$ :

$$\mu = \frac{\delta_u}{\delta_y} \quad (6.2)$$

The deflection at the ultimate limit state also has got different interpretations in different works. Whereas in [157]  $\delta_u$  is defined as the deflection corresponding to 80% of peak load along the descending branch of force-displacement curve, by some other researchers [188] is treated as deflection corresponding to sharp decrease on the force-displacement curve. These different interpretations of mid-span deflection at the ultimate

limit state  $\delta_u$  are reasonable if we take into account different possible force-displacement paths (fig. 6.1).

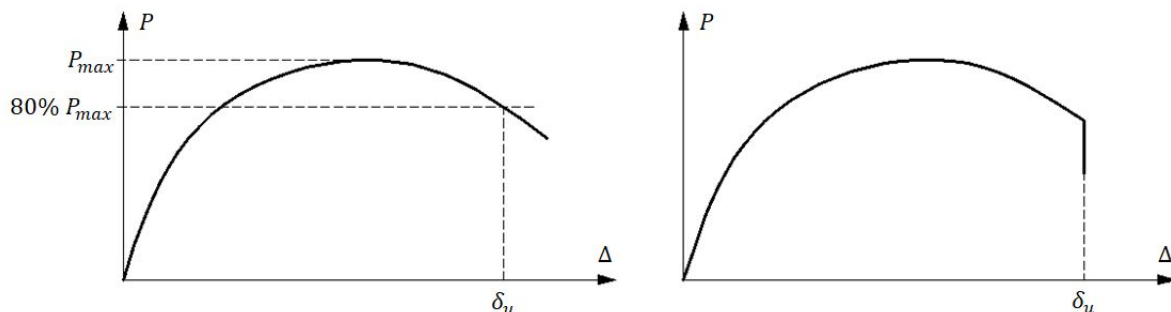


**Fig. 6.1:** Different interpretations of  $\delta_u$  regarding force-displacement path

As another measurement of ductility, **fracture energy**  $G_f$  can be considered. It is calculated as the area under the force-displacement curve divided by the area of specimen cross-section:

$$G_f = \frac{1}{bh} \int_0^{\delta_B} P d\Delta \quad (6.3)$$

where:  $b$  and  $h$  denotes the width and the height of the sample, respectively. Generally, the fracture energy is perceived as energy required to separate specimen [107] - then the upper limit of integration  $\delta_B$  in formula (6.3) is taken as the displacement where the sample is broken ( $\delta_B = \delta_u$ ). The greater fracture energy can be interpreted as the greater ductility. However, it is worth noting we do not consider which part of area under force-displacement graph is before and after peak of load. It is very common to test beams with the notch - then the height of the section  $h$  in the formula (6.3) should be reduced by the height of the notch.

Two different measurements using fracture energy and material properties are found in practice: characteristic length  $l_{ch}$  and ductility length  $D_l$ .

The **characteristic length**  $l_{ch}$  according to Hillerborg's definition can be perceived as half the length of a tensile bar, being able to store the same amount of elastic energy as dissipated in the fracture process [107]. The higher values of characteristic length describe ductile materials, whereas the small ones are related to the brittle materials. The characteristic length can be calculated by the formula:

$$l_{ch} = \frac{G_f E}{f_{ct}^2} \quad (6.4)$$

The ratio of fracture energy  $G_f$  to tensile strength  $f_{ct}$  is called as the **ductility length**:

$$D_l = \frac{G_f}{f_{ct}} \quad (6.5)$$

In a significant number of works, where the ductility of fibre reinforced concrete beams is investigated, researchers use toughness indices. There is obviously the difference between

*ductility* and *toughness* - one could say *toughness* is a more general term - it refers to the ductility and to the strength as well. Nevertheless, the wide range of applications of ASTM C1018 method [201] and JSCE SF-4 method [211] allows one to treat toughness indices as ductility measurements.

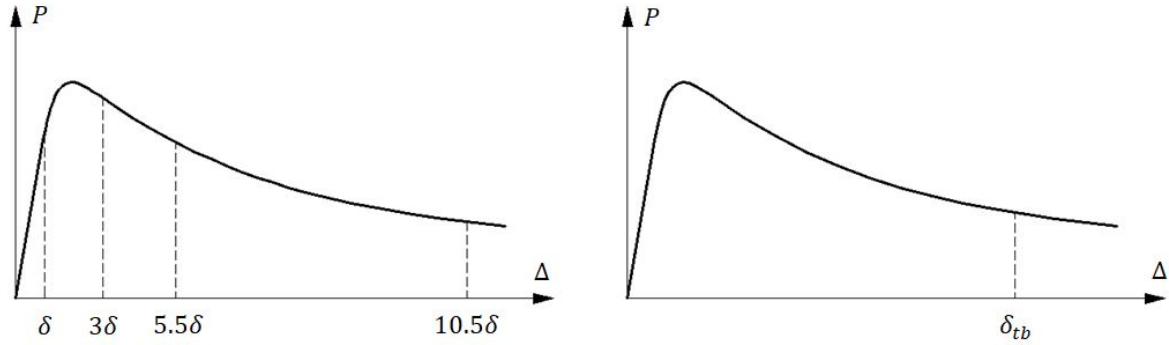


**Fig. 6.2:** Force-displacement graphs with marked important deflections according to (on the left:) ASTM C1018 [201] and (on the right:) JSCE SF-4 [211]

According to ASTM C1018 [201] we can distinguish three different toughness indices:  $I_5$ ,  $I_{10}$  and  $I_{20}$ . They can be calculated as the ratios of the area under force-displacement curve up to 3, 5.5 and 10.5 times the first crack displacement respectively, divided by the area up to the first crack displacement [21]. The load-displacement graph with marked important points according to ASTM C1018 [200] is on the left of the figure 6.2. The toughness indices can be expressed as:

$$I_5 = \frac{\int_0^{3\delta} Pd\Delta}{\int_0^{\delta} Pd\Delta}, \quad I_{10} = \frac{\int_0^{5.5\delta} Pd\Delta}{\int_0^{\delta} Pd\Delta}, \quad I_{20} = \frac{\int_0^{10.5\delta} Pd\Delta}{\int_0^{\delta} Pd\Delta} \quad (6.6)$$

The labelling of individual toughness indices could be the source of consternation on first sight. The subscripts 5, 10 and 20 appear to have no relevance to multiples of deflection at the linear elastic limit  $\delta$  ( $3\delta$ ,  $5.5\delta$  and  $10.5\delta$ , respectively). The explanation is as follows: in the case of elastic brittle material all indices:  $I_5$ ,  $I_{10}$  and  $I_{30}$  should equal 1 [102], whereas for the elastic-ideal plastic material should be equaled to 5, 10 and 30, respectively [21].

The method of test flexural toughness JSCE-SF4 has also many references in literature. There is worth mentioning that despite the fact that the Standard [211] is dedicated to testing steel fibre reinforced concrete, the method is also adopted by many scientists in experimental research of different fibre reinforcement. In this method there is only one point marked on the deflection axis and it depends on the length of the span (right part of the fig. 6.2).

The flexural toughness according to JSCE-SF4 [211] can be expressed as:

**Tab. 6.1:** Toughness indices  $I_5$ ,  $I_{10}$  and  $I_{20}$  according to ASTM C1018 [200]

Variant	No. of specimen	$I_5$	$I_{10}$	$I_{20}$
I-2	I-2-b1	4.36	9.67	21.10
	I-2-b2	4.50	10.17	21.96
	I-2-b3	4.41	9.57	20.04
	<b>Mean value</b>	<b>4.42</b>	<b>9.80</b>	<b>21.03</b>
	Stand. deviation	0.07	0.32	0.96
	Coef. of variation	1.6%	3.3%	4.6%

$$T_b = \int_0^{\delta_{tb}} P d\Delta \quad (6.7)$$

where  $\delta_{tb}$  depends on the length of span  $l$  according to formula:

$$\delta_{tb} = \frac{l}{150} \quad (6.8)$$

The flexural toughness factor according to JSCE-SF4 [211] can be calculated by using the following formula:

$$\bar{\sigma}_b = \frac{T_b}{\delta_{tb}} \frac{l}{bh^2} \quad (6.9)$$

## 6.2 Ductility of laboratory beams (10x10x50cm)

The influence of polypropylene fibres on ductility is clearly evident in the force-displacement relationship. In figure 4.38 (section 4.7 of the thesis) force-displacement graphs in laboratory beams (10x10x50 cm) with (1-2-(b1-b3)) and without (I-3-(b1-b3)) polypropylene fibres are shown. The change of failure mechanism from the brittle one into ductile one can be observed. For abovementioned variants toughness indices according to ASTM C1018 [201] and JSCE SF-4 [211] are calculated. In the table 6.1 results of calculation based on American standard are catalogued. The magnitudes of  $I_5$ ,  $I_{10}$  and  $I_{20}$  were obtained on the basis of formula 6.6. Taking into account the fact that value of 1.0 represents brittle material and 5, 10 and 20, respectively the ideal-plastic material the great improvement of ductility can be noticed. The table 6.2, which contains the results of calculation according to JSCE SF-4 [211], allows us to come to a similar conclusion.

**Tab. 6.2:** Flexural toughness  $T_b$  [Nm] and flexural toughness factor  $\bar{\sigma}_b$  [MPa] based on JSCE SF-4 [211] in laboratory beams (10x10x50cm)

Variant	No. of specimen	$T_b$	$\bar{\sigma}_b$
I-2	I-2-b1	30.47	4.57
	I-2-b2	28.17	4.23
	I-2-b3	26.53	3.98
	<b>Mean value</b>	<b>28.39</b>	<b>4.26</b>
	Stand. deviation	1.98	0.30
	Coef. of variation	7.0%	7.0%

### 6.3 Ductility of full-scale beams (12x24x260cm)

For all tested full-scale beams the following basic measurements of ductility were determined: fracture energy  $G_f$  (according to formula 6.3), characteristic length  $l_{ch}$  (according to formula 6.4) and ductility length  $D_l$  (according to formula 6.5).

In tested beams due to the presence of reinforcement and high ductility no fragmentation of sample can be observed even when the mid-span deflection reaches 1/30 of the length span. Therefore in the calculation of fracture energy the upper limit of integration  $\delta_B$  was assumed as constant and determined as 40 mm, which corresponds to the fraction of 1/60 of the effective length span.

The results of calculation with standard deviations and coefficients of variation are catalogued in table 6.3, whereas in figures 6.3, 6.4 and 6.5, column diagrams of mean values of fracture energy, characteristic length and ductility length are presented, respectively.

In addition the calculation of toughness indices according to JSCE SF-4 was carried out. The results of this computing are catalogued in table 6.4.

The fracture energy exceeds 40 kN/m in the case of beams with both reinforcement (PP fibres + longitudinal steel bars with diameter of 8 mm) concreted in the laboratory. When industrial conditions are taken into account, the results are slightly smaller (35.84 and 37.53 kN/m), whereas a considerable difference can be noticed in cases with one type of reinforcement. The fracture energy when only fibres are provided (variant I-2) is over two times smaller, on the other hand in variant with steel reinforcement without fibres (variant I-3') the fracture energy is at the level of 31.76 kN/m. It could be concluded that in this research the addition of polypropylene fibres into the concrete mix results in the one-third increase of fracture energy.

The similar tendencies can be observed in results of characteristic length and ductility length, which is not surprising considering that both of abovementioned ductility measures are functions of the fracture energy.

It is worth to take a look on the flexural toughness factor  $\bar{\sigma}'_b$  according to JSCE-SF4 [211]. The results for variant I-2, which is without steel bars can be compared with laboratory beams, which also do not have any steel bars. Although flexural toughness differ distinctly (what is obvious taking into account the area under force-displacement graph), the flexural toughness factors are on the similar level: 4.26 MPa (laboratory beams) and

4.70 MPa (full-scale beams). The noticeable difference could be a consequence of size effect.

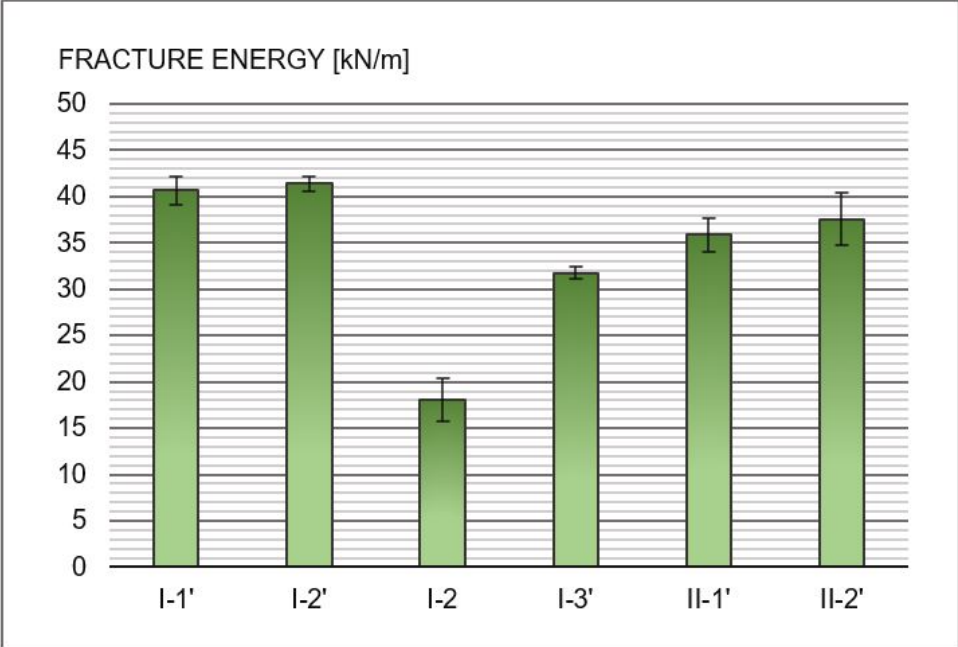


Fig. 6.3: Fracture energy [kN/m] in full-scale beams - column diagram

**Tab. 6.3:** Fracture energy  $G_f$  [kN/m], characteristic length  $l_{ch}$  [m] and ductility length  $D_l$  [mm] in full-scale beams

Variant	No. of specimen	$G_f$ [kN/m]	$l_{ch}$ [m]	$D_l$ [mm]
I-1'	I-1'-B1	42.03	50.36	7.17
	I-1'-B2	39.09	46.84	6.67
	I-1'-B3	40.76	48.84	6.95
	<b>Mean value</b>	<b>40.63</b>	<b>48.68</b>	<b>6.93</b>
	Stand. deviation	1.47	1.77	0.25
	Coef. of variation	3.6%	3.6%	3.6%
I-2'	I-2'-B1	41.16	52.78	7.32
	I-2'-B2	42.22	54.14	7.51
	I-2'-B3	40.74	52.24	7.24
	<b>Mean value</b>	<b>41.37</b>	<b>53.05</b>	<b>7.36</b>
	Stand. deviation	0.76	0.98	0.14
	Coef. of variation	1.8%	1.8%	1.8%
I-2	I-2-B4	15.44	19.80	2.74
	I-2-B5	19.30	24.75	3.43
	I-2-B6	19.59	25.12	3.48
	<b>Mean value</b>	<b>18.11</b>	<b>23.22</b>	<b>3.22</b>
	Stand. deviation	2.32	2.97	0.41
	Coef. of variation	12.8%	12.8%	12.8%
I-3'	I-3'-B1	31.20	36.39	4.93
	I-3'-B2	32.47	37.87	5.13
	I-3'-B3	31.61	36.87	5.00
	<b>Mean value</b>	<b>31.76</b>	<b>37.05</b>	<b>5.02</b>
	Stand. deviation	0.65	0.76	0.10
	Coef. of variation	2.0%	2.0%	2.0%
II-1'	II-1'-B1	37.20	51.18	6.53
	II-1'-B2	33.71	46.37	5.92
	II-1'-B3	36.60	50.35	6.42
	<b>Mean value</b>	<b>35.84</b>	<b>49.30</b>	<b>6.29</b>
	Stand. deviation	1.87	2.57	0.33
	Coef. of variation	5.2%	5.2%	5.2%
II-2'	II-2'-B1	34.61	47.66	6.08
	II-2'-B2	37.72	51.97	6.63
	II-2'-B3	40.25	55.42	7.07
	<b>Mean value</b>	<b>37.53</b>	<b>51.68</b>	<b>6.59</b>
	Stand. deviation	2.82	3.89	0.50
	Coef. of variation	7.5%	7.5%	7.5%

**Tab. 6.4:** Flexural toughness  $T_b$  [Nm] and flexural toughness factor  $\bar{\sigma}_b$  [MPa] based on JSCE SF-4 [211] in full-scale beams

Variant	No. of specimen	$T_b$ [Nm]	$\bar{\sigma}_b$ [MPa]
I-1'	I-1'-B1	370.86	8.05
	I-1'-B2	336.34	7.30
	I-1'-B3	344.03	7.47
	<b>Mean value</b>	<b>350.41</b>	<b>7.61</b>
	Stand. deviation	18.12	0.39
	Coef. of variation	5.2%	5.2%
I-2'	I-2'-B1	362.58	7.87
	I-2'-B2	353.31	7.67
	I-2'-B3	361.04	7.84
	<b>Mean value</b>	<b>358.98</b>	<b>7.79</b>
	Stand. deviation	4.97	0.11
	Coef. of variation	1.4%	1.4%
I-2	I-2-B4	216.47	4.70
	I-2-B5	201.73	4.38
	I-2-B6	231.27	5.02
	<b>Mean value</b>	<b>216.49</b>	<b>4.70</b>
	Stand. deviation	14.77	0.32
	Coef. of variation	6.8%	6.8%
I-3'	I-3'-B1	273.28	5.93
	I-3'-B2	261.51	5.68
	I-3'-B3	277.46	6.02
	<b>Mean value</b>	<b>270.75</b>	<b>5.88</b>
	Stand. deviation	8.27	0.18
	Coef. of variation	3.0%	3.0%
II-1'	II-1'-B1	334.26	7.25
	II-1'-B2	310.72	6.74
	II-1'-B3	334.07	7.25
	<b>Mean value</b>	<b>326.35</b>	<b>7.08</b>
	Stand. deviation	13.54	0.29
	Coef. of variation	4.1%	4.1%
II-2'	II-2'-B1	329.96	7.16
	II-2'-B2	343.37	7.45
	II-2'-B3	362.55	7.87
	<b>Mean value</b>	<b>345.29</b>	<b>7.49</b>
	Stand. deviation	16.38	0.36
	Coef. of variation	4.7%	4.7%

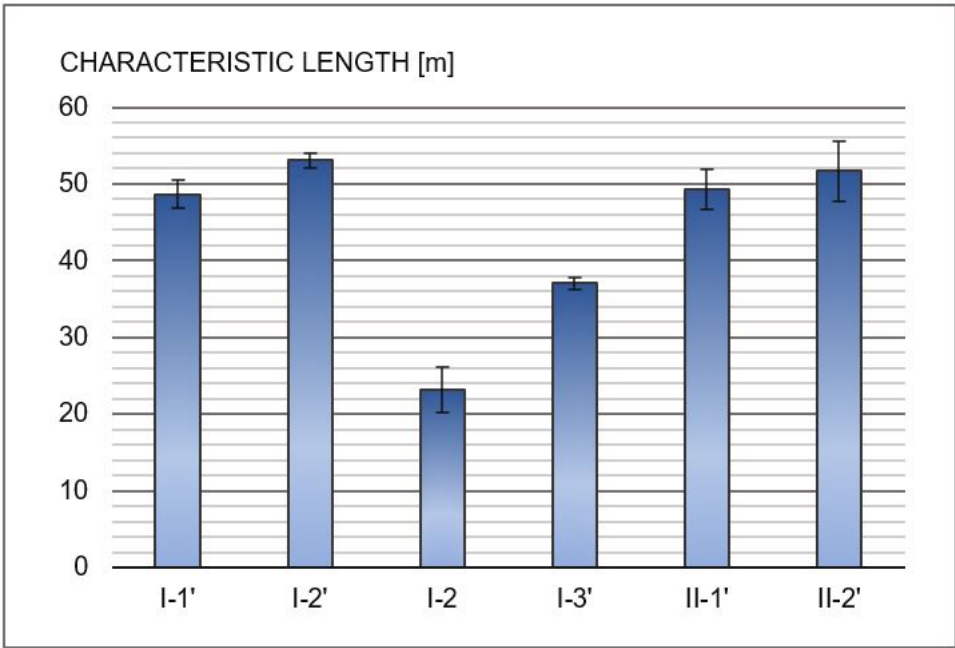


Fig. 6.4: Characteristic length [m] in full-scale beams - column diagram

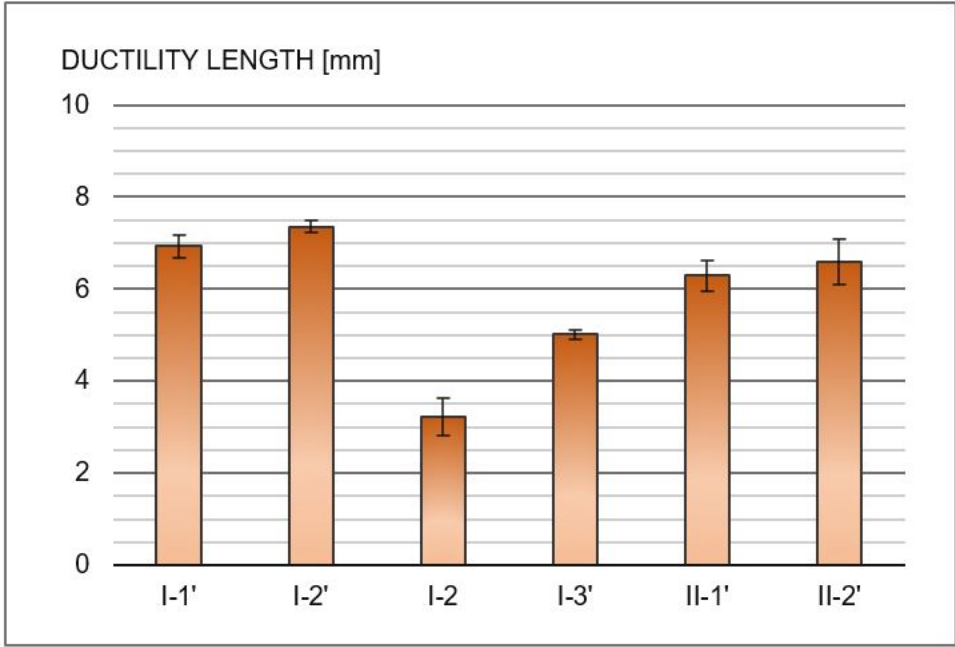


Fig. 6.5: Ductility length [mm] in full-scale beams - column diagram



# Chapter 7

## Conclusions and future research

### 7.1 Conclusions

Based on the considerations and results presented in the previous chapters the following conclusions can be drawn:

1. Application of polypropylene fibres into high performance concrete mix meaningfully changes the failure mechanism of bended samples - from the brittle and rapid into ductile one (see figures 4.37 and 4.38).
2. Application of polypropylene fibres enhanced the extreme path of force-displacement graph: in figure 7.1 by  $g(\Delta)$  the force-displacement relationship in beams with steel bars only is presented, whereas  $f(\Delta)$  shows the course of the force-displacement relation when polypropylene fibres are provided too. The  $\alpha$  coefficient, which is the ratio of  $f(\Delta)$  to  $g(\Delta)$  increases rapidly about two times at the beginning and then reaches the constant level of approximately 1.25 (25% of improvement).

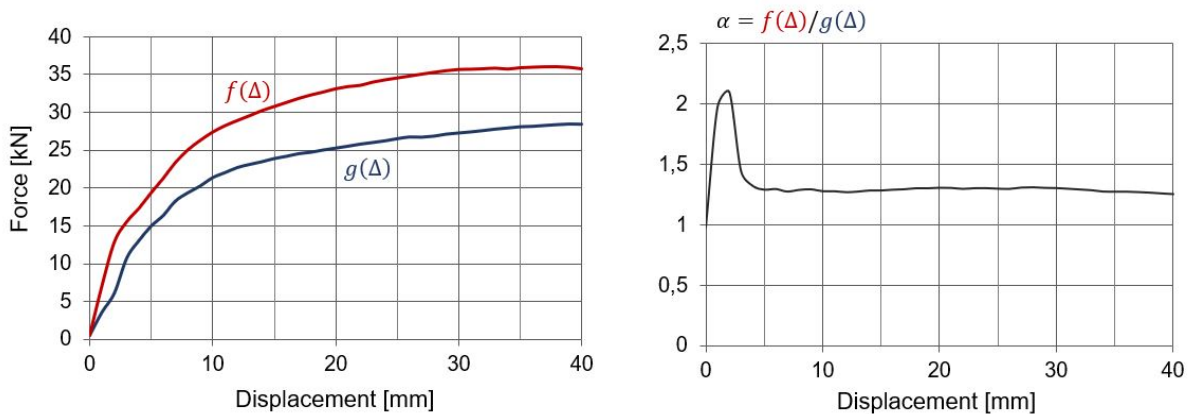


**Fig. 7.1:** Comparison of force-displacement envelopes for full-scale beams with steel bars ( $g(\Delta)$ ) and steel bars and PP fibres ( $f(\Delta)$ )

3. The increases of all considered ductility measurements (the fracture energy, the characteristic length, the ductility length, the toughness indices) have been observed (fig. 7.2).

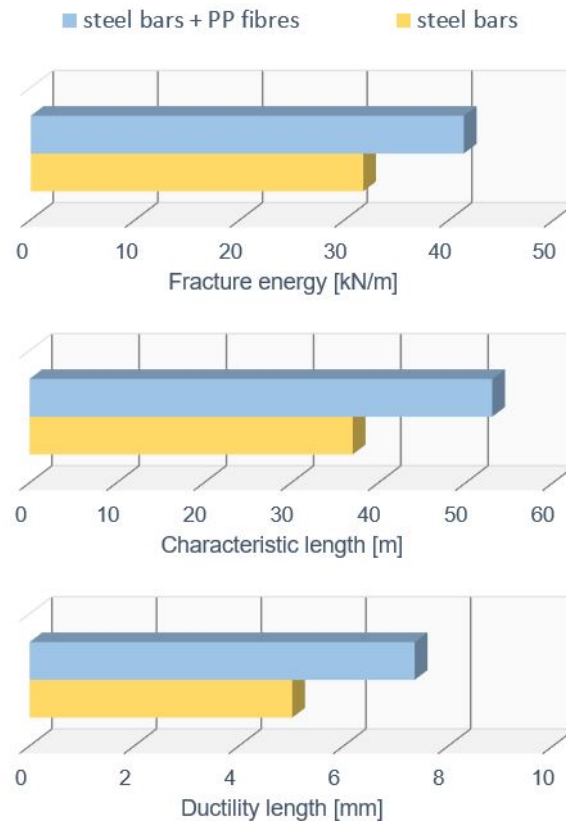


**Fig. 7.2:** Comparison of fracture energy, characteristic length and ductility length for B-type beams with steel bars and steel bars and PP fibres

Thereby, the main hypothesis of the dissertation about the significant improvement of flexural behaviour and ductility of high performance concrete beams thanks to application of polypropylene fibre reinforcement was proved.

In addition, after the conducted research a series of other accompanying conclusions can be mentioned:

- a. Laboratory testing of the used cement allowed us to classify it as CEM I 52.5 R, which confirms the manufacturer information.
- b. Utilized replacement of 15% of cement with silica fume will result in roughly of 7% increase of standard flexural strength and approximately 16% increase of standard compressive strength in testing of cement, whereas at an early age (2 days) flexural strength as well as compressive strength are slightly smaller than in testing of specimens without silica fume.

- c. Used high dosage of polypropylene fibres will result in a decrease of compressive strength of concrete; on the other hand the mechanism of failure under compression changes and in case of the polypropylene fibres presence is not so destructible (compare figures: 4.26 and 4.24)
- d. Young's modulus of elasticity of PFRHP concrete exhibits a several percentage increase compared to its initial value.
- e. Poisson's ratio in polypropylene fibre reinforced high performance concrete used in the research can be taken as the same like for normal-strength concrete, i.e.  $\nu = 0.20$ ;
- f. Displacements of the beams were recorded simultaneously by using three different measurement systems (INSTRON 8505, LVDT and ARAMIS 6M). The obtained results are in very good agreement.
- g. The replacement of the silica fume and aggregates by similar materials provided by other manufacturer does not cause any noticeable changes in the force-displacement relationship determined in laboratory tests (fig. 4.49).
- h. Full-scale beams prepared in laboratory conditions showed higher load bearing capacity than specimens concreted in industrial conditions, although in the first linear parts the load-displacement path are practically the same (fig. 4.52).
- i. The obtained results demonstrate a slight influence of small difference in the length of polypropylene fibres (60 mm vs 48 mm) on the behaviour of the beam (fig. 4.53).
- j. Permanent part of the mid-span deflection measured in the loading-unloading cycles on full-scale beams is nearly the same for the most of tested samples.
- k. A clear difference in horizontal strain distribution was observed depending on the applied reinforcement. The presence of longitudinal steel bars results in cracks distributed along the beam, whereas in beams where polypropylene fibres are used as the only one type of reinforcement we observe only one (optionally a few) greater, concentrated horizontal strains
- l. The used uniaxial tensile stress-strain relationship (equation 5.29) for polypropylene fibre reinforced high performance concrete can be an effective method of taking fibre reinforcement into account in modelling of polypropylene fibre reinforced high performance concrete beams.

## 7.2 Future research directions

In the light of the conducted research other questions and ideas of next investigations have emerged. I would like in the future to consider following issues:

- experimental research of polypropylene fibre reinforced high performance concrete beams with smaller fibre dosage, e.g. 0.5% and 1% (taking into account greater number of samples in one variant);
- experimental research of high performance concrete reinforced by different polypropylene fibres, which will differ substantially in geometry of fibre from provided in this research;
- development of an efficient algorithm for simulation of cyclic loading-unloading processes conducted in this dissertation;
- multi-scale modelling of PFRHPC;
- experimental tests on PFRHPC specimens subjected to impact loading.

Polypropylene fibre reinforced high performance concrete is a material of great potential which can be further developed in the nearest future. I would like to be the one of the researchers to put some contribution into better comprehension of the PFRHPC.

# Appendix A

## Force-displacement graphs in full-scale beams

In this Appendix force-displacement graphs for individual full-scale beams are presented:

- variant I-1'-(B1-B3) – figures A.2 – A.4,
- variant I-2'-(B1-B3) – figures A.5 – A.7,
- variant I-2-(B4-B6) – figures A.8 – A.10 (variant without steel reinforcement),
- variant I-3'-(B1-B3) – figures A.11 – A.13 (variant without polypropylene fibre),
- variant I-1'-(B1-B3) – figures A.14 – A.16,
- variant I-2'-(B1-B3) – figures A.17 – A.19.



**Fig. A.1:** Full-scale beam (I-1'-B1) on test setup

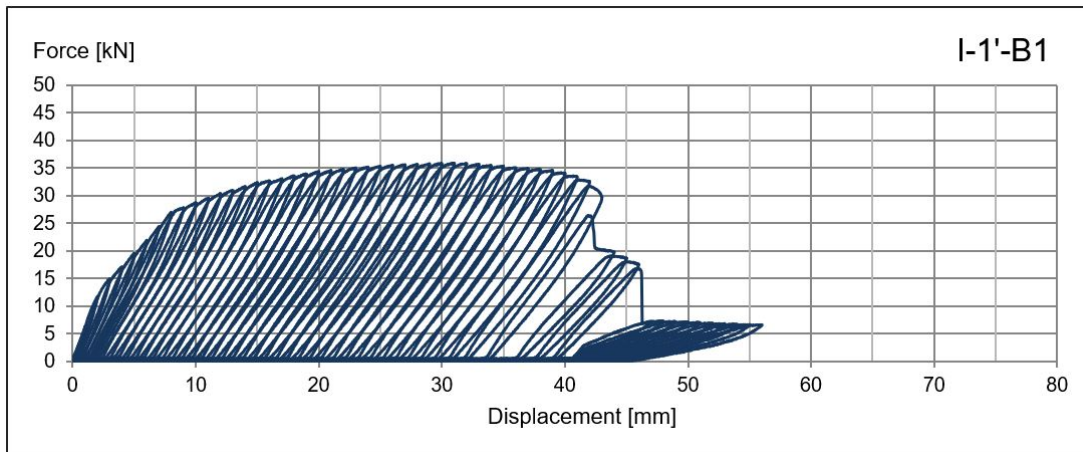


Fig. A.2: Force-displacement graph in beam I-1'-B1

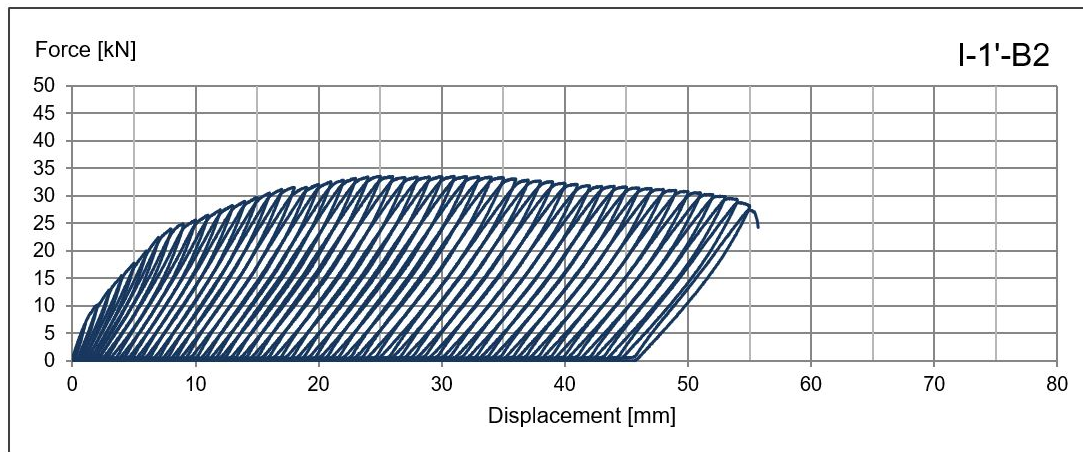


Fig. A.3: Force-displacement graph in beam I-1'-B2

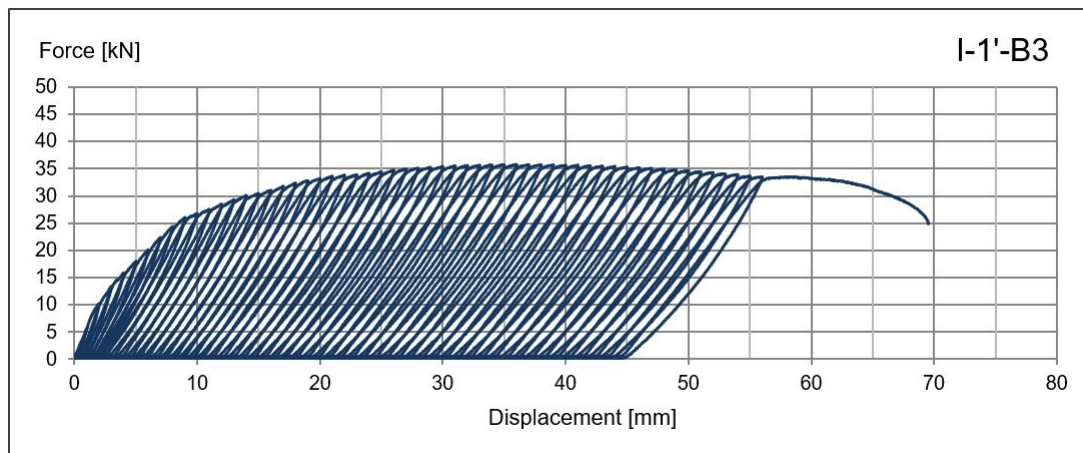
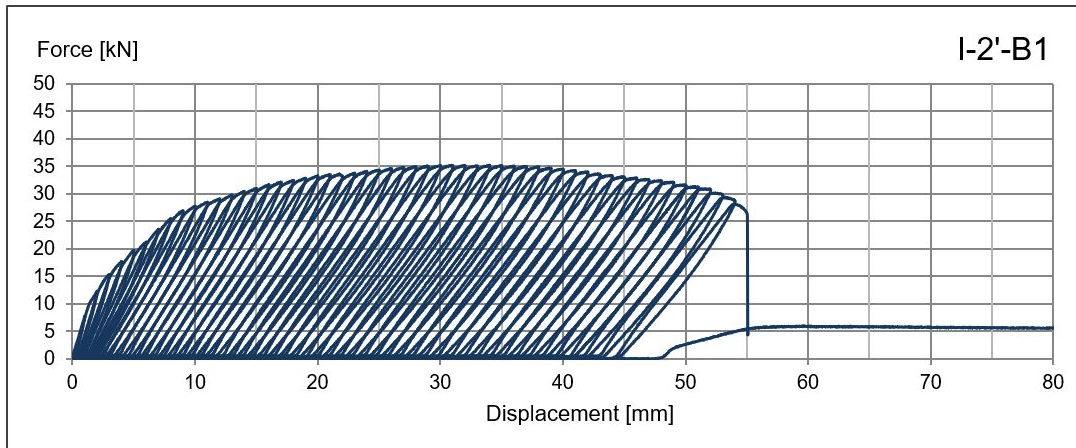
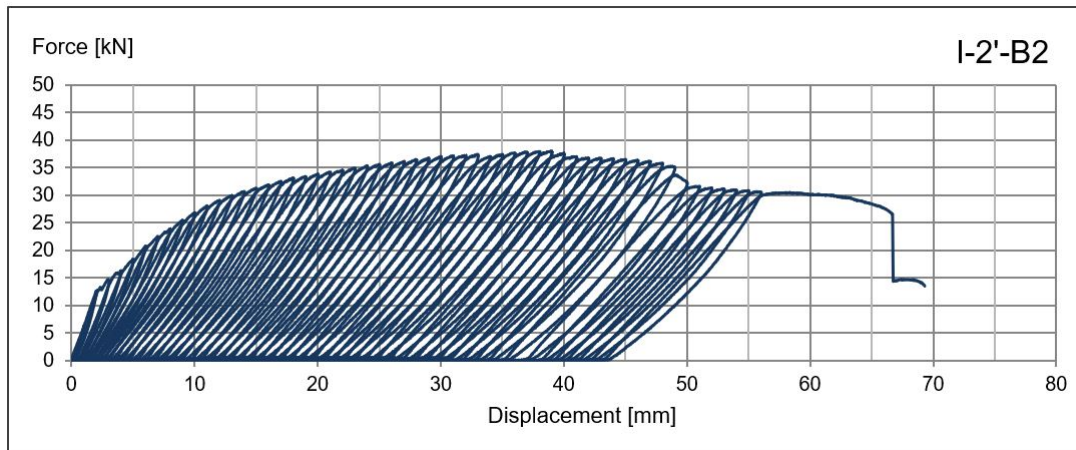


Fig. A.4: Force-displacement graph in beam I-1'-B3



**Fig. A.5:** Force-displacement graph in beam I-2'-B1



**Fig. A.6:** Force-displacement graph in beam I-2'-B2

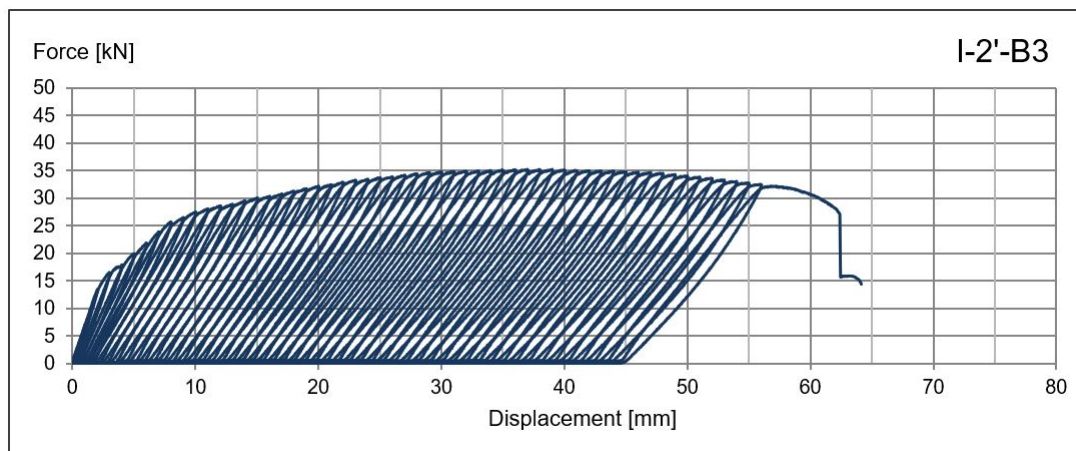


**Fig. A.7:** Force-displacement graph in beam I-2'-B3

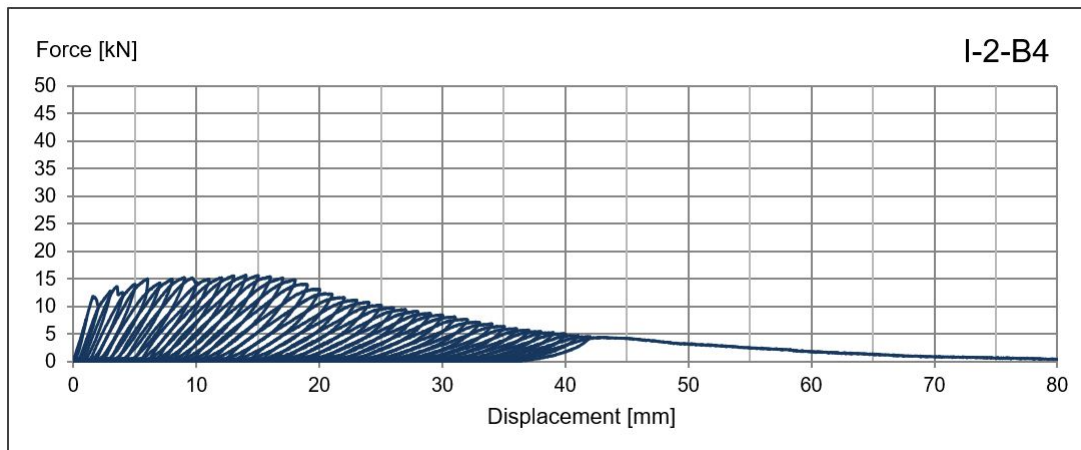


Fig. A.8: Force - displacement graph in beam I-2-B4

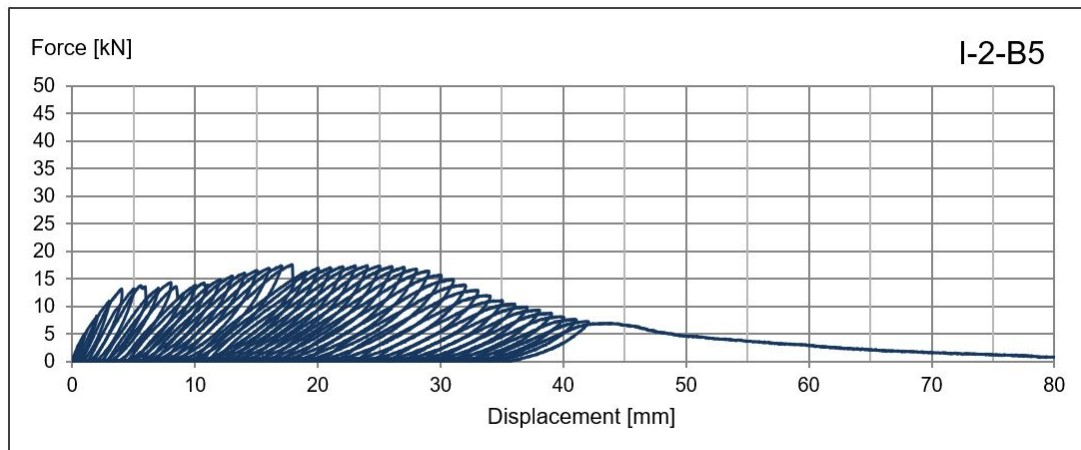


Fig. A.9: Force - displacement graph in beam I-2-B5

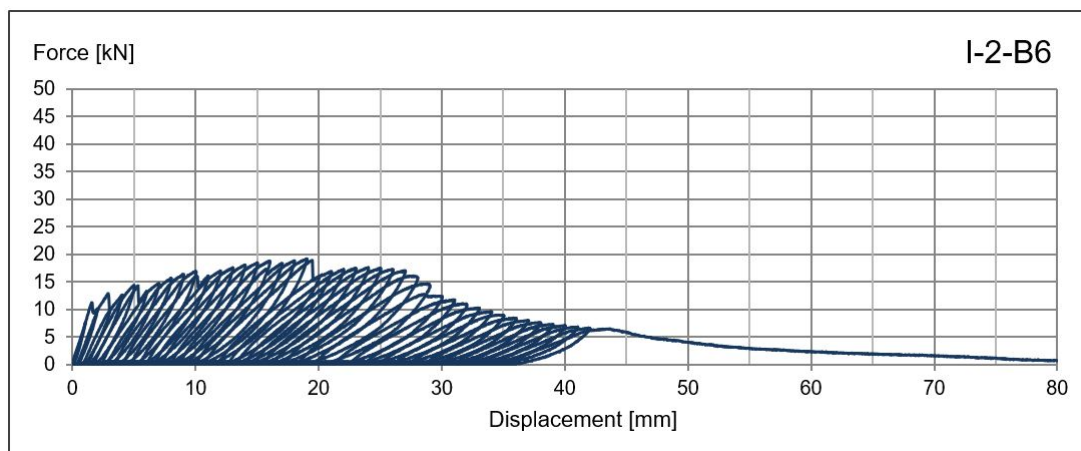
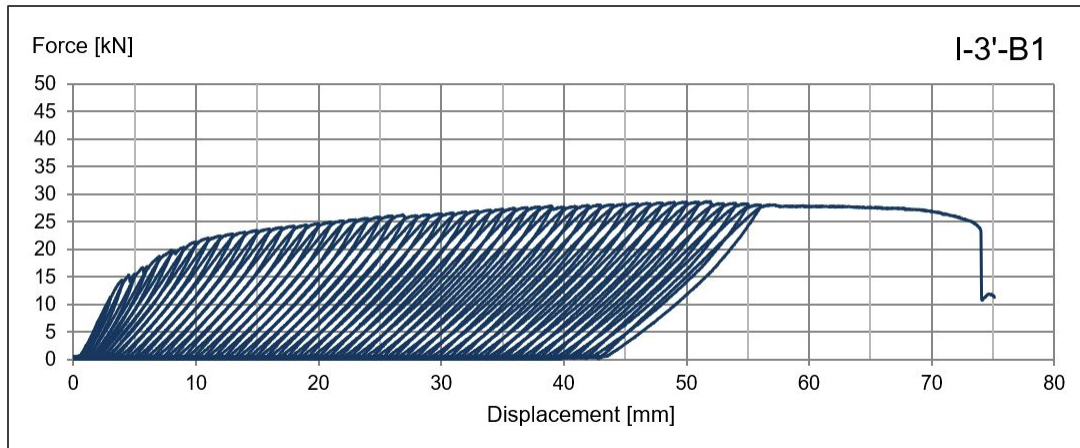
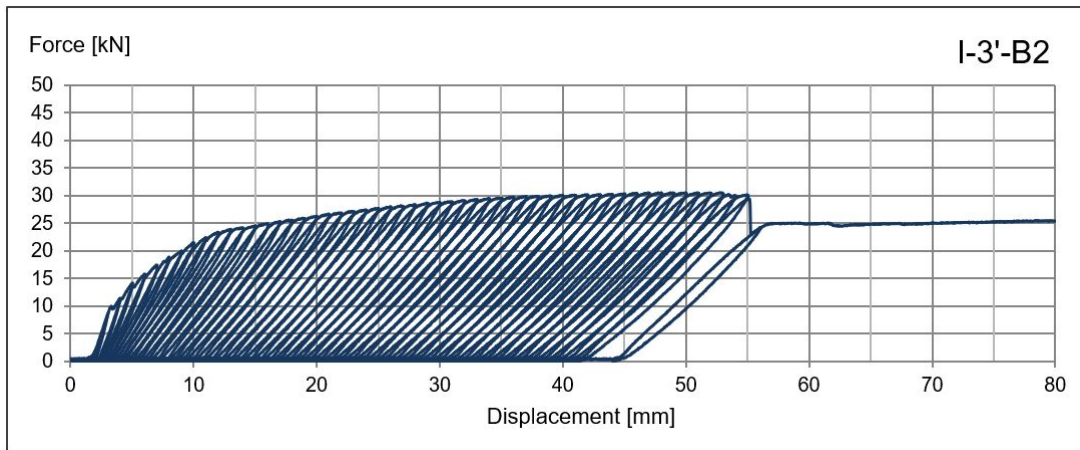


Fig. A.10: Force - displacement graph for beam I-2-B6



**Fig. A.11:** Force - displacement graph for beam I-3'-B1



**Fig. A.12:** Force - displacement graph for beam I-3'-B2

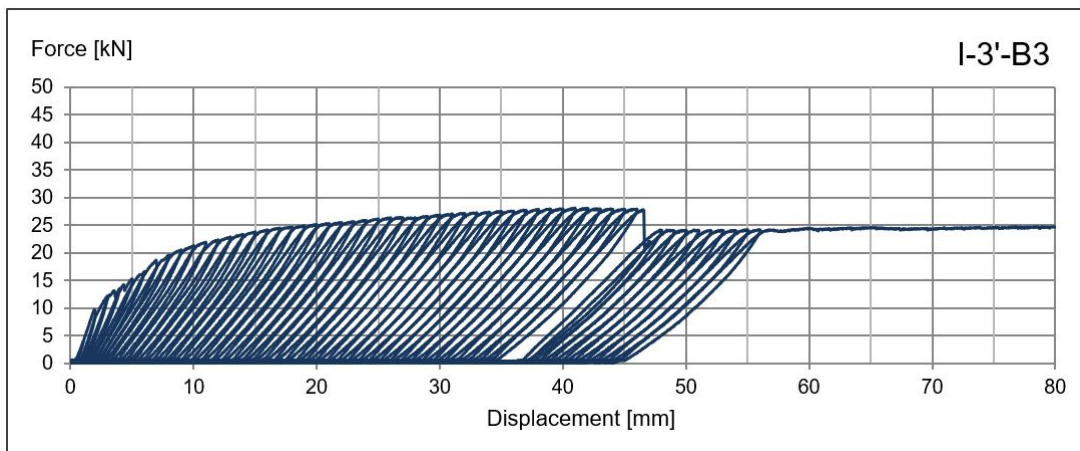


**Fig. A.13:** Force - displacement graph for beam I-3'-B3

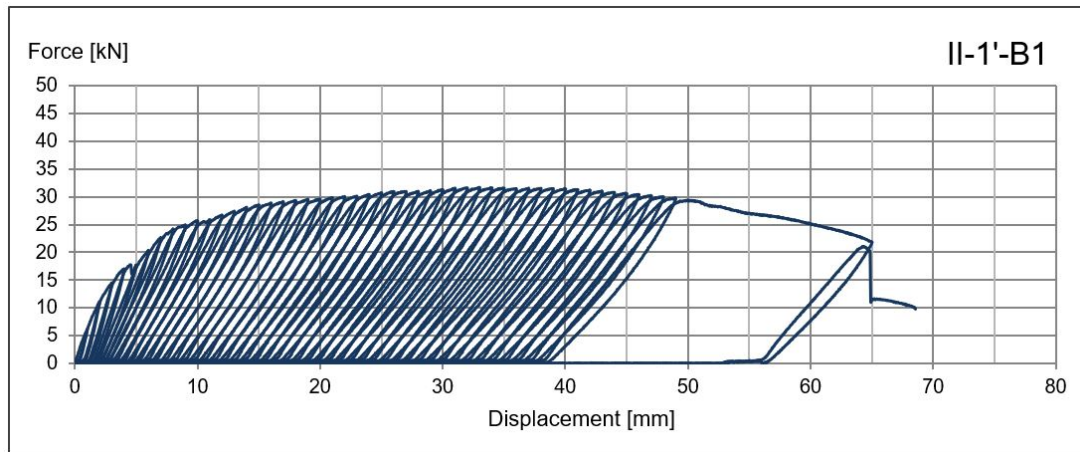


Fig. A.14: Force - displacement graph for beam II-1'-B1

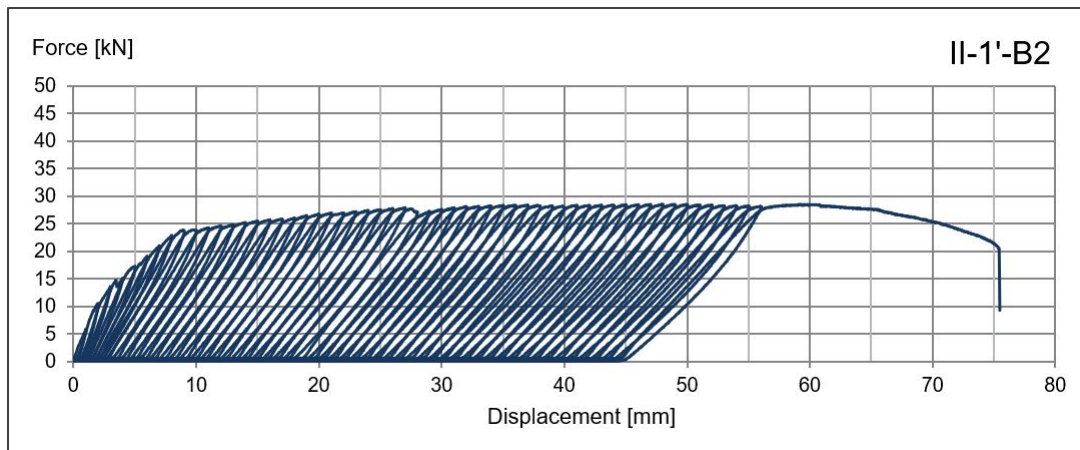


Fig. A.15: Force - displacement graph for beam II-1'-B2

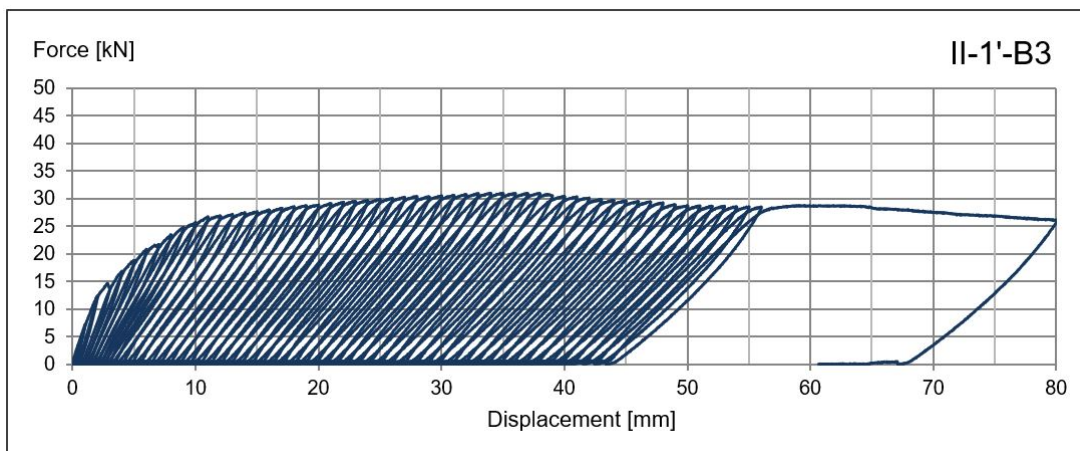


Fig. A.16: Force - displacement graph for beam II-1'-B3

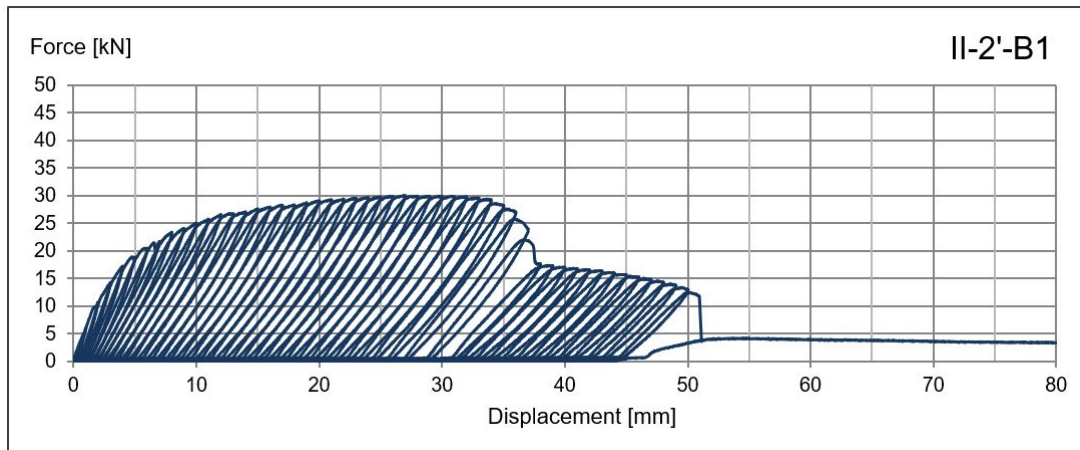


Fig. A.17: Force - displacement graph for beam II-2'-B1

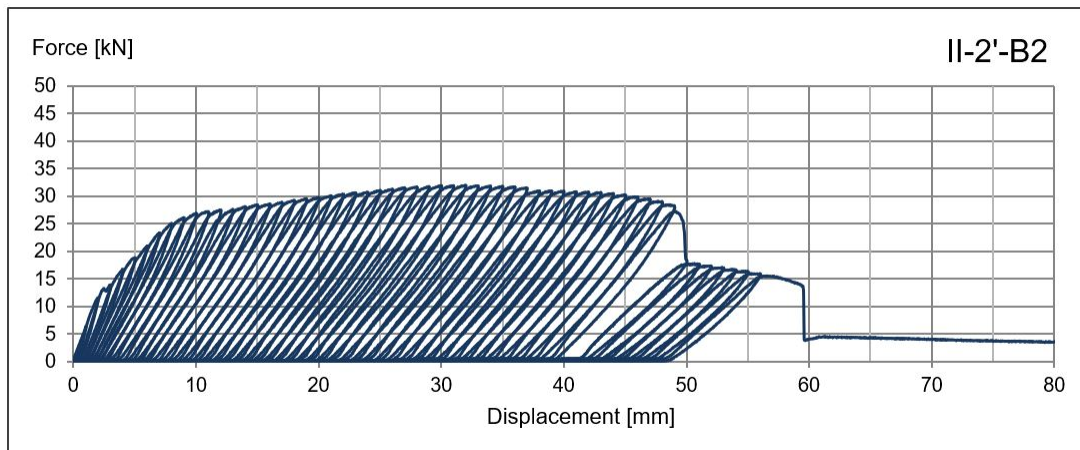


Fig. A.18: Force - displacement graph for beam II-2'-B2

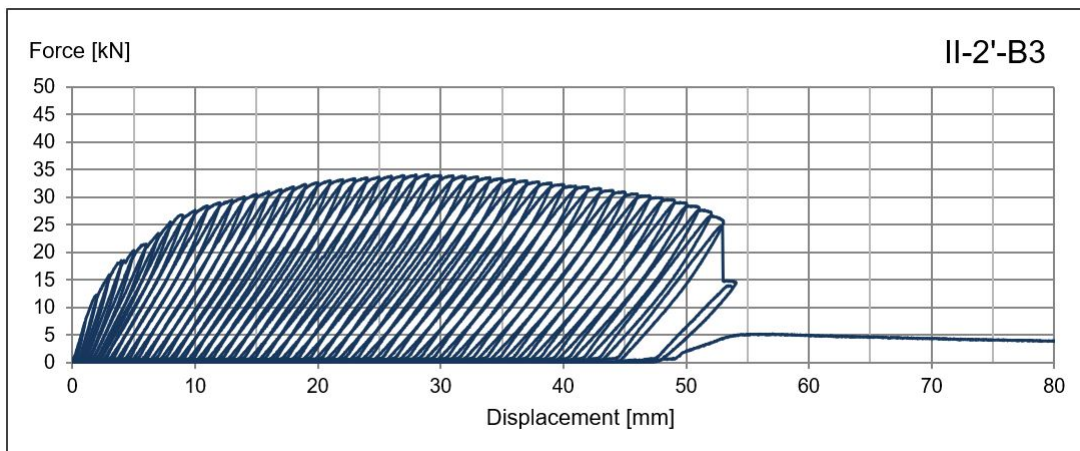


Fig. A.19: Force - displacement graph for beam II-2'-B3



# Appendix B

## Maps of horizontal strains in full-scale beams

In the Appendix B maps of horizontal strains after selected (5th and 10th) cycles of loading in full-scale beams are presented. Maps were obtained by the means of non-contact measuring system ARAMIS.



**Fig. B.1:** The view from ARAMIS camera

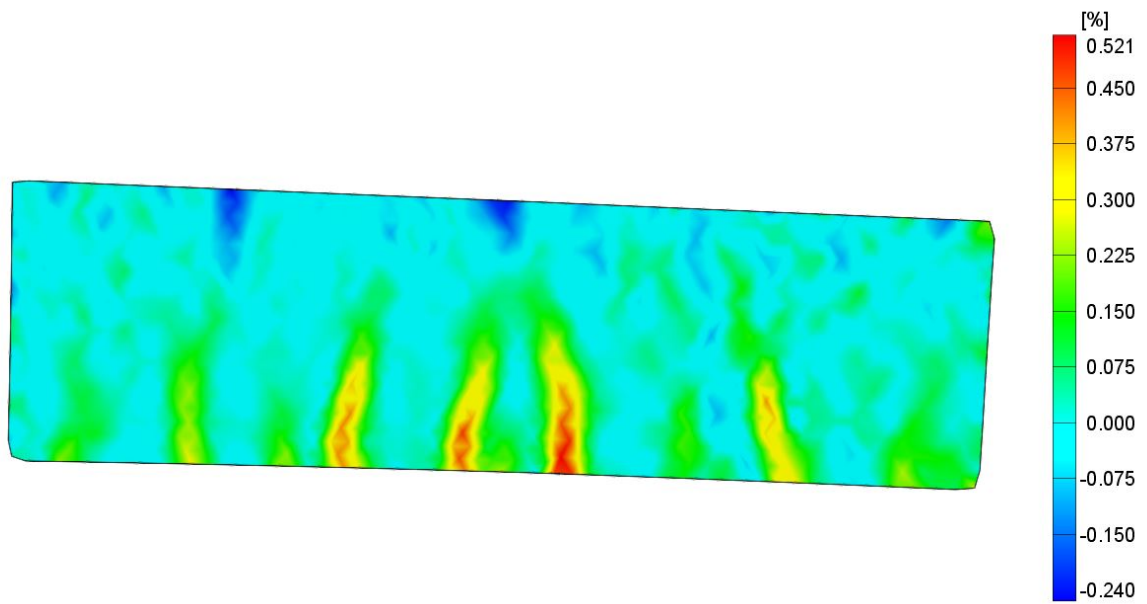


**Fig. B.2:** Map of horizontal strains in beam I-1'-B1 after 5th cycle of loading

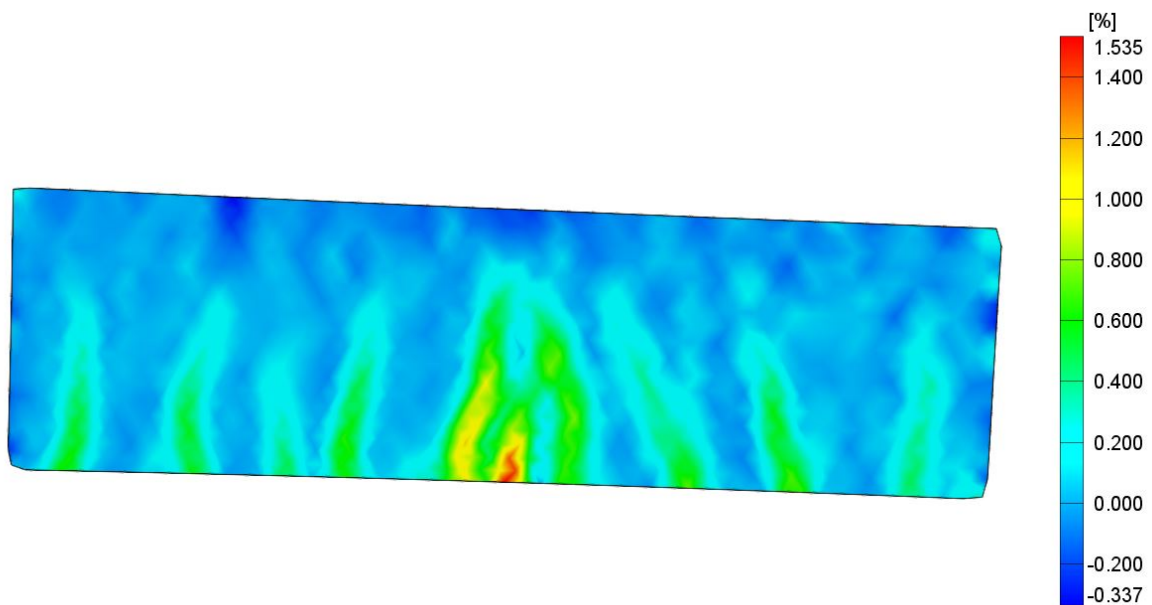


**Fig. B.3:** Map of horizontal strains in beam I-1'-B1 after 10th cycle of loading

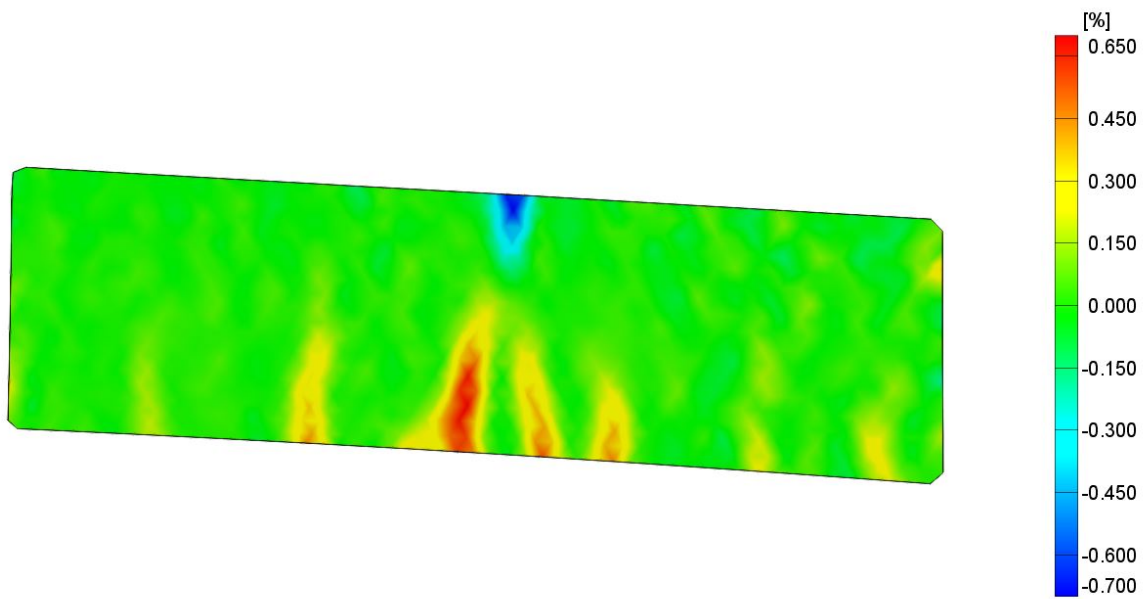


**Fig. B.4:** Map of horizontal strains in beam I-1'-B2 after 5th cycle of loading

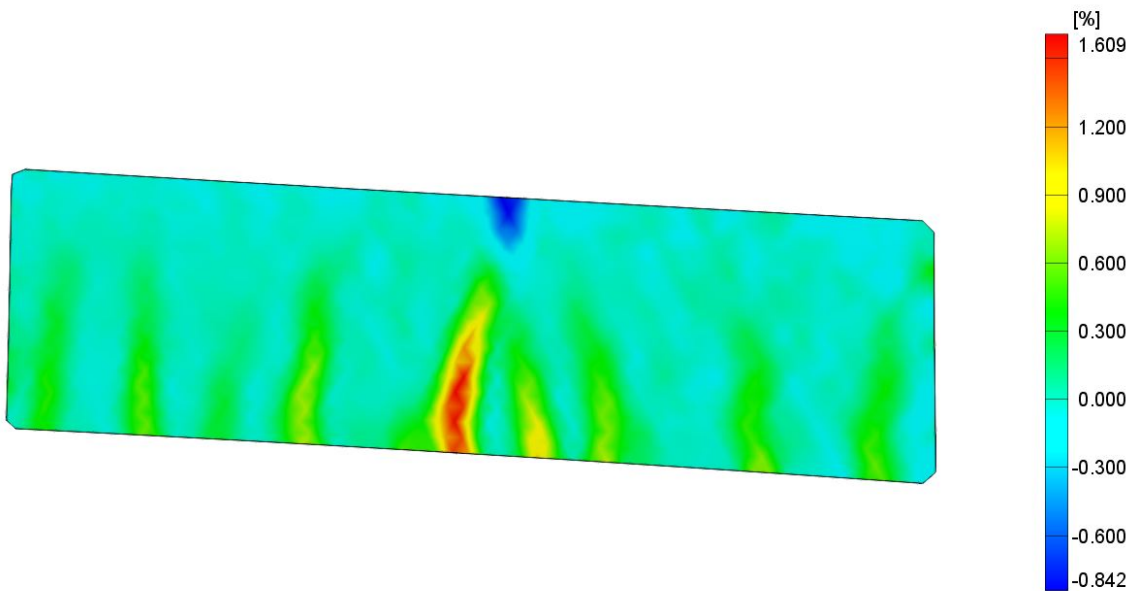


**Fig. B.5:** Map of horizontal strains in beam I-1'-B2 after 10th cycle of loading

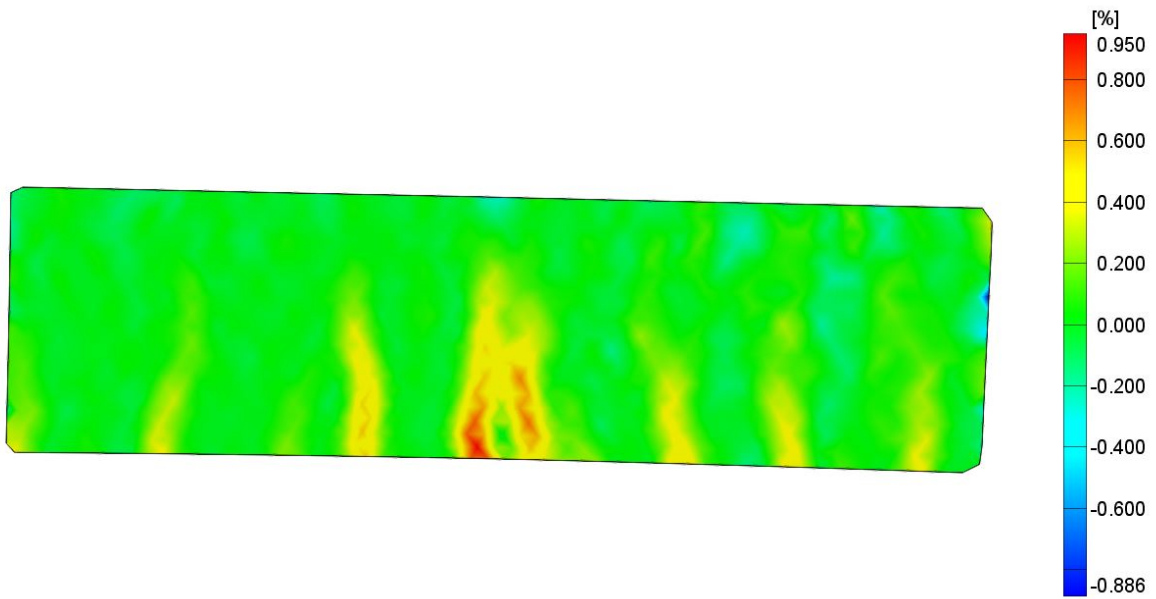


**Fig. B.6:** Map of horizontal strains in beam I-1'-B3 after 5th cycle of loading

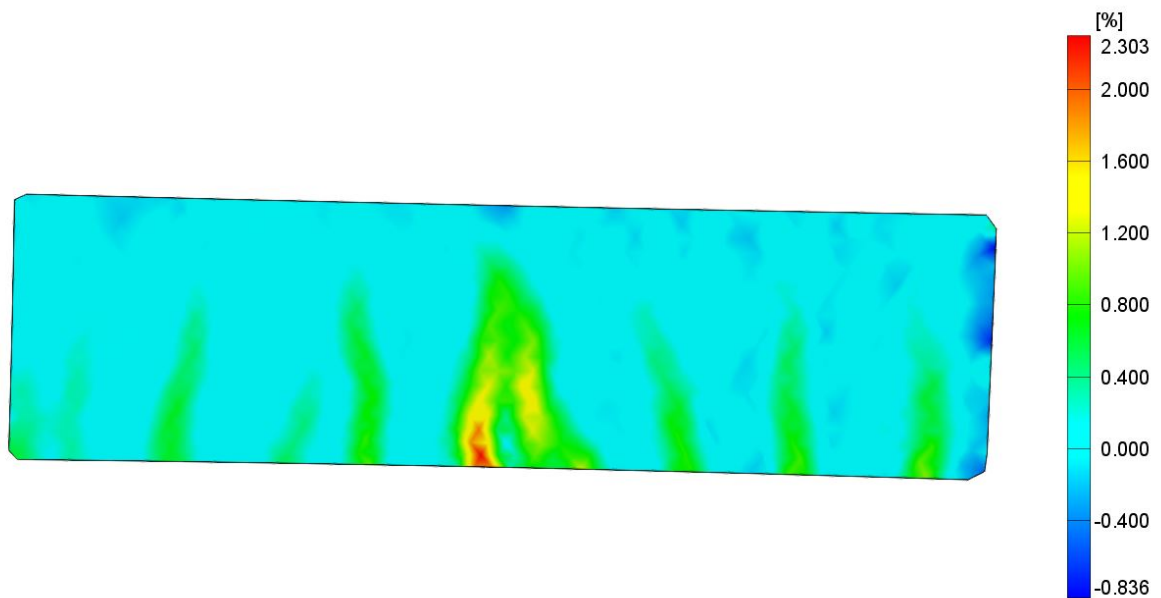


**Fig. B.7:** Map of horizontal strains in beam I-1'-B3 after 10th cycle of loading

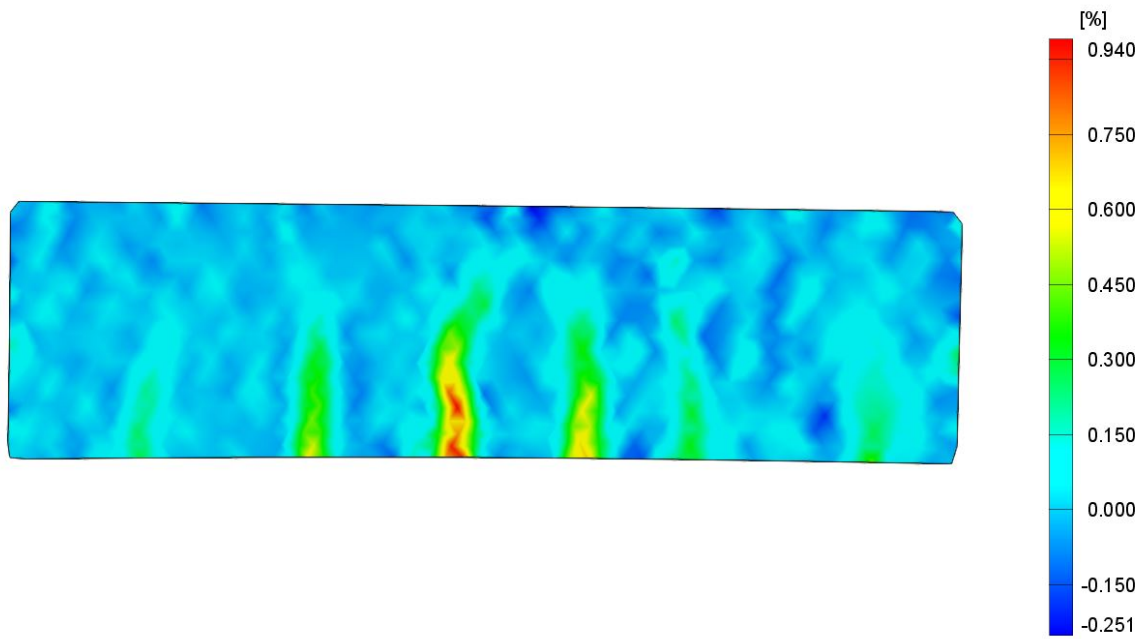


**Fig. B.8:** Map of horizontal strains in beam I-2'-B1 after 5th cycle of loading

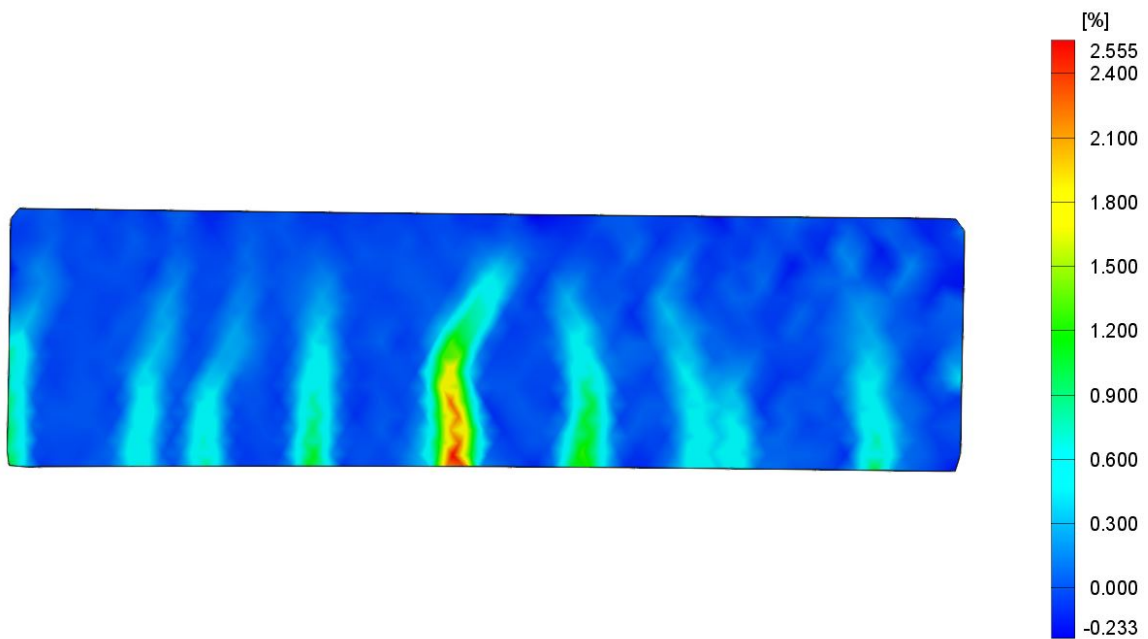


**Fig. B.9:** Map of horizontal strains in beam I-2'-B1 after 10th cycle of loading

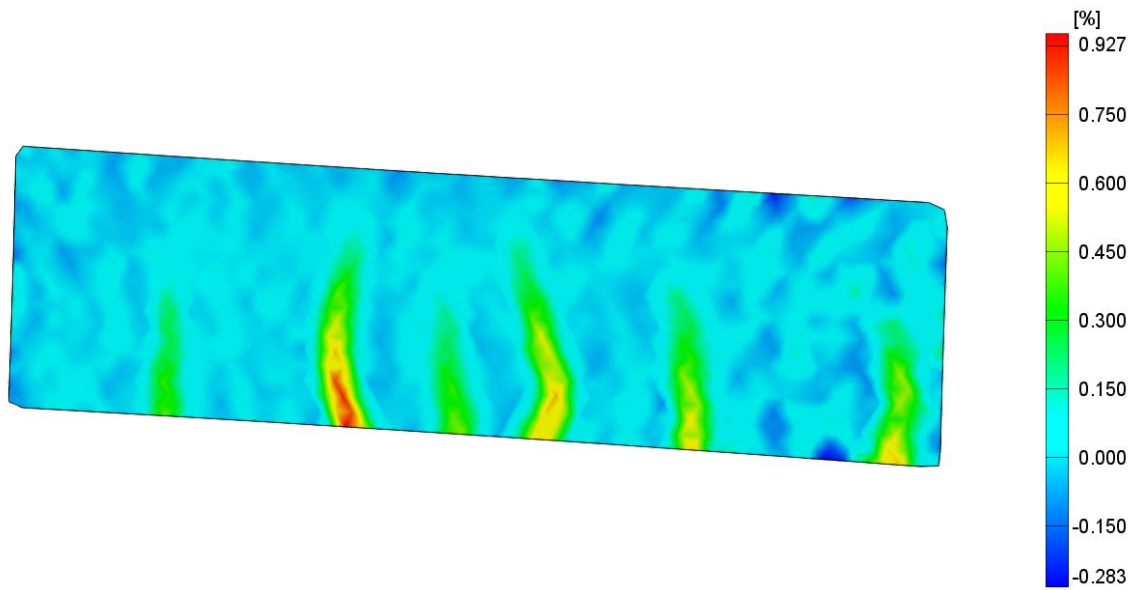


Fig. B.10: Map of horizontal strains in beam I-2'-B2 after 5th cycle of loading

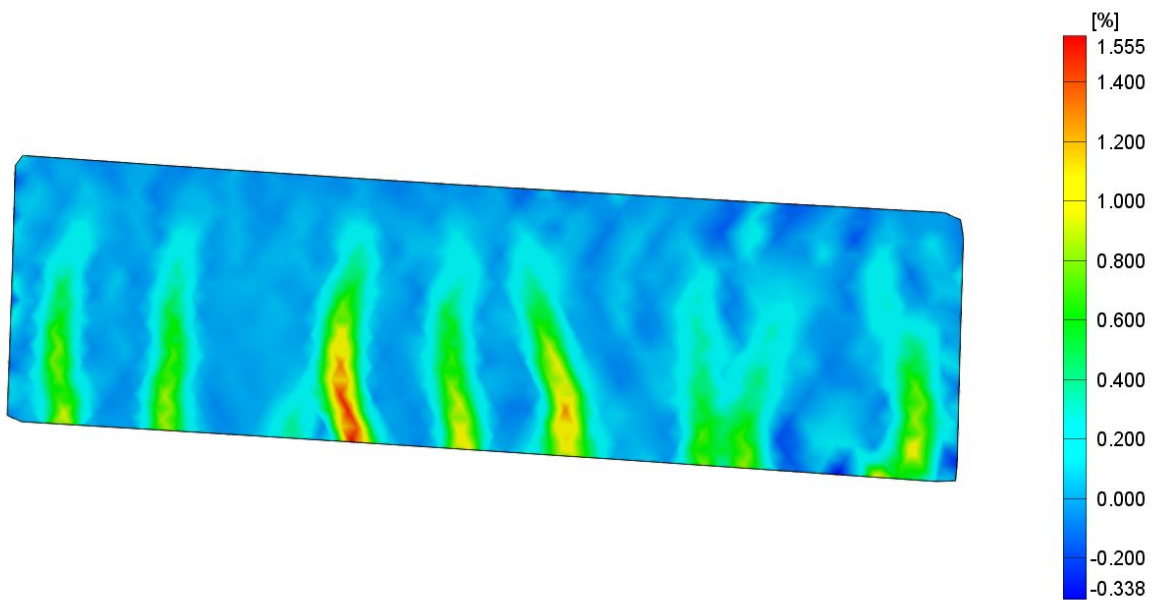
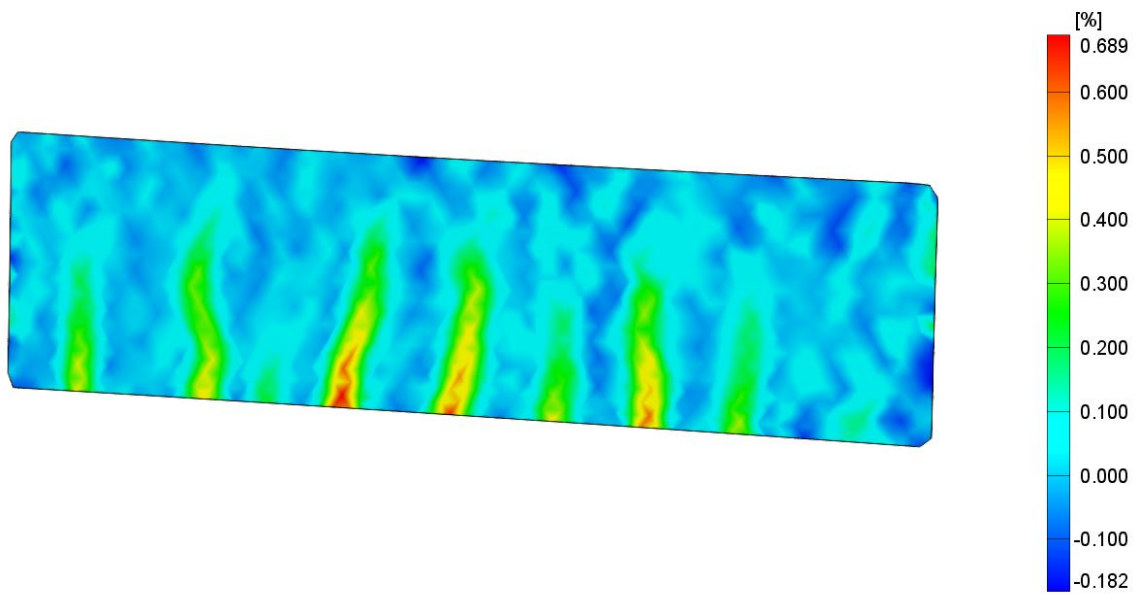
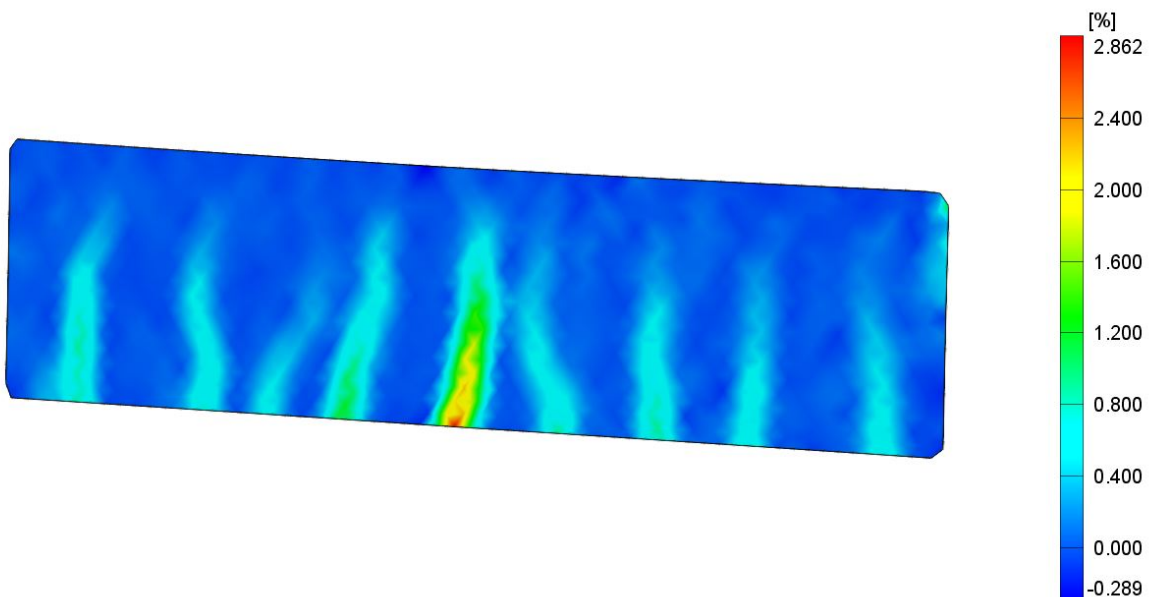


Fig. B.11: Map of horizontal strains in beam I-2'-B2 after 10th cycle of loading



**Fig. B.12:** Map of horizontal strains in beam I-2'-B3 after 5th cycle of loading



**Fig. B.13:** Map of horizontal strains in beam I-2'-B3 after 10th cycle of loading

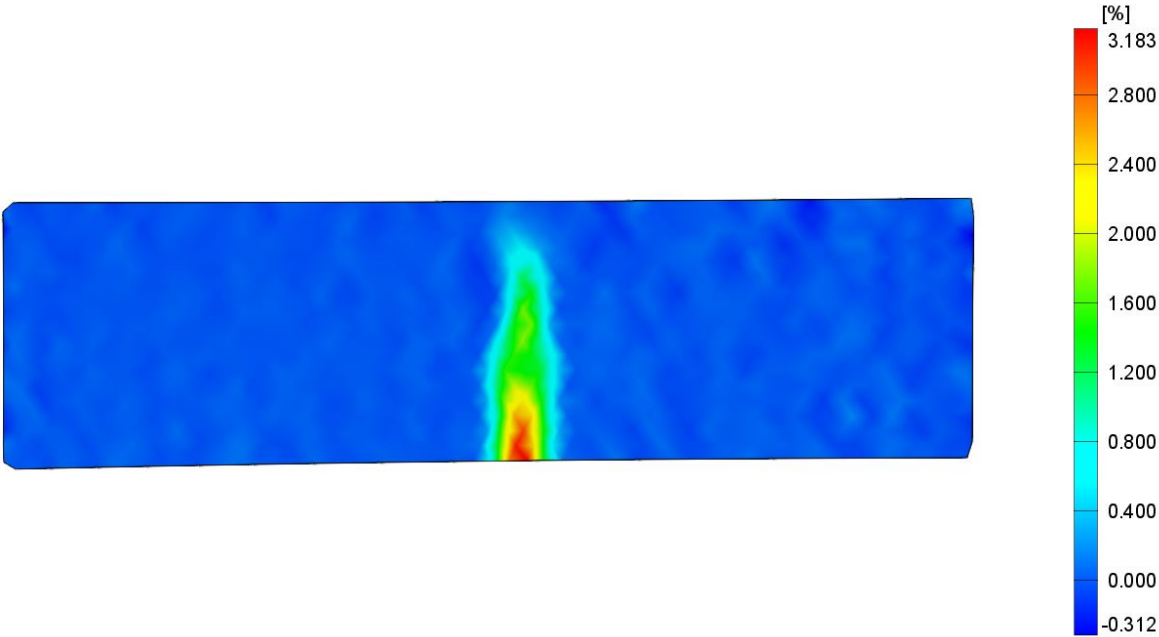


Fig. B.14: Map of horizontal strains in beam I-2-B4 after 5th cycle of loading

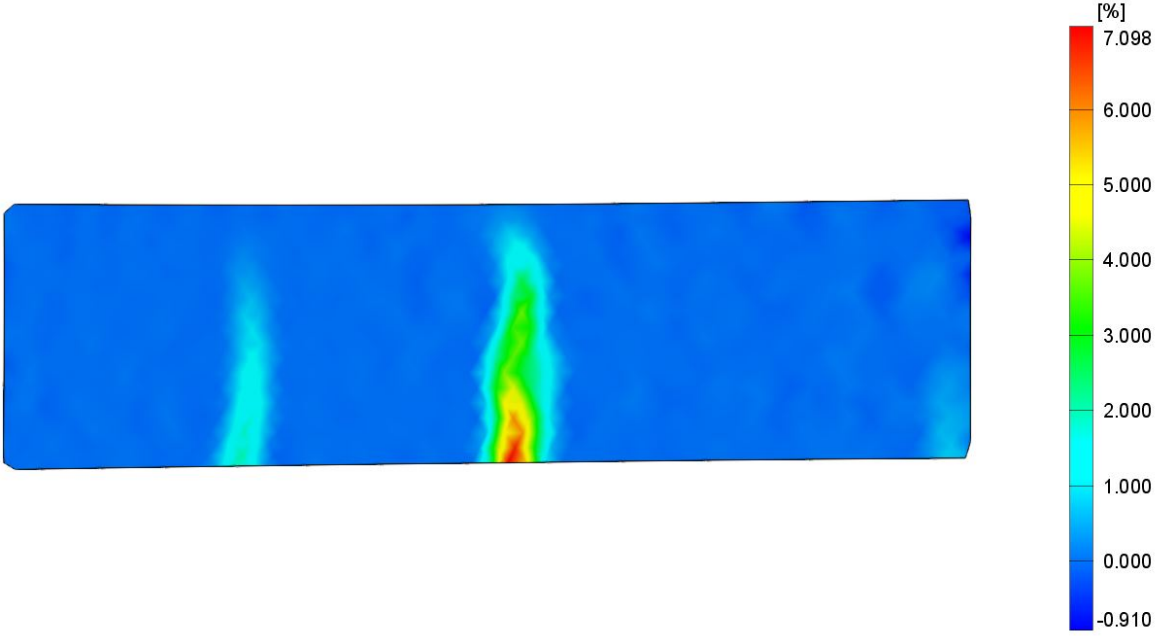
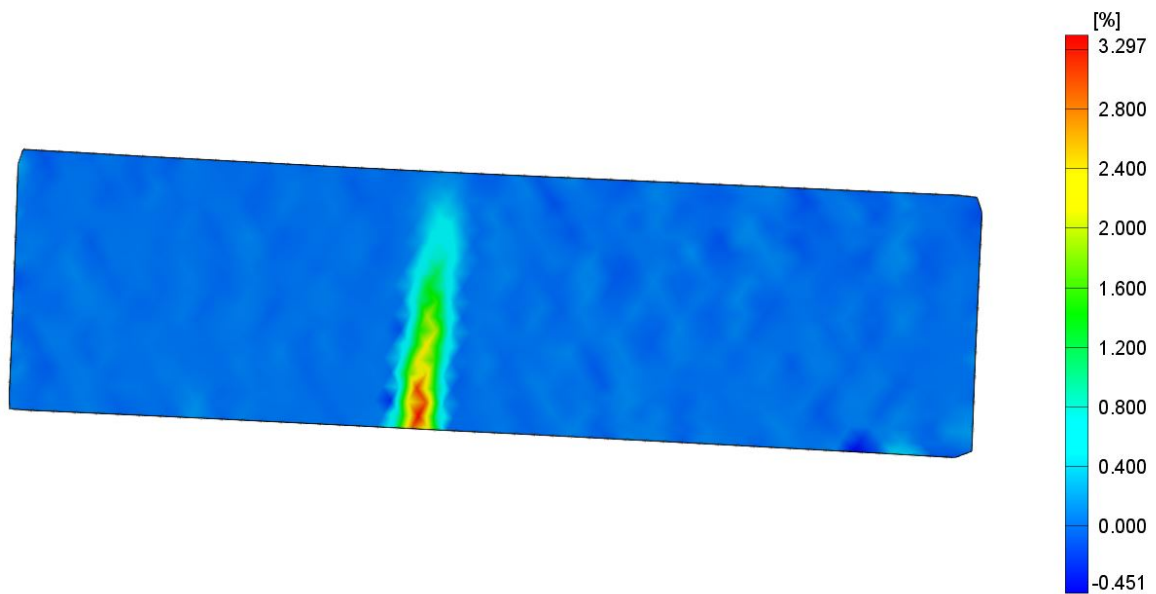
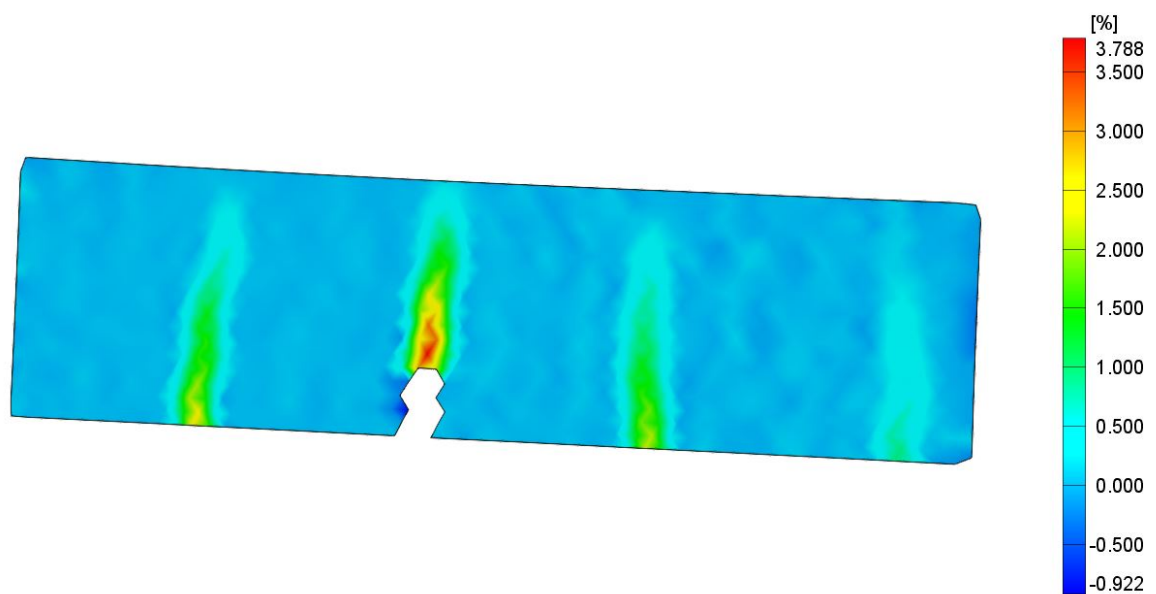


Fig. B.15: Map of horizontal strains in beam I-2-B4 after 10th cycle of loading



**Fig. B.16:** Map of horizontal strains in beam I-2-B5 after 5th cycle of loading



**Fig. B.17:** Map of horizontal strains in beam I-2-B5 after 10th cycle of loading

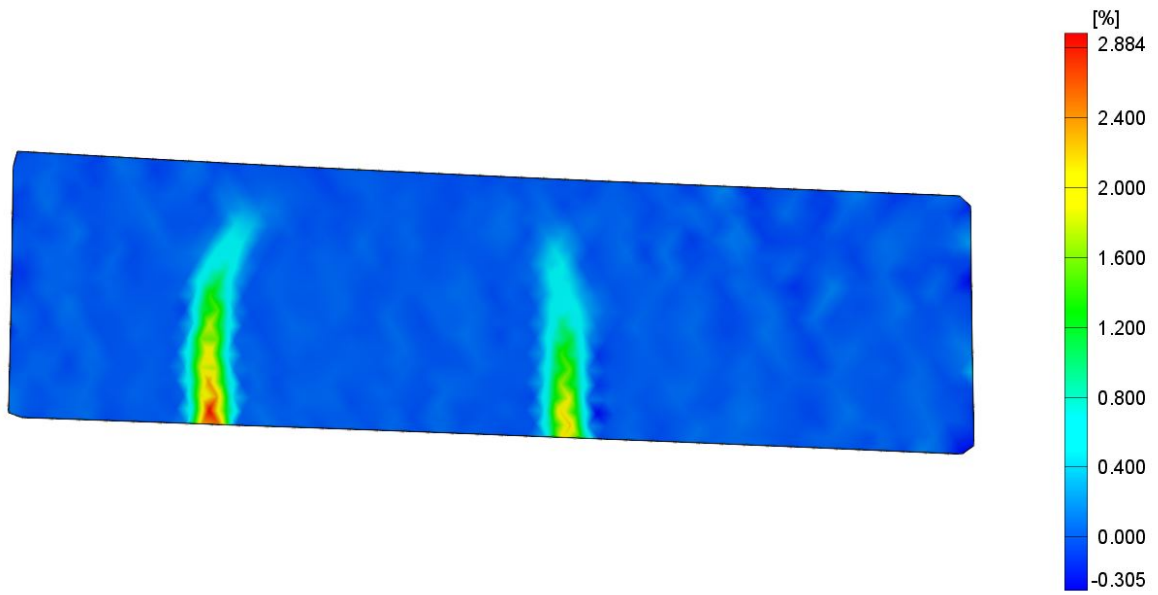


Fig. B.18: Map of horizontal strains in beam I-2-B6 after 5th cycle of loading

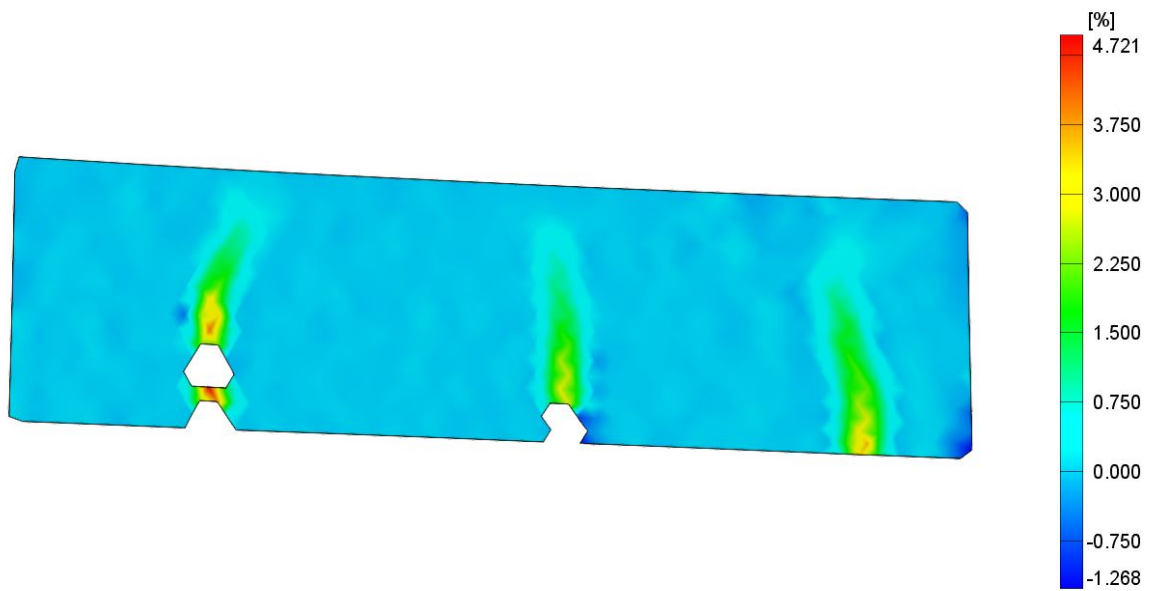
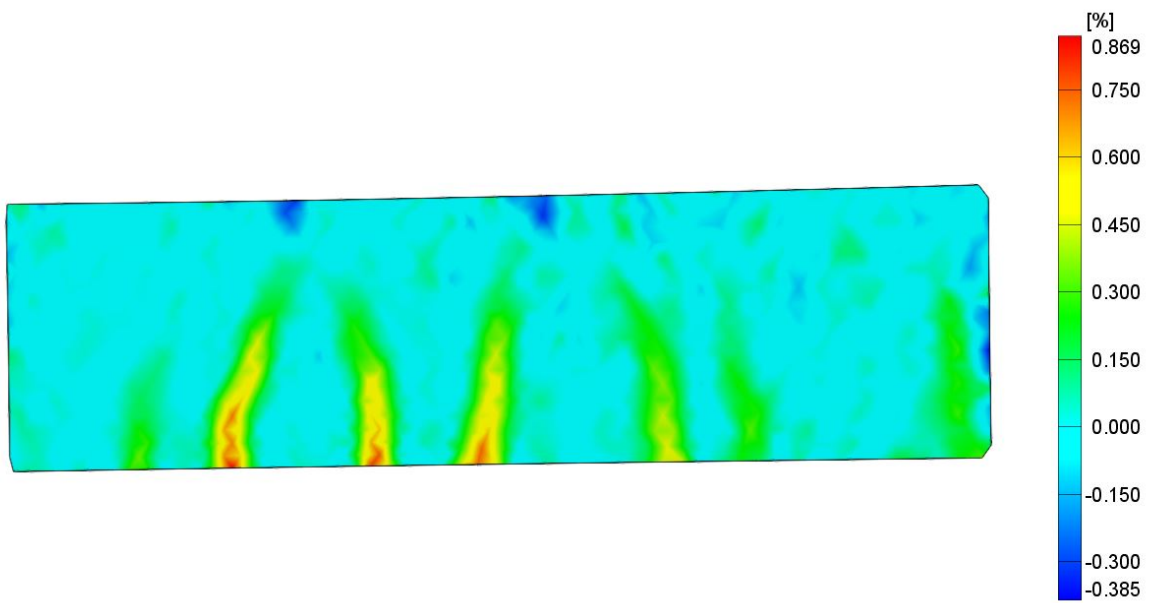
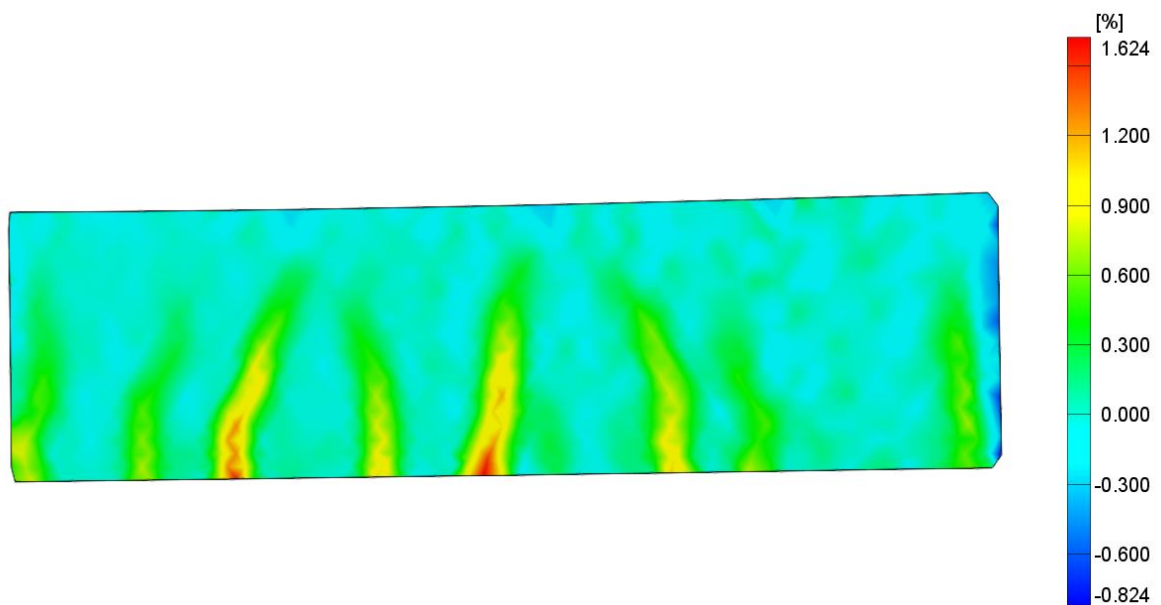


Fig. B.19: Map of horizontal strains in beam I-2-B6 after 10th cycle of loading



**Fig. B.20:** Map of horizontal strains in beam I-3'-B1 after 5th cycle of loading



**Fig. B.21:** Map of horizontal strains in beam I-3'-B1 after 10th cycle of loading

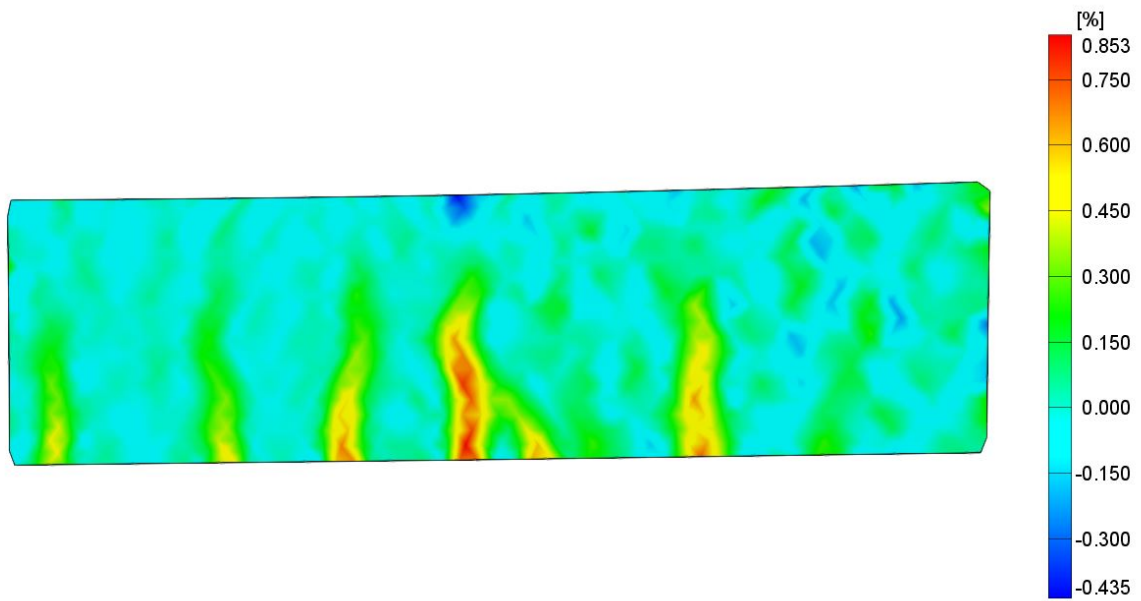


**Fig. B.22:** Map of horizontal strains in beam I-3'-B2 after 5th cycle of loading

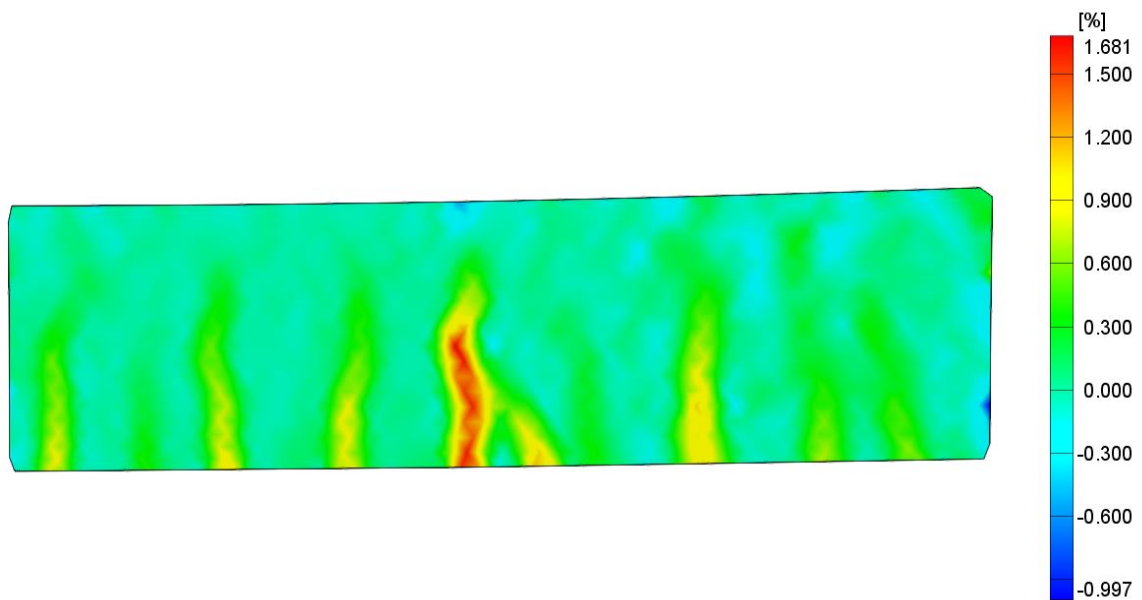


**Fig. B.23:** Map of horizontal strains in beam I-3'-B2 after 10th cycle of loading

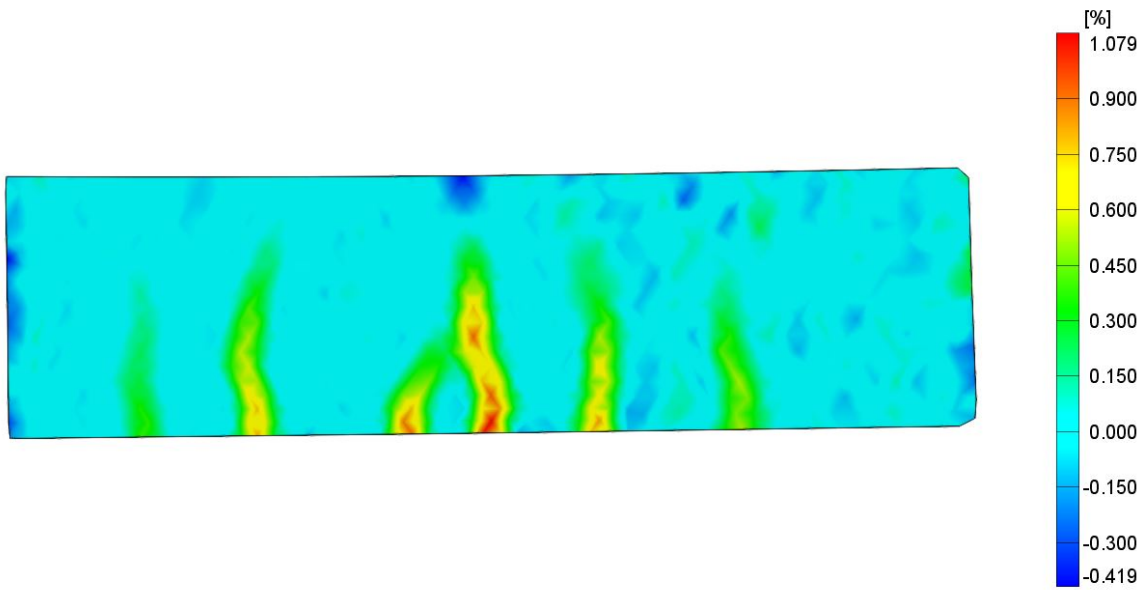


**Fig. B.24:** Map of horizontal strains in beam I-3'-B3 after 5th cycle of loading

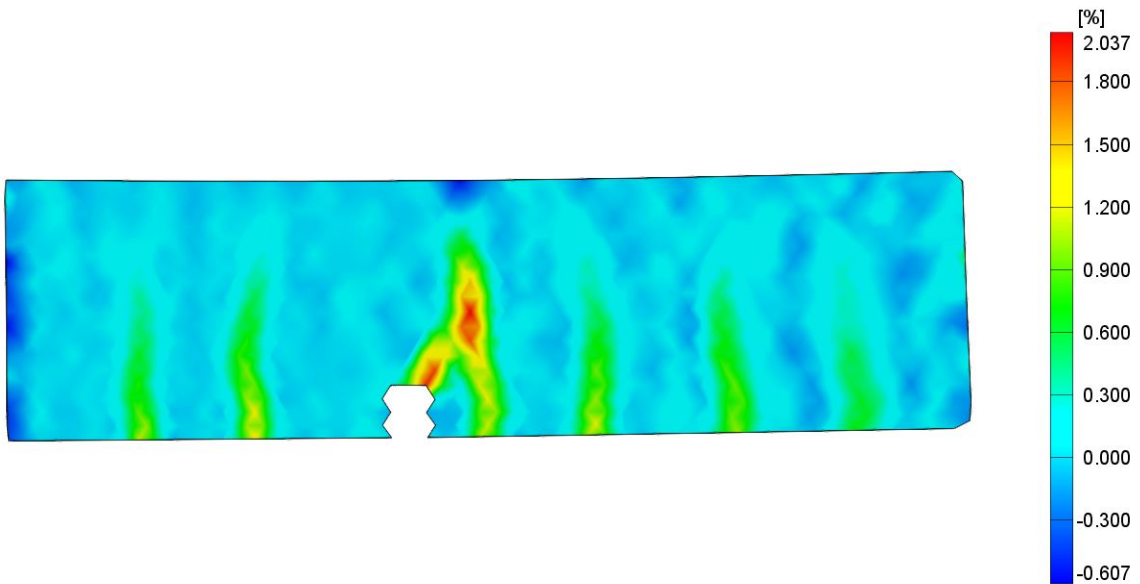


**Fig. B.25:** Map of horizontal strains in beam I-3'-B3 after 10th cycle of loading

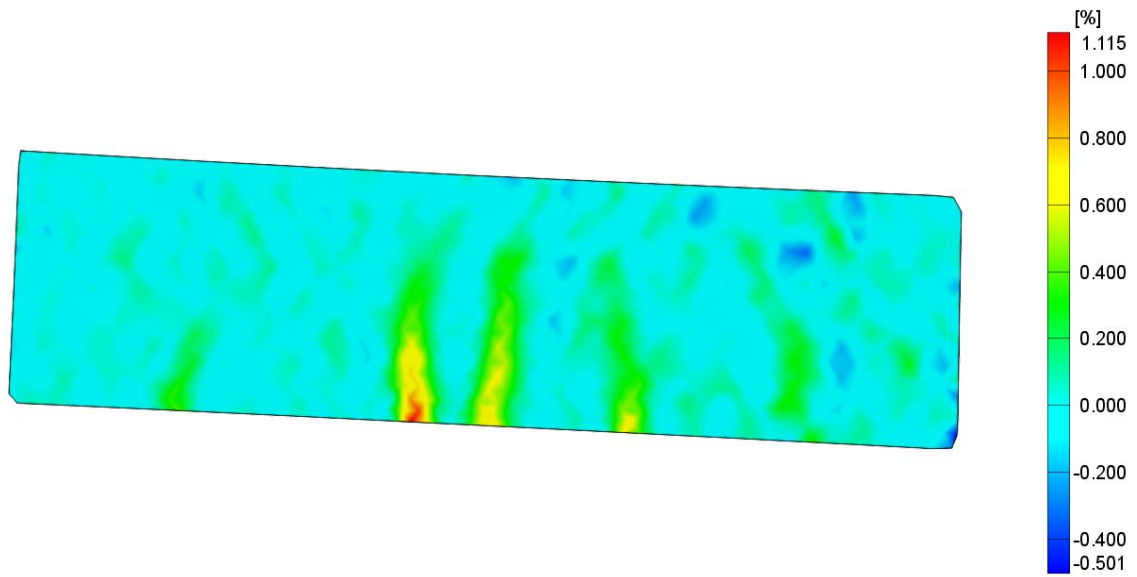


**Fig. B.26:** Map of horizontal strains in beam II-1'-B1 after 5th cycle of loading

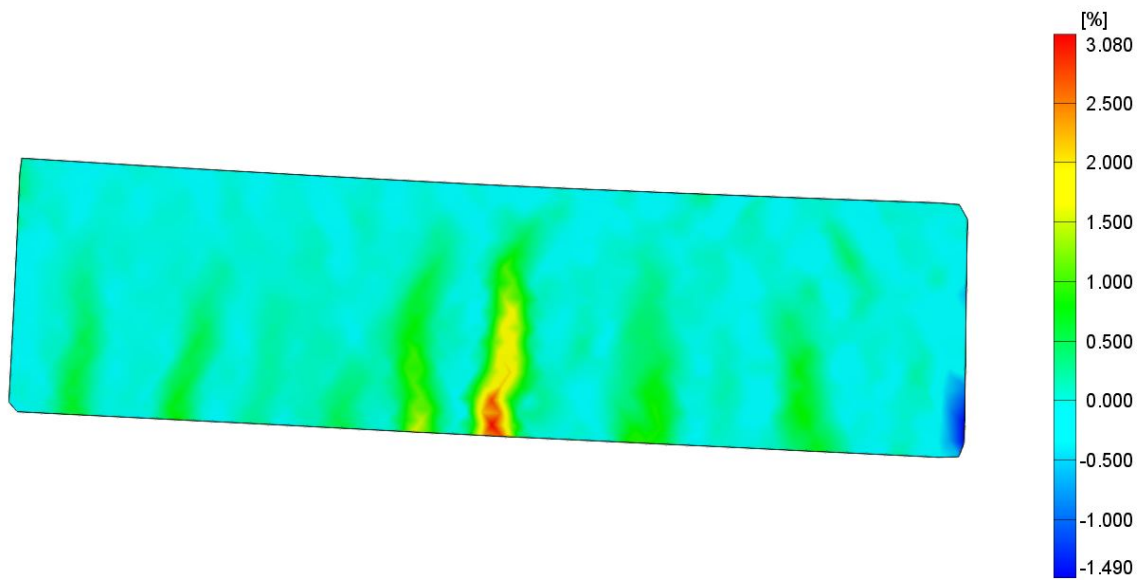


**Fig. B.27:** Map of horizontal strains in beam II-1'-B1 after 10th cycle of loading

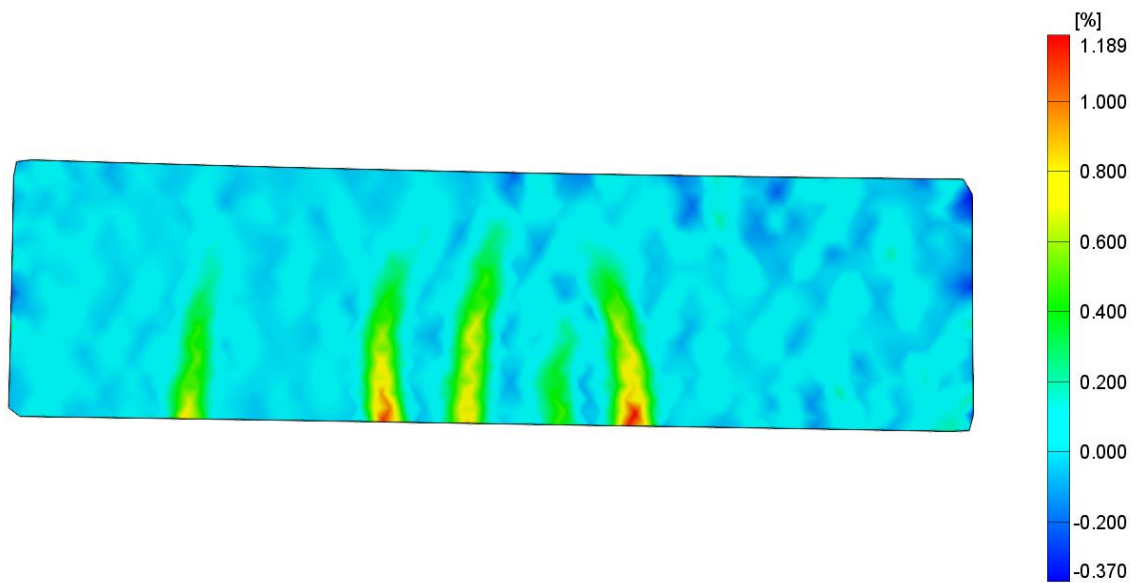


**Fig. B.28:** Map of horizontal strains in beam II-1'-B2 after 5th cycle of loading

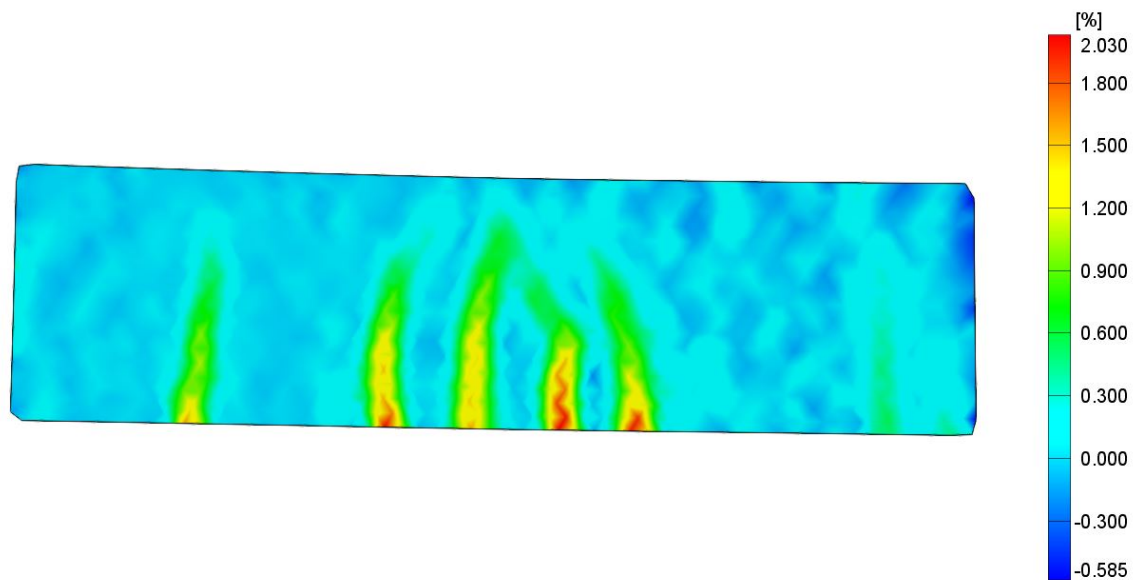


**Fig. B.29:** Map of horizontal strains in beam II-1'-B2 after 10th cycle of loading

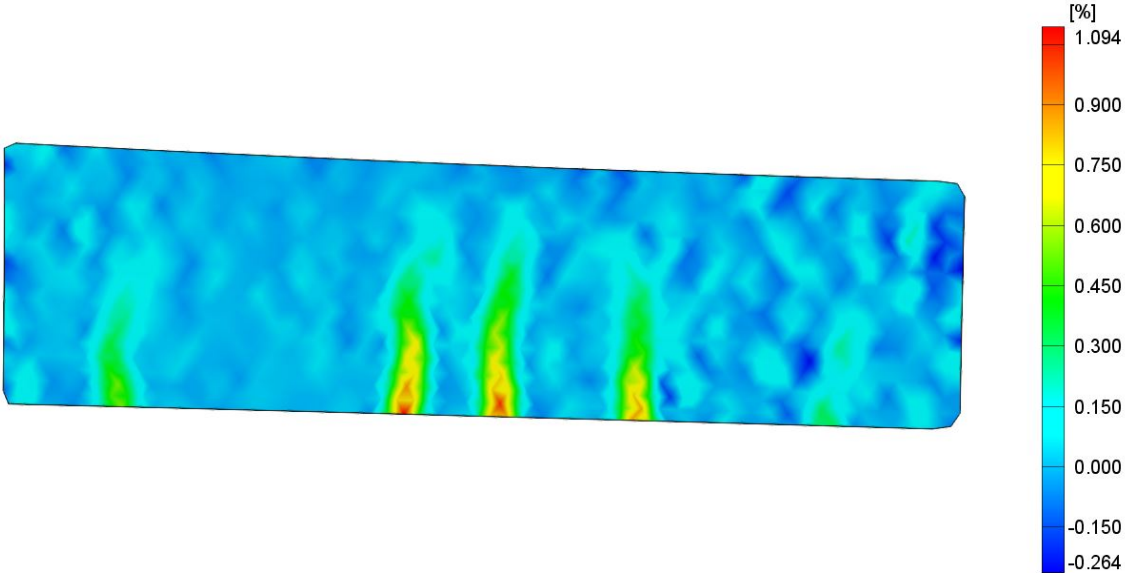


Fig. B.30: Map of horizontal strains in beam II-1'-B3 after 5th cycle of loading

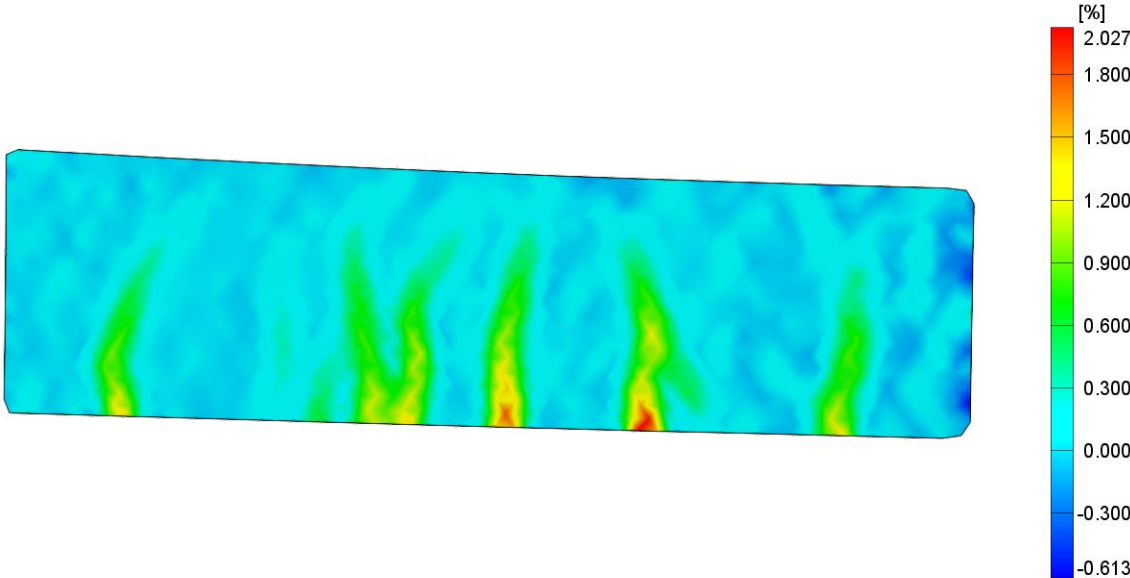
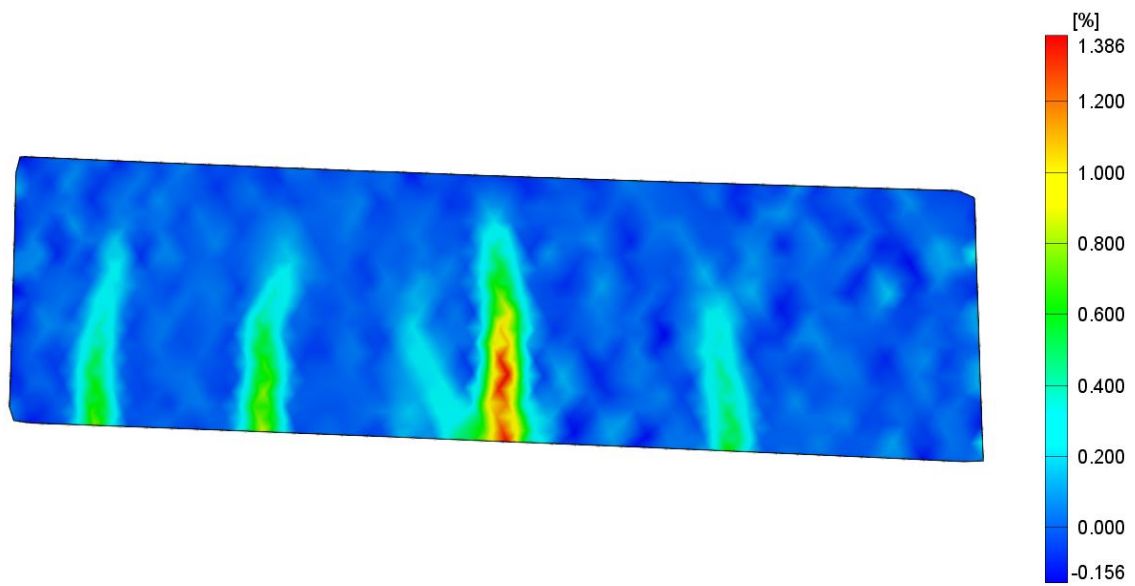
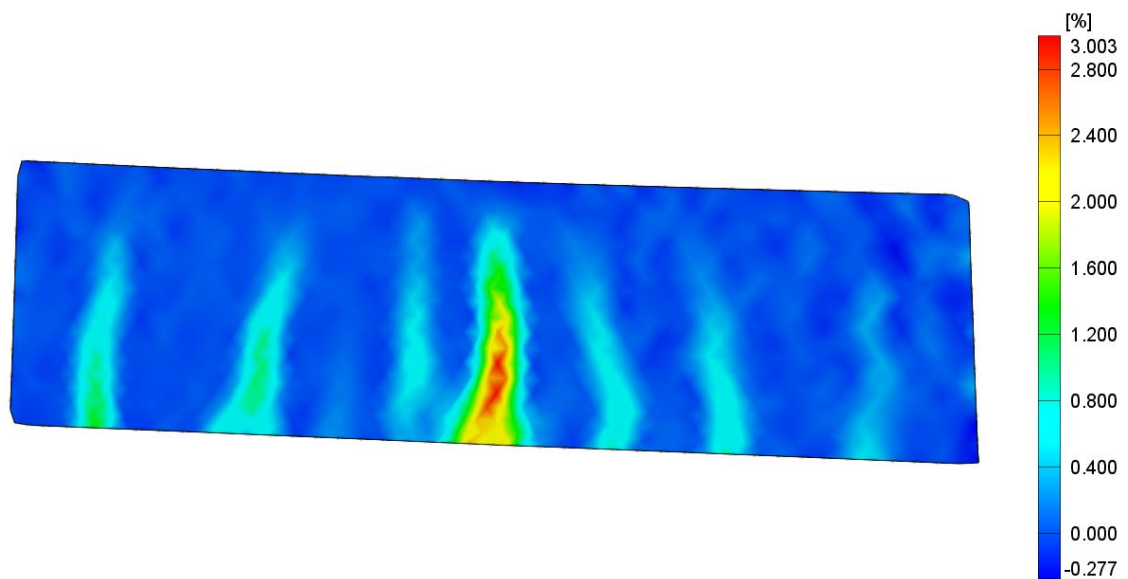


Fig. B.31: Map of horizontal strains in beam II-1'-B3 after 10th cycle of loading



**Fig. B.32:** Map of horizontal strains in beam II-2'-B1 after 5th cycle of loading



**Fig. B.33:** Map of horizontal strains in beam II-2'-B1 after 10th cycle of loading

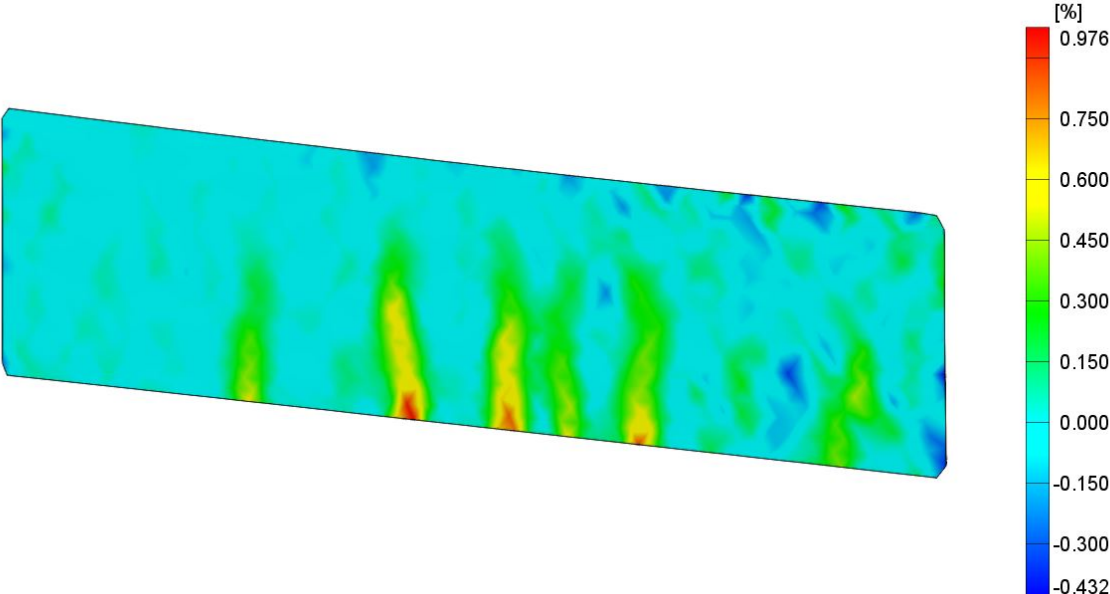


Fig. B.34: Map of horizontal strains in beam II-2'-B2 after 5th cycle of loading

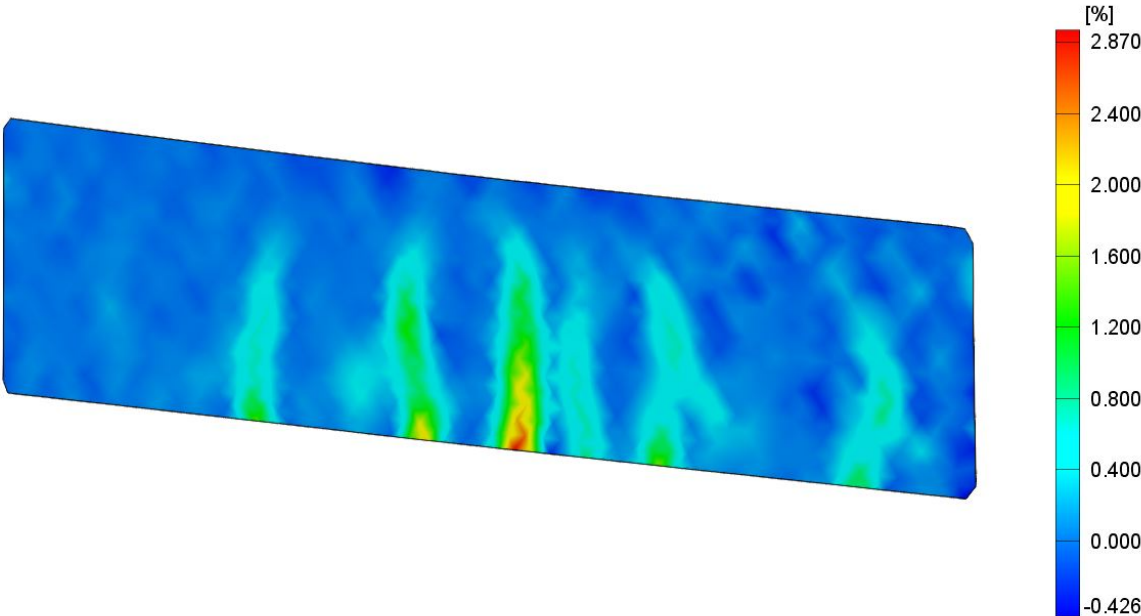
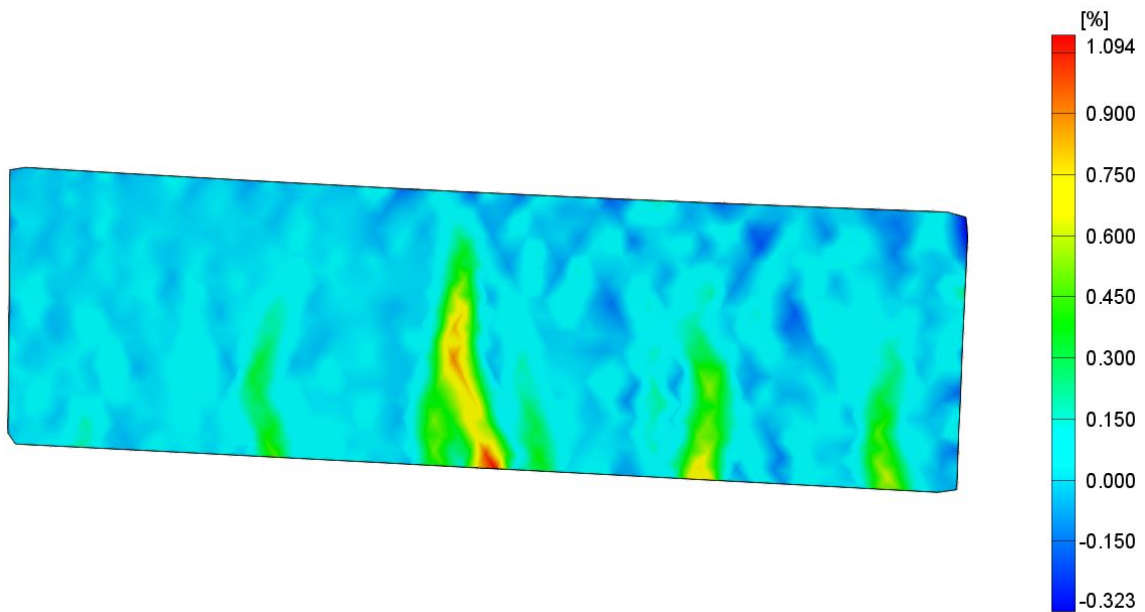
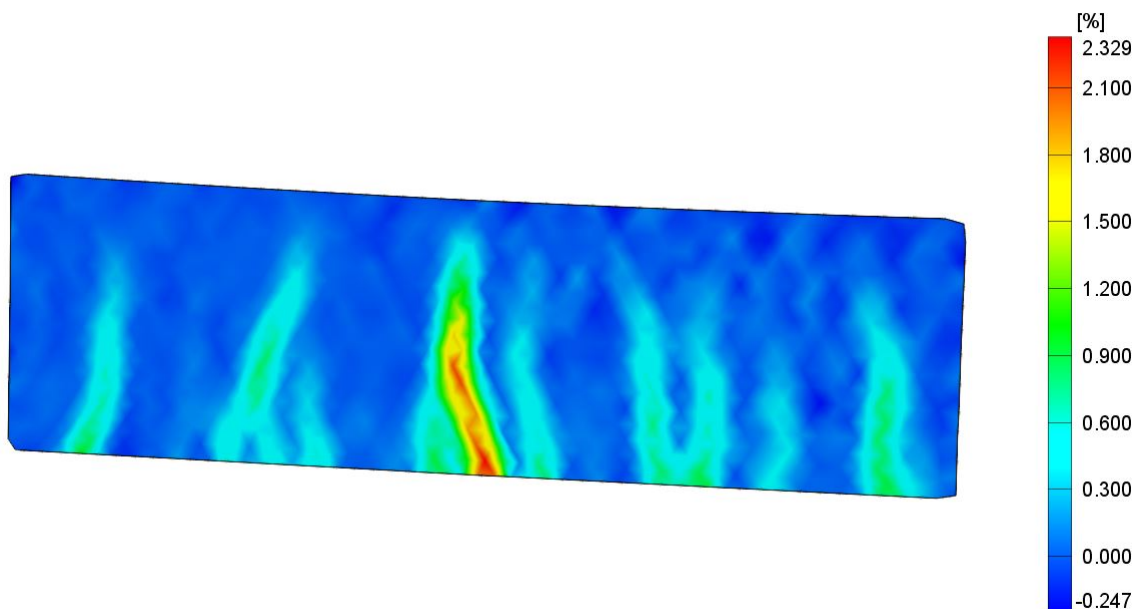


Fig. B.35: Map of horizontal strains in beam II-2'-B2 after 10th cycle of loading



**Fig. B.36:** Map of horizontal strains in beam II-2'-B3 after 5th cycle of loading



**Fig. B.37:** Map of horizontal strains in beam II-2'-B3 after 10th cycle of loading



# Bibliografia

Bibliography is prepared in the alphabetical order (according to the surname of the first author) in separation of references to standards used in the dissertation.

Papers published in the Polish language are denoted with [PL].

- [1] *ABAQUS 6.14, Analysis User's Guide*, Simulia Manuals, Dessault Systemes, 2014.
- [2] Abbass W., Khan M.I., Mourad S., *Evaluation of mechanical properties of steel fiber reinforced concrete with different strengths of concrete*, Construction and Building Materials (168), p. 556-569, 2018.
- [3] Afroughsabet V., Biolzi L., Monteiro P.J.M., *The effect of steel and polypropylene fibers on the chloride diffusivity and drying shrinkage of high-strength concrete*, Composites Part B (139), p. 84-96, 2018.
- [4] Afroughsabet V., Biolzi L., Ozbakkaloglu T., *High-performance fiber-reinforced concrete: a review*, J Mater Sci (51), p. 6517-6551, 2016.
- [5] Afroughsabet V., Ozbakkaloglu T., *Mechanical and durability properties of high-strength concrete containing steel and polypropylene fibers*, Construction and Building Materials (94), p. 73-82, 2015.
- [6] Ahmed T.A.H., Daoud O.M.A., *Influence of polypropylene fibres on concrete properties*, IOSR Journal of Mechanical and Civil Engineering (5), p. 9-20, 2016.
- [7] Ahmed T.W., Ali A.A.M., Zidan R.S., *Properties of high strength polypropylene fiber concrete containing recycled aggregate*, Construction and Building Materials (241-118010), 2020.
- [8] Akça K.R., Çakir O., İpek M., *Properties of polypropylene fibre reinforced concrete using recycled aggregates*, Construction and Building Materials (98), p. 620-630, 2015.
- [9] Alberti M.G., Enfedaque A., Gálvez J.C., *Fracture mechanics of polyolefin fibre reinforced concrete: Study of the influence of the concrete properties, casting procedures, the fibre length and specimen size*, Engineering Fracture Mechanics (154), p. 225-244, 2016.

- [10] Alfarah B., López-Almansa F., Oller S., *New methodology for calculating damage variables evolution in Plastic Damage Model for RC structures*, Engineering Structures (132), p. 70-86, 2017.
- [11] Algourdin N., Pliya P., Beaucour A.-L., Simon A., Noumowé A., *Influence of polypropylene and steel fibres on thermal spalling and physical and mechanical properties of concrete under different heating rates*, Construction and Building Materials (259-119690), 2020.
- [12] Alhozaimy A.M., Soroushian P., Mirza F., *Mechanical properties of polypropylene fiber reinforced concrete and the effects of pozzolanic materials*, Cement & Concrete Composites (18), p. 85-92, 1996.
- [13] Ali B., Qureshi L.A., Kurda R., *Environmental and economic benefits of steel, glass and polypropylene fiber reinforced cement composite application in jointed plain concrete pavement*, Composite Communications (22-100437), 2020.
- [14] Alsadey S., *Effect of polypropylene fiber on properties of mortar*, International Journal of Energy Science and Engineering (2), p. 8-12, 2016.
- [15] Alsalman A., Dang C.N., Prinz G.S., Hale W.M., *Evaluation of modulus of elasticity of ultra-high performance concrete*, Construction and Building Materials (153), p. 918-928, 2017.
- [16] Altalabani D., Bzeni D.K.H., Linsel S., *Mechanical properties and load deflection relationship of polypropylene fiber reinforced self-compacting lightweight concrete*, Construction and Building Materials (252-119084), 2020.
- [17] Amin M., Tayeh B.A., Saad Agwa I., *Investigating the mechanical and microstructure properties of fibre-reinforced lightweight concrete under elevated temperatures*, Case Studies in Construction Materials (13-e00459), 2020.
- [18] Aslani F., Jowkarmeimandi R., *Stress-strain model for concrete under cyclic loading*, Magazine of Concrete Research (64), p. 673-685, 2012.
- [19] Aslani F., Nejadi S., *Self-compacting concrete incorporating steel and polypropylene fibers: Compressive and tensile strengths, moduli of elasticity and rupture, compressive stress-strain curve, and energy dissipated under compression*, Composites: Part B (53), p. 121-133, 2013.
- [20] Aulia T.B., *Effects of polypropylene fibres on the properties of high-strength concretes*, LACER (7), p. 43-59, 2002.
- [21] Balendran R.V., Zhou F.P., Nadeem A., Leung A.Y.T., *Influence of steel fibres on strength and ductility of normal and lightweight high strength concrete*, Building and Environment (37), p. 1361-1367, 2002.

- [22] Banthia N., Gupta R., *Influence of polypropylene fiber geometry on plastic shrinkage cracking in concrete*, Cement and Concrete Research (26), p. 1263-1267, 2006.
- [23] Banthia N., Mindness S., Trottier J. *Impact resistance of steel fiber reinforced concrete*, ACI Materials Journal, p. 472-479, 1996.
- [24] Bayasi Z., Zeng J., *Properties of polypropylene fiber reinforced concrete*, ACI Materials Journal (90), p. 605-610, 1993.
- [25] Bažant Z.P., Oh B.H., *Crack band theory for fracture of concrete*, Materials and Structures (16), p. 155-177, 1983.
- [26] Bažant Z.P., Pijaudier-Cabot G., Pan J.Y., *Ductility snapback size effect, and redistribution in softening beams and frames*, ASCE J. of Structural Engrg. 113 (12), p. 2348-2364, 1987.
- [27] Behfarnia K., Behravan A., *Application of high performance polypropylene fibers in concrete lining of water tunnels*, Materials and Design (55), p. 274-279, 2014.
- [28] Bentur A., Mindness S., *Fiber Reinforced Cementitious Composites*, Taylor & Francis, 2007.
- [29] Bhogone M.V., Subramaniam K.V.L., *Early-age tensile constitutive relationships for steel and polypropylene fiber reinforced concrete*, Engineering Fracture Mechanics (244-107556), 2021.
- [30] Blazy J., Blazy R., *Polypropylene fiber reinforced concrete and its application in creating architectural forms of public spaces*, Case Studies in Construction Materials (14-e00549), 2021.
- [31] Bolat H., Şimşek O., Çullu M., Durmuş G., Can Ö., *The effects of macro synthetic fiber reinforcement use on physical and mechanical properties of concrete*, Composites: Part B (61), p. 191-198, 2014.
- [32] Brandt A.M., *Fibre reinforced cement-based (FRC) composites after over 40 years of development in building and civil engineering*, Composite Structures (86), p. 3-9, 2008.
- [33] Broda J., *Application of polypropylene fibrillated fibres for reinforcement of concrete and cement mortars*, High Performance Concrete Technology and Application, InTech, p. 189-205, 2016.
- [34] Broda J., Gawłowski A., Slusarczyk Cz., Wlochowicz A., Fabia J., *The influence of additives on the structure of polypropylene fibres*, Dyes and Pigments (74), p. 508-511, 2007.

- [35] Buratti N., Mazzotti C., Savoia M., *Post-cracking behaviour of steel and macro-synthetic fibre-reinforced concretes*, Construction and Building Materials (25), p. 2713-2722, 2011.
- [36] Caggiano A., Gambarelli S., Martinelli E., Nisticò N., Pepe M., *Experimental characterization of the post-cracking response in Hybrid Steel/Polypropylene Fiber-Reinforced Concrete*, Construction and Building Materials (125), p. 1035-1043, 2016.
- [37] Castillo-Lara J.F., Flores-Johnson E.A., Valadez-Gonzalez A., Herrera-Franco P., Carrillo J.G., Gonzalez-Chi P.I., Li Q.M., *Mechanical properties of natural fiber reinforced foamed concrete*, Materials (13-3060), 2020.
- [38] Castoldi R.S., Souza L.M.S., Andrade Silva F., *Comparative study on the mechanical behaviour and durability of polypropylene and sisal fiber reinforced concretes*, Construction and Building Materials (211), p. 617-628, 2019.
- [39] Chen W.F., *Plasticity in reinforced concrete*, McGraw-Hill Book Company, 1982.
- [40] Das C.S., Dey T., Dandapat R., Mukharjee B.B., Kumar J., *Performance evaluation of polypropylene fibre reinforced recycled aggregate concrete*, Construction and Building Materials (189), p. 649-659, 2018.
- [41] Das S., Singh P., Negi V., *Strength and durability properties of polypropylene fiber reinforced, recycled coarse aggregate concrete*, Indian Concrete Journal, p. 62-69, 2018.
- [42] De Borst R., *Fracture in quasi-brittle materials: a review of continuum damage-based approaches*, Engineering fracture mechanics (69), p. 95-112, 2002.
- [43] Demby M., Kuczma M., *Analysis of Polypropylene Fibre Reinforced High Performance Concrete Beams*, 4th Polish Congress of Mechanics and 23rd International Conference on Computer Methods in Mechanics PCM-CMM, Krakow, 2019.
- [44] Demby M., Kuczma M., *Finite element analysis of ultra-high performance concrete beams*, 22nd International Conference on Computer Methods in Mechanics CMM, Lublin, 2017.
- [45] Demby M., Kuczma M., *Badania i analiza wyników nowego betonu zbrojonego włóknami metalowymi, cz.I-III*, the research report, 2021, [PL].
- [46] Demby M., Kuczma M., *Badania i analiza wyników nowego betonu zbrojonego włóknami metalowymi, cz.I-III*, the research report, 2021, [PL].
- [47] Demin W., Fukang H., *Investigation for plastic damage constitutive models of the concrete material*, Procedia Engineering (210), p. 71-78, 2017.

- [48] Denisiewicz A., *Modelowanie dwuskalowe związkow konstytutywnych betonu z proszkow reaktywnych i ich walidacja doswiadczalna*, supervisor: Prof. Mieczyslaw Kuczma, Uniwersytet Zielonogorski, 2013, [PL].
- [49] Denisiewicz A., Kuczma M., *Two-scale numerical homogenization of the constitutive parameters of reactive powder concrete*, Journal for Multiscale Computational Engineering (12), p. 361-374, 2014.
- [50] Ding Y., Wang Q., Pacheco-Torgal F., Zhang Y., *Hybrid effect of basalt fiber textile and macro polypropylene fiber on flexural load-bearing capacity and toughness of two-way concrete slabs*, Construction and Building Materials (261-119881), 2020.
- [51] Dwivedi M., Mishra S., Singh V., *Effect of polypropylene fibres on flexural strength of M30 grade concrete*, IOSR Journal of Mechanical and Civil Engineering (11), p. 93-97, 2014.
- [52] Fédération Internationale du Béton, Task Group 8.2, *Constitutive modelling of high strength/high performance concrete*, International Federation for Structural Concrete, (*fib*) Bulletin no. 42, 2008.
- [53] Feng J., Yang F., Qian S., *Improving the bond between polypropylene fiber and cement matrix by nano calcium carbonate modification*, Construction and Building Materials (269-121249), 2021.
- [54] Flores Medina N., Barluenga G., Hernández-Olivares F., *Combined effect of Polypropylene fibers and Silica Fume to improve the durability of concrete with natural Pozzolans blended cement*, Construction and Building Materials (96), p. 556-566, 2015.
- [55] Garg R., Garg R., *Performance evaluation of polypropylene fiber waste reinforced concrete in presence of silica fume*, Materials Today: Proceedings (43), p. 809-816, 2021.
- [56] Geers M.G.D., *Continuum damage mechanics. Fundamentals, high-order theories and computational aspects*, Eindhoven University of Technology, 1998.
- [57] Geers M.G.D., *Experimental analysis and computational modelling of damage and fracture*, Eindhoven University of Technology, 1997.
- [58] Gencil O., Ozel C., Brostow W., Martínez-Barrera G., *Mechanical properties of self-compacting concrete reinforced with polypropylene fibres*, Materials Research Innovations (15), p. 216-225, 2011.
- [59] Ghafari E., Costa H., Júlio E., *Statistical mixture design approach for eco-efficient UHPC*, Cement & Concrete Composites (55), p. 17-25, 2015.
- [60] Glinicki M., *Beton ze zbrojeniem strukturalnym*, XXV Ogólnopolskie Warsztaty Pracy Projektanta Konstrukcji, p. 279-308, Szczyrk, 2010, [PL].

- [61] Glinicki M., *Energy absorption capacity of glass fibre reinforced cement composites*, Archives of Civil Engineering (XLIII), p. 71-84, 1997.
- [62] Głodkowska W., Kobaka J., *Modelling of properties and distribution of steel fibres within a fine aggregate concrete*, Construction and Building Materials (44), p. 645-653, 2013.
- [63] Grassl P., Xenos D., Nyström U., Rempling R., Gylltoft K., *CDPM2: A damage-plasticity approach to modelling the failure of concrete*, International Journal of Solids and Structures (50), p. 3805-3816, 2013.
- [64] Grdic Z.J., Curcic G.A.T., Ristic N.S., Despotovic I.M., *Abrasion resistance of concrete micro-reinforced with polypropylene fibers*, Construction and Building Materials (27), p. 305-312, 2012.
- [65] Groeneveld A.B., Ahlborn T.M., Crane C.K., Burchfield C.A., Landis E.N., *Dynamic strength and ductility of ultra-high performance concrete with flow -induced fiber alignment*, International Journal of Impact Engineering (111), p. 37-45, 2018.
- [66] Guo H., Jiang L., Tao J., Chen Y., Zheng Z., Jia B., *Influence of a hybrid combination of steel polypropylene fibers on concrete toughness*, Construction and Building Materials (275-122132), 2021.
- [67] Hadi M.N.S., *An investigation of the behaviour of steel and polypropylene fibre reinforced concrete slabs*, 7th International Conference. Concrete: Construction's Sustainable Option - Harnessing Fibres for Concrete Construction, Dundee, Scotland, 2008.
- [68] Hager I., Mróz K., Tracz T., *Contribution of polypropylene fibres melting to permeability change in heated concrete - the fibre amount and length effect*, IOP Conf. Series: Materials Science and Engineering (706-012009), 2019.
- [69] Hafezolghorani M., Hejazi F., Vaghei R., Jaafar M.S.B., Karimzade K., *Simplified Damage Plasticity Model for Concrete*, Structural Engineering International (1), p. 68-78, 2017.
- [70] Han J.-W., Jeon J.-H., Park C.-G., *Bond characteristics of macro polypropylene fiber in cementitious composites containing nanosilica and styrene butadiene latex polymer*, International Journal of Polymer Science (2015-207456), 2015.
- [71] Hongbo Z., Haiyun Z., Hongxiang G., *Characteristics of ductility enhancement of concrete by a macro polypropylene fiber*, Results in Materials (100087), 2020.
- [72] Horszczaruk E., *Abrasion resistance of high-performance hydraulic concrete with polypropylene fibers*, Tribologia (1), p. 63-72, 2012.
- [73] Hsie M., Tu Ch., Song P.S., *Mechanical properties of polypropylene hybrid fiber-reinforced concrete*, Material Science and Engineering A (494), p. 153-157, 2008.

- [74] Hussain I., Ali B., Akhtar T., Jameel M.S., Raza S.S., *Comparison of mechanical properties of concrete and design thickness of pavement with different types of fiber-reinforcements (steel, glass, and polypropylene)*, Case Studies in Construction Materials (13-e00429), 2020.
- [75] Jacob G.C., Starbuck J.M., Fellers J.F., Simunovic S., Boeman R.G., *The effect of loading rate on the fracture toughness of fiber reinforced polymer composites*, Journal of Applied Polymer Science (96), p. 899-904, 2005.
- [76] Jain R., Gupta R., Khare M.G., Dharmadhikari A.A., *Use of polypropylene fibre reinforced concrete as a construction material for rigid pavements*, The Indian Concrete Journal (85), p. 45-53, 2011.
- [77] Jankowiak T., *Kryteria zniszczenia betonu poddanego obciążeniom quasi-statycznym i dynamicznym (Failure criteria for concrete under quasi-static and dynamic loadings)*, Wydawnictwo Politechniki Poznańskiej, 2011, [PL].
- [78] Jankowiak T., Łodygowski T., *Identification of parameters of concrete damage plasticity constitutive model*, Foundations of Civil and Environmental Engineering (6), p. 53-69, 2005.
- [79] Jasiczak J., Wdowska A., Rudnicki T., *Betony ultrawysokowartościowe - właściwości, technologie, zastosowania*, Stowarzyszenie Producentów Cementu, 2008, [PL].
- [80] Juhász K.P., Schaul P., Nagy L., *Effect of the loading rate on fibre reinforced concrete beams*, IOP Conference Series: Materials Science and Engineering (246-012040), 2017.
- [81] Kachanov L. M., *Introduction to continuum damage mechanics*, Martinus Nijhoff Publishers, 1986.
- [82] Kakooei S., Akil H.M., Jamshidi M., Rouhi J., *The effects of polypropylene fibers on the properties of reinforced concrete structures*, Construction and Building Materials (27), p. 73-77, 2012.
- [83] Kalifa P., Chéné G., Gallé C., *High-temperature behaviour of HPC with polypropylene fibres. From spalling to microstructure*, Cement and Concrete Research (31), p. 1487-1499, 2001.
- [84] Karahan O., Atiş C.D., *The durability properties of polypropylene fiber reinforced fly ash concrete*, Materials and Design (32), p. 1044-1049, 2011.
- [85] Karimipour A., Ghalehnovi M., Brito J., Attari M., *The effect of polypropylene fibres on the compressive strength, impact and heat resistance of self-compacting concrete*, Structures (25), p. 72-87, 2020.

- [86] Kato J., Ramm E., *Optimization of fiber geometry for fiber reinforced composites considering damage*, Finite Elements in Analysis and Design (46), p. 401-415, 2010.
- [87] Katzer J., *Krajowe włókna stalowe uszlachetniające beton*, Warstwy (4), p. 136-139, 1997, [PL].
- [88] Khan M.I., Abbas Y.M., Fares G., *Review of high and ultrahigh performance cementitious composites incorporating various combinations of fibers and ultrafines*, Journal of King Saud University (29), p. 339-347, 2017.
- [89] Kmiecik P., Kamiński M., *Modelling of reinforced concrete structures and composite structures with concrete strength degradation taken into consideration*, Archives of Civil and Mechanical Engineering (3), 2011.
- [90] Köksal F., Şahin Y., Gencil O., Yiğit I., *Fracture energy-based optimisation of steel fibre reinforced concretes*, Engineering Fracture Mechanics (107), p. 29-37, 2013.
- [91] Kuczma M., Whiteman J.R., *Variational inequality formulation for flow theory plasticity*, Int. J. Engng Sci. (33), p. 1153-1169, 1995.
- [92] Kuczma M., Demby M., *High performance concrete: modelling, simulation and testing*, 10th German-Greek-Polish Symposium "Recent Advances in Mechanics", 2020.
- [93] Kuczma M., Demby M., *Modelling and simulation of HPC structural elements*, 89th GAMM Annual Meeting, Munich, Germany, 2018.
- [94] Kuczma M., Demby M., *Opracowanie dotyczące wyników badań wytrzymałości resztkowej na rozciąganie przy zginaniu belek betonowych zbrojonych włóknami stalowymi*, the research report, 2020, [PL].
- [95] Kusumawardaningsih Y., Fehling E., Ismail M., *UHPC compressive strength test specimens: Cylinder or cube?*, The 5th International Conference of Euro Asia Civil Engineering Forum, Procedia Engineering (125), p. 1076-1080, 2015.
- [96] Kusumawardaningsih Y., Fehling E., Ismail M., Aboubakr A., *Tensile strength behaviour of UHPC and UHPFRC*, The 5th International Conference of Euro Asia Civil Engineering Forum, Procedia Engineering (125), p. 1081-1086, 2015.
- [97] Kwan A.K.H., Ho J.C.M., Pam H.J., *Flexural strength and ductility of reinforced concrete beams*, Structures & Buildings (152), p. 361-369, 2002.
- [98] Labib W.A., *Fibre Reinforced Cement Composites*, Cement Based Materials, In-techOpen, 2018.

- [99] Lanzoni L., Nobili A., Tarantino A.M., *Performance evaluation of a polypropylene-based draw-wired fibre for concrete structures*, Construction and Building Materials (28), p. 798-806, 2012.
- [100] Lee J., Fenves G.L., *Plastic-damage model for cyclic loading of concrete structures*, Journal of Engineering Mechanics (124), p. 892-900, 1998.
- [101] Leong G.W., Mo K.H., Loh Z.P., Ibrahim Z., *Mechanical properties and drying shrinkage of lightweight cementitious composite incorporating perlite microspheres and polypropylene fibers*, Construction and Building Materials (246-118410), 2020.
- [102] Li B., Chen M., Cheng F., Liu L., *The mechanical properties of polypropylene fiber reinforced concrete*, Journal of Wuhan University of Technology, 2004.
- [103] Li D., Liu S., *Macro polypropylene fiber influences on crack geometry and water permeability of concrete*, Construction and Building Materials (231-117128), 2020.
- [104] Li J., Niu J., Wan C., Liu X., Jin Z., *Comparison of flexural property between high performance polypropylene fiber reinforced lightweight aggregate concrete and steel fiber reinforced lightweight aggregate concrete*, Construction and Building Materials (157), p. 729-736, 2017.
- [105] Liu F., Ding W., Qiao Y., *An experimental investigation on the integral waterproofing capacity of polypropylene fiber concrete with fly ash and slag powder*, Construction and Building Materials (212), p. 675-686, 2019.
- [106] Lohaus L., Anders S., *Ductility and Fatigue Behaviour of Polymer-Modified and Fibre-Reinforced High-Performance Concrete*, Advances in Construction Materials, p. 165-172, 2007.
- [107] Lohaus L., Anders S., *Effects of polymer- and fibre modifications on the ductility, fracture properties and micro-crack development of ultra-high performance concrete*, Ultra High Performance Concrete (UHPC) - Proceedings of the International Symposium on Ultra High Performance Concrete, Kassel, Germany, 2004.
- [108] Lubliner J., Oliver J., Oller S., Onate E., *A plastic-damage model for concrete*, International Journal of Solid Structures (25), p. 229-326, 1989.
- [109] Mahdikhani M., Bamshad O., Shirvani M.F., *Mechanical properties and durability of concrete specimens containing nano silica in sulfuric acid rain condition*, Construction and Building Materials (167), p. 929-935, 2018.
- [110] Majewski S., *The mechanics of structural concrete in terms of elasto-plasticity*, Silesian Polytechnic Publishing House, Gliwice, 2003.
- [111] Małek M., Jackowski M., Łasica W., Kadela M., *Characteristics of recycled polypropylene fibers as an addition to concrete fabrication based on Portland cement*, Materials (13), 2020.

- [112] Małek M., Jackowski M., Łasica W., Kadela M., *Influence of polypropylene, glass and steel fibre on the thermal properties of concrete*, Materials (14), 2021.
- [113] Małek M., Łasica W., Kadela M., Kluczynski J., Dudek D., *Physical and mechanical properties of polypropylene fibre-reinforced cement-glass composite*, Materials (14), 2021.
- [114] Mardani-Aghabaglou A., Ilhan M., Özen S., *The effect of shrinkage reducing admixture and polypropylene fibers on drying shrinkage behaviour of concrete*, Cement Wapno Beton (3), p. 227-237, 2019.
- [115] Marković I., *High-Performance Hybrid-Fibre Concrete*, DUP Science DUP, Delft, 2006.
- [116] Mashrei M. A., Sultan A. A., Mahdi A. M., *Effects of polypropylene fibers on compressive and flexural strength of concrete material*, International Journal of Civil Engineering and Technology (9), p. 2208-2217, 2018.
- [117] Mazloom M., Ramezaniyanpour A.A., Brooks J.J., *Effect of silica fume on mechanical properties of high-strength concrete*, Cement & Concrete Composites (26), p. 347-357, 2004.
- [118] McCormick N., Lord J., *Digital Image Correlation*, Materials Today (13), p. 52-54, 2010.
- [119] Meng C., Li W., Cai L., Shi X., Jiang C., *Experimental research on durability of high-performance synthetic fibers reinforced concrete: Resistance to sulfate attack and freezing-thawing*, Construction and Building Materials (262-120055), 2020.
- [120] Meng K., Xu L., Chi Y., *Experimental investigation on the mechanical behavior of hybrid steel-polypropylene fiber reinforced concrete under conventional triaxial cyclic compression*, Construction and Building Materials (291-123262), 2021.
- [121] Meza de Luna A., Ortiz J.Á., Peralta L., Pacheco J., Soto J.J., Rangel S.H., Padilla R., Alvarado J., *Experimental mechanical characterization of steel and polypropylene fiber reinforced concrete*, Revista Técnica de la Facultad de Ingeniería Universidad del Zulia (37), p. 106-115, 2014.
- [122] Mohajerani A., Hui S.-Q., Mirzababaei M., Arulrajah A., Horpibulsuk S., Kadir A.A., Rahman M.T., Maghool F., *Amazing types, properties, and applications of fibers in construction materials*, Materials (12-2513), 2019.
- [123] Mohammadhosseini H., Alrshoudi F., Tahir M.M., Alyousef R., Alghamdi H., Alharbi Y.R., Alsaif A., *Durability and thermal properties of prepacked aggregate concrete reinforced with waste polypropylene fibers*, Journal of Building Engineering (101723), 2020.

- [124] Monteiro V., Lima L., Silva F., *On the mechanical behaviour of polypropylene, steel and hybrid fiber reinforced self-consolidating concrete*, Construction and Building Materials (188), p. 280-291, 2018.
- [125] Najimi M., Farahani F.M., Pourkhorshidi A.R., *Effects of polypropylene fibers on physical and mechanical properties of concretes*, In Proceedings of the 3rd International Conference on Concrete & Development, Iran, p. 1073-1081, 2009.
- [126] Naziri B., Maj M., Ubysz A., *Odkształcenia sprężyste i trwałe w żelbetowej belce wspornikowej z betonu o wysokiej wytrzymałości*, Materiały Budowlane (6), p. 74-75, 2015, [PL].
- [127] Necevska-Cvetanovska G., Petrusevska-Apostolska R., *Strength and ductility capacity of high strength concrete elements*, 13th World Conference on Earthquake Engineering, Vancouver, B.C., Canada, paper no. 3128, 2004.
- [128] Neville A. M., *Properties of concrete*, 5th Edition, Prentice Hall, 2012.
- [129] Nguyen G., Korsunsky A., *Damage-plasticity modelling of concrete: calibration of parameters using separation of fracture energy*, International Journal of Fracture (139), p. 325-332, 2006.
- [130] Nili M., Afroughsabet V., *The effects of silica fume and polypropylene fibers on the impact resistance and mechanical properties of concrete*, Construction and Building Materials (24), p. 927-933, 2010.
- [131] Ozawa M., Morimoto H., *Effects of various fibres on high-temperature spalling in high-performance concrete*, Construction and Building Materials (71), p. 83-92, 2014.
- [132] Ozawa M., Parajuli S.S., Uchida Y., Zhou B., *Preventive effects of polypropylene and jute fibers on spalling of UHPC at high temperatures in combination with waste porous ceramic fine aggregate as an internal curing material*, Construction and Building Materials (206), p. 219-225, 2019.
- [133] Pajak M., Janiszewski J., *Steel fibre reinforced self-compacting concrete subjected to quasi-static and dynamic loading conditions*, AIP Conference Proceedings (2239-020037), 2020.
- [134] Pam H.J., Kwan A.K.H., Islam M.S., *Flexural strength and ductility of reinforced normal- and high-strength concrete beams*, Structures & Buildings (146), p. 381-389, 2001.
- [135] Peerlings R. H. J., De Borst R., Brekelmans W.A.M., De Vree J. H. P., *Gradient enhanced damage for quasi-brittle materials*, International Journal for Numerical Methods in Engineering (39), p.3391-3403, 1996.
- [136] Petri M., *Włókna do mikrozbrojenia betonu*, Materiały Budowlane (2), p. 53-54, 1998, [PL].

- [137] Piatek-Sierek E., *Kalibracja parametrów określających właściwości betonu opisanego modelem plastyczno-degradacyjnym zaimplementowanym w programie Abaqus*, supervisor: Prof. Adam Podhorecki, Uniwersytet Technologiczno-Przyrodniczy w Bydgoszczy, 2013, [PL].
- [138] Pietrzak A., Ulewicz M., *The effect of the addition of polypropylene fibres on improvement on concrete quality*, MATEC Web of Conferences (183-02011), 2018.
- [139] Pyo S, Alkaysi M., El-Tawil S., *Crack propagation speed in ultra high performance concrete (UHPC)*, Construction & Building Materials (114), p.109-118, 2016.
- [140] Qin Y., Zhang X., Chai J., Xu Z., Li S., *Experimental study of compressive behaviour of polypropylene-fiber-reinforced and polypropylene-fiber-fabric-reinforced concrete*, Construction and Building Materials (194), p. 216-225, 2019.
- [141] Ramesh B., Gokulnath V., Kumar M.R., *Detailed study on flexural strength of polypropylene fiber reinforced self-compacting concrete*, Materials Today: Proceedings (22), p. 1054-1058, 2020.
- [142] Ramezaniyanpour A.A., Esmaeili M., Ghahari S.A., Najafi M.H., *Laboratory study on the effect of polypropylene fiber on durability, and physical and mechanical characteristic of concrete for application in sleepers*, Construction and Building Materials (44), p. 411-418, 2013.
- [143] Randl N., Steiner T., Baumgartner E., Mészöly T., *Development of UHPC mixtures from an ecological point of view*, Construction and Building Materials (67), p. 373-378, 2014.
- [144] Rashid M.U., *Experimental investigation on durability characteristics of steel and polypropylene fiber reinforced concrete exposed to natural weathering action*, Construction and Building Materials (250-118910), 2020.
- [145] Renade R., Li V.C., Heard W.F., Williams B.A., *Impact resistance of high strength-high ductility concrete*, Cement and Concrete Research (98), p. 24-35, 2017.
- [146] Richardson A.E., *Compressive strength of concrete with polypropylene fibre additions*, Structural Survey (24), p. 138-153, 2006.
- [147] Richardson A.E., Dave U.V., *The effect of polypropylene fibres within concrete with regard to fire performance in structures*, Structural Survey (26), p. 435-444, 2008.
- [148] Rinaldi Z., Grimaldi A., Galli G., *Ductility of R.C. beams reinforced with FRC*, 13th World Conference on Earthquake Engineering, Vancouver, B.C., Canada, 2004.
- [149] Romualdi J., Baston G., *Mechanics of crack arrest in concrete*, Proceedings ASCE (89), p. 147-168, 1963.

- [150] Sabet F.A., Libre N.A., Shekarchi M., *Mechanical and durability properties of self consolidating high performance concrete incorporating natural zeolite, silica fume and fly ash*, Construction and Building Materials (44), p. 175-184, 2013.
- [151] Sadiqul Islam G.M., Das Gupta S., *Evaluating plastic shrinkage and permeability of polypropylene fiber reinforced concrete*, International Journal of Sustainable Built Engineering (5), p. 345-354, 2016.
- [152] Said S.H., Razak H.A., *The effect of synthetic polyethylene fiber on the strain hardening behaviour of engineered cementitious composite (ECC)*, Materials and Design (86), p. 447-457, 2015.
- [153] Satisha N.S., Shruthi C.G., Kiran B.M., Sanjith J., *Study on effect of polypropylene fibres on mechanical properties of normal strength concrete with partial replacement of cement by GGBS*, International Journal of Advanced Research Trends in Engineering and Technology (5), p. 23-51, 2018.
- [154] Schmidt M., Fehling E., *Ultra-High-Performance Concrete: Research, Development and Application in Europe*, The 7th International Symposium on the Utilization of High-Strength/High-Performance Concrete, p. 51-78, 2005.
- [155] Shen D., Liu X., Zeng X., Zhao X., Jiang G., *Effect of polypropylene plastic fibers length on cracking resistance of high performance concrete at early age*, Construction and Building Materials (244-117874), 2020.
- [156] Shi F., Pham T.M., Hao H., Hao Y., *Post-cracking behaviour of basalt and macro polypropylene hybrid fibre reinforced concrete with different compressive strengths*, Construction and Building Materials (262-120108), 2020.
- [157] Shin S.W., Ghosh S.K., Moreno J., *Flexural ductility of ultra-high-strength concrete members*, ACI Structural Journal (86), p. 394-400, 1989.
- [158] Singh V.K., *Effect of polypropylene fiber on properties of concrete*, International Journal of Engineering Sciences & Research Technology (3), p. 312-317, 2014.
- [159] Singh N.K., Rai B., *A review of fiber synergy in hybrid fiber reinforced concrete*, Journal of Applied Engineering Sciences (8), p. 41-50, 2018.
- [160] Sivakumar A., Santhanam M., *Mechanical properties of high strength concrete reinforced with metallic and non-metallic fibres*, Cement & Concrete Composites (29), p. 603-608, 2007.
- [161] Smarzewski P., *Effect of curing period on properties of steel and polypropylene fibre reinforced ultra-high performance concrete*, IOP Conf. Series: Materials Science and Engineering (245-032059), 2017.
- [162] Soliman N.A., Tagnit-Hamou A., *Development of ultra-high-performance concrete using glass powder - Towards ecofriendly concrete*, Construction and Building Materials (125), p. 600-612, 2016.

- [163] Soliman N.A., Tagnit-Hamou A., *Using glass sand as an alternative for quartz sand in UHPC*, Construction and Building Materials (145), p. 243-252, 2017.
- [164] Soutsos M.N., Le T.T., Lampropoulos A.P., *Flexural performance of fibre reinforced concrete made with steel and synthetic fibres*, Construction and Building Materials (36), p. 704-710, 2012.
- [165] Sukontasukkul P., *Toughness evaluation of steel and polypropylene fibre reinforced concrete beams under bending*, Thammasat Int. J. Sc. Tech. (9), 2004.
- [166] Sümer Y., Aktaş M., *Defining parameters for concrete damage plasticity model*, Challenge Journal of Structural Mechanics (3), p. 149-155, 2015.
- [167] Szczecina M., Winnicki A., *Calibration of the CDP model parameters in Abaqus*, The 2015 World Congress on Advances in Structural Engineering and Mechanics (ASEM15), 2015.
- [168] Szelag M., *Evaluation of cracking patterns of cement paste containing polypropylene fibers*, Composite Structures (220), p. 402-411, 2019.
- [169] Szwed A., Kaminska I., *Modification of Concrete Damage Plasticity model. Part I: Modified plastic potential*, MATEC Web of Conferences (117), 2017.
- [170] Śliwiński J., Zych T., *Wpływ zawartości zaczynu i różnych rodzajów włókien na wytrzymałość fibrobetonu na ściskanie*, Warstwy, p.117-118, 1999, [PL].
- [171] Tadepalli P.R., Mo Y.L., Hsu T.T., *Mechanical properties of steel fibre concrete*, Magazine of Concrete Research (65), p.462-474, 2013.
- [172] Tang M.-Ch., *High Performance Concrete - Past, Present, Future*, International Symposium on Ultra High Performance Concrete, p. 3-9, Kassel, 2004.
- [173] Tanyildizi H., *Statistical analysis for mechanical properties of polypropylene fiber reinforced lightweight concrete containing silica fume exposed to high temperature*, Materials and Design (30), p. 3252-3258, 2009.
- [174] Thompson R.P., Clegg W.J. *Predicting whether a material is ductile or brittle*, Current Opinion in Solid State & Material Science 22, p.100-108, 2018.
- [175] Trtík K., *Concrete reinforced by combination of steel and polypropylene fibres*, XVI Konferencja Naukowo-Techniczna JADWISIN, 1998.
- [176] Ulańska D., Figa M., Stawicka Agnieszka, *Wlasciwosci betonu z dodatkiem wlokien polipropylenowych w zbrojonych elementach zginanych*, Inzynieria i Budownictwo (11), p. 615-619, 2000, [PL].
- [177] Velasco R.V., Filho R.D.T., Fairbairn E.M.R., Lima P.R.L., Neumann R., *Spalling and stress-strain behaviour of polypropylene fibre reinforced hpc after exposure to high temperature*, 6th RILEM Symposium on Fibre-Reinforced Concretes (BE-FIB), p. 699-708, 2004.

- [178] Vítěk J.L., Coufal R., Čítek D., *UHPC - Development and testing on structural elements*, Procedia Engineering (65), p. 218-223, 2013.
- [179] Wadekar A.P., Pandit R.D., *Study on different types fibres used in high strength fibre reinforced concrete*, International Journal of Innovative Research in Advanced Engineering (1), p. 225-230, 2014.
- [180] Wafa F., Ashour S., *Mechanical Properties of High-Strength Fiber Reinforced Concrete*, ACI Materials Journal (5), p. 449-455, 1992.
- [181] Wan Ibrahim M.H.,Mangi S.A.,Burhanudin M.K., Ridzuan M.B., Jamaluddin N., Shahidan S., Wong Y., Faisal S., Fadzil M.A., Ramadhansyah P.J., Ayop S.S.,Othman N.H., *Compressive and flexural strength of concrete containing palm oil biomass clinker and polypropylene fibres*, IOP Conf. Series: Materials Science and Engineering (271-012011), 2017.
- [182] Wang T., Hsu T.T.C., *Nonlinear finite element analysis of concrete structures using new constitutive models*, Computers and Structures (79), p. 2781-2791, 2001.
- [183] Wang D., Ju Y., Shen H., Xu L., *Mechanical properties of high performance concrete reinforced with basalt and polypropylene fiber*, Construction and Building Materials (197), p. 464-473, 2019.
- [184] Wang S., Zhang M.-H., Quek S.T., *Mechanical behaviour of fiber-reinforced high-strength concrete subjected to high strain-rate compressive loading*, Construction and Building Materials (31), p. 1-11, 2012.
- [185] Widodo S., *Fresh and hardened properties of Polypropylene fiber added Self-Consolidating Concrete*, International Journal of Civil and Structural Engineering (3), p. 85-93, 2012.
- [186] Wolska-Kotanska Cz., *Kształtowanie wytrzymałości betonu pyłami krzemionkowymi*, Inżynieria i Budownictwo (9), p. 379-392, 1993, [PL].
- [187] Wu Z., Shi C., He W., Wang D., *Static and dynamic compressive properties of ultra-high performance concrete (UHPC) with hybrid steel fiber reinforcements*, Cement and Concrete Composites (79), p. 148-157, 2017.
- [188] Yang I.H., Joh C., Kim B., *Structural behaviour of ultra high performance concrete beams subjected to bending*, Engineering Structures (32), p. 3478-3487, 2010.
- [189] Yang J., Wang R., Zhang Y., *Influence of dually mixing with latex powder and polypropylene fiber on toughness and shrinkage performance of overlay repair mortar*, Construction and Building Materials (261-120521), 2020.
- [190] Yap S.P., Bu C.H., Alengaram U.J., Mo K.H., Jumaat M.Z., *Flexural toughness characteristics of steel-polypropylene hybrid fibre-reinforced oil palm shell concrete*, Materials and Design (57), p. 652-659, 2014.

- [191] Yew M.K., Mahmud H.B., Ang B.C., Yew M.C., *Influence of different types of polypropylene fibre on the mechanical properties of high-strength oil palm shell lightweight concrete*, Construction and Building Materials (90), p. 36-43, 2015.
- [192] Yoo D.-Y., Yoon Y.-S., *Structural performance of ultra-high performance concrete beams with different steel fibers*, Engineering Structures (102), p. 409-423, 2015.
- [193] Yousefieh N., Joshaghani A., Hajibandeh E., Shekarchi M., *Influence of fibers on drying shrinkage in restrained concrete*, Construction and Building Materials (148), p. 833-845, 2017.
- [194] Yu R., Spiesz P., Brouwers H.J.H., *Mix design and properties assessment of Ultra-High Performance Fibre Reinforced Concrete (UHPC)*, Cement and Concrete Research (56), p. 29-39, 2014.
- [195] Zeiml M., Leithner D., Lackner R., Mang H.A., *How do polypropylene fibers improve the spalling behaviour of in-situ concrete?*, Cement and Concrete Research (36), p. 929-942, 2006.
- [196] Zhang P., Li Q., *Effect of polypropylene fiber on durability of concrete composite containing fly ash and silica fume*, Composites: Part B (45), p. 1587-1594, 2013.
- [197] Zienkiewicz O., Taylor C., Leroy R., Fox D. D., *The finite element method for solid and structural mechanics*, Butterworth-Heinemann, 1990-2005.
- [198] Zych T., Krasodomski W., *Polyolefin fibres used in cementitious composites - manufacturing, properties and application*, Technical Transactions Civil Engineering (3-B), p. 155-178, 2016.
- [199] Zollo R.F., *Fiber-reinforced concrete: an overview after 30 years of development*, Cement and Concrete Composites (19), p. 107-122, 1997.

## Standards and reports:

- [200] ACI Committee 544, *Measurement of Properties of Fiber Reinforced Concrete*, (ACI 544. 2R-89), American Concrete Institute, Detroit, 1989.
- [201] ASTM 1018-85, *Standard Test Method for Flexural Toughness and First-Crack Strength of Fiber-Reinforced Concrete (Using Beam with Third-Point Loading)*, American Concrete Institute.
- [202] 1097-3:2000 *Badania mechanicznych i fizycznych właściwości kruszyw - Oznaczanie gęstości nasypowej i jamistości*, Polski Komitet Normalizacyjny, 2006.
- [203] PN-EN 12390-1 *Badania betonu - Część 1: Kształt, wymiary i inne wymagania dotyczące próbek do badania i form / Testing hardened concrete - Part 1: Shape, dimensions and other requirements for specimens and moulds*, Polski Komitet Normalizacyjny, 2013.

- [204] PN-EN 12390-2 *Badania betonu - Część 2: Wykonywanie i pielęgnacja próbek do badań wytrzymałościowych / Testing hardened concrete - Part 2: Making and curing specimens for strength tests*, Polski Komitet Normalizacyjny, 2011.
- [205] PN-EN 12390-3 *Badania betonu - Część 3: Wytrzymałość na ściskanie próbek do badań / Testing hardened concrete - Part 3: Compressive strength of test specimens*, Polski Komitet Normalizacyjny, 2011.
- [206] PN-EN 12390-4 *Badania betonu - Część 4: Wymagania dla maszyn wytrzymałościowych / Testing hardened concrete - Part 4: Compressive strength. Specification for testing machines*, Polski Komitet Normalizacyjny, 2001.
- [207] PN-EN 12390-5 *Badania betonu - Część 5: Wytrzymałość na zginanie próbek do badania / Testing hardened concrete - Part 5: Flexural strength of test specimens*, Polski Komitet Normalizacyjny, 2009.
- [208] PN-EN 12390-13 *Badania betonu - Część 13: Wyznaczanie siecznego modułu sprężystości przy ściskaniu / Testing hardened concrete - Part 13: Determination of secant modulus of elasticity of concrete in compression*, Polski Komitet Normalizacyjny, 2014.
- [209] PN-EN 14889-2 *Włókna do betonu. Część 2: Włókna polimerowe. Definicje, wymagania i zgodność / Fibers for concrete. Part 2: Polymer fibres. Definitions, specifications and conformity*, Polski Komitet Normalizacyjny, 2007.
- [210] PN-EN 1992-1-1 *Projektowanie konstrukcji z betonu. Część 1-1: Reguły ogólne i reguły dla budynków / Design of concrete structures. Part 1-1: General rules and rules for buildings*, Polski Komitet Normalizacyjny, 2008.
- [211] JSCE-SF4 *Method of tests for flexural strength and flexural toughness of steel fiber reinforced concrete*, 1984.
- [212] *Global Cement Report*, 13th edition.



# Spis rysunków

1.1	Author of the dissertation with his supervisor at PEKABEX's facilities . . .	2
3.1	Packing effect (source: [154]) . . . . .	6
3.2	Failure mechanism of concrete members without and with fiber (based on [116]) . . . . .	7
4.1	Types of specimens used in the research . . . . .	15
4.2	The method of interpretation of the specimens notation (explanation of symbols in the text) . . . . .	17
4.3	Arrangement of mounting brackets in the full-scale beam . . . . .	18
4.4	Steel reinforcement in most of full-scale beams . . . . .	18
4.5	PEKABEX concrete batching plant . . . . .	18
4.6	Scheme of loading for determination of flexural strength [mm] . . . . .	19
4.7	Prism half during compression test . . . . .	20
4.8	Silica fume used in the research . . . . .	26
4.9	Max. flexural stress [MPa] of cement and cement mixed with silica fume - column diagram . . . . .	27
4.10	Max. compressive stress [MPa] of cement and cement mixed with silica fume - column diagram . . . . .	27
4.11	Coarse aggregate (basalt) used in the research (COLAS) . . . . .	28
4.12	Grading curve for fine aggregate (PEKABEX) . . . . .	29
4.13	Grading curve for fine aggregate (SIKA) . . . . .	29
4.14	Grading curve for coarse aggregate (PEKABEX) . . . . .	30
4.15	Grading curve for coarse aggregate (COLAS) . . . . .	30
4.16	Bulk density test setup . . . . .	31
4.17	Polypropylene fibre used in the research . . . . .	32
4.18	Cement mixer in the laboratory of Poznań University of Technology . . . .	33
4.19	Testing machines: INSTRON 8505 (on the left) and INSTRON SATEC 300DX (on the right) . . . . .	34
4.20	Contact free measuring system ARAMIS 6M . . . . .	34
4.21	A few specimens after testing in the preliminary stage of work . . . . .	35
4.22	Full-scale beam in a test stand subjected 3-point bending in the preliminary stage of work . . . . .	35
4.23	Cylinder specimen mounted on compressive strength test setup . . . . .	37

4.24	Examples of specimens after compressive strength test . . . . .	37
4.25	Compressive strength [MPa] test results (after 28 days) - column diagram .	38
4.26	The failure of cylinder under compression - specimen without polypropylene fibres (I-3-W1) . . . . .	40
4.27	Preparation of specimens for testing of material parameters . . . . .	41
4.28	Cylinder specimens for testing of material parameters . . . . .	41
4.29	Cycles for determination of initial and stabilized secant modulus of elasticity	42
4.30	Stress - strain graph for cylinder I-1-W4 . . . . .	44
4.31	Secant modulus of elasticity - column diagram . . . . .	45
4.32	Poisson's ratio - column diagram . . . . .	45
4.33	ARAMIS system during the testing of modulus of elasticity . . . . .	48
4.34	The cylinder II-2-W4 subjected to testing . . . . .	49
4.35	Laboratory beam (10x10x50cm) mounted on test setup . . . . .	50
4.36	Static scheme of laboratory beam . . . . .	50
4.37	The failure mechanism of beam without (on the left) and with (on the right) polypropylene fibre reinforcement . . . . .	51
4.38	Force-displacement graphs for beams without (I-3) and with (I-2) polypro- pylene fibre . . . . .	53
4.39	Forces [kN] - column diagram . . . . .	53
4.40	Three measuring systems used simultaneously in testing of full-scale beams	54
4.41	The full-scale beam during testing . . . . .	55
4.42	Force-displacement graph for one of the full-scale beam . . . . .	55
4.43	Forces [kN] in 5th, 10th, 20th and 30th cycle of loading - column diagram .	56
4.44	Force-displacement graphs (selected cycles) in full-scale beams (I-1' and I-2')	58
4.45	Force-displacement graph (envelope) for the full scale beam I-1'-B3 . . . .	59
4.46	Permanent part of deflection [mm] in 5th, 10th, 20th and 30th cycle of loading - column diagram . . . . .	59
4.47	Force-displacement graphs (envelopes) in full-scale beams . . . . .	60
4.48	Permanent part of mid-span deflection in full-scale beams . . . . .	62
4.49	Comparison of results depending on used silica fume and aggregate (I-1' vs. I-2') . . . . .	63
4.50	Comparison of results depending on the presence of steel bars (I-2' vs. I-2)	63
4.51	Comparison of results depending on the presence of polypropylene fibres (I-2' vs. I-3') . . . . .	64
4.52	Comparison of results depending on place of concreting (I-1' vs. II-1') . . .	64
4.53	Comparison of results depending on polypropylene fibre length (II-1' vs. II-2') . . . . .	65
4.54	Mid-span deflection according to time (first 850 sec) in full-scale beam (I- 1'-B1) measured by different measuring systems . . . . .	65
4.55	The ARAMIS system during testing of full-scale beam . . . . .	66
4.56	The full-scale beam during testing – view from the side of ARAMIS . . . .	66
4.57	Map of horizontal strain in beam I-2'-B1 after 5th cycle of loading . . . . .	67

4.58	Map of horizontal strain in beam I-2'-B1 after 10th cycle of loading . . . . .	67
4.59	Map of horizontal strain in beam I-2-B4 after 5th cycle of loading . . . . .	68
4.60	Map of horizontal strain in beam I-2-B4 after 10th cycle of loading . . . . .	68
5.1	The idea of coupling between plasticity and degradation: (a) plastic model, (b) degradation model, (c) plasticity-based damaged model . . . . .	73
5.2	Non-associated plastic flow [137] . . . . .	74
5.3	The physical interpretation of the eccentricity $\epsilon$ and the dilation angle $\Psi$ .	75
5.4	Yield surfaces in the deviatoric plane [1] . . . . .	76
5.5	Yield surface in plane stress [1] . . . . .	77
5.6	General stress-strain relation for concrete in compression [1] . . . . .	78
5.7	General stress-strain relation for concrete in tension [1] . . . . .	78
5.8	Geometric parameters of the computational model (dimensions in mm) . .	79
5.9	Tensile stress-strain relations provided in the analysis . . . . .	81
5.10	Force-displacement graphs obtained in the analysis . . . . .	81
5.11	Different density of meshes with FE size: 80 mm, 40 mm, 20 mm, 10 mm .	82
5.12	Force-displacement graphs for different FE size: 80 mm, 40 mm, 20 mm, 10 mm . . . . .	82
6.1	Different interpretations of $\delta_u$ regarding force-displacement path . . . . .	86
6.2	Force-displacement graphs with marked important deflections according to (on the left:) ASTM C1018 [201] and (on the right:) JSCE SF-4 [211] . . .	87
6.3	Fracture energy [kJ/m] in full-scale beams - column diagram . . . . .	90
6.4	Characteristic length [m] in full-scale beams - column diagram . . . . .	93
6.5	Ductility length [mm] in full-scale beams - column diagram . . . . .	93
7.1	Comparison of force-displacement envelopes for full-scale beams with steel bars ( $g(\Delta)$ ) and steel bars and PP fibres ( $f(\Delta)$ ) . . . . .	95
7.2	Comparison of fracture energy, characteristic length and ductility length for B-type beams with steel bars and steel bars and PP fibres . . . . .	96
A.1	Full-scale beam (I-1'-B1) on test setup . . . . .	99
A.2	Force-displacement graph in beam I-1'-B1 . . . . .	100
A.3	Force-displacement graph in beam I-1'-B2 . . . . .	100
A.4	Force-displacement graph in beam I-1'-B3 . . . . .	100
A.5	Force-displacement graph in beam I-2'-B1 . . . . .	101
A.6	Force-displacement graph in beam I-2'-B2 . . . . .	101
A.7	Force-displacement graph in beam I-2'-B3 . . . . .	101
A.8	Force - displacement graph in beam I-2-B4 . . . . .	102
A.9	Force - displacement graph in beam I-2-B5 . . . . .	102
A.10	Force - displacement graph for beam I-2-B6 . . . . .	102
A.11	Force - displacement graph for beam I-3'-B1 . . . . .	103
A.12	Force - displacement graph for beam I-3'-B2 . . . . .	103
A.13	Force - displacement graph for beam I-3'-B3 . . . . .	103
A.14	Force - displacement graph for beam II-1'-B1 . . . . .	104

A.15	Force - displacement graph for beam II-1'-B2 . . . . .	104
A.16	Force - displacement graph for beam II-1'-B3 . . . . .	104
A.17	Force - displacement graph for beam II-2'-B1 . . . . .	105
A.18	Force - displacement graph for beam II-2'-B2 . . . . .	105
A.19	Force - displacement graph for beam II-2'-B3 . . . . .	105
B.1	The view from ARAMIS camera . . . . .	107
B.2	Map of horizontal strains in beam I-1'-B1 after 5th cycle of loading . . . .	108
B.3	Map of horizontal strains in beam I-1'-B1 after 10th cycle of loading . . . .	108
B.4	Map of horizontal strains in beam I-1'-B2 after 5th cycle of loading . . . .	109
B.5	Map of horizontal strains in beam I-1'-B2 after 10th cycle of loading . . . .	109
B.6	Map of horizontal strains in beam I-1'-B3 after 5th cycle of loading . . . .	110
B.7	Map of horizontal strains in beam I-1'-B3 after 10th cycle of loading . . . .	110
B.8	Map of horizontal strains in beam I-2'-B1 after 5th cycle of loading . . . .	111
B.9	Map of horizontal strains in beam I-2'-B1 after 10th cycle of loading . . . .	111
B.10	Map of horizontal strains in beam I-2'-B2 after 5th cycle of loading . . . .	112
B.11	Map of horizontal strains in beam I-2'-B2 after 10th cycle of loading . . . .	112
B.12	Map of horizontal strains in beam I-2'-B3 after 5th cycle of loading . . . .	113
B.13	Map of horizontal strains in beam I-2'-B3 after 10th cycle of loading . . . .	113
B.14	Map of horizontal strains in beam I-2-B4 after 5th cycle of loading . . . .	114
B.15	Map of horizontal strains in beam I-2-B4 after 10th cycle of loading . . . .	114
B.16	Map of horizontal strains in beam I-2-B5 after 5th cycle of loading . . . .	115
B.17	Map of horizontal strains in beam I-2-B5 after 10th cycle of loading . . . .	115
B.18	Map of horizontal strains in beam I-2-B6 after 5th cycle of loading . . . .	116
B.19	Map of horizontal strains in beam I-2-B6 after 10th cycle of loading . . . .	116
B.20	Map of horizontal strains in beam I-3'-B1 after 5th cycle of loading . . . .	117
B.21	Map of horizontal strains in beam I-3'-B1 after 10th cycle of loading . . . .	117
B.22	Map of horizontal strains in beam I-3'-B2 after 5th cycle of loading . . . .	118
B.23	Map of horizontal strains in beam I-3'-B2 after 10th cycle of loading . . . .	118
B.24	Map of horizontal strains in beam I-3'-B3 after 5th cycle of loading . . . .	119
B.25	Map of horizontal strains in beam I-3'-B3 after 10th cycle of loading . . . .	119
B.26	Map of horizontal strains in beam II-1'-B1 after 5th cycle of loading . . . .	120
B.27	Map of horizontal strains in beam II-1'-B1 after 10th cycle of loading . . . .	120
B.28	Map of horizontal strains in beam II-1'-B2 after 5th cycle of loading . . . .	121
B.29	Map of horizontal strains in beam II-1'-B2 after 10th cycle of loading . . . .	121
B.30	Map of horizontal strains in beam II-1'-B3 after 5th cycle of loading . . . .	122
B.31	Map of horizontal strains in beam II-1'-B3 after 10th cycle of loading . . . .	122
B.32	Map of horizontal strains in beam II-2'-B1 after 5th cycle of loading . . . .	123
B.33	Map of horizontal strains in beam II-2'-B1 after 10th cycle of loading . . . .	123
B.34	Map of horizontal strains in beam II-2'-B2 after 5th cycle of loading . . . .	124
B.35	Map of horizontal strains in beam II-2'-B2 after 10th cycle of loading . . . .	124
B.36	Map of horizontal strains in beam II-2'-B3 after 5th cycle of loading . . . .	125
B.37	Map of horizontal strains in beam II-2'-B3 after 10th cycle of loading . . . .	125

# Spis tabel

3.1	Classification of polymer fibers according to [209]	8
3.2	Influence of polypropylene fiber inclusion to the concrete on different properties [30]	12
4.1	Amount of specimens according to their type and stage of work	16
4.2	Research variants	17
4.3	Standard (28 days) flexural strength of cement - test results	20
4.4	Early (2 days) flexural strength of cement - test results	20
4.5	Standard (28 days) compressive strength of cement - test results	21
4.6	Early (2 days) compressive strength of cement - test results	21
4.7	Standard (28 days) flexural strength of cement mixed with silica fume (KL) - test results	23
4.8	Early (2 days) flexural strength of cement mixed with silica fume (KL) - test results	23
4.9	Standard (28 days) flexural strength of cement mixed with silica fume (KS) - test results	23
4.10	Early (2 days) flexural strength of cement mixed with silica fume (KS) - test results	24
4.11	Standard (28 days) compressive strength of cement mixed with silica fume (KL) - test results	24
4.12	Early (2 days) compressive strength of cement mixed with silica fume (KL) - test results	24
4.13	Standard (28 days) compressive strength of cement mixed with silica fume (KS) - test results	25
4.14	Early (2 days) compressive strength of cement mixed with silica fume (KS) - test results	25
4.15	Comparison of test results for cement and cement mixed with silica fume	26
4.16	Different providers of aggregate	28
4.17	Results of testing of bulk density	31
4.18	Mix proportions	36
4.19	Results of compressive strength test	39
4.20	Cube strength [MPa] after 28 days and 1 year (variant I-1)	40
4.21	The characteristics of applied electric resistance wire strain gauges	42
4.22	Strains along measuring line at lower stress after third preloading cycle	43

4.23	Initial and stabilized secant modulus of elasticity - results of calculation . . .	46
4.24	Poisson's ratio . . . . .	47
4.25	Modulus of elasticity by the means of extensometers and Aramis [GPa] . . . . .	49
4.26	Max. force [kN] and corresponding flexural stress [MPa] in laboratory beams	52
4.27	Forces [kN] in 5th, 10th, 20th and 30th loading cycle in testing of full-scale beams . . . . .	57
4.28	Permanent part of deflection after 5th, 10th, 20th and 30th loading cycle in testing of full-scale beams . . . . .	61
5.1	Applied Concrete Damage Plasticity parameters . . . . .	76
6.1	Toughness indices $I_5$ , $I_{10}$ and $I_{20}$ according to ASTM C1018 [200] . . . . .	88
6.2	Flexural toughness $T_b$ [Nm] and flexural toughness factor $\bar{\sigma}_b$ [MPa] based on JSCE SF-4 [211] in laboratory beams (10x10x50cm) . . . . .	89
6.3	Fracture energy $G_f$ [kJ/m], characteristic length $l_{ch}$ [m] and ductility length $D_l$ [mm] in full-scale beams . . . . .	91
6.4	Flexural toughness $T_b$ [Nm] and flexural toughness factor $\bar{\sigma}'_b$ [MPa] based on JSCE SF-4 [211] in full-scale beams . . . . .	92